Geomorphic Hazard Analyses in Tectonically-Active Mountains: Application to the Western Southern Alps, New Zealand

A thesis submitted in partial fulfilment of the requirements for the

Degree of

Doctor of Philosophy in Hazard and Disaster Management

in the

Department of Geological Sciences

University of Canterbury

by

Theodosios Kritikos

2013

Franz Josef Glacier, West Coast, South Island New Zealand

"Human society is organized for a stable earth; its whole machinery supposes that, while the other familiar elements of air and water are fluctuating and untrustworthy, the earth affords a foundation which is firm. Now and then this implied compact with nature is broken, and the ground trembles beneath our feet. At such times we feel a painful sense of shipwrecked confidence; we learn how very precious to us was that trust in the earth which we gave without question. If the disturbance be of a momentary an unimportant kind we may soon forget it, as we forget the rush word of a friend; if it be violent, we lose one of the substantial goods of life, our instinctive confidence in the earth beneath our feet"

by N. S. Shaler, March 1887 "The Stability of the Earth," Scribner's Magazine, Vol.1, No.3, p.259.

Abstract

On-going population growth and urbanization increasingly force people to occupy environments where natural processes intensely affect the landscape, by way of potentially hazardous natural events. Tectonic plate boundaries, active volcanic regions and rapidly uplifting mountain ranges are prominent examples of geomorphically hazardous areas which today accommodate some of the world's largest cities. These areas are often affected by more than one hazard such as volcanic eruptions, earthquakes, landslides, tsunamis, floods, storms and wildfires, which frequently interact with each other increasing the total impact on communities. Despite progress in natural hazards research over the last two decades, the increasing losses from natural disasters highlight the limitations of existing methodologies to effectively mitigate the adverse effects of natural hazards. A major limitation is the lack of effective hazard and risk assessments incorporating hazard interactions and cascade effects. Most commonly, the assessment of risks related to different hazards is carried out through independent analyses, adopting different procedures and time-space resolutions. Such approaches make the comparison of risks from different hazard sources extremely difficult, and the implicit assumption of independence of the risk sources leads to neglect of possible interactions among hazard processes. As a result the full hazard potential is likely to be underestimated and lead to inadequate mitigation measures or land-use planning. Therefore there is a pressing need to improve hazard and risk assessments and mitigation strategies especially in highly dynamic environments affected by multiple hazards.

A prominent example of such an environment is the western Southern Alps of New Zealand. The region is located along an actively deforming plate boundary and is subject to high rates of uplift, erosion and orographically-enhanced precipitation that drive a range of interrelated geomorphic processes and consequent hazards. Furthermore, the region is an increasingly popular tourist destination with growing visitor numbers and the prospect for future development, significantly increasing societal vulnerability and the likelihood of serious impacts from potential hazards. Therefore the mountainous landscape of the western Southern Alps is an ideal area for studying the interaction between a range of interrelated geomorphic hazards and human activity.

In an effort to address these issues this research has developed an approach for the analysis of geomorphic hazards in highly dynamic environments with particular focus on tectonically-active mountains using the western Southern Alps as a study area. The approach aims to provide a framework comprising the stages required to perform multi-hazard and risk analyses and inform land-use planning.

This aim was approached through four main objectives integrating quantitative geomorphology, hazard assessments and GIS. The first objective was to identify the dominant geomorphic processes, their spatial distribution and interrelationships and explore their implications in hazard assessment and modelling. This was achieved through regional geomorphic analysis focusing on catchment morphometry and the structure of the drainage networks. This analysis revealed the strong influence and interactions between frequent landslides / debris-flows, glaciers, orographic precipitation and spatially-variable uplift rates on the landscape evolution of the western Southern Alps, which supports the need for hazard assessment approaches incorporating the interrelationships between different processes and accounting for potential event cascades.

The second and third objectives were to assess the regional susceptibility to rainfall-generated shallow landslides and river floods respectively, as these phenomena are most often responsible for extensive damage to property and infrastructure, injury, and loss of lives in mountainous environments. To achieve these objectives a series of GIS-based models was developed, applied and evaluated in the western Southern Alps. Evaluation results based on historical records indicated that the susceptibility assessment of shallow landslides and river floods using the proposed GIS-based models is feasible. The output from the landslide model delineates the regional spatial variation of shallow landslide susceptibility and potential runout zones while the results from the flood modelling illustrate the hydrologic response of major ungauged catchments in the study area and identify flood-prone areas. Both outputs provide critical insights for land-use planning.

Finally, a multi-hazard analysis approach was developed by combining the findings from the previous objectives based on the concepts of *interaction* and *emergent properties* (cascade effects) inherent in complex systems. The integrated analysis of shallow landslides, river floods and expected ground shaking from a M8 plate-boundary fault (Alpine fault) earthquake revealed the areas with the highest and lowest total susceptibilities. Areas characterized by the highest total susceptibility require to be prioritized in terms of hazard mitigation, and areas with very low total susceptibility may be suitable locations for future development.

This doctoral research project contributes to the field of hazard research, and particularly to geomorphic hazard analyses in highly dynamic environments such as tectonically active mountains, aiming to inform land-use planning in the context of sustainable hazard mitigation.

Acknowledgments

This research project has benefited from the help and support of many people. First and foremost I would like to express my deepest appreciation to my senior supervisor Professor Tim Davies for his fantastic support, guidance, encouragement throughout my PhD journey. His open mind and critical thinking were invaluable for developing my research skills.

Special thanks to my associate supervisor Dr. Thomas Wilson who offered great advice and support over the duration of the project. His sharp eye for the detail and insightful comments have been instrumental in continuously improving the quality of my research.

I would also like to express my gratitude to the University of Canterbury for financial support through the Doctoral Scholarship and Mason Trust.

I wish to acknowledge the special contribution of Noah Snyder who provided many useful discussions on geomorphic analysis and I am grateful to have worked with him. Acknowledgement must be extended to Erin Hawke and Rodney Barker from the Department of Conservation who kindly provided useful data and information during the initial stages of my research project. Huge thank you to all the fantastic technical and administrative staff of the Department of Geological Sciences for their support and assistance.

To my fellow postgraduate students, the many wonderful friends and my officemates thank you for making me feel at home in a place far, far away...from mine.

Finally, I owe my deepest gratitude to my family and my partner. Thank you for believing in me, your never-ending support, patience and understanding throughout the doctorate, and over my university years. I couldn't have done this without you.

Table of contents

List of Figures

List of Tables

Terminology

Hazards research involves many different disciplines, each with its own perspective. This inevitably results in the development and use of different terminology within each discipline. Although considerable progress has been made in terms of consistency of fundamental terms, as a result of the increasing number of hazard studies in recent years, a commonly-understood terminology still remains a challenge in the field of hazards. Therefore it is important to clarify the meaning of frequently-used and potentially-confusing terms throughout the study. The following term definitions are based on various published articles and reports investigating hazard and risk.

Assets (elements at risk): Humanly/socially valued entities threatened by a hazard. (Schmidt et al. 2011)

Consequences: The negative effects of a disaster expressed in terms of human, economic, environmental and political/social impacts (ISO 31010).

Exposure: People, property, systems, or other elements present in hazard zones that are thereby subject to potential losses (UNISDR 2009).

Hazard: A dangerous phenomenon, substance, human activity or condition that may cause loss of life, injury or other health impacts, property damage, loss of livelihoods and services, social and economic disruption, or environmental damage (UNISDR 2009).

Natural hazard: Natural process or phenomenon that may cause loss of life, injury or other health impacts, property damage, loss of livelihoods and services, social and economic disruption, or environmental damage (UNISDR 2009).

Geomorphic hazard: A landform or landscape change that adversely affects the human (population, economics, culture, politics) and constructed systems (buildings, roads, infrastructure etc.).

Technological hazard: A hazard originating from technological or industrial conditions, including accidents, dangerous procedures, infrastructure failures or specific human activities, that may cause loss of life, injury, illness or other health impacts, property damage, loss of livelihoods and services, social and economic disruption, or environmental damage (UNISDR 2009).

Hazard assessment: The process of identifying the nature, location, probability and magnitude of a potentially damaging event.

Hazardscape: A dynamic spatial entity which reflects the physical susceptibility of a place and vulnerability of human life and assets to various hazards in a given human ecological system (Khan 2012).

Land-use planning: The process undertaken by public authorities to identify, evaluate and decide on different options for the use of land, including consideration of long term economic, social and environmental objectives and the implications for different communities and interest groups, and the subsequent formulation and promulgation of plans that describe the permitted or acceptable uses (UNISDR 2009).

Land-use suitability analysis: the process of identifying the most suitable places for locating future land-uses (Collins et al. 2001).

Multi-Hazard analysis: The implementation of methodologies and approaches aimed at assessing and mapping the potential occurrence of different types of natural hazards in a given area. Analytical methods and mapping have to take into account the characteristics of the single hazardous events (e.g. affected area, intensity/magnitude, frequency of occurrence) as well as their mutual interactions and interrelations (e.g. landslide-induced earthquake, floods and landslides triggered by extreme rainfall, natural disasters as secondary effects from main disaster types) (Delmonaco et al. 2006).

Multi-Risk analysis: The implementation of methodologies and approaches aimed at assessing and mapping the potential damage/expected loss due to the occurrence of different types of natural or human-induced hazards on social, environmental and economic settings of a given area. Analytical methods and mapping have to consider the occurrence and impact of all potential hazardous events, exposure of elements at risk and their vulnerability (Delmonaco et al. 2006).

Resilience: The ability of a system, community or society exposed to hazards to resist, absorb, accommodate to and recover from the effects of a hazard in a timely and efficient manner, including through the preservation and restoration of its essential basic structures and functions (UNISDR 2009).

Risk: The combination (i.e. product) of the probability of an event and its negative consequences (UNISDR 2009).

Risk assessment: A methodology to determine the nature and extent of risk by analysing potential hazards and evaluating existing conditions of vulnerability that together could potentially

harm exposed people, property, services, livelihoods and the environment on which they depend (UNISDR 2009).

Susceptibility: Expected occurrence of a geomorphic event due to a set of predisposing factors. Susceptibility does not imply the temporal probability of occurrence or magnitude of the event. Herein it is determined from statistical relationships between historical events and predisposing factors.

Vulnerability: The characteristics and circumstances of a community, system or asset that make it susceptible to the damaging effects of a hazard (UNISDR 2009).

Chapter 1: Introduction

Whether induced by earthquakes, floods, landslides or other climatic and geomorphic processes, natural hazards can have devastating impacts on communities with short- and long-term adverse effects. According to the Global Assessment Report on Disaster Risk Reduction (UNISDR 2013) over one trillion U.S. dollars have been lost in the last decade (2000-2012) due to disasters, 2.9 million people have been affected and more than one million people killed. Although these figures illustrate very high losses they may present a conservative picture of global disaster impacts, as they don't take into account uninsured losses associated with recurrent, smaller-scale extensive disasters, particularly in developing countries.

The rapid growth of population and expansion of infrastructure worldwide has led to equally rapid development of land. This development often forces people to occupy highly dynamic environments where natural processes intensely affect the landscape and, when their effects are combined with the vulnerabilities of human systems, result in disasters with major impacts. Tectonic plate boundaries, active volcanic regions and rapidly uplifting mountain ranges are only a few of the geomorphic-hazard-threatened areas which accommodate densely populated cities. A recent study investigating global patterns of loss of life from non-seismically triggered landslides illustrates that landslides are a major hazard particularly in areas with high rates of tectonic activity, high relief, intense rainfall, and high population density (Petley 2012). According to the global dataset presented in the study, 32,322 deaths have been recorded between 2004 and 2010, clustering in tectonically-active regions.

However, the significant increase in fatalities and economic losses over the past few decades due to natural catastrophic events is not only a direct result of the growth of population density in hazard-prone areas, but also due to the consequent increase of possible cascade effects that derive from the interactions between various natural and human systems (Marzocchi et al. 2009). The concept of "cascading effects" refers to a chain of events where a primary hazard triggers a series of subsequent hazards with catastrophic cumulative impact. Cascading disasters such as the 2011 Tohoku earthquake (Japan) that generated a tsunami and subsequent damage to the Fukushima nuclear power plant, in addition to major economic losses, demonstrate the interactions among different natural and technological hazards with severe societal and environmental impacts. Cascading hazards in highly dynamic environments are also generated from the interactions

between geomorphic processes. A prominent chain of events in mountainous environments is the triggering of mass movements due to earthquake shaking which block rivers forming landslide-dams and induce consequent dam-break floods (Huang & Fan 2013).

From the above it is clear that development of innovative hazard and risk assessment approaches recognising and incorporating hazard interactions is crucial for effectively reducing risk, especially in highly dynamic environments with high population densities or prospects of future development. Nevertheless, to date the evaluation of risks related to different hazards has generally been carried out through independent analyses, adopting different procedures and time-space resolutions. Such an approach of assessing hazards and risks has some obvious major limitations, as it is extremely difficult to compare risks of from different hazard sources, and the implicit assumption of independence of the risk sources leads to neglect of possible interactions among hazard processes (Marzocchi et al. 2009). On the other hand the implementation of multi-risk approaches requires dealing with a variety of practical issues. Given the wide spectrum of natural and man-made hazards with diverse characteristics such as magnitude, intensity, duration, extent, recurrence interval and impacts, the main difficulties are related to the disparate methodologies and spatio-temporal resolutions used for the assessments, as well as the extremely demanding data requirements.

The limitations of existing hazard assessment methodologies, and increasing disaster losses in highly dynamic environments, stress the pressing need for research focusing on the development of approaches for multi-hazard and risk analyses which would incorporate the interactions between different processes, have relatively low data requirements and associated costs and provide meaningful results for planning purposes.

1.1 Tectonically active mountains

The spectacular landscapes of mountains have caught the attention of humankind for centuries. A significant percentage of the world's population (20%) lives today in mountainous environments or mountain-front regions, and half of humankind depends in some way on mountain resources (mainly water) (Körner & Ohsawa 2005). Formed by tectonic forces and often located in tectonically active zones, mountains are particularly susceptible to seismicity, volcanoes, landslides and a range of hydro-meteorological processes (Hewitt 1983, 1997; Wohl & Oguchi 2004) which frequently result in significant loss of life and property.

The earth's lithosphere is divided into rigid plates moving in different directions. Where these plates meet, their relative motion creates three types of boundaries: divergent, convergent and transform.

At convergent zones tectonic plates move toward one another and collide, usually one plate is forced beneath the other and is recycled back down into the mantle (subduction). This process creates different types of mountain belts depending on the types of lithospheric crust involved (Fig.1.1). For example at the margins of ocean-to-ocean convergence zones, island arc volcanic chains are formed (e.g Mariana, Aleutian Islands). In ocean-to-continent convergent margins the less buoyant oceanic material is forced to pass beneath the continental landmass creating Andean-type mountain ranges, whereas at continent-to-continent convergence zones, collisional-type mountain ranges develop (e.g. Himalaya). Conversely, where tectonic plates are diverging new crustal material is being generated at extensional centre rift zones by magma rising from the mantle (e.g. the submerged mountain range of Mid-Atlantic Ridge).

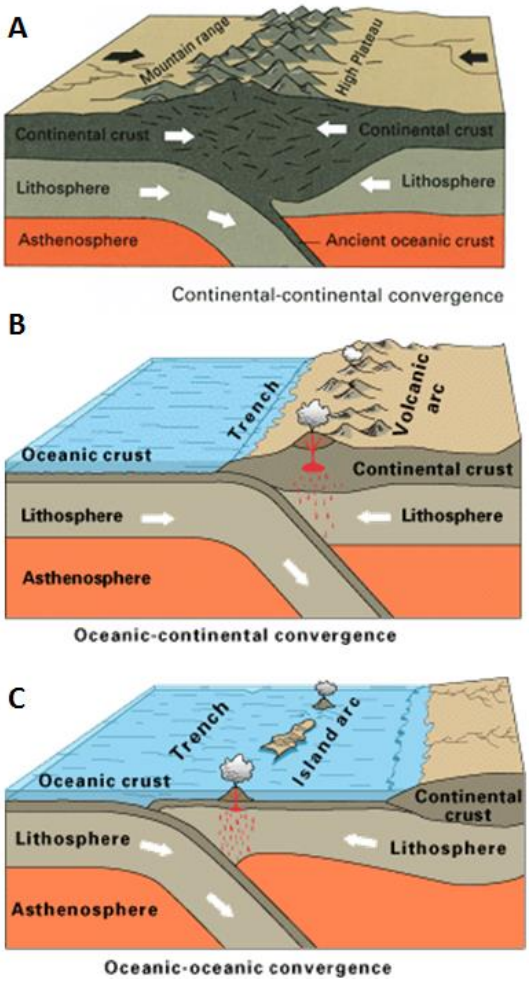

Figure 1.1 Three types of subduction zones and associated types of mountain ranges (Source USGS 2012).

Mountain geomorphic systems are the result of complex interactions between tectonics, climate and surface processes, all of which operate over different spatial and temporal scales. They exist as part of a spatial continuum that makes up the Earth's surface without clear separation from systems at low attitudes (Shroder & Bishop 2004). However the greater topographic complexity of mountainous

landscapes dictates strong spatial and temporal constraints that govern surface processes and feedback mechanisms (Bishop & Shroder 2000; Bishop et al. 2002). Slaymaker 2010 argues that mountain geo- systems are not exceptionally fragile but they demonstrate a greater range of vulnerability to disturbance than many landscapes. In addition to the highly dynamic physical environment Hewitt & Mehta (2012) recognize the social organization and histories of mountain communities as key factors for their increased susceptibility to hazards and consider the consequent risks as embedded in human land uses, activities and interactions.

Therefore the combination of extreme climatic and geomorphic processes with ongoing population growth, land use modifications and social organization of mountain communities are the primary factors of the observed increased disaster losses in these environments. Common hazards at tectonically active mountains include earthquakes, volcanic eruptions, floods, rainfall-induced landslides and debris-flows, rock avalanches, dam-break floods, glacial lake outbursts and snow avalanches as well as a range of other climate-related hazards such as strong wind, tornadoes, hail, snow, ice, drought, extreme temperatures and wildfires.

1.1.1 The western Southern Alps hazardscape

New Zealand is a tectonically active region located on the transpressive boundary of the Australian and Pacific tectonic plates. The plate boundary consists of two opposite-dipping obliquely convergent subduction systems linked by the Alpine fault and Malborough fault zones (Pettinga et al. 2001). The Pacific Plate is subducting westward beneath the Australian Plate along the Hikurangi Trench in the northeast, while the Australian Plate is subducting eastward below the Pacific Plate along the Puysegur Trench in the south-west of New Zealand (Fig. 1.2). The total rate of displacement across the plate boundary is approximately 40-50 mm yr^{-1} (Beavan et al. 2002, Wallace et al 2007; De Mets et al. 2010). Along the west coast of the South Island at least 70-75% of the total plate boundary motion is accommodated through the Alpine Fault (Norris et al. 1990) which forms an approximately 450 km linear feature with both right-lateral strike- and dip-slip components (Norris & Cooper 2000).

Total displacement of 480 km has occurred across the plate boundary over the last 25 million years as the eastern South Island has been displaced south-westward relative to the Australian Plate (Norris et al. 1990). Due to the oblique convergence across the plate boundary during the late Cenozoic, approximately 25 km of vertical displacement has also occurred across the Alpine Fault, creating the Southern Alps mountain range (Norris et al. 1990). The Southern Alps form a linear

mountain belt, with a length of around 350 km, as measured from the Hurunui River in the NE to Arawata River in the SW (Tippett & Hovius 2000), rising to more than 3km a.s.l. (Mt Cook; 3754 m).

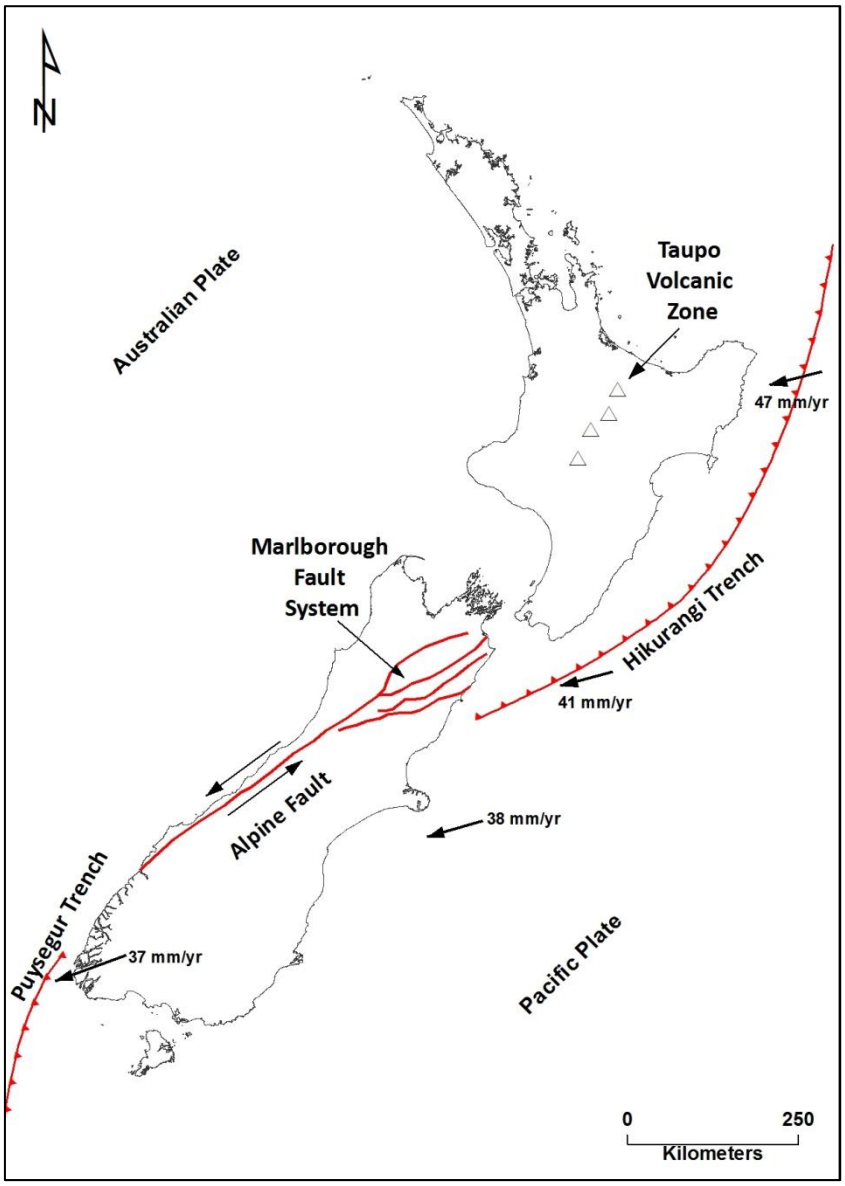

Figure 1.2 New Zealand tectonic setting. Plate motion from Anderson & Webb (1994).

Due to its geographic position and the highly dynamic processes shaping its landscape the Southern Alps are an ideal place for studying the interaction between plate tectonics and mountain range evolution and have been the subject of extensive research for at least three decades. Summerfield (1989) states "Much of the attraction of the southern Alps for assessing relationships between uplift rates and modes of landscape development lies in their relative tectonic simplicity, at least in comparison with convergent margins composed of displaced Terranes" while Tippet & Hovius (2000) argue that "the Southern Alps present an unparalleled opportunity to understand relationships between tectonics, surface processes and topography in a collisional setting". Nevertheless Tippett

& Kamp (1993) note that "Despite the apparent tectonic simplicity of the South Island collision zone, little is known about its dynamics".

The Alpine Fault lies at the north-western margin of the Southern Alps dividing the study area into two distinct geological regions. Southeast of the Alpine fault, lithologies are predominantly quartzofeldspathic indurated sedimentary rocks of the Torlesse composite terrane, which have in places been metamorphosed to semischist or schist (Cox & Barrell 2007). Northwest of the Alpine fault early Paleozoic metasedimentary and plutonic rocks comprise the basement lithologies covered by moraine ridges and outwash surfaces formed where glaciers previously extended out from the Southern Alps (Cooper 1989; Cooper & Tulloch 1992; Mortimer et al. 1999). Large lateral moraines from the last glacial maximum (LGM: ~ 23000 BP) are very well preserved and confine the fans and outwash surfaces of the major rivers, which are the sites of most societal activity.

The climate of the western South Island is a major factor of the landscape evolution of the Southern Alps, as it affects the relief and is affected by it (Bonnet & Crave 2003). The rugged mountainous landscape of Southern Alps forms a barrier to the strong westerly-dominated atmospheric circulation. When the warm humid westerly air masses from the Tasman Sea reach the West Coast, they rise over the topographic barrier of western Southern Alps and cool. As a result the water vapour condenses and produces heavy rainfall at the western flank of the mountains. Once over the Main Divide, the air masses descend and warm up while the moisture gradually evaporates resulting in a much drier climate at the eastern side of the mountain range and Canterbury Plains. Precipitation rates reach up to 14 m yr^{-1} west of the Main Divide (Henderson & Thomson 1999) but there is a strong east–west precipitation gradient so that they fall to 1000 mm yr-1 or less east of the Alps (Griffiths & McSaveney 1983).

The ice and snow forming the glaciers are produced and maintained by New Zealand's humid maritime climate and the orientation of the main axial range across the dominant Southern Hemisphere westerlies (Fitzharris et al. 1992). There are more than 3100 glaciers in New Zealand that exceed 0.01 km^2 in area, comprising a total of c. 53.3 km^3 of ice volume (Chinn 1989). Tasman Glacier is the largest glacier flowing south along the eastern flanks of Mt Cook, while the well-known Franz Josef and Fox Glaciers flow westwards from the slopes of Mt Cook down steep-sided valleys to their termini in temperate rain forest at approximately 300 m a.s.l (Fitzharris et al. 1999).

As a result of the interplay between tectonic, geomorphic and climatic processes driving the landscape evolution of the mountain range, the region is subject to a broad range of hazards. Flooding is the most frequent hazard in the region, inducing extensive economic and physical

impacts, and has probably caused more loss of life than any other hazard to date (DTec 2002).The extremely high orographically-enhanced precipitation, steep topography (Griffiths & McSaveney 1983) and the fact that most settlements and infrastructure are located on active floodplains and fans are the main factors underlying the very high flood risk in the region. Approximately 471 flood events have been recorded in a 156 year period indicating the high frequency of flooding in the area (Benn 1990; DTec 2002). Floods, however, can occur due to a number of other processes besides heavy rainfall such as river aggradation (McSaveney & Davies 1998; Davies et al 2003a, Korup 2005b; Davies & McSaveney 2006; Davies & Korup 2007) landslide dam break floods (Davies & Scott 1997; Davies 2002; Korup 2005a; Hancox et al 2005) and glacier bursts (Davies et al. 2003b; Korup & Tweed 2007).

Landslides are common in landscape evolution of the western Southern Alps (Hovius et al. 1997; Korup 2005b,c; Korup 2006; Hewitt 2006; Hewitt et al. 2008; Korup et al. 2009) and pose a serious hazard in the region (Whitehouse 1983; Whitehouse & Griffiths 1983; Bell 1994; Davies & Scott 1997; McSaveney & Davies 1998; Benn 2005; Hancox et al. 2005; Korup 2005a; Davies 2002, 2007), frequently damaging property and infrastructure as well as causing injury and loss of lives. A combination of high tectonic uplift rates, steep topography, intense or prolonged rainfalls and earthquakes controls the occurrence of mass movements varying from debris-flows and rockfalls to catastrophic rock avalanches with volumes > 10^6 m^3 (Hancox et al. 2005; Chevalier et al. 2009; Dufresne et al. 2009; Wright 1999; Barth 2013). However, small-magnitude, high-frequency landslides, triggered by intense or prolonged rainfall, have caused the most damage to property and infrastructure and at least 36 fatalities in the region (Benn 2005).

Due to the region's high tectonic activity the west coast of the South Island has also very high seismic hazard. The Alpine fault as a major active tectonic structure was first identified by Wellman & Willett (1942) and few years later (1950s) Wellman indicated its dextral strike-slip displacement of about 480 km. Since then several studies have investigated the Alpine fault providing age constraints for surface-rupturing earthquakes (Adams 1980; Bull 1996; Berryman et al. 1998; Wells et al. 1999; Yetton 2000; Wells & Goff 2007; Berryman et al. 2012; De Pascale & Langridge 2012), studying its structure (Norris & Cooper 1995, 2000) and exploring its role as a hazard by indicating its various potential impacts (McCahon et al. 2006a, 2006b, 2006c; Orchiston 2010; Robinson & Davies 2013). The greatest potential seismic hazard in the region is associated with the Alpine Fault. Ground shaking and consequent geomorphic hazards from a great Alpine fault earthquake (M = 8+ every 250-300 years; Rhoades & Van Dissen 2003) are expected to affect the entire region on time scales

varying from immediately after the earthquake up to decades (Hewitt et al. 2008; Robinson & Davies 2013).

Further hazards threatening the study area are coastal hazards (e.g. coastal erosion, storm surge, tsunami, sea level rise), climatic hazards (e.g. strong wind, tornadoes, hail, snow, ice, droughts, wildfires), landslide-induced lake tsunamis and glacier outburst floods (DTec 2002).

The regional population (Westland district) currently stands at approximately 8403 almost 40% of whom live in Hokitika (3078) (Statistics New Zealand 2006). The remaining population lives in rural areas and small townships such as Franz Josef, Fox Glacier, Harihari, Ross and Haast (Fig. 1.3). During the early years of settlement natural resources have been the major drivers of the local economy with industries such as mining, farming and forestry. Gold mining in particular attracted early settlers to the region in the 1860s and spurred the development of farming, agriculture and forestry (Balcar & Pearce 1996). In recent years, nature-based tourism has been more important with annual visitor numbers reaching up to approximately 2 million (including international and domestic visitors in the broader West Coast region). The main attractions are the low-level Fox and Franz Josef Glaciers as well as several heritage sites associated with gold and coal mining.

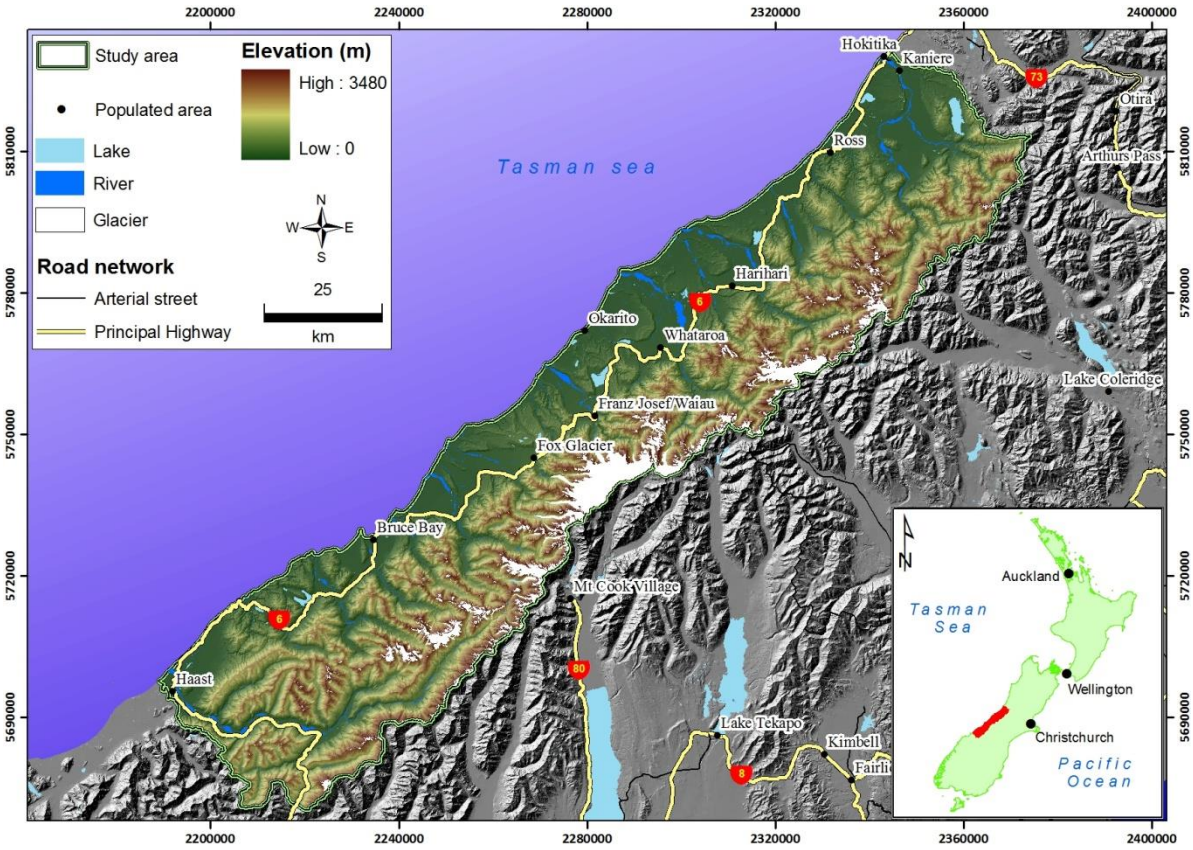

Figure 1.3 Location map of the study area.

The relatively low rates of loss of life from floods, landslides and historical earthquakes in the area are primarily due to the low population density. However, given the prospect of future development, population growth and the increase of both domestic and international visitors, societal vulnerability is also increasing and the likelihood of serious impacts from geomorphic hazards is likely to increase.

1.1.2 Hazard and disaster management in Westland

The field of disaster or emergency management has its origin in the period of the Cold War when planning for nuclear war and the building of bomb shelters was encouraged (Pierce 2003). The modern approach has a much broader perspective aiming to protect societies in times of peace as well as in times of war, as defined by the civil defence acts in different countries (e.g. CDEM Act 2002, New Zealand). Lyndell & Perry (1992) divide emergency management activities into four discrete but interconnected categories distinguished by the time relative to disaster impact. Thus, mitigation and preparedness activities are generally seen as taking place before the impact of any given disaster, whereas response and recovery are post-impact activities. During the pre-impact period, hazard, vulnerability and risk assessments are necessary in order to identify the potential hazards and evaluate their impacts on human and constructed systems. According to Mileti (1999), among the sustainable mitigation components of a good comprehensive plan are the hazard identification, impact assessment and loss estimation. Based on this general concept, over the last three decades hazard and risk assessment methods have been the subject of research by many institutions, organizations and governments around the world in an effort to effectively predict, where possible, the spatial and temporal occurrence of catastrophic events and reduce disaster losses (FEMA 1997; Guzzetti et al. 1999; European Commission 2000; Van Westen 2010).

Emergency management in New Zealand involves a generic framework referred to as the 4Rs, emphasizing the stages of reduction, readiness, response, and recovery. Reduction includes the activities to identify risks to human life and property from hazards, and aims to eliminate these risks if possible or to reduce their likelihood and the magnitude of their impact. Readiness mainly concerns the development of operational systems and capabilities before an emergency happens, through a variety of response programmes for emergency services, lifeline utilities (infrastructure providers), the general public and other agencies. Response takes place immediately before, during or directly after an emergency focusing on saving lives and property as well as setting the grounds for recovery. Finally, recovery activities aim at immediate, medium- and long-term regeneration of a community following an emergency.

The Resource Management Act 1991 (RMA), the Civil Defence Emergency Management Act 2002 (CDEM Act) and the Building Act 2004 are the main pieces of legislation that promote the assessment of hazards and risks as well as environmental management in New Zealand. Particularly, the purpose of the Resource Management Act (RMA) is to promote the sustainable management of natural and physical resources. Under the RMA, both regional councils and territorial authorities have responsibilities to avoid or mitigate natural hazards. The CDEM Act was enacted in 2002 to replace the existing Civil Defence Act 1983. The Act promotes a co-operative, integrated, 4R approach that aims at the sustainable management of hazards and encourages communities to achieve acceptable levels of risk. It also specifies the role and function of civil defence emergency management organisations, and the responsibilities of government departments, lifeline utilities, and emergency services in the context of the 4Rs (reduction, readiness, response, and recovery) to ensure they are well prepared for any type of emergency. The CDEM Act also requires the formation of regional CDEM Groups and the preparation of corresponding CDEM Group plans. Each CDEM Group comprises a regional group of local authorities, emergency services, health organisations, and lifeline utilities with the tasks to identify hazards and mitigation activities, as well as highlight gaps in hazard knowledge and limitations in mitigation strategies. Lastly, the Building Act 2004 provides the means to ensure the safety and integrity of structures by setting out specific criteria to which buildings and structures must conform.

In order to fulfil its responsibilities under the RMA 1991 and the Civil Defence Act 1983, the West Coast Regional Council (WCRC) initiated a series of mapping projects and reports in the early 1990s, in an attempt to assess the major hazards in the region and provide recommendations for hazard mitigation strategies (Benn 1990, 1991a, 1991b, 1992a, 1992b, 1993; Hoey 1990). Since the late 1990s the WCRC has commissioned or been involved in several hazard research projects (McSaveney & Davies 1998; Goff et al. 2001; Connell 2001; Rouse 2001; DTec 2002; McCahon et al. 2006a, 2006b, 2006c, 2007; Langridge & Ries 2009; Langridge & Beban 2011; Hall 2012).

A study by McSaveney & Davies (1998) indicates the major geomorphic hazards posing a threat to the community of Franz Josef Glacier, primarily due to the community's proximity to the Waiho / Callery River system and the Alpine Fault. In their report they also suggest possible options for future management of the Waiho River and ways to decrease the community's vulnerability to seismic hazards. A few years later the WCRC Hazards Review (DTec 2002) summarized the existing literature on all natural hazards relevant to the region, identified progress and gaps in knowledge and provided recommendations for future research based on regional council’s needs for hazard management. Further research commissioned by the WCRC and various district councils investigated

the impact of a major natural disaster, using an Alpine Fault earthquake as an example of a worst-case scenario, on essential lifelines, including transportation, energy, water supply, sewerage and telecommunications (McCahon et al. 2006a, 2006b, 2006c, 2007).

All the above projects and reports illustrate the high level of hazard from various geomorphic and climatic processes in the region, identify gaps in hazard knowledge, indicate data constraints and establish the basis for future hazard research. Nevertheless, methodologies for mapping the spatial variation of hazard or susceptibility to dominant geomorphic processes in the region, (e.g. floods, landslides) have yet to be developed. Exceptions are the model for estimating mean erosion rates and sediment discharge under different land-use scenarios developed by Dymond et al. (2010) and the GIS-based statistical approach for regional landslide susceptibility mapping applied by England (2011) in the West Coast region.

1.2 Geomorphology and hazard research

The field of hazard research was established by Gilbert F. White who observed that losses from flooding in the U.S. had increased between 1942 and 1956 despite substantial investment in flood control works and concluded that increasing numbers of people occupying apparently protected flood-prone areas, results in greater losses when flooding occurred (White et al. 1958). Motivated by these findings, White (1974) proposed the fundamental components of hazard research focusing on the extent of human population in areas subject to natural hazards, people's perceptions of extreme events and consequent hazards as well as the range of potential hazard mitigation actions. Although only indirectly recognized in these early components, the role of physical systems (e.g. atmosphere, lithosphere, hydrosphere etc.) in hazard research has received increased attention over the years. Burton et al. (1978) highlight the significance of the physical system to natural hazards research by describing the most important physical parameters of an event that affect human response and a qualitative scale for each, these are: magnitude (high-low), frequency (frequent- rare), duration (long-short), areal extent (widespread-limited), speed of onset (slow-fast), spatial dispersion (diffuse-concentrated), and temporal spacing (regular-random).

Natural hazards result from tectonic, climatic or other geomorphic events are part of the spectrum of natural processes continuously reshaping the landscape in order to maintain the equilibrium between endogenous and exogenous processes, therefore they are not isolated events but tend to recur. The frequency of a hazard event can be regarded as the number of events of a given magnitude in a particular period of time. A recurrence interval for an event is often determined in terms of the average length of time between events of a certain size. However, the limited historical

records that usually reflect only a fraction of landscape evolution time scales are not sufficient for predicting the occurrence of these events with meaningful reliability for emergency management planning. Despite limitations in current knowledge that do not allow predicting the timing and magnitude of potentially hazardous natural events, there has been remarkable progress on methods to study the spatial distribution, frequency and mechanisms of these processes. Focusing on landform dynamics and landscape evolution, geomorphology has played an especially important role in the progress of hazard research. The field of geomorphology encompasses a wide range of different approaches and sub-disciplines including fluvial, hillslope, glacial, tectonic, coastal and desert geomorphology, biogeomorphology and karst geomorphology. All the above subdivisions are mainly concerned with landforms, landscape dynamics, driving mechanisms, process rates and time-scales providing the means for quantitative analysis of interconnected processes. A growing number of studies have applied geomorphological methods to investigate landslide hazards (Brunsden 1999; Glade 2005; Petley 2010), flood hazards (Rodriguez-Iturbe & Valdes 1979; Baker 1976; Baker 2008; Lastra et al 2008; Benito & Hudson 2010), paleoseismology of faults and earthquake hazards (Panizza 1991; Crozier 2009; Bull 2007, 2010), coastal hazards (Walker & McGraw 2010) and volcanic hazards (Thouret 2010). The significant contribution of geomorphology in the field of hazard research has been recognized by several authors (Baker 1994; Evans & Glague 1994; Gares at al. 1994; Rosenfeld 1994; Sheidegger 1994; Alcantara–Ayala 2002, 2010) who argue that geomorphology can be useful in various aspects of hazard research, in particular, for the mapping of hazard-prone areas, constructing the history of occurrence of past hazardous events and establish their frequency and magnitudes, predicting the occurrence and location of future events and indicating appropriate mitigation strategies.

1.3 GIS applications in hazard management

A geographic information system (GIS) can be broadly defined as a computer-based system that facilitates the acquisition, compilation, storage, transformation, analysis, display and dissemination of geographic information by integrating the fields of computer science, cartography and statistical analysis. Goodchild (1992) first introduced the term Geographic information science (GIScience) as the "*research on the generic issues that surround the use of GIS technology, impede its successful implementation, or emerge from an understanding of its potential capabilities*" p.41. GIScience is essentially a multidisciplinary field that explores space-time relationships, with a focus on geographic representation, spatial analysis, modelling and communication of these relationships as well as studying the fundamental principles of geographic information systems. These principles

include issues of representation, uncertainty, scale, visualization and at a less technical level the impacts that GIS has on society (Goodchild 2004).

In dealing with natural hazards, many of the critical issues that arise are inherently spatial. Common tasks involved in hazard and disaster management such as identifying hazards, critical vulnerabilities and impact consequences, land use planning and coordinating emergency response or planning for rebuild following a disaster, have a strong spatial component (Cova 1999). Linking spatial to non-spatial information is a fundamental process of decision making. Several studies have illustrated the important role of GIS in all phases of emergency management (mitigation, preparedness, response, and recovery) (Johnson 1992; Bruzewicz 1994; Mondschein 1994; Cova 1999) in natural hazards (Wadge et al 1993; Coppock 1995; Carrara & Guzzetti 1995; Wohl & Oguchi 2004; Van Westen 2010), risk (Rejeski 1993) and environmental hazard management (Emani 1996; Gatrell & Vincent 1991). The practical value of GIS in emergency management lies in the benefits of integrating a technology designed to support spatial decision making into a field with a strong need to address numerous critical spatial decisions. Therefore, it provides emergency managers with a powerful tool to manage large amounts of spatial information, visualize spatial relationships and reveal trends critical to planning and response phases.

As GIS technologies facilitate spatial analysis and modelling, they also improve our understanding of interactions between processes and their implications, as well as providing insight into scale dependencies thus significantly enhancing our ability to assess hazards. Furthermore, geographical information systems and digital topography provide sophisticated tools for landscape analyses and visualization advancing the methods of quantitative geomorphology and landscape evolution modelling. In particular, DEM-based analyses implemented through GIS have significantly improved our ability to quantitatively analyze landforms. Today these analyses are widely used in the hydrological and geophysical sciences for both data visualization and as analytical frameworks, facilitating the development and implementation of multi-input, spatially distributed models of surface processes (Maidment et al. 1993, 1996; Muzik 1996; Saghafian et al. 2000; Martinez et al. 2002; Melesse et al. 2004; Noto & Loggia 2007; Du et al. 2009). These capabilities make GISs particularly useful in addressing natural hazards in mountainous regions. They allow combining and comparing various types of spatial and numerical data, facilitate the updating of databases as new information becomes available and enhance visualization of spatial relations producing comprehensive maps. Therefore they can be effectively used to model the spatial distribution, frequency and magnitude of hazardous processes as well as to model the spatial variation of land susceptibility to such processes.

An increasing number of hazard and susceptibility assessments are based on the identification of various predisposing factors (e.g. slope gradient, fault locations, lithologic units, land cover etc.) and their combination via GIS (Carrara et al. 1991; Carrara & Guzzetti 1995; Guzzetti et al. 1999; Guzzetti 2006; Malczewski 2000, 2006; Ohlmacher & Davis 2003; Ayalew et al. 2004; Ayalew & Yamagishi 2005; Lee 2005; He & Beighley 2008). This approach is especially useful in areas where direct instrumental or historical records of hazardous processes are not available, but where morphometric, geological, land cover, soil data that control these processes are available or may be extracted using existing maps, aerial photographs or satellite imagery. By facilitating quantitative comparisons among different types of data, GIS technologies provide new insights into the location as well as controlling and triggering factors of potentially hazardous processes.

GIS is a fundamental component of the present research used in various analyses, modelling and visualization procedures. It is applied to perform regional geomorphic analyses, develop a series of susceptibility models, carry out exposure analysis, evaluate modelling outputs and generate corresponding maps.

1.4 Thesis aim and objectives

This research project integrates quantitative geomorphology, hazard assessments and GIS to develop an approach for the analysis of multiple geomorphic hazards in highly dynamic environments such as tectonically active mountains. Particular focus is given to shallow landslides / debris flows and river floods triggered by prolonged or high intensity rainfall, as these phenomena are often responsible for extensive damage to property and infrastructure, injury, and loss of lives in mountainous environments. The approach ultimately aims to provide a framework comprising the stages required to perform multi-hazard and risk assessment and inform land-use planning in highly dynamic environments. This is addressed with the following four objectives:

Objective One

Explore the dominant geomorphic processes, driven by tectonic activity and climate, and identify their interrelationships as well as their links with the occurrence and magnitude of geomorphic hazards in the active mountainous environment of the Western Southern Alps (WSA) of New Zealand.

Objective two

Assess the spatial variation of rainfall-generated shallow landslide /debris-flow susceptibility.

Objective three

Evaluate the susceptibility of major catchments to rainfall-induced river flooding.

The common theme of the objectives two and three is to develop approaches for susceptibility assessment with relatively low data requirements yet able to generate meaningful results for regional-scale planning. Through the modelling procedures it is also aimed to identify the most important factors controlling the occurrence of debris-flows and river floods as well as revealing limitations in evaluating these processes and the main sources of uncertainty.

Objective four

Develop an approach for multi-hazard and risk assessment suitable for highly dynamic environments. The proposed approach aims to provide a conceptual framework for multi-hazard / risk analysis.

1.5 Thesis structure

This thesis is organised into six chapters. Because of the inter-disciplinary nature of the study, chapters 2, 3 and 4 focus on different aspects of hazard analysis and include a review of relevant literature, description of methods, results, discussion and conclusions. These different aspects are brought together in chapter 5 to formulate the main stages of a multi-hazard analysis framework. In chapter six the conclusions and implications from each chapter are discussed through the lens of pre-event land use planning in the context of sustainable hazard mitigation at tectonically active mountains.

Chapter 2 explores regional patterns of landscape morphometric parameters in an effort to investigate tectonic, climate and surface processes which control the landscape evolution of the WSA and consequent hazards. Methods of quantitative geomorphology are applied via GIS to analyse the spatial variation of catchment morphometric parameters, the structure of drainage networks, channel longitudinal profiles of major rivers and valley geometries. Results provide insight into the spatial variation of uplift rates and dominant interrelated geomorphic processes. Recognizing the link between the dominant geomorphic processes and hazards, the findings are used to identify the hazardscape of the WSA and reveal critical implications in hazard assessment and modelling.

In chapter 3 a GIS-based approach for shallow landslide and debris-flow susceptibility assessment is developed. Since slope failures are complex phenomena and their prediction involves many uncertainties, the application of fuzzy set theory in a GIS environment is investigated as a potential landslide susceptibility assessment approach, in an effort to minimize the uncertainties derived from non-linear relationships between conditioning factors and slope instability. A GIS-based model to estimate the runout path and distance of potential future shallow slope failures is also developed. Both models are applied and evaluated in WSA.

Chapter 4 is concerned with modelling the spatial variation of rainfall-induced river flood susceptibility in the region. Initially the development of a GIS-based spatially distributed unit hydrograph model is described. The model aims to investigate the hydrologic response of major ungauged catchments in the study area based on their morphometry, land cover and soil characteristics, as well as providing a tool to predict runoff hydrographs using real rainfall intensity data. The model's predictive performance and its potential as a tool to inform planning are evaluated by comparing the results with observed hydrographs. A GIS-based approach to delineate flood-prone areas is also developed. The relations between five critical factors and flood occurrence are established using fuzzy logic and historical flood events in the region. Finally, the factors are combined to generate the regional flood susceptibility map.

Chapter 5 integrates the results from chapters 2-4 and develops an approach for multi-hazard and risk analysis suitable for highly dynamic environments. The approach aims to provide a conceptual framework of the key stages underlying effective hazard and risk analysis in environments where geomorphic processes and consequent hazards are strongly interrelated. Each stage of the procedure is separately discussed using examples from the WSA. Particular focus is given to the various types of interactions between processes and an attempt is made to classify them in specific categories. To demonstrate the practical application of the proposed approach, a regional multi-hazard and exposure analysis was carried out in the central WSA.

In Chapter 6 the key findings from the four main objectives are outlined, followed by a discussion on the implications of the thesis' findings for land suitability analysis and land use planning in the context of sustainable risk reduction and hazard mitigation.

1.6 References

Adams J 1980. Contemporary uplift and erosion of the Southern Alps, New Zealand: Summary. Geological Society of America Bulletin, 91, 2-4.

Alcántara-Ayala I 2002. Geomorphology, natural hazards, vulnerability and prevention of natural disasters in developing countries. Geomorphology 47: 107–124.

Alcántara-Ayala I 2010. Geomorphology and coastal hazards. In: Geomorphological hazards and disaster prevention in (eds) I. Alcantara-Ayala and A. Goudie. Cambridge : Cambridge University Press, 2010. pp. 269 - 276.

Anderson H, Webb T 1994. New Zealand seismicity: patterns revealed by the upgraded National Seismograph Network. New Zealand Journal of Geology and Geophysics, 37, 477-493.

Ayalew L, Yamagishi H, Ugawa N 2004. Landslide susceptibility mapping using GIS-based weighted linear combination, the case in Tsugawa area of Agano River, Niigata Prefecture, Japan. Landslides 1:73–81.

Ayalew L, Yamagishi H 2005. The application of GIS-based logistic regression for landslide susceptibility mapping in the Kakuda-Yahiko Mountains, Central Japan. Geomorphology, 65(1-2), 15-31.

Baker VR 1976. Hydrogeomorphic methods for the regional evaluation of hazards. Environmental Gelogy, 1, 261-281.

Baker VR 1994. Geomorphological understanding of floods. Geomorphology 10: 139–156.

Baker VR 2008. Paleoflood hydrology: origin, progress, prospects. Geomorphology, 101(1-2), 1-13.

Balcar MJ, Pearce DG 1996. Heritage tourism on the West Coast of New Zealand. Tourism Management, 17(3), 203-212.

Barth NC 2013. A tectono-geomorphic study of the Alpine Fault, New Zealand. PhD thesis, University of Otago, New Zealand. 303p.

Beavan J, Tregoning P, Bevis M, Kato T, Meertens C 2002. The motion and rigidity of the Pacific Plate and implications for plate boundary deformation, J. Geophys. Res., 107(B10), 2261, doi:10.1029/ 2001JB000282.

Bell DH 1994. Landslide hazards. In: Canterbury Regional Council Report 94 (19), Natural hazards in Canterbury, 55–76.

Benito G, Hudson PF 2010. Flood hazards: the context of fluvial geomorphology. In: Geomorphological hazards and disaster prevention in (eds) I. Alcantara-Ayala and A. Goudie. Cambridge : Cambridge University Press, 2010. pp. 111 - 123.

Benn JL 1990. A Chronology of Flooding on the West Coast, South Island, New Zealand: 1846 – 1990. The West Coast Regional Council, Greymouth. 159p.

Benn JL 1991a. Grey River Catchment Flood Hazard Maps. The West Coast Regional Council, Greymouth.

Benn JL 1991b. Buller River Catchment Flood Hazard Maps. The West Coast Regional Council, Gremouth. 6p plus 21 Flood Hazard Maps.

Benn JL 1992a. Hokitika River Catchmemt Flood Hazard Maps. The West Coast Regional Council, Greymouth. 6p plus 4 Flood Hazard Maps.

Benn JL 1992b. Review of Earthquake Hazards on the West Coast. The West Coast Regional Council, Greymouth. 62p.

Benn JL 1993. Karamea and Arahura River Catchment Flood Hazard Maps. The West Coast Regional Council, Greymouth. 5p plus 3 Flood Hazards Maps.

Benn JL 2005. Landslide events on the West Coast, South Island, 1867-2002. New Zealand Geographer 61: 3-13.

Berryman K, Cooper AF, Norris RJ, Sutherland R, Villamor P 1998. Paleoseismic investigation of the Alpine Fault at Haast and Okuru. Geological Society of New Zealand Miscellaneous Publication, 101A, 44.

Berryman KR, Cochran UA, Clark KJ, Biasi GP, Langridge RM, Villamor P 2012. Major Earthquakes Occur Regularly on an Isolated Plate Boundary Fault. Science 336, 1690. DOI: 10.1126/science.1218959.

Bishop MP, Shroder JF 2000. Remote sensing and geomorphometric analysis for assessing topographic complexity and erosion dynamics in the Nanga Parbat Himalaya, in Khan, M.A., Treloar, P.J., Searle, M.P., and J.M. Qasim, eds., Tectonics of the Nanga Parbat Syntaxis and Western Himalaya: Geological Society of London Special Publication 170, p. 181–200.

Bishop MP, Shroder JF, Bonk R, Olsenholler J 2002. Geomorphic change in high mountains: a western Himalayan perspective. Global and Planetary Change, 32: 311–29.

Bonnet S, Crave A 2003. Landscape response to climate change: insights from experimental modelling and implications for tectonic versus climatic uplift of topography. Geology, 31, 123 – 126.

Brunsden D 1999. Some geomorphological considerations for the future development of landslide models. Geomorphology 30, 13–24.

Bruzewicz AJ 1994 Remote sensing and GIS for emergency management. Proceedings, First Federal Geographic Technology Conference. Washington DC, GIS World Inc. Vol 1: 161–4.

Bull WB 1996. Prehistorical earthquakes on the Alpine fault, New Zealand: Journal of Geophysical Research, v. 101, no. B3, p. 6037–6050, doi:10.1029/95JB03062.

Bull WB 2007. Tectonic Geomorphology of Mountains: A New Approach to Paleoseismology. Blackwell Publishing. 316p.

Bull W 2010. Regional seismic shaking hazards in mountains. In: Geomorphological hazards and disaster prevention in (eds) I. Alcantara-Ayala and A. Goudie. Cambridge : Cambridge University Press, 2010. pp. 5 - 11.

Burton I, Kates RW, White GF 1978. The Environment as Hazard. 1st ed. Oxford Univ. Press, New York, 240 pp.

Carrara A, Cardinali M, Detti R, Guzzetti F, Pasqui V, Reichenbach P, 1991. GIS Techniques and statistical models in evaluating landslide hazard. Earth Surface Processes and Landform 16, 427–445.

Carrara A, Guzzetti F 1995. Geographical Information Systems in assessing natural hazard. Selected Contribution from the International Workshop held in Perugia on Sept. 20–22 1993, Kluver Academic Publisher, Dordrecht/Boston/London, pp 354 (Advances in Natural Technological Hazard Research Series, Volume 5).

Chevalier G, Davies T, McSaveney M 2009. The prehistoric Mt Wilberg rock avalanche, Westland, New Zealand, Landslides 6: 253–262.

Chinn TJH 1989. Glaciers of New Zealand. US Geological Survey Professional Paper 1386-H2. Washington, DC: US Government Printing Office.

Connell RJ 2001. Grey River – Greymouth: Hydraulic Review of Flood Capacity. Report Prepared for the West Coast Regional Council (Greymouth) by CH Modelling Ltd, (Christchurch). 41p.

Cooper RA 1989. Early Paleozoic terranes of New Zealand. Journal of the Royal Society of New Zealand 19: 73–112.

Cooper RA, Tulloch AJ 1992. Early Palaeozoic terranes in New Zealand and their relationship to the Lachlan Fold Belt. Tectonophysics 214(1/4): 129-144.

Coppock JT 1995. GIS and natural hazards: an overview from a GIS perspective. In Carrara A, Guzzetti F (eds) Geographical information systems in assessing natural hazards. Dordrecht, Kluwer: 21–34.

Cova TJ 1999. GIS in emergency management. In: Geographical Information Systems: Principles, Techniques, Applications, and Management, P.A. Longley, M.F. Goodchild, D.J. Maguire, D.W. Rhind (eds.), John Wiley & Sons, New York, 845-858.

Cox SC, Barrell DJA (compilers) 2007. Geology of the Aoraki area. Institute of Geological & Nuclear Sciences 1:250 000 geological map 15. 1 sheet + 71 p. Lower Hutt, New Zealand. GNS Science.

Crozier MJ 2009. Landslide geomorphology: An argument for recognition, with examples from New Zealand, Geomorphology, doi:10.1016/j.geomorph.2009.09.010.

Davies TR, Scott BK 1997. Dambreak Flood Hazard from the Callery River, Westland New Zealand. New Zealand Journal of Hydrology, Vol. 36 (1), pp 1-13.

Davies TRH 2002. Landslide dambreak flood hazards at Franz Josef Glacier township, NewZealand: a risk assessment. Journal of Hydrology (New Zealand) 41: 1-17.

Davies TR, McSaveney MJ, Clarkson PJ 2003a. Anthropic Aggradation of the Waiho River, Westland, New Zealand: Microscale Modelling. Earth Surf. Process. Landforms 28, 209–218.

Davies TR, Smart CC, Turnbull JM 2003b. Water and Sediment Outbursts from Advanced Franz Josef Glacier, New Zealand. Earth Surface Processes and Landforms, 28, 1081–1096.

Davies TR, McSaveney MJ 2006. Geomorphic constraints on the management of bedloaddominated rivers. Journal of Hydrology (New Zealand) 45 (2): 69-88.

Davies TR, Korup O 2007. Alluvial fanhead trenching resulting from catastrophic sediment inputs. Earth Surface Processes and Landforms 32: 725-742.

Davies TR 2007. Potential for rock avalanche hazard at Franz Josef glacier village, Westland. Confidential report to west coast regional council. Natural Hazards Research Centre Dept of Geological Sciences University of Canterbury, New Zealand, 14p.

DeMets C, Gordon RG, Argus DF 2010. Geologically current plate motions. Geophys. J. Int. 181, 1–80. doi: 10.1111/j.1365-246X.2009.04491.x

De Pascale GP, Langridge RM 2012. New on-fault evidence for a great earthquake in A.D. 1717, central Alpine fault, New Zealand. Geology, doi: 10.1130/G33363.1.

DTec Consulting Ltd 2002: West Coast Regional Council: Natural Hazards Review. Report prepared for West Coast Regional Council by Dtec Consulting Ltd. Client Reference: 1065.136WCRC, Greymouth. 140 p.

Dufresne A, Davies TR, McSaveney MJ 2009. Influence of runout-path material on emplacement of the Round Top rock avalanche, New Zealand. Earth Surface Processes and Landforms. DOI: 10.1002/esp.1900.

Du J, Xie H, Hu Y, Xu Y, Xu C 2009. Development and testing of a new storm runoff routing approach based on time variant spatially distributed travel time method. Journal of Hydrology 369: 44-54.

Dymond JR, Betts HD, Schierlitz CS 2010. An erosion model for evaluating regional land-use scenarios. Environmental Modelling & Software 25, 289–298.

Emani S 1996. Applications in hazard assessment and management. Explorations in Geographic Information Systems Technology, Vol. 6. Worcester (USA), United Nations Institute for Training and Research (UNITAR).

England K 2011. A GIS approach to landslide hazard management for the West Coast region, New Zealand. Unpublished MSc thesis, University of Canterbury, Christchurch, New Zealand.

European Commission DG XII, Environment and Climate Program, 2000. TEMRAP: The European Multi-Hazard Risk Assessment Project, contract ENV4-CT97-0589.

Evans SG, Clague JJ 1994. Recent climatic change and catastrophic geomorphic processes in mountain environments. Geomorphology 10, 107–128.

FEMA 1997. Multi hazard identification and risk assessment: a cornerstone of the national mitigation strategy, 1th Edition, United States.http://www.fema.gov/library/viewRecord.do?id=2214.

Fitzharris BB, Hay JE, Jones PD 1992. Behaviour of New Zealand glaciers and atmospheric circulation changes over the past 130 years. The Holocene2, 97–106.

Fitzharris B, Lawson W, Owens I 1999. Research on glaciers and snow in New Zealand. Progress in Physical Geography 23, 4 pp. 469–500.

Gares PA, Sherman DJ, Nordstrom KF 1994. Geomorphology and natural hazards. Geomorphology 10:1– 18.

Gatrell AC, Vincent P 1991. Managing natural and technological hazards. In Masser I, Blakemore M (eds) Handling geographical information: methodology and potential applications. Harlow, Longman/New York, John Wiley & Sons, Inc: 148–80.

Glade T 2005. Linking debris-flow hazard assessments with geomorphology. Geomorphology 66, 189– 213.

Goff JR, Nichol SL, Chagué-Goff C 2001. Evidence for Catastrophic Inundation of the West Coast: Okarito Lagoon. Report prepared for The West Coast Regional Council, Greymouth. 34p.

Goodchild MF 1992. Geographical information science. International Journal of Geographical Information Systems, 6 (1): 31-45.

Goodchild 2004. Foreword (GIScience perspective). In, M.P. Bishop, ed., Geographic Information Science and Mountain Geomorphology. Praxis Scientific Publishing, Chichester, UK, pp. 309-341.

Griffiths GA, McSaveney MJ 1983. Distribution of mean annual precipitation across some steepland regions of New Zealand: New Zealand Journal of Science, v. 26, p. 197–209.

Guzzetti F, Carrara A, Cardinali M, Reichenbach P 1999. Landslide hazard evaluation: a review of current techniques and their application in a multi-scale study, central Italy. Geomorphology 31, 181–216.

Guzzetti F, Reichenbach P, Ardizzone F, Cardinali M, Galli M 2006. Estimating the quality of landslide susceptibility models. Geomorphology 81(1-2): 166-184.

Hall RJ 2012. Waiho River Future Management. West Coast Regional Council, Greymouth 74p.

Hancox GT, McSaveney MJ, Manville VR, Davies TRH 2005. The October 1999 Mt Adams rock avalanche and subsequent landslide dam-break flood and effects in Poerua River, Westland, New Zealand. New Zealand Journal of Geology & Geophysics 48: 683-705.

He YP, Beighley RE 2008. GIS-based regional landslide susceptibility mapping: a case study in southern California. Earth Surface Processes and Landforms, 33(3), 380-393.

Henderson RD, Thompson SM 1999. Extreme rainfalls in the Southern Alps of New Zealand. Journal of Hydrology (New Zealand) 38: 309-330.

Hewitt K 1983. Human geography and mountain environments. The Canadian Geographer / Le Géographe canadien, 27: 96–102. doi: 10.1111/j.1541-0064.1983.tb00687.x

Hewitt K 1997. Risk and disasters in mountain lands. In B Messerli and JD Ives (eds), Mountains of the World: A global priority, Carnforth: Parthenon 371-408.

Hewitt K 2006. Disturbance regime landscapes: mountain drainage systems interrupted by large rockslides. Progress in Physical Geography, Vol. 30, No. 3, 365-393.

Hewitt K, Clague JJ, Orwin JF 2008. Legacies of catastrophic rock slope failures in mountain landscapes. Earth-Science Reviews 87, 1-38.

Hewitt K, Mehta M 2012. Rethinking risk and disasters in mountain areas. Revue de géographie alpine / Journal of Alpine Research [En ligne], 100-1 | 2012, mis en ligne le 14 mai 2012, consulté le 30 juin 2013. URL:http://rga.revues.org/1653, DOI : 10.4000/rga.1653.

Hoey T 1990. Aggradation in the Waiho River. Final Report for the West Coast Regional Council. 23p.

Hovius N, Stark CP, Allen PA 1997. Sediment flux from a mountain belt derived from landslide mapping. Geology 25, 231– 234.

Huang R, Fan X 2013. The landslide story Nature Geoscience, 6 (5), 325-326.

Johnson GO 1992. GIS applications in emergency management. URISA Journal 4: 66–72.

Körner C, Ohsawa M 2005. Mountain Systems. In Millennium Ecosystem Assessment. Current State and Trends: Findings of the Condition and Trends Working Group. Ecosystems and Human Well-being. Vol 1. Island Press, Washington, DC, 681–716.

Korup O 2005a. Geomorphic hazard assessment of landslide dams in South Westland, New Zealand – fundamental problems and approaches. Geomorphology 66, 167-188.

Korup O 2005b. Large landslides and their effect on alpine sediment flux: South Westland, New Zealand. Earth Surface Processes and Landforms 30, 305-323.

Korup O 2005c. Geomorphic imprint of landslides on alpine river systems, southwest New Zealand. Earth Surface Processes and Landforms 30, 783-800.

Korup O 2006. Effects of deep-seated bedrock landslides on hillslope morphology, Southern Alps, New Zealand. Journal of Geophysical Research 111, F01018, doi:10.1029/2004JF000242.

Korup O, Tweed F 2007. Ice, moraine, and landslide dams in mountainous terrain. Quaternary Science Reviews 26, 3406–3422.

Korup O, Densmore AL, Schlunegger F 2009. The role of landslides in mountain range evolution. Geomorphology, doi:10.1016/j.geomorph.2009.09.017.

Langridge R, Ries W 2009. Mapping and Fault Rupture Avoidance Zonation for the Alpine Fault in the West Coast Region. GNS Science Consultancy Report 2009/18. 47 p.

Langridge RM, Beban JG 2011. Planning for a Safer Franz Josef/Waiau Community, Westland District: Considering Fault Rupture of the Alpine Fault GNS Science Consultancy Report 2011/217. 61p.

Lastra J, Fernadez E, Diez-Herrero A, Marquinez J 2008. Flood hazard delineation combining geomorphological and hydrological methods: an example in the Northern Iberian Peninsula. Nat Hazards 45:277–293.

Lee S 2005. Application of logistic regression model and its validation for landslide susceptibility mapping using GIS and remote sensing data, International Journal of Remote Sensing, 26:7, 1477-1491.

Lindell MK, Perry RW 1992. Behavioral Foundations of Community Emergency Planning. Hemisphere Publishing Co., New York. 309p.

Maidment DR 1993. Developing a spatially distributed unit hydrograph by using GIS. In HydroGIS 93: Application of Geographic Information Systems in Hydrology and Water Resources, Proceedings of the Vienna Conference, eds. K. Dovar and H. P. Natchnebel, 181 - 192. Vienna: Int. Assoc. of Hydrological Sci. Publ. no 211.

Maidment DR, Olivera F, Calver A, Eatherall A, Fraczek W 1996. Unit hydrograph derived from a spatially distributed velocity field. Hydrological Processes 10: 831-844.

Malczewski J 2000. On the use of Weighted Linear Combination Method in GIS: common and best practice approaches. Transactions in GIS, 4(1): 5-22.

Malczewski J 2006. GIS-based multicriteria decision analysis: a survey of the literature. International Journal of of Geographical Information Science, Vol. 20, No. 7, pp. 703-726.

Martinez V, Garcia AI, Ayuga F 2002. Distributed routing techniques developed on GIS for generating synthetic unit hydrograph. Trans ASAE 45(6):1825–1834.

Marzocchi W, Mastellone M, Ruocco A Di, Novelli P, Romeo E, Gasparini P 2009. Principles of multi-risk assessment: interactions amongst natural and man-induced risks. European Commission.

McCahon I, Elms D, Dewhirst R 2006a. Buller District Lifelines Study: Alpine fault earthquake scenario. A report prepared for the Buller District Council, 208 p.

McCahon I, Elms D, Dewhirst R 2006b. Westland District Council Lifelines Study: Alpine fault earthquake scenario. A report prepared for the Westland District Council. Greymouth, 210 p.

McCahon I, Elms D, Dewhirst R 2006c. West Coast Engineering Lifelines Group Study: Alpine fault earthquake scenario. A report prepared for the West Coast Engineering Lifelines Group and the West Coast Regional Council. Greymouth, 204 p.

McCahon I, Elms D, Dewhirst R 2007. Grey District Lifelines Plan: Alpine fault earthquake scenario and lifelines vulnerability assessment. A report prepared for the Grey District Council. Greymouth, 299 p.

McSaveney MJ, Davies TR 1998. Natural Hazard Assessment for the township of Franz Josef Glacier and its Environs. Client Report 43714B.10, Institute of Geological and Nuclear Sciences, Lower Hutt, 58 p.

Melesse AM, Graham WD 2004. Storm runoff prediction based on a spatially distributed travel time method utilizing remote sensing and GIS. *Journal of American Water Resources Association* 40(4): 863-879.

Mileti DS 1999. Disasters by Design: A reassessment of natural Hazards in the United States. Washington, D.C. Joseph Henry Press. 351p.

Mondschein LG 1994. The role of spatial information systems in environmental emergency management. Journal of the American Society for Information Science 45: 678–85.

Mortimer N, Tulloch AJ, Spark RN, Walker NW, Ladley E, Allibone A, Kimbrough DL 1999. Overview of the Median Batholith, New Zealand: a new interpretation of the geology of the Median Tectonic Zone. Journal of African Earth Sciences 29: 257–268.

Muzik I 1996. Flooding modelling with GIS-derived distributed unit hydrographs. Hydrological Processes 10: 1401-1409.

Norris RJ, Koons PO, Cooper AF 1990. The obliquely-convergent plate boundary in the South Island of New Zealand: Implications for ancient collision zones, Journal of Structural Geology, 12, 715–725.

Norris RJ, Cooper AF 1995. Origin of small-scale segmentation and transpressional thrusting along the Alpine fault, New Zealand, Bull. Geol. Soc. Am., 107, 231–240.

Norris RJ, Cooper AF 2000. Late Quaternary slip rates and slip partitioning on the Alpine Fault, New Zealand. Journal of Structural Geology 23: 507–520.

Noto LV, Loggia GL 2007. Derivation of a distributed unit hydrograph integrating GIS and remote sensing. Journal of Hydrologic Engineering 12(6): 639-650.

Ohlmacher GC, Davis JC 2003. Using multiple logistic regression and GIS technology to predict landslide hazard in northeast Kansas, USA. Engineering Geology 69: 331–343.

Orchiston CHR 2010. Tourism and Seismic Risk: Perceptions, preparedness and resilience in the zone of the Alpine Fault, Southern Alps, New Zealand. PhD thesis, University of Otago, New Zealand. 317p.

Panizza M 1991. Geomorphology and seismic risk. Earth-Science Reviews, 31, 11-20.

Pearce L 2003. Disaster management and community planning, and public participation: How to achieve sustainable hazard mitigation. Natural Hazards Vol. 28: pp 211-228.

Pettinga JR, Yetton MD, Van Dissen RJ, Downes G 2001. Earthquake source identification and characterization for the Canterbury Region, South Island, New Zealand. Bulletin of the New Zealand Society for Earthquake Engineering 34: 282-317.

Petley D 2010. Landslide hazards. In: Alcantara-Ayala I, Goudie A ed. Geomorphological hazards and disaster prevention. Cambridge, Cambridge University Press, 2010. pp. 13 - 28.

Petley D 2012. Global patterns of loss of life from landslides. Geology, v. 40; no. 10; p. 927–930.

Rejeski D 1993. GIS and risk: a three culture problem. In Goodchild M F, Parks B O, Steyart L T (eds) Environmental modeling with GIS. New York, Oxford University Press: 319–31.

Rhoades DA, Van Dissen RJ 2003. Estimates of the time-varying hazard of rupture of the Alpine Fault, New Zealand, allowing for uncertainties. New Zealand Journal of Geology and Geophysics, 46: 4, 479-488.

Robinson TR, Davies TRH 2013. Review Article: Potential geomorphic consequences of a future great (Mw = 8.0+) Alpine Fault earthquake, South Island, New Zealand. Nat. Hazards Earth Syst. Sci., 13, 2279–2299.

Rodriguez-Iturbe I, Valdes JB 1979. The geomorphological structure of hydrologic response. Water Resources Res. 15(6):1409-1420.

Rosenfeld CL 1994. The geomorphological dimensions of natural disasters. Geomorphology 10: 27–36.

Rouse HL 2001. Natural Hazard Identification and Emergency Management: Strategic Directions 2001-2003. WCRC Internal Report, Greymouth. 44p.

Saghafian B, van Lieshout AM, Rajaei HM 2000. Distributed catchment simulation using a raster GIS. International Journal of Applied Earth Observation and Geoinformation 2(3-4): 199-203.

Scheidegger AE 1994. Hazards: singularities in geomorphic systems. Geomorphology 10: 19– 25.

Shroder JF, Bishop MP 2004. Mountain geomorphic systems. In: Bishop MP ed. Geographic Information Science and Mountain Geomorphology. Praxis Scientific Publishing, Chichester, UK, pp. 33 – 66.

Slaymaker O 2010. Mountain hazards. In: Alcantara-Ayala I, Goudie A ed. Geomorphological hazards and disaster prevention. Cambridge, Cambridge University Press, 2010. pp. 33 - 44.

Summerfield MA 1989. Tectonic geomorphology: convergent plate boundaries, passive continental margins and supercontinent cycles. Progress in Physical Geography, Vol. 13, No. 3, 431-441.

Thouret J-C 2010. Volcanic hazards and risks: a geomorphological perspective. In: Alcantara-Ayala I, Goudie A ed. Geomorphological hazards and disaster prevention. Cambridge, Cambridge University Press, 2010. pp. 13 - 28.

Tippett JM, Kamp PJJ 1993. Dynamics of Pacific Plate Crust in the South Island (New Zealand) Zone of Oblique Continent-Continent Convergence. Journal of Geophysical Research, Vol. 98, No B9, p. 16,105-16,118.

Tippett JM, Hovius N 2000. Geodynamic processes in the Southern Alps, New Zealand. In: Summerfield MA ed. Geomorphology and Global Tectonics. John Wiley, Hoboken, N. J. pp. 109– 134.

UNISDR 2013. From Shared Risk to Shared Value –The Business Case for Disaster Risk Reduction. Global Assessment Report on Disaster Risk Reduction. Geneva, Switzerland: United Nations Office for Disaster Risk Reduction (UNISDR).

Van Westen CJ 2010. GIS for the assessment of risk from geomorphological hazards. In: Alcantara-Ayala I, Goudie A ed. Geomorphological hazards and disaster prevention. Cambridge, Cambridge University Press, 2010. pp. 205 - 218.

Wadge G, Wislocki AP, Pearson EJ 1993. Spatial analysis in GIS for natural hazard assessment. In Goodchild M F, Parks B O, Steyaert L T (eds) Environmental Modeling with GIS. New York, Oxford University Press: 332–8.

Walker H, McGraw M 2010. Geomorphology and disaster prevention. In: Geomorphological hazards and disaster prevention in (eds) I. Alcantara-Ayala and A. Goudie. Cambridge : Cambridge University Press, 2010. pp. 129 - 142.

Wallace LM, Beavan RJ, McCaffrey R, Berryman K, Denys P 2007. Balancing the plate motion budget in the South Island, New Zealand using GPS, geological and seismological data. Geophysical Journal International 168, 332-352.

Wellman HW, Willett RW 1942. The geology of the West Coast from Abut Head to Milford Sound – Part 1. Transactions of the Royal Society of New Zealand 71(4): 282-306.

Wells A, Yetton MD, Duncan RP, Stewart GH 1999. Prehistoric dates of the most recent Alpine fault earthquakes, New Zealand: Geology, v. 27, p. 995–998.

Wells A, Goff J 2007. Coastal dunes in Westland, New Zealand, provide a record of paleoseismic activity on the Alpine fault: Geology, v. 35, p. 731–734, doi:10.1130/G23554A.1.

White GF, Calef WC, Hudson JW, Mayer HM, Sheaffer JR, Volk DJ. 1958. Changes in human occupance of flood plains in the United States. Dept. of Geogr. Res. Paper #57. Univ. Chicago Press, Chicago, 235 pp.

White GF 1974. Natural hazards research: concepts, methods and policy implications. In: G.F. White (Editor), Natural Hazards: Local, National, Global. Oxford Univ. Press, New York, pp. 3-16.

Whitehouse IE 1983. Distribution of large rock avalanche deposits in the central Southern Alps, New Zealand. New Zealand Journal of Geology and Geophysics 26: 272-279.

Whitehouse IE, Griffiths GA 1983. Frequency and Hazard of Large Rock Avalanches in the Central Southern Alps, New Zealand. Geology, Vol. 11, pp 331-334.

Wohl E, Oguchi T 2004. GIS and mountain hazards. In, M.P. Bishop, ed., Geographic Information Science and Mountain Geomorphology. Praxis Scientific Publishing, Chichester, UK, pp. 309-341.

Wright CA 1999. The AD 930 long-runout Round Top debris avalanche, Westland, New Zealand. New Zealand Journal of Geology and Geophysics 41: 493–497.

Yetton MD 2000. The probability and consequences of the next Alpine Fault earthquake, South Island, New Zealand. Unpublished Ph.D. thesis, Christchurch, New Zealand, University of Canterbury, 312 p.

Chapter 2: Regional geomorphic analysis

2.1 Introduction

Geomorphic hazards such as earthquakes, landslides, soil erosion and floods are not randomly distributed across the planet; instead they are concentrated in specific regions. These regions frequently coincide with plate boundaries that delineate tectonically active environments. The Southern Alps of New Zealand's South Island are the topographic expression of the active oblique continental convergence of the Australian and Pacific plates. The western side of the mountain range is subject to tectonic and climatic forcing expressed through high rates of uplift, erosion, orographically-enhanced precipitation and seismicity (Korup 2005a). These processes create a highly dynamic open geomorphic system that makes the transitional geomorphology between the mountains and plains potentially hazardous to the increasing human developments and land-uses in the region. Contemporary research on mountain hazard and risk assessment (Bell & Glade 2004; Glade & von Elverfeldt 2005; Kappes et al. 2010) argues that independent assessments of single processes might lead to a misjudgement of the real hazard potential in highly dynamic landscapes, as the possible interactions between geomorphic processes, and their cascade effects, are often neglected. Therefore, approaches incorporating the interdependence of geomorphic processes are necessary in order to effectively mitigate risk in highly dynamic mountainous environments. A key prerequisite of such approaches is identifying the dominant geomorphic processes, their spatial and temporal distribution as well as understanding how they interact.

2.1.1 Geomorphic processes and hazard assessment

Although widely used terms such as natural, geological, geophysical and hydro-meteorological hazards are quite clearly defined within international literature the concept of geomorphological / geomorphic hazard remains ipoorly-defined (Alcantara – Ayala 2010). Different conceptual terms have been proposed in literature to define the term geomorphic hazard. Schumm (1988) describes as geomorphic hazard any landform or landscape change that adversely affects the geomorphic stability of a site. According to Gares (1994) geomorphic hazards must be regarded as a group of threats to human resources arising from landform response to surface processes. Panizza (1996) defines geomorphological hazards as the probability that the economic and social consequences of a particular phenomenon reflecting geomorphic instability will exceed a certain threshold. Rosenfeld (2004) discussing geomorphological hazards states that "*Hazards exist when landscape developing*

processes conflict with human activity, often with catastrophic results." (p. 423). However, despite the apparent differences in their definitions, all the above authors stress the importance of landscape change and its potential impact on human activity. Thus, it is clear that if there are no people affected, there is no *hazard* and if the landform or landscape is unchanged there is no *geomorphic* hazard (Slaymaker 2010). While the landscape change is an ongoing natural process, the rapid expansion of human communities and infrastructure worldwide has led to equally rapid development of land, forcing people to increasingly occupy tectonically active and highly dynamic environments. This stresses the need for better understanding of the geomorphic processes underlying the landscape evolution of tectonically active mountains, with their inter-dependent effects as well as their interaction with the human system.

The significant practical contribution of geomorphology to hazards research has been discussed in several studies such as those of Baker (1994), Evans & Clague (1994), Gares at al. (1994), Rosenfeld (1994), Scheidegger (1994) and Alcantara – Ayala (2002, 2010). Tectonic geomorphology, in particular, has played a significant role in the understanding of the links between tectonics, climate and surface processes (erosional - depositional) controlling the landscape evolution of mountains and has been recognized for its contribution to paleoseismology and earthquake hazard assessment (Bull & McFadden 1977; Burbank & Anderson 2001; Harkins et al. 2005; Bull 2007). As it is mainly concerned with active tectonic processes, including earthquakes resulting from faulting, tectonic geomorphology provides the means to estimate the recurrence intervals between seismic events and identify the faults responsible for major earthquake hazards (Hancock & Skinner, 2000). Bull (2007) argues that the landscape evolution in tectonic settings with different uplift rates generates distinct landforms that can be used as a reconnaissance tool in assessing regional earthquake hazards, highlighting the strong relationship between geomorphology and hazards research. Nevertheless, Alcántara-Ayala (2002), by analysing a list of major geomorphology-related natural disasters of the world for the period 1900-1999, investigates the role of geomorphology in the prevention of natural disasters in developing countries and argues that "...*despite the innumerable works related to natural hazards that have represented the significance of geomorphology to the natural disaster field, little has been done to associate geomorphology and natural disasters directly*." (p.114). This statement clearly raises the issue that while an increasing number of studies explores the natural processes which generate and modify landforms, providing substantial knowledge about the landscape evolution and geomorphology, few efforts have in fact been made to integrate research findings about the geomorphic processes into disaster management planning and decision making. This thesis makes such an attempt.

2.1.2 The western Southern Alps of New Zealand

The study area is located in the West Coast of New Zealand's South Island and it is bounded by the Tasman Sea to the NW and the Main Divide of the Southern Alps to the SE. The major tectonic structure in the region is the Alpine fault which delineates the active boundary of a dextral transpressional continent–continent collision between the Indo-Australian and Pacific Plates with a total rate of plate convergence of approximately 40 - 50 mm yr^{-1} (Wallace et al. 2007; DeMets et al. 2010). As a result of this oblique continental collision rapid uplift rates of the order of 10mm y^{-1} (Norris & Cooper 2000) and extreme precipitation (~ 10,000 mm y^{-1}) have formed the Southern Alps, an approximately 450 km linear mountain range, extending along much of the length of the Alpine Fault.

Previous research on the landscape evolution of the Southern Alps has made a significant contribution in identifying the dominant geomorphic processes and landforms in the region. Adams (1980) comparing uplift rates with sediment load carried by major rivers in Southern Alps, pointed out that the rugged landscape of the Southern Alps is the result from the combined action of runoff, fluvial erosion and uplift, and suggested that the mountain range is in steady state (erosion rates equal uplift rates). According to Whitehouse (1988) the geomorphology of the Southern Alps reflects the interaction of uplift, produced by the plate collision, rapid erosion as a result of the heavy orographic precipitation and the degree of preservation of the Pleistocene glacial landforms. He also divided the mountain range into three distinct geomorphological regions: the western, dominated by steep, fluvially-dissected, almost rectilinear slopes covered by a thin regolith creating V-shaped valleys with very steep river gradients; the axial, which delineates the region of highest elevation and relief characterized by the presence of glacially-eroded bedrock forms with frequent rockfalls and rock avalanches; and the eastern, a region with significant depositional features and generally older landforms. He identifies as dominant erosion processes as fluvial processes, debris flows and rock falls / avalanching. Koons (1989, 1990) investigating the relationship between tectonic uplift and erosion through numerical modelling, described the Southern Alps as an asymmetric orogenic wedge with rapid uplift and erosion on the western side. Research on regional relief characteristics and denudation patterns of the western Southern Alps by Korup et al. (2005) identified as dominant geomorphic processes fluvial processes in low-altitude valleys, surface runoff and frequent landsliding on hillslopes, "relief dampening" by glaciers, and rock falls or avalanches on steep high slopes. Further, Herman & Braun (2006) recognized strong orographic precipitation combined with extreme rates of tectonic uplift as the processes that dominate the development and evolution of a mixed glacial-fluvial landscape on the western side of the Southern Alps. Hovius et al. (1997)

described the western side of the mountain range as a landscape characterized by dissected, rectilinear slopes, frequently steeper than 45^{o} with thin regolith cover (<1m), and identified high-magnitude low-frequency landslide events as the dominant erosion process controlling landscape evolution. Other important studies (Korup 2006b; Hewitt et al. 2008; Korup et al. 2009) have also recognized the contribution of large-scale landslides in shaping the mountain range, their role as the major sources of sediment in the area (Whitehouse 1983; Korup et al. 2004; 2005b) as well as their impact on drainage network and in developing distinct landforms (Korup O 2005a, Hewitt 2006). Landslide dams have also been identified as the dominant persistent geomorphic imprints of bedrock landslides in the region, often affecting the behaviour of the drainage networks and inducing other geomorphic processes / hazards such as outburst floods, backwater ponding, river aggradation, channel instability and debris flows (Korup 2005a; 2005c; 2006a; Korup et al. 2006). More recently, Shulmeister et al. (2009) suggested a link between rock avalanches and glacier behaviour by discovering evidence for the landslide origin of terminal moraines. They found that rock avalanches are the source of much of the debris that forms glacial moraines in active mountains, while Tovar et al. (2008) state that landslides of the magnitude required to form the Waiho Loop moraine (>10^{8} m^{3}) are recorded by similar deposits in several parts of the Southern Alps and are probably associated with the intense seismicity of the area (M8 earthquakes). All the above studies clearly illustrate a highly dynamic environment shaped by various interrelated geomorphic processes. However, relatively few studies directly associate findings on landscape evolution and geomorphic processes in WSA with various types of hazards (Zarn & Davies 1994; McSaveney & Davies 1998; Korup 2005c; Davies & McSaveney 2006; Welsh & Davies 2011; Robinson & Davies 2013).

In this study, widely-applied methodologies and techniques of quantitative geomorphology with well-established theoretical backgrounds are used to identify the dominant geomorphic processes, their spatial distribution and inter-dependent effects, and explore their implications in hazard assessment and modelling. The main focus is on the drainage network as it is directly linked to tectonic forcing and therefore contains potentially useful information on differential rock uplift rates across the landscape as well as, reflecting critical relationships between tectonic, climatic and surface processes (Wobus et al. 2006; Tucker & Bras 1998).

2.2 Methodology

In recent years a growing body of literature has investigated the interactions between climate, surface processes and tectonics and their role in the landscape evolution of mountains (Koons 1989;

Molnar & England 1990; Beaumont et al. 1992, 2001; Willett 1999; Wobus 2003). The availability of high-quality digital topographic data, GIS and remote sensing has significantly improved the capability of quantitative geomorphology techniques allowing the statistical analysis and comparison of different terrain types at multiple scales (Burrough & McDonnell 1998; Wood 1996; Bishop & Shroder 2004). Various morphometric indices and techniques have been proposed to quantitatively describe landforms (Horton 1945; Strahler 1952, 1964; Schumm 1956; Hack 1973), identify geomorphic processes (Church & Mark 1980; Moore et al. 1991; Willgoose & Hancock 1998; Verstraeten & Poesen 2001; Wilford et al. 2004) and deduce rates of current and past tectonic activity directly from topography (Bull & McFadden 1977; Kirby & Whipple 2001; Frankel & Pazzaglia 2006; Bull 2007; Pelletier 2008; Burbank & Anderson 2012). Nevertheless, any results that derive from such techniques based on digital terrain analysis should be interpreted with caution as they may be strongly dependent on the scale of the DEM (Wolock & Price 1994; Schneider 2001, Jamieson et al 2004).

In this study we focus on the central western Southern Alps and particularly at the region between the Hokitika and Haast Rivers. Topographic and morphometric data from 22 catchments with areas between 11 and 1313 km^2, that drain the western side of the mountain range, were extracted using a 25m DEM. Different techniques of quantitative geomorphology in GIS environment have been employed to analyse the drainage network, catchment morphometry, stream longitudinal profiles and valley topography in order to identify the dominant geomorphic processes, their spatial distribution and their interdependencies. The premise of this analysis is that the form of the landscape and its morphometric patterns are driven by complex and interrelated processes taking place over a range of spatial and temporal scales (Walsh et al. 1998). The analysis has been carried out at regional scale (1:50000).

2.2.1 Data

For this study a 25 m DEM developed by Landcare Research in 2002 was used. The DEM was generated from 20 m contours and spot heights supplied by Land Information New Zealand (LINZ). Comparison with a very high resolution LIDAR-derived DEM (2m) indicated that the spatial accuracy of the DEM varies between different landforms (lakes, river channels, riverbeds, floodplains etc.) and the areas of greatest errors are predominantly confined to valley floors (Barringer et al. 2002). However, with overall RMS error of 8.15 m the DEM meets the internationally-accepted accuracy standards as set out by US Geological Survey (USGS, 1997) and is of sufficient quality for regional - scale studies such as the present one.

Drainage network is a fundamental landscape feature, controlled by lithology, tectonic, climatic and surface processes. Therefore accurate representation of the study area's drainage network is a prerequisite in quantitative geomorphic analyses. Direct delineation of streams using the 25m DEM resulted in a very poor representation of the existing drainage patterns, especially in the floodplains NW of the Alpine Fault. According to Barringer et al. (2002) the primary objective of Landcare Research's DEM was absolute elevation correctness and speed of interpolation rather than hydrological correctness and slope continuity. To overcome this limitation the surface elevation of the DEM was adjusted to be consistent with the drainage network from the topographic maps (1:50000) by implementing the DEM reconditioning method AGREE (Hellweger 1997). The DEM processing and reconditioning were performed using the ArcHydro tools 9 (v1.4) in ArcGIS 9.3 environment (Fig. 2.1).

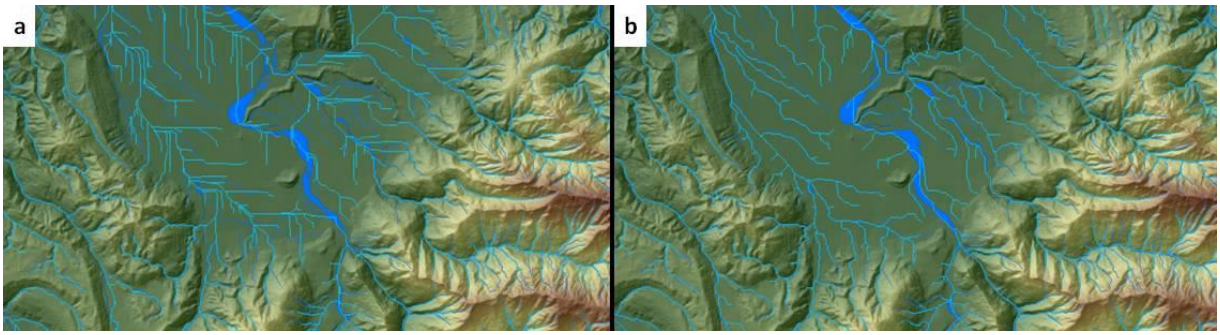

Figure 2.1 a) Mismatch between the drainage networks from the topographic maps 1:50000 and the DEM b) After the implementation of AGREE method there is a distinct improvement on the representation of the drainage network.

2.2.2 Regional drainage network analysis

On the western side of the Southern Alps, the major catchments are short (catchment lengths range from 10 to 44 km) and have been developed sub-perpendicular to the Main Divide with dendritic drainage network patterns and closely spaced interfluves (Fig. 2.2). Near the divide, due to the region's humid maritime climate and the orientation of the main axial range across the dominant Southern Hemisphere westerlies (Fitzharris et al. 1992), the catchments hold glaciers which flow westwards through steep valleys. In particular Waiho and Fox-Cook catchments, which are located at the central part of the western Southern Alps, have up to 20-25% of their total catchment areas covered by glaciers that reach low elevations of approximately 300m. The main tectonic structure in the region is the Alpine Fault which divides the study area into two distinct geological provinces. The underlying lithologies SE of the AF are predominately quartzo-feldspathic schist and semi-schist of the Torlesse composite terrane, whereas NW of the AF the metasedimentary rocks of the Buller terrane (Cooper 1989) with igneous intrusions (Cooper & Tulloch 1992; Mortimer et al. 1999) are

covered by Quaternary moraines and clastic sediments (consisting of unconsolidated gravels, sand and silt). Land cover at lower- and mid- altitudes mainly consists of indigenous forests, scrub and shrubland while floodplains are predominantly covered by grasslands. At higher altitudes common land cover types are tall tussock grasslands, lightly vegetated areas covered with alpine grass-/herbfields, bare gravel and rock areas as well as permanent snow and ice.

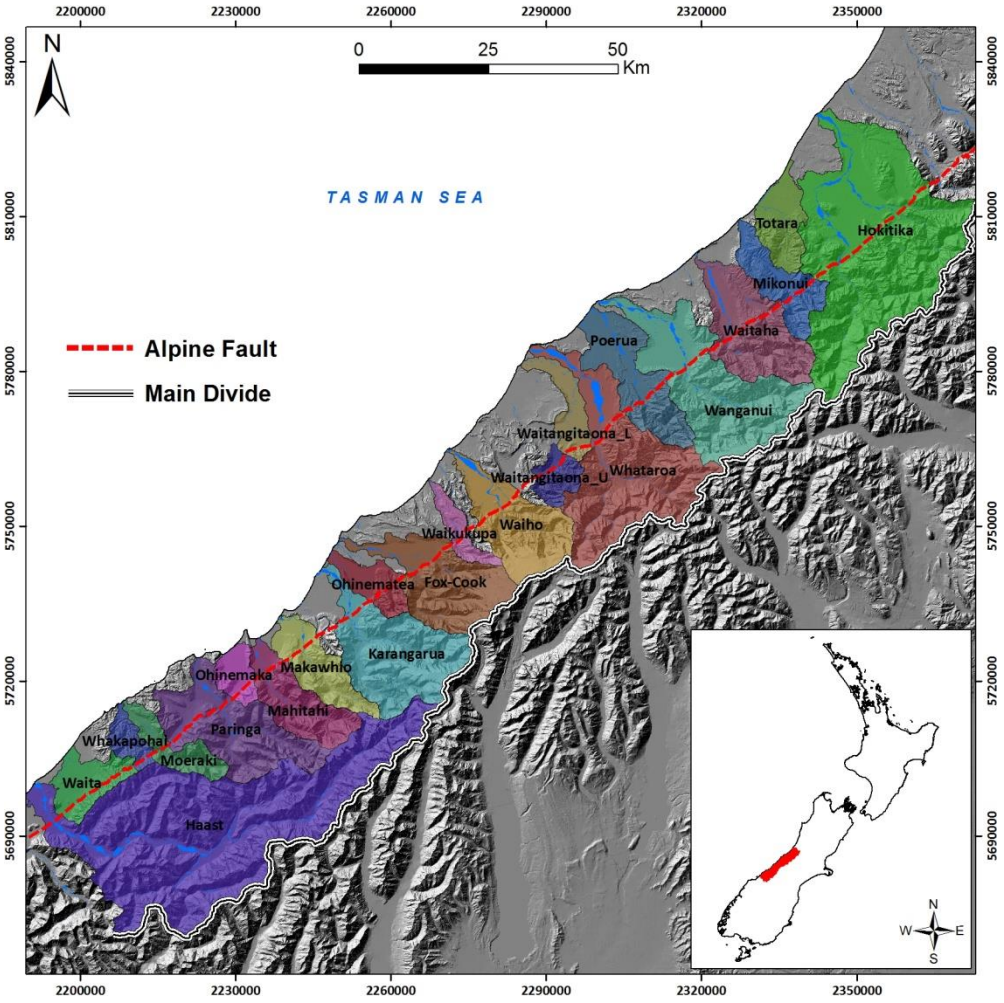

Figure 2.2 Major river catchments of WSA.

The investigation of catchment morphometry in mountainous environments has been found useful in the identification of dominating fluvial or debris-flow processes (Jackson et al. 1987; De Scally & Owens 2004; Wilford et al. 2004; Welsh & Davies 2011). The extraction of morphometric parameters for each major catchment was initially carried out in order to observe patterns in the structure of catchment topography in NE–SW direction driven by geomorphic processes. Morphometric characteristics of major drainage basins are given in Tables 2.1-2.3. Additionally, specific morphometric parameters were estimated considering only catchments east of the AF, in order to eliminate the effect of the flat and low-slope terrain of the floodplains in the analysis (Table 2.4).

Table 2.1 Morphometric characteristics (1) of major catchments in the western Southern Alps (WSA).

Catchment	Area (km^2)	Max Elevation (m)	Relief (m)	Mean Elevation (m)	Glacier area (km^2)	Glaciers %	Area % East of the AF	Glaciers Min Elevation (m)	Glaciers Mean Elevation (m)
Hokitika	1066	2600	2600	669	13.6	1.3	58.2	900	1856
Totara	135.6	1145	1145	233	-	-	-	-	-
Mikonui	157.8	2132	2132	662	0.3	0.2	37.7	1800	1942
Waitaha	315.6	2580	2580	780	8.1	2.6	57.1	1277	1870
Wanganui	521.3	2640	2639	846	48.0	9.2	68.3	1080	1924
Poerua	257.7	2440	2440	438	2	0.8	34.3	1230	1777
Whataroa	592.6	3100	3099	970	62.7	10.6	81.3	758	1839
Waitangitaona (lower)	102.5	1480	1480	108	-	-	7.8	-	-
Waitangitaona (upper)	73.9	2140	2053	824	1	1.4	77.9	1513	1837
Waiho	290.2	3093	3086	1034	73	25.2	72.6	370	2016
Waikukupa	65.7	2320	2317	652	3	4.6	42.8	1340	1941
Fox-Cook	323.6	3480	3480	1055	69.9	21.6	75.2	280	2034
Ohinematea	96.8	1955	1954	366	-	-	32.4	1790	1878
Karangarua	408.1	3120	3120	1039	39.3	9.6	92.1	951	1958
Makawhio	169.6	2380	2380	741	2.1	1.3	70.2	1053	1821
Mahitahi	197.4	2640	2640	816	7.3	3.7	85.8	1030	1894
Ohinemaka	70.7	1500	1499	239	-	-	18.5	-	-
Paringa	365.4	2620	2617	633	9.3	2.5	69.2	939	1850
Moeraki	106.7	1900	1898	561	-	-	60.3	1736	1763
Whakapohai	58.4	1283	1282	419	-	-	10.2	-	-
Waita	130.2	1319	1319	286	-	-	27	-	-
Haast	1354	2720	2720	950	55.7	4.1	97.6	596	1899

Table 2.2 Morphometric characteristics (2) of major catchments in the western Southern Alps (WSA).

Catchment	Order	Mean Rb	Mean RL	Mean Ra	Total stream length (km)	Total stream Number	Drainage Density	Stream Frequency
Hokitika	6	4.22	1.98	3.87	1655.1	1649	1.55	1.55
Totara	5	3.61	1.50	3.33	237.0	184	1.75	1.36
Mikonui	5	4.02	2.01	3.45	252.7	263	1.60	1.67
Waitaha	5	4.54	2.06	4.04	493.2	481	1.56	1.52
Wanganui	5	5.09	2.57	4.96	742.2	815	1.42	1.56
Poerua	5	4.39	1.92	4.30	392.5	337	1.52	1.31
Whataroa	6	3.92	1.96	3.56	798.8	908	1.35	1.53
Waitangitaona (upper)	4	4.72	2.02	4.15	107.4	129	1.45	1.74
Waiho	6	3.42	1.69	3.04	333.1	346	1.15	1.19
Waikukupa	4	4.69	4.00	5.74	88.6	88	1.35	1.34
Fox-Cook	5	4.32	2.29	4.33	395.0	426	1.22	1.32
Ohinematea	4	4.71	2.57	4.30	140.8	129	1.46	1.33
Karangarua	6	3.94	1.84	3.49	595.3	710	1.46	1.74
Makawhio	5	3.87	1.97	3.47	252.2	274	1.49	1.62
Mahitahi	5	4.28	1.89	3.75	286.3	325	1.45	1.65
Ohinemaka	5	3.16	1.38	2.87	104.2	112	1.47	1.58
Paringa	5	4.77	2.05	4.48	525.3	573	1.44	1.57
Moeraki	4	5.04	7.04	6.23	153.5	154	1.44	1.44
Whakapohai	4	4.60	2.14	3.71	84.2	84	1.44	1.44
Waita	5	3.63	1.49	3.42	203.7	189	1.56	1.45
Haast	6	4.71	2.30	4.37	1885.5	2066	1.39	1.53

Elevation in the central WSA ranges from 18 m (Haast) up to approximately 3480 m (Fox-Cook) between the Alpine fault and the main divide. The maximum elevation in the Southern Alps is located a few kilometres to the east of the main divide (Mt Cook; 3754 m). In several tectonically active mountain ranges the main divide separates regions of contrasting drainage patters and landforms as well as variable rock uplift and exhumation rates (e.g. Andes, Taiwan, Southern Alps of New Zealand). Migration of the divide through various possible mechanisms, the nature of which still remains unclear, has therefore the potential to significantly impact the evolution of drainage systems and affect rock uplift and exhumation patterns in an active orogen (Herman & Braun 2006). The main divide has a length of 312 km in the study area, with elevations between 564 m (Haast Pass) and 3480 m (Mt Tasman at Fox-Cook catchment) with a mean of 2115 m. Its distance to the Alpine fault is a minimum of approximately 14 km at the Fox-Cook and Waiho catchments (where

the highest mean elevations are observed) and a maximum of about 34 km at the Haast river catchment (where mean elevation values are the lowest).

Table 2.3 Morphometric characteristics (3) of major catchments in the western Southern Alps (WSA).

Catchment	Perimeter (km)	Elongation ratio	Length (km)	Relief ratio	Ruggedness number
Hokitika	274.6	0.94	39.1	0.066	4037
Totara	86.9	0.89	14.8	0.077	2002
Mikonui	107.2	0.55	25.7	0.083	3413
Waitaha	132.7	0.61	32.9	0.079	4031
Wanganui	205.1	0.67	38.6	0.068	3757
Poerua	136.1	0.57	31.9	0.077	3716
Whataroa	230.9	0.63	43.3	0.072	4178
Waitangitaona (upper)	59.3	0.98	9.9	0.208	2982
Waiho	123.8	0.62	30.8	0.100	3542
Waikukupa	75.0	0.43	21.5	0.108	3125
Fox-Cook	138.5	0.72	28.3	0.123	4249
Ohinematea	72.0	0.59	18.8	0.104	2843
Karangarua	150.2	0.67	33.9	0.092	4551
Makawhio	99.9	0.55	26.8	0.089	3541
Mahitahi	100.0	0.61	26.0	0.102	3829
Ohinemaka	52.0	0.85	11.1	0.135	2210
Paringa	161.2	0.76	28.4	0.092	3762
Moeraki	91.4	0.53	22.1	0.086	2730
Whakapohai	57.5	0.66	13.1	0.098	1847
Waita	87.1	1.00	12.8	0.103	2063
Haast	353.9	0.93	44.5	0.061	3788

The hypsometric curve describes the distribution of elevation in a given area and it is usually represented by plotting relative catchment area against relative height. The hypsometric integral (HI) provides a simple way to characterize the shape of the hypsometric curve and it is defined as the relative area below the curve. The shapes of hypsometric curves and the HI have been used to interpret landform age (Schumm 1956; Strahler 1952, 1964), to examine the hypsometry of glaciated landscapes (Brozovic et al. 1997; Brocklehurst & Whipple 2004), to infer lithologic, climatic, tectonic, or scale-dependent influences on basin geomorphometry (Willgoose & Hancock 1998) and to investigate changes in the relative importance of fluvial, glacial, and tectonic processes (Montgomery et al. 2001). Willgoose & Hancock (1998) classify high HI values (> 0.5) as indicative of catchments dominated by diffusive erosion processes (concave-down hypsometric curve) whereas lower HI values (< 0.5) represent fluvial dominated catchments (concave up hypsometric curve).

Table 2.4 Morphometric characteristics of catchments areas east of the Alpine fault.

Catchment	Area (km^2)	Min Elevation (m)	Max Elevation (m)	Relief (m)	Mean Elevation (m)	Mode Elevation (m)	Median Elevation (m)	Hypsometric Integral	Mean Slope (deg.)	Mode Slope (deg.)	Relief ratio
Hokitika	620.5	79	2600	2521	1031	1100	1030	0.378	32	38	0.118
Mikonui	59.5	220	2130	1910	1101	1100	1087	0.461	36	38	0.232
Waitaha	180.1	119	2580	2461	1171	1060	1180	0.427	33	38	0.156
Wanganui	356	88	2640	2552	1175	1120	1180	0.426	32	38	0.117
Poerua	88.3	120	2440	2320	1070	1200	1070	0.409	36	38	0.183
Whataroa	481.9	87	3100	3013	1178	1480	1200	0.362	33	38	0.129
Waitangitaona (upper)	57.6	136	2140	2004	996	1160	1020	0.429	36	38	0.289
Waiho	210.5	140	3093	2953	1376	1080	1380	0.418	32	38	0.186
Waikukupa	28.1	219	2320	2101	1168	1180	1180	0.451	34	38	0.230
Fox-Cook	243.4	117	3480	3363	1361	1300	1300	0.370	31	38	0.207
Ohinematea	31.4	120	1955	1835	913	480	920	0.432	33	38	0.307
Karangarua	375.9	37	3100	3063	1124	1100	1120	0.355	32	38	0.126
Makawhio	119.1	37	2380	2343	1012	1200	1030	0.416	33	38	0.118
Mahitahi	169.4	37	2640	2603	940	1000	920	0.347	32	38	0.133
Ohinemaka	13.1	64	1500	1436	651	1120	640	0.409	31	38	0.423
Paringa	252.9	38	2620	2582	830	59	800	0.307	30	38	0.121
Moeraki	64.3	60	1900	1840	778	219	780	0.390	30	38	0.159
Whakapohai	6	444	1283	839	894	1060	900	0.537	29	38	0.489
Waita	35.2	20	1319	1299	660	620	680	0.493	29	38	0.350
Haast	1321	18	2720	2702	972	1100	970	0.353	30	38	0.080

The HI values for major catchments in the study area are between 0.3 and 0.54 demonstrating an inverse correlation with catchment area and therefore scale dependence. Korup et al. (2005) observed that hypsometric curves of presently strongly-glaciated basins in the WSA (e.g. Waiho, Fox) show a distinct convexity, which however is similar to some of the larger basins dominated by fluvial processes (e.g. Waitaha, Wanganui) concluding that the HI values cannot be used to distinguish between glacial or fluvial processes in the region without additional information.

The ratio between catchment total relief and length (measured as the longest dimension of the catchment parallel to the main stream channel; Strahler 1964), known as relief ratio (Rh), represents the overall steepness of a drainage basin (Schumm 1956). A high relief ratio corresponds to a more pronounced topography and thus can be used as an indicator of erosion intensity (Verstraeten & Poesen, 2001). Relief ratio values range from 6×10^{-2} at the Haast catchment up to 0.2 at the upper Waitangitaona catchment. In the study area, catchments with higher denudation rates (as estimated by Hovius et al. 1997) generally, demonstrate somewhat higher R_h values (when R_h is estimated for catchments east of the AF) (Fig. 2.3). R_h also shows an inverse correlation with catchment area and thus is scale dependent.

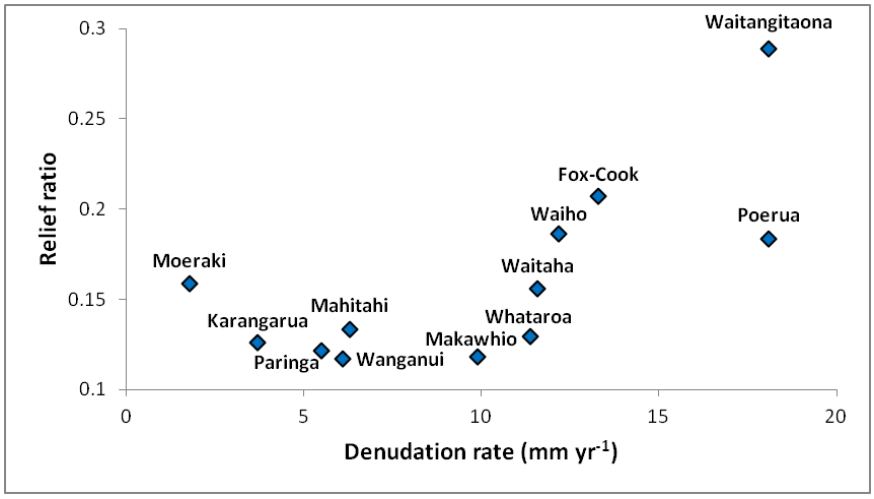

Figure 2.3 Relief ratio compared with denudation rates from Hovius et al. (1997). Relief ratio was estimated for catchments east of the Alpine Fault.

The ruggedness number (Rn) originally defined by Strahler (1952) as the product of drainage density and relief is a dimensionless number to describe the intrinsic structural complexity of catchment topography. Different forms of ruggedness number have been proposed (Schumm 1956, Melton 1957) as indicators of catchment dynamics as well as to identify the dominant geomorphic processes in the context of hazard studies (Wilford et al. 2004; Welsh 2008; Welsh & Davies 2011). The underlying assumption is that as the topography becomes more complex the associated increased ruggedness number reflects the incidence and intensity of geomorphic processes and consequent

hazards. In WSA it was observed that catchments with high ruggedness numbers (> 3500) such as Waitaha, Wanganui, Whataroa, Waiho, Fox-Cook and Karangarua have also high sediment discharges (> 10^6 m^3 yr^{-1}; Hovius et al. 1997) whereas Moeraki with a lower Rn = 2730 has also a low sediment discharge of 12 x 10^4 m^3 yr^{-1} (Fig. 2.4).

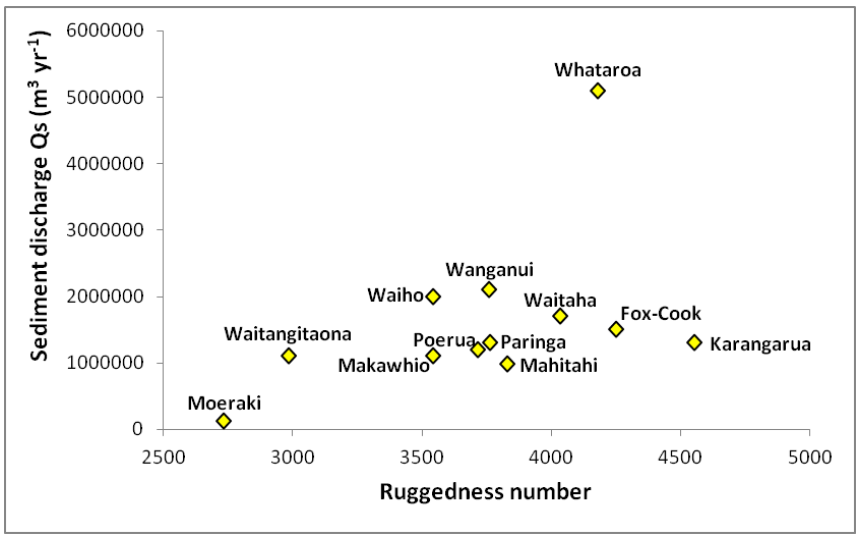

Figure 2.4 Ruggedness number and sediment discharge from Hovius et al. (1997)

Elongation ratio (ER) is a commonly-applied morphometric index that describes catchment shape. It is calculated by normalizing the diameter of a circle with same area as the catchment by the catchment length (Schumm 1956). As the elongation ratio approaches 1 the shape of the drainage basin approaches circular. The elongation ratio has important hydrological implications because, in contrast to more elongated catchments, circular and semi-circular catchments produce narrow, high peak hydrographs as the runoff from the most distant parts of the drainage area generally arrives at the outlet faster (low time of concentration). Most of the catchments in the study area are elongated with ratios < 0.7. More circular-shaped catchments with elongation ratios > 0.8 are those of Hokitika, Totara, Waitangitaona, Ohinemaka, Waita and Haast rivers.

Drainage density (Dd), introduced by Horton (1945) as the total length of all the streams channels in a drainage basin divided by the total catchment area, is a widely applied measure of how well a catchment is drained by its drainage network or how dissected the landscape is by its stream channels, thus it reflects both the tendency of the drainage basin to generate surface runoff and the erodibility of the surface materials. Dd is influenced by climate, lithology, relief, soil characteristics, land cover and land use as well as the stage of drainage network development (Slaymaker 2010). A wide range of drainage density values has been reported in literature from very high (e.g. 968 km^{-1} in the badlands of Perth Amboy, New Jersey; Schumm 1956) to <1 on un-dissected plateaus (Slaymaker 2010). Drainage density in the western side of the Southern Alps was estimated between 1.15 km^{-1}

(Waiho) and 1.75 km^{-1} (Totara) with a regional mean value of 1.45 km^{-1}. The relatively low regional value and the fact that the lowest values 1.15 km^{-1} and 1.22 km^{-1} are observed in the central section where relief is higher, are consistent with findings from previous studies (Kirkby 1980, 1993; Oguchi 1997; Tucker & Brass 1998) which have argued that under a humid climate drainage density demonstrates an inverse correlation with relief. Furthermore, Brocklehurst & Whipple (2007) investigating the response of glaciated landscapes to rapid rock uplift, also argued that replacement of valley floors by steep hillslopes allows headwalls to grow and causes drainage density to decrease.

In NE-SW direction mean catchment slope varies from 29^{o} to 36^{o} with an average regional value of 32^{o}.The most frequent slope in the study area is 38^{o}. Of course, as discussed by Finlayson and Montgomery (2003) and Korup et al. (2005), given the resolution of the DEM, it is likely that these slope values are underestimates of real values. Various authors have suggested that hillslopes in rapidly-uplifted landscapes respond to river incision into bedrock by steepening to a maximum stable or threshold angle and have observed that landslide erosion rates increase nonlinearly as hillslope angles approach the threshold value (Burbank et al. 1996; Montgomery 2001; Montgomery & Brandon 2002; Larsen & Montgomery 2012). To test the above hypothesis in the study area a reclassified slope grid (class interval 5^{o}) was overlaid with a landslide inventory (Fig. 2.5). The uniform mode slope angle and the fact that most landslides are observed between 35^{o}-40^{o} suggest a regional threshold slope angle of $38^{0}\pm2^{0}$ (Fig. 2.6).

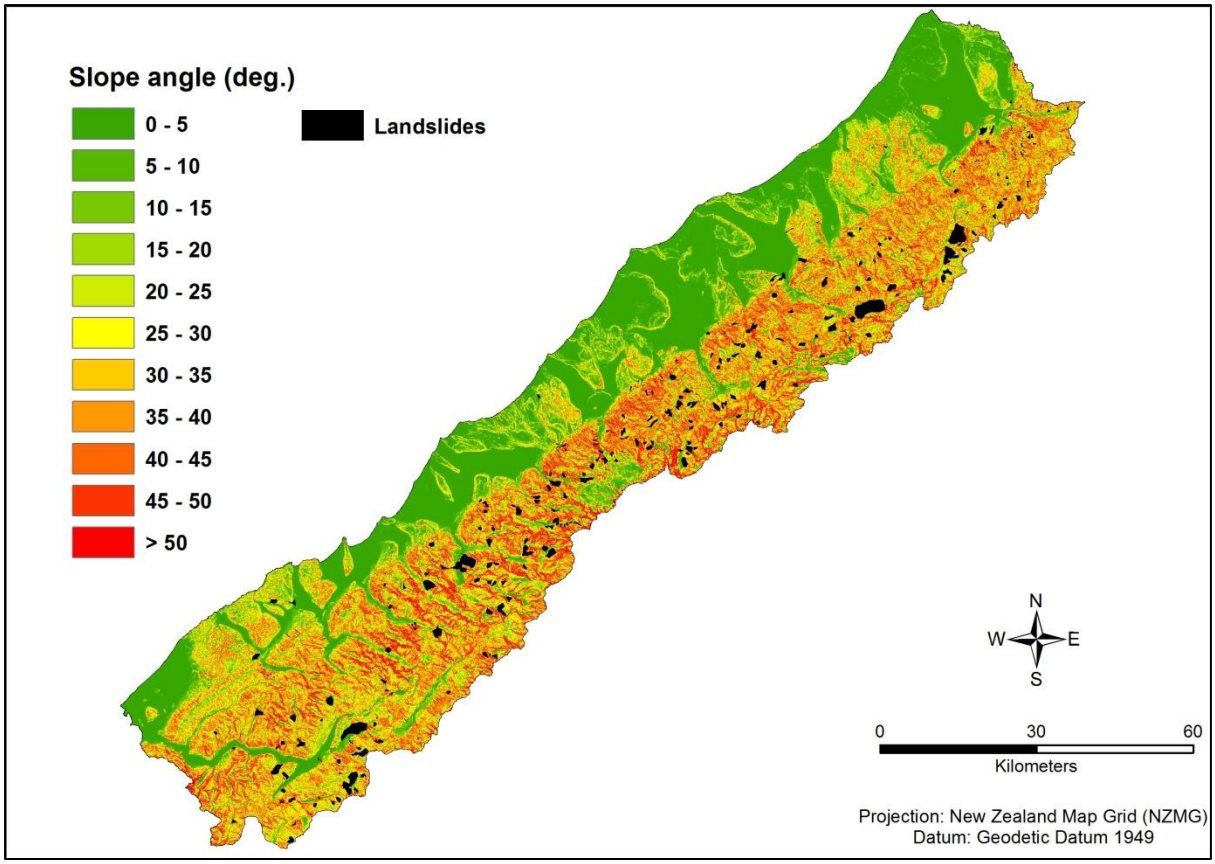

Figure 2.5 Slope gradient and landslides in the study area. The landslide polygons were extracted from QMAP, NZ Land Cover Database, England (2011) and Google Earth (see chapter 3, section 3.3.1).

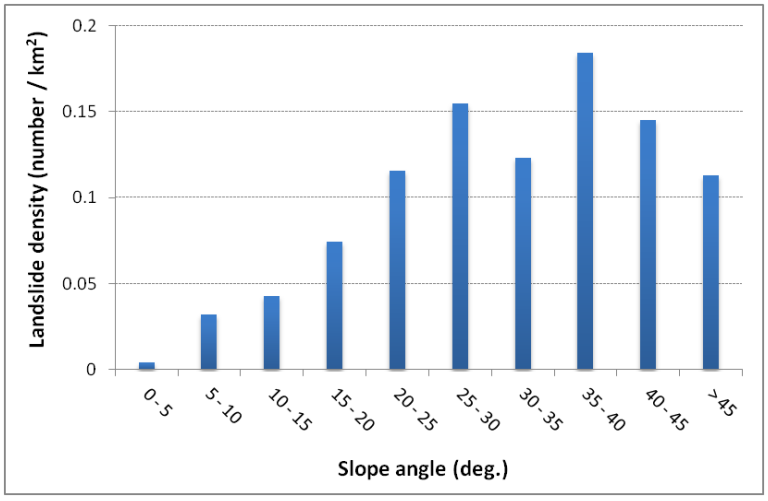

Figure 2.6 Slope angle (5° class interval) and corresponding landslide density.

Strahler (1952) by modifying Horton's (1945) method proposed an approach to define the relative stream size based on the hierarchy of its tributaries, known as the Strahler stream order. The stream order is essentially a measure of the degree of stream branching within a catchment. Each segment

of channel network is indicated by its order (1st order, 2nd order, etc.). A first-order stream is an unbranched tributary, a second-order stream is a tributary formed by two or more first-order streams. A third-order stream is a tributary formed by two or more second-order streams and so on. In general, an nth order stream is a tributary formed by two or more streams of order (n-1) and streams of lower order. Ultimately the order of the entire watershed is defined by the order of its main channel. Figure 2.7 shows part of the drainage network classified in stream orders. Based on the concept of stream order other morphometric parameters such as the bifurcation, length and area ratios can be estimated. The bifurcation ratio (R_b) is defined as the ratio of the number of streams (N) of any order (i) to the number of streams of the next highest order and it is calculated as:

$$R_b = \frac{N_i}{N_{i+1}} \tag{2.1}$$

From this, Horton (1945) developed two statistical relationships known as the "*Law of Stream Numbers*" which relates the number of streams of order i (Ni) to the bifurcation ratio and the principal stream order (u):

$$N_i = R_b^{u-1} \tag{2.2}$$

and the "*Law of Stream Lengths*", in which the average lengths of the streams (L) of successive orders are related by a length ratio R_L:

$$R_L = \frac{L_{i+1}}{L_i} \tag{2.3}$$

$$L_i = L_1 \, \mathrm{r_L^{i-1}} \tag{2.4}$$

Following a similar rationale, Schumm (1956) proposed the "*Law of Stream Areas*" to relate the average areas (A_i) drained by streams of successive order:

$$R_A = \frac{A_{i+1}}{A_i} \tag{2.5}$$

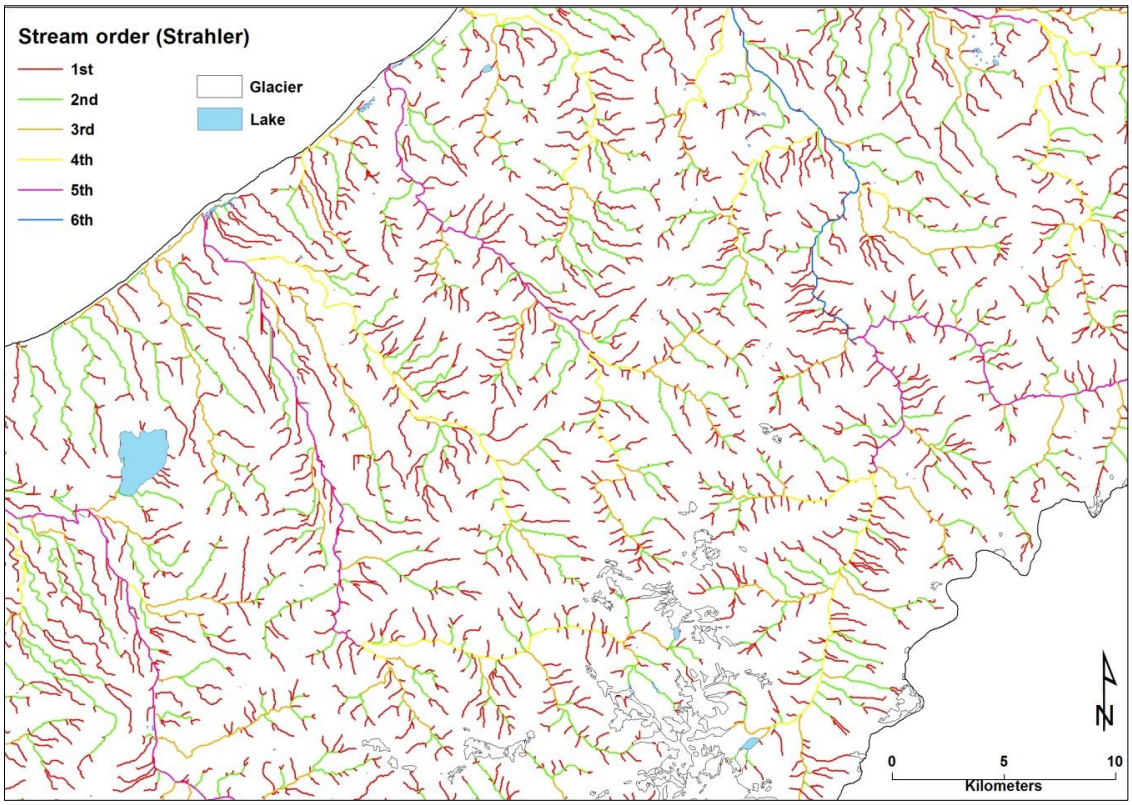

Figure 2.7 Stream orders calculated using ArcGIS 9.3; based on the stream ordering method proposed by Strahler (1952). Stream order increases when streams of the same order intersect.

Systematic deviations from the above statistical relationships might be indicative of tectonic, climatic and surface processes that affect the drainage patterns. Negative deviations from the law of stream numbers were recorded in the majority of the catchments, indicating that the observed streams are fewer than those predicted from Horton's statistical relationship. In contrast, positive deviations from the predicted stream lengths and catchment areas are systematically observed along the range front (Appendix 1; Table A1.1). The glacier cover and the frequent landsliding on the steep slopes of WSA impede channel formation particularly close to the headwaters. On the other hand, the high runoff due to the extremely high orographically-enhanced precipitation, impermeable lithologies and low stream frequency contribute to increasing the length of the existing channels. Furthermore the low drainage frequency forces the existing stream channels to drain larger catchment areas providing a possible explanation for the positive deviations from the predicted catchment areas per stream order.

2.2.3 Stream longitudinal profile analysis

In a variety of natural environments previous research (Hack 1973; Flint 1974; Howard & Kerby 1983) has illustrated that stream channels generally exhibit power-law scaling between local channel gradient and contributing catchment area:

$$S = k_s A^{-\theta} \quad (2.6)$$

where k_s is known as steepness index and θ is channel concavity. Sklar & Dietrich (1998) and Wobus et al., (2006) point out that the above equation applies only for catchment areas above a critical threshold (Acr) that delimits the transition between debris-flow to fluvial processes. Several studies have investigated the response of rivers to changes in rock uplift rate (U) (Kobor & Roering 2004; Lague & Davy 2003; Snyder et al. 2000; Whipple 2004; Wobus et al. 2006; Whittacker et al. 2008). They have shown that, in general, the concavity index (θ) is insensitive to rock uplift rate, whereas the steepness index (k_s) (normalized by a regional reference concavity), demonstrates a positive correlation and can be used to quantify differential uplift and erosional rates. Nevertheless, although there is strong empirical support relating the steepness index to uplift rate, several other factors (e.g. climate, lithology, fluvial erosion, extent of alluvial cover etc) which are not incorporated in this simple equation also affect this relationship (Wobus et al. 2006). Therefore, the relationship between k_s and U is expected to vary depending on the geo-tectonic setting. Although stream profiles are generally assumed to exhibit a single slope-area scaling for their entire length, segments of an individual profile are often characterized by different values of k_s, θ or both. Based on these differences we can extract tectonic information from the channel profiles.

Initially, longitudinal profiles for the main channel in each catchment (following the direction of maximum flow accumulation) were extracted from the hydrologically-corrected 25m DEM by intersecting downstream flow length with 20 m interpolated contour intervals (Kirby et al. 2003; Korup 2006a). Longitudinal profiles of major rivers in the WSA (Fig. 2.8) range from concave to convex and stepped profiles (Fig. 2.9). Major knickpoints with discrete steps in channel elevation (> 25 m) were also extracted and analyzed. The selected knickpoints did not exhibit any consistency in their location relative to the AF or elevation. However they demonstrate spatial coincidence with landslide dam locations (Korup O 2006a) and faults (Fig. 2.10).

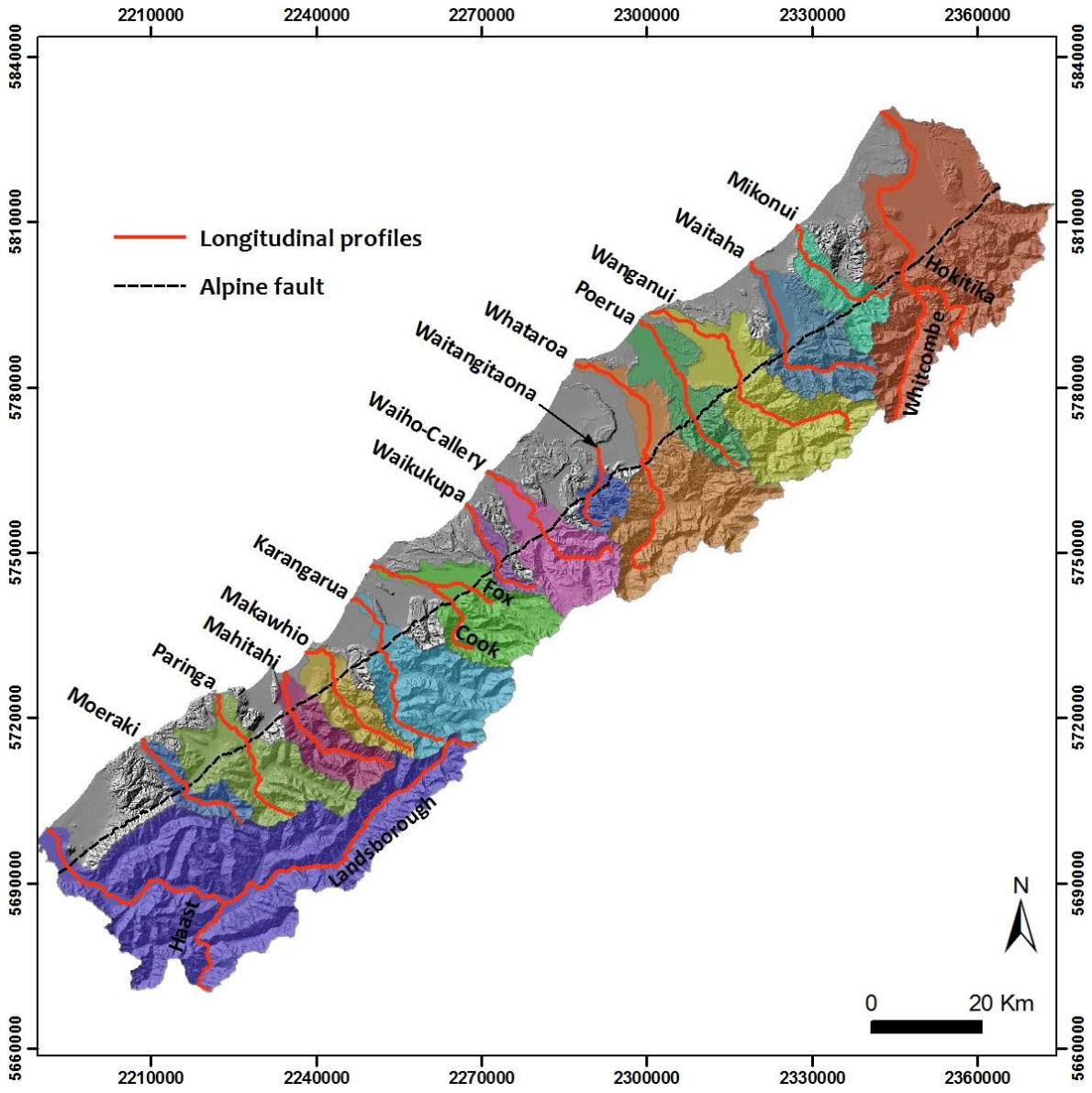

Figure 2.8 Longitudinal profiles of major rivers.

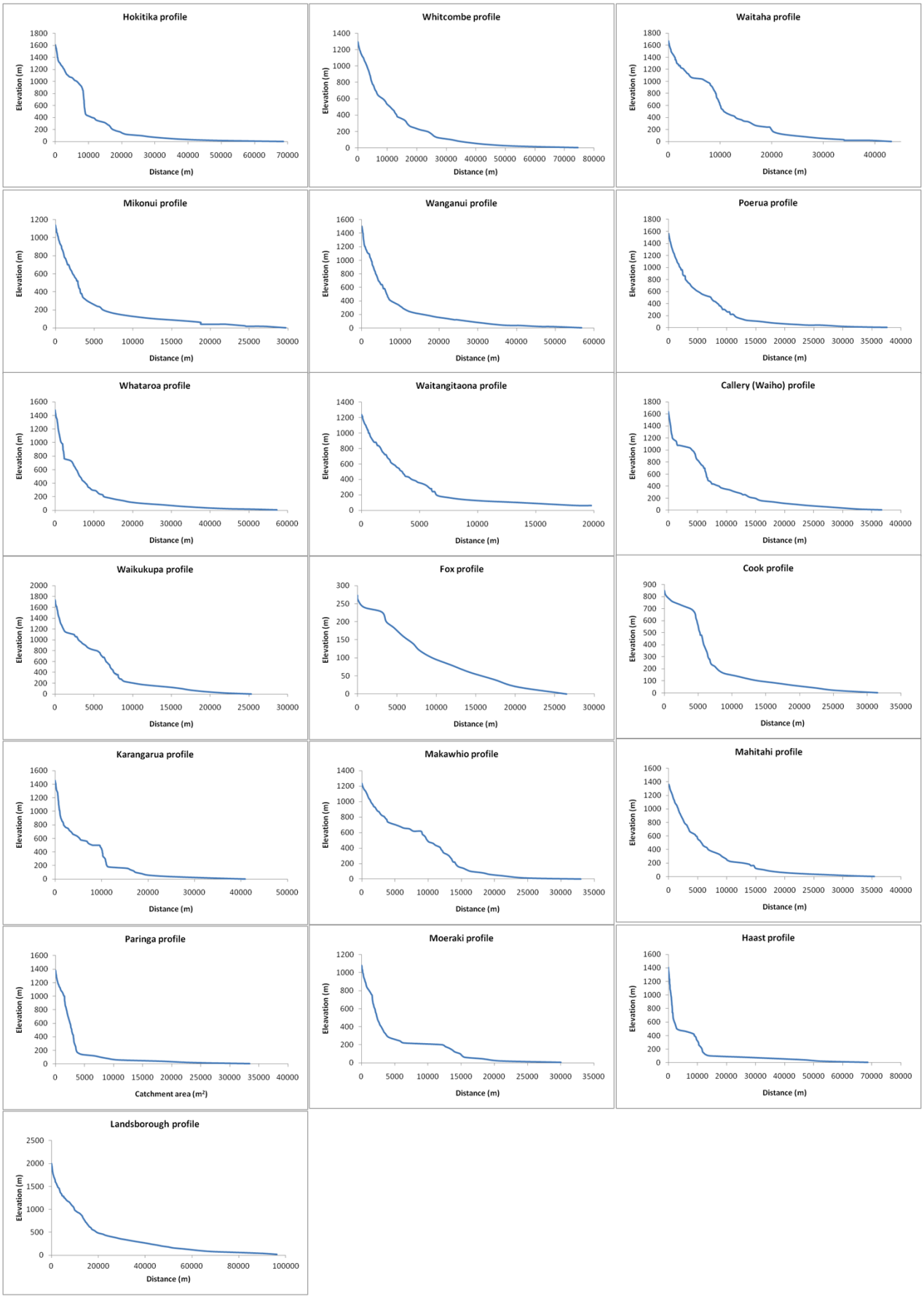

Figure 2.9 Channel profiles extracted by intersecting flow length with 20 m interpolated contour intervals.

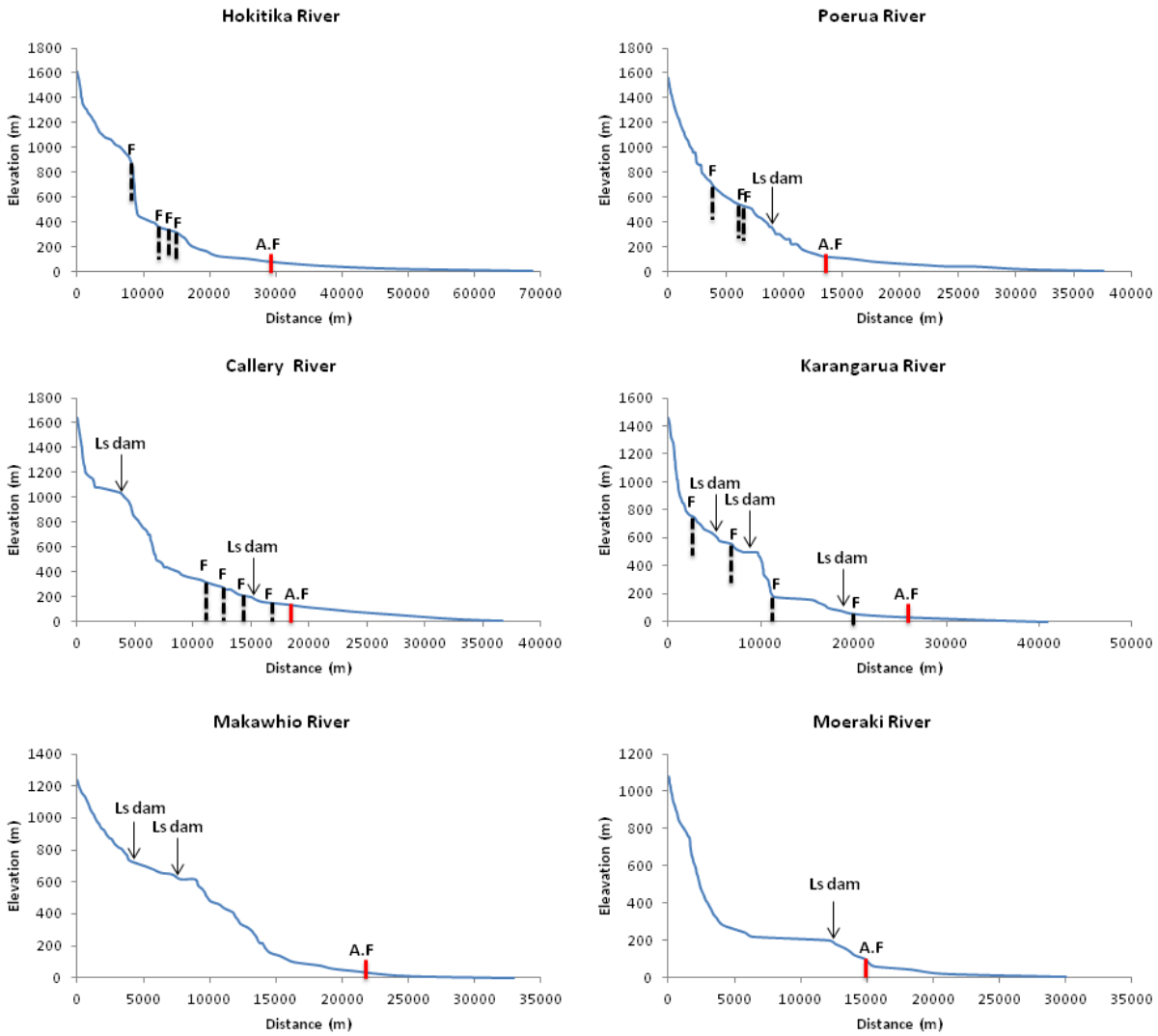

Figure 2.10 Major knickpoints associated with fault and landslide dam locations by Korup O. (unpublished data).

Channel steepness k_s and concavity θ were derived by linear regression of *S* and *A* in log-log space using the software developed by Whipple et al. (2007) (Fig. 2.11). The software implements the methods developed by Snyder (2000) and Kirby et al. (2003) which utilize a group of built-in functions in ArcGIS to generate flow accumulation and delineate drainage basins from a DEM and a suite of MATLAB scripts to extract and analyse stream profile data from these basins. Several issues with raw slope grids can adversely affect profile analysis results. These issues often derive from the DEM's resolution and the interpolation of the digitized topographic data to generate the DEM. The suite of algorithms in the Stream Profiler tool provides the means to overcome these limitations by resampling the raw elevation data at equal vertical intervals, using the contour interval from the original data source. Detailed description of the methodology and the algorithms can be found in Wobus et al. (2006) and Whipple et al. (2007).

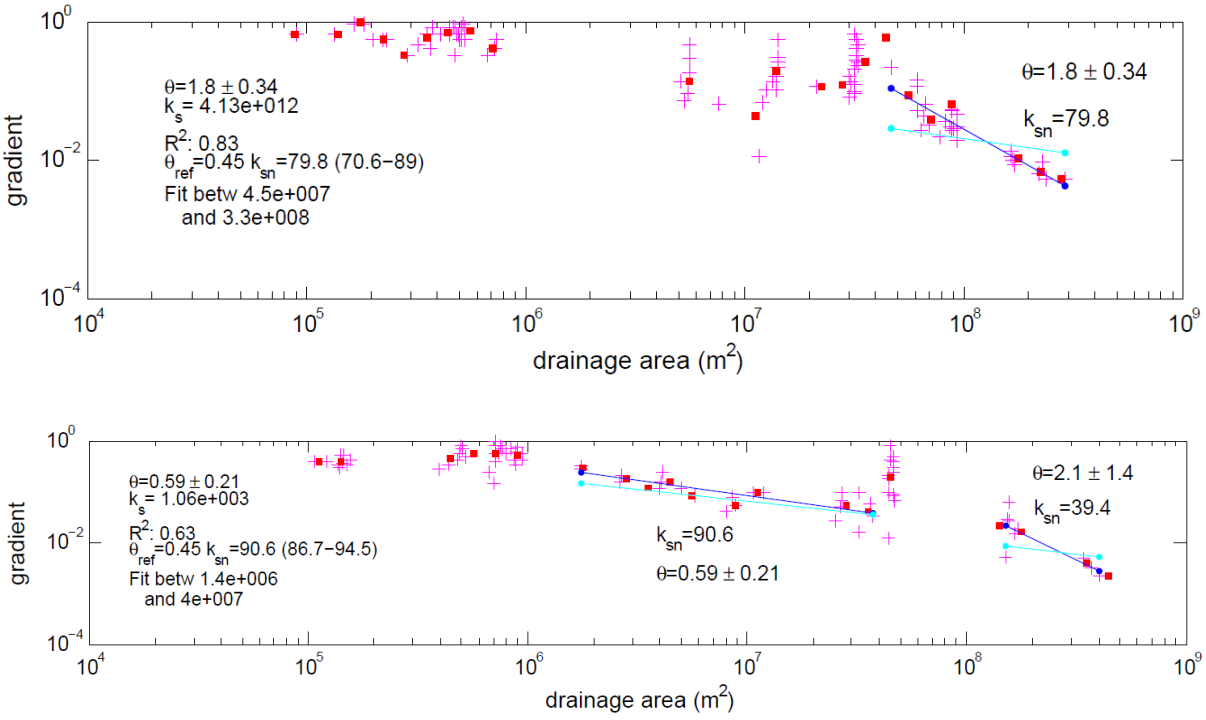

Figure 2.11 Example of linear regression of slope gradient and drainage area in log-log space of Callery river (upper figure) and Karangarua river (lower figure). *S-A* plots are provided in Appendix 2 (Figs. A2.1- A2.16).

The plan view distribution of normalized steepness indices for all the tributaries in a catchment can be an extremely useful tool for delineating the geomorphic signature of tectonics on the landscape (Kirby et al. 2003; Wobus et al. 2003, 2006). Herein the steepness index map is used to identify spatially-variable uplift rates assuming that at the regional scale, rivers respond to higher rock uplift rates by steepening their channel gradients throughout the drainage network.

2.2.3.1 Channel concavity (θ)

The longitudinal profiles of the study area rivers generally exhibit high channel concavities from 0.59 ± 0.13 (Mahitahi) up to 2.6 ± 0.52 (Waikukupa) (Table 2.5). In most river profiles, especially in those that have significant flow lengths east of the AF, three main segments characterized by different concavities can be identified: (1) a region with a relatively constant steep slope gradient (almost linear in the S-A plot) close to the headwaters (A=0.1-1 km^2) which probably represents the debris flow / rockfall dominated part of the channel network (Stock & Dietrich 2003; Wobus et al. 2006), (2) a middle section of medium to high concavity (0.5-1) where the presence of glaciers, bedrock incision and frequent landsliding interact, creating the very distinct rugged topography of WSA and (3) a lower segment, generally west of the AF, where concavity is very high (> 1), reflecting the part of the profile dominated by fluvial processes. Brocklehurst & Whipple (2007) examining the long profiles from rivers in WSA and Nanga Parbat, Pakistan also identified three distinct zones with

different concavities over longer reaches, suggesting that the presence of these zones is characteristic of glacial long profiles.

Table 2.5 *S-A* regression analysis results for major rivers.

Channel profile	Concavity (θ)	Normalized steepness index (k_{sn})
Hokitika	1.3 ± 0.25	56.2
Mikonui	0.83 ± 0.29	39.8
Waitaha	1.8 ± 0.99	92.1
Wanganui	1.4 ± 0.19	78.5
Poerua	2.4 ± 0.53	74.9
Whataroa	1.4 ± 0.18	95.1
Waitangitaona (upper)	1.5 ± 0.31	61.7
Callery	1.8 ± 0.34	79.8
Waikukupa	2.6 ±0.52	94.6
Cook	1.5 ± 0.47	47.1
Karangarua	2.1 ± 1.4	39.4
Makawhio	1 ± 0.25, 3 ± 0.63	85.2, 81.7
Mahitahi	0.59 ± 0.13	132
Paringa	1.2 ± 0.25	32.1
Moeraki	0.97 ± 0.18	145
Haast	1.9 ± 4.4	23.5

The very high concavities (>1) are somewhat expected in WSA rivers as their channel profiles cross different geomorphic processes (erosional-depositional) as well as uplift gradients between the main divide and the AF (based on measured vertical deformation rates in a transect across the Southern Alps; Beavan et al. 2010). The headward glacial erosion propagation model proposed by Shuster et al. (2011) who studied the topographic evolution of the glacial landscape of Fiordland, in New Zealand provides another possible explanation for the very high concavity of longitudinal profiles of major river valleys. Nevertheless, more research is required before conclusions can be drawn about the role of glaciers, differential uplift rates and landslide erosion in the evolution of channel long profiles in tectonically active glaciofluvial landscapes.

Therefore, although the spatial distribution of concavities downstream and in NE-SW direction cannot provide adequate information on the variability of uplift rates it clearly shows that the drainage network is affected by different geomorphic processes that vary both in space and time.

2.2.3.2 Channel steepness (k_s)

Assuming a regional reference concavity (θ) of 0.45, considered as typical value for rivers in active mountain belts (Whipple 2004; Korup 2006a), a normalized channel steepness index (k_{sn}) was estimated throughout the drainage network in the study area (Fig. 2.12). The values of k_{sn} vary spatially both downstream and in NE-SW direction. The mean k_{sn} was extracted from each catchment in order to investigate potential regional patterns. The major spatial variability in the mean k_{sn} is in NE-SW direction, where the values tend to increase from Hokitika to Callery river catchments (highest mean k_{sn}) and then exhibit a systematic decrease to the SE (Fig. 2.13).

The spatial pattern of the mean k_{sn}, assuming that reflects the adjustment of channel gradient to variable rock-uplift rates in the study area, suggests that the highest uplift rates occur in the Waiho catchment and decrease in both NE and SW directions. The most pronounced decrease however is observed in the SW (lowest mean k_{sn} at Haast catchment). The spatial pattern of mean k_{sn} was also found to resemble the spatial variation of mean elevation (Fig. 2.14). This observation is in agreement with Tippet & Kamp (1995) who found a close relation ($r^2 > 0.8$) between rock uplift rate and elevation. A positive correlation between mean k_{sn} and denudation rates (Hovius et al. 1997) was also observed (Fig. 2.15) illustrating the relation between uplift and erosion rates expressed through steep channel reaches.

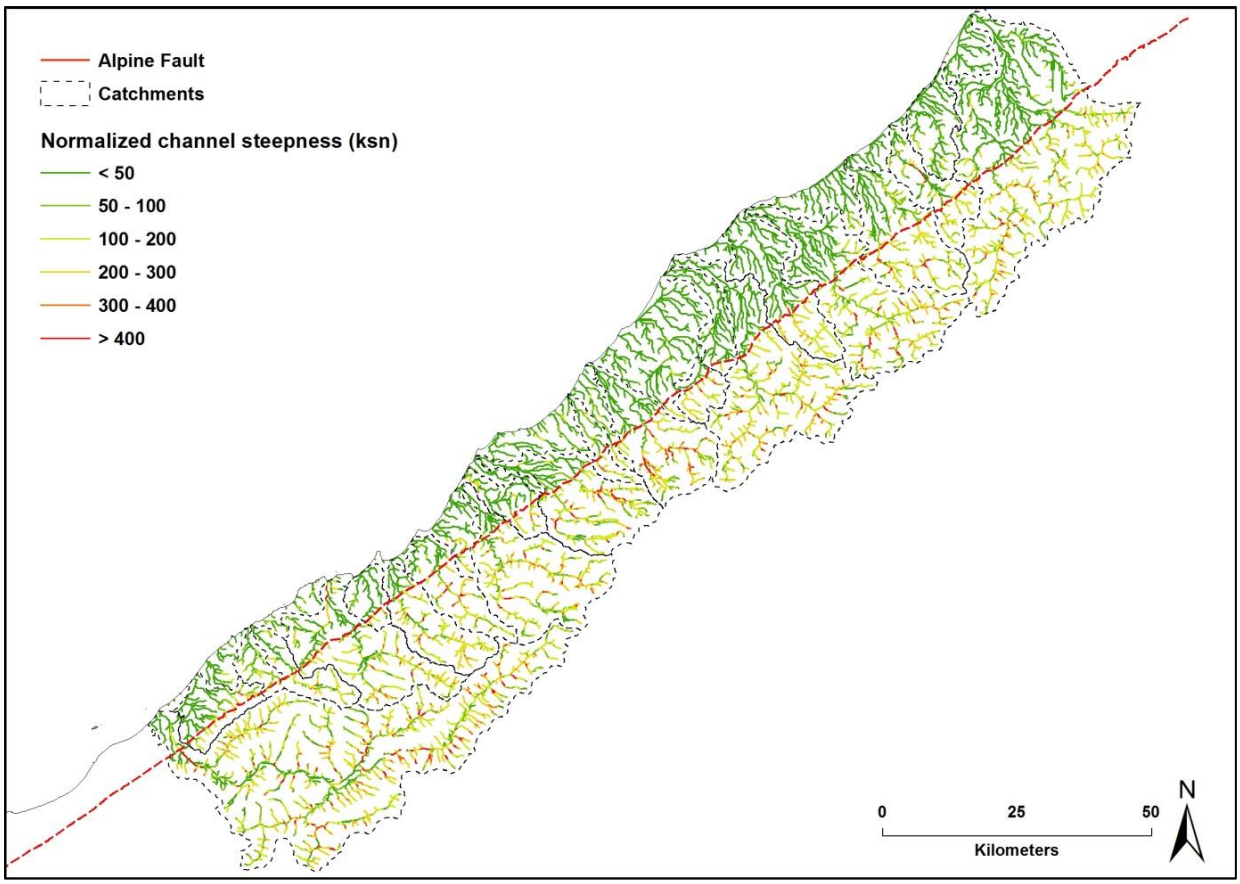

Figure 2.12 Map of normalized channel steepness (k_{sn} in $m^{0.9}$) for the study area channels (tributaries and main channels) with A > 1 km^2.

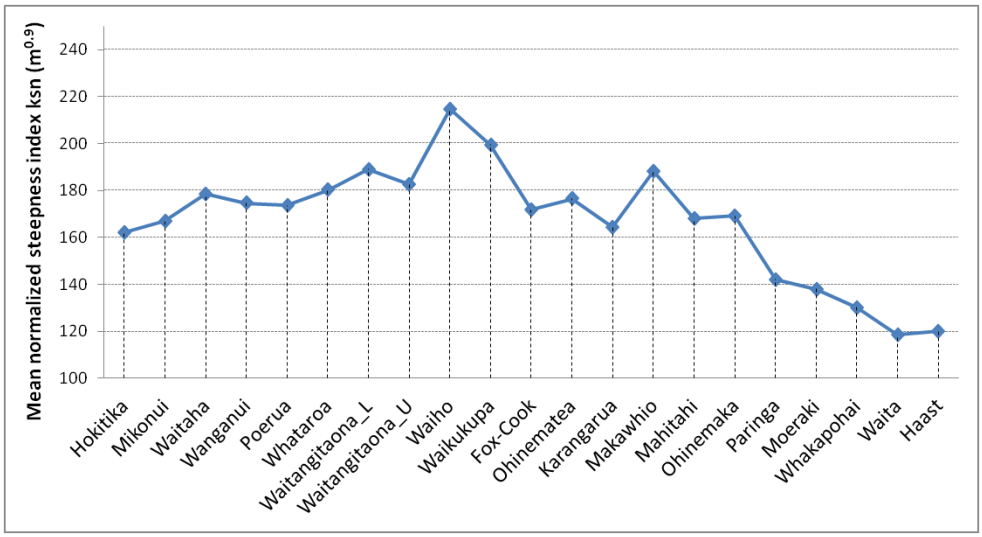

Figure 2.13 Mean normalized channel steepness index extracted for each major river catchment in the study area. The graph shows the variation of mean k_{sn} ($m^{0.9}$) in NE-SW direction.

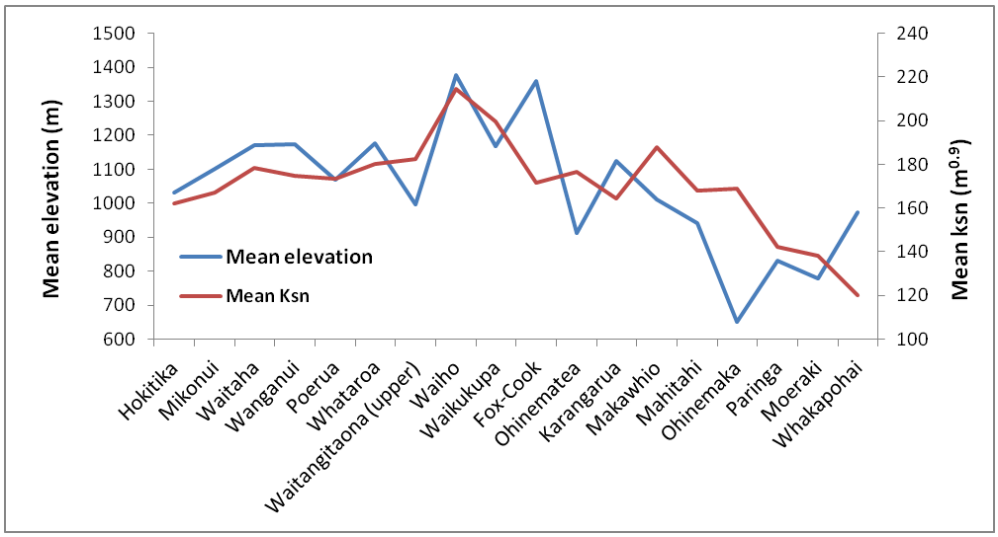

Figure 2.14 Variation of catchment mean elevation and mean k_{sn} in NE-SW direction.

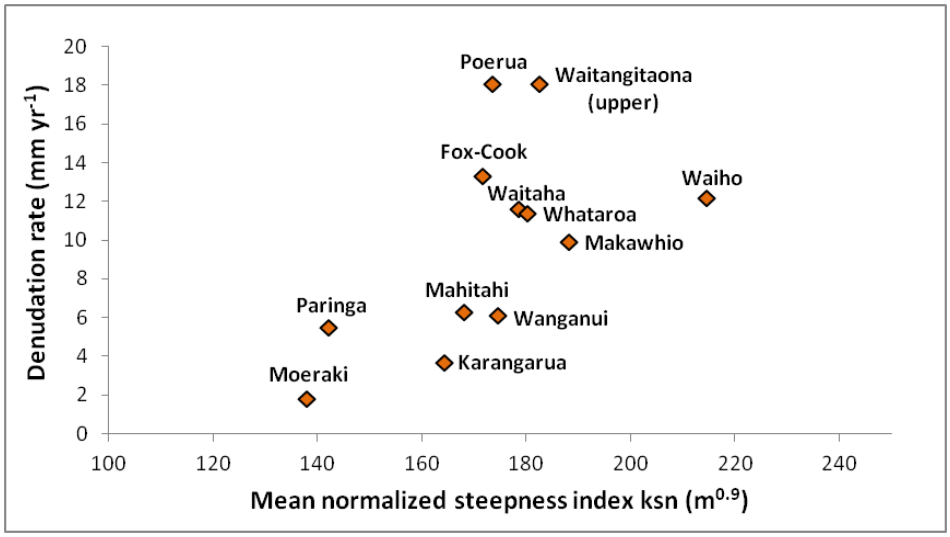

Figure 2.15 Mean k_{sn} plotted against denudation rates from Hovius et al. (1997).

2.2.3.3 Stream power

The stream-power model has been extensively used in a variety of landscapes as a basis to quantify sediment transport and erosion rates, model fluvial bedrock channel incision, explore downstream changes of channel geometry and investigate the evolution of riparian environments (Howard & Kerby 1983; Stock & Montgomery 1999; Whipple & Tucker 1999; Snyder et al. 2000; Kobor & Roering 2004; Whipple 2004). The model is based on downstream hydraulic relations describing bedrock channel incision as a power-law function of contributing catchment area, as proxy for discharge, and channel gradient as proxy for the energy grade line of the channel:

$$E = K\,A^m S^n \tag{2.7}$$

where *K* is the erosion coefficient, *A* is catchment area, *S* is slope gradient and *m*, *n* are empirically derived constants depending on a variety of parameters such as basin hydrology, hydraulic geometry and erosion rates, and therefore may significantly vary in different environments. Different values for m and n have been proposed in literature for three different types of models: for a total stream power model m=1, n=1; for a stream power per unit channel width model m=1/2, n =1; and for a shear stress model m=1/2, n =2/3 (Howard & Kerby 1983; Whipple & Tucker 1999). Also, the values of K range over several orders of magnitude, depending on channel characteristics (e.g. geometry, sediment cover), lithology, sediment transport rates, climate, orographic precipitation and differential rock uplift (Sklar & Dietrich 1998; Stock & Montgomery 1999; Kobor & Roering 2004). Despite its simplicity, the stream power model is considered a useful tool to study spatial variations of fluvial bedrock incision at regional scales (Korup et al. 2005). In particular, Finlayson et al. (2002) in order to investigate the relative erosion in the Himalayas, proposed a spatially distributed index (ε) based on the concept of bedrock incision models, assuming uniform bedrock resistance to fluvial erosion (eq. 2.8). In WSA Korup et al. (2005) adapted the method of Finlayson et al. (2002) and modelled the specific stream power for major rivers in order to observe the potential for fluvial incision along the mountain range (eq. 2.9).

$$\varepsilon = E/K = A^m S^n \tag{2.8}$$

$$\varepsilon = A^{0,5}\,S \tag{2.9}$$

Herein, we use the above simplified stream power model to examine the spatial distribution of fluvial erosion and deposition in the study area. The model utilizes the corrected slope used for the estimation of k_{sn}. Figure 2.16 shows the variation of mean stream power index in the study area. The most prominent spatial variability of stream power index occurs downstream where its values show an abrupt decrease as river channels emerge from the steep confined mountain valleys SE of the AF and flow onto the low slope plains. The abrupt decrease of stream power index values delineates the transition between fluvial erosion and deposition processes, immediately west of the mountain front. Relatively higher mean values are observed in the central part of WSA (Waiho, Waikukupa catchments) indicating that, in general, steep channel reaches (high k_{sn}) have also higher stream power index values.

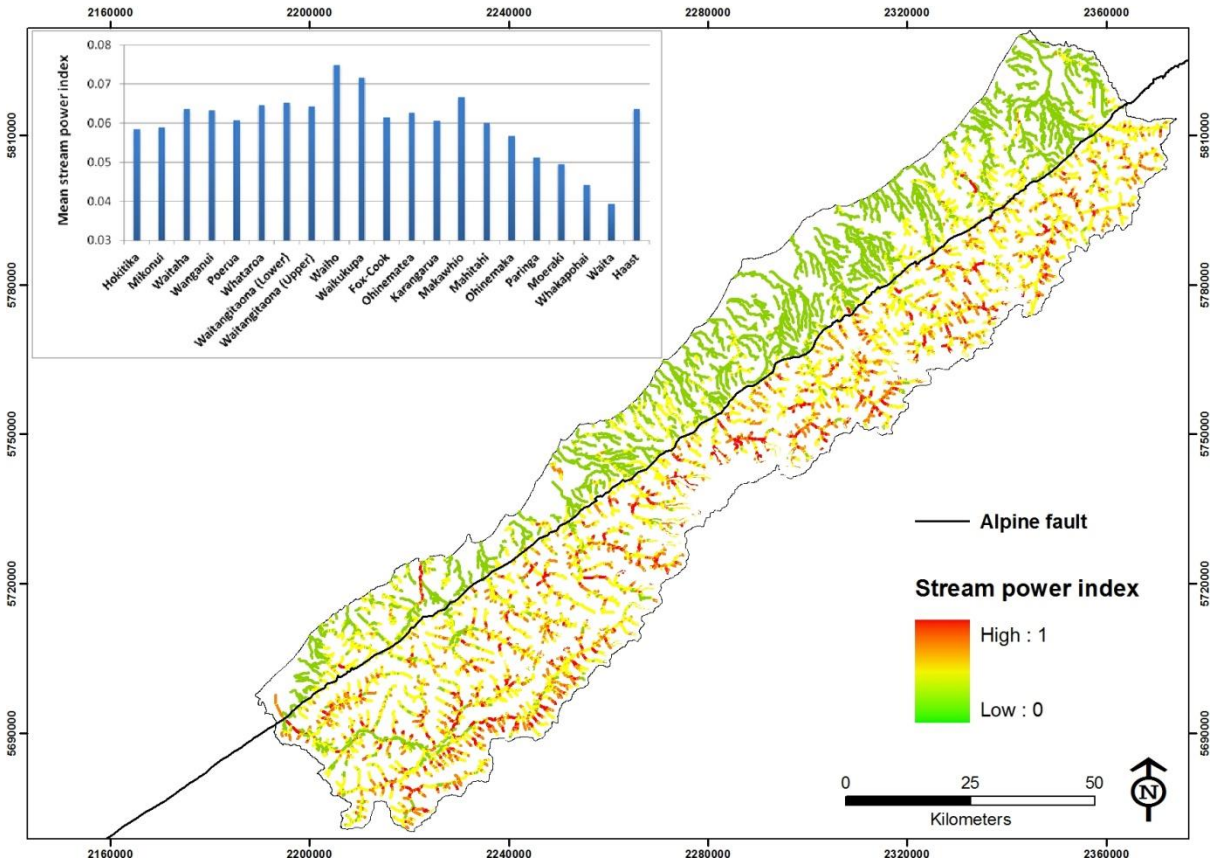

Figure 2.16 Regional spatial variation of stream power index ($\varepsilon = A^{0.5} S$). Inset graph shows the mean stream power index extracted for each catchment.

2.2.4 Valley Floor Width – Valley Height Ratio

The valley floor width-valley height ratio is an index sensitive to recent and ongoing uplift introduced by Bull & McFadden (1977), who found significant differences (at the 0.99 confidence level) in the means of V_f ratios of tectonically active and inactive mountain fronts. They suggested that if V_{fw} is the width of a valley floor, A_{ld} and A_{rd} are the altitudes of the left and right divides (looking downstream) respectively and A_{sc} is the altitude of the stream channel, then the valley floor width-valley height ratio (V_f) is estimated as:

$$V_f = \frac{V_{fw}}{\frac{(A_{ld} - A_{sc}) + (A_{rd} - A_{sc})}{2}} \quad (2.10)$$

The applicability of the ratio is based on the observation that valley-floor widths generally increase with watershed size, erodibility of rock type, and with decrease of uplift rate whereas valley heights decrease with the passage of time after the cessation of uplift, but not as fast valleys-floors widen.

The V_f ratio is particularly sensitive to late Quaternary tectonic base-level falls because narrowing of a valley floor is accomplished quickly by the downcutting action of streams (Bull 2007). Although the ratio has been developed to indirectly measure tectonic activity, herein it is applied in order to investigate the spatial variability of relative tectonic activity, expressed through uplift rates, in the NE-SW direction and over the distance between the Alpine Fault and the main divide.

Topographic cross-sections from 339 locations in valleys along the range-front were extracted and analysed in GIS environment (Fig. 2.17). Bull (2007) noted that careful selection of measurement sites is very important in order for the V_f values to be representative of the relative degree of tectonic base-level fall and not reflect differences in rock resistance or variation of stream power due to upstream catchment area size. Therefore all measurement sites were selected based on the following criteria: 1) at least 2 km away from the AF fault line and major river confluences 2) constant distance of 2 km between each site and 3) on similar rock types.

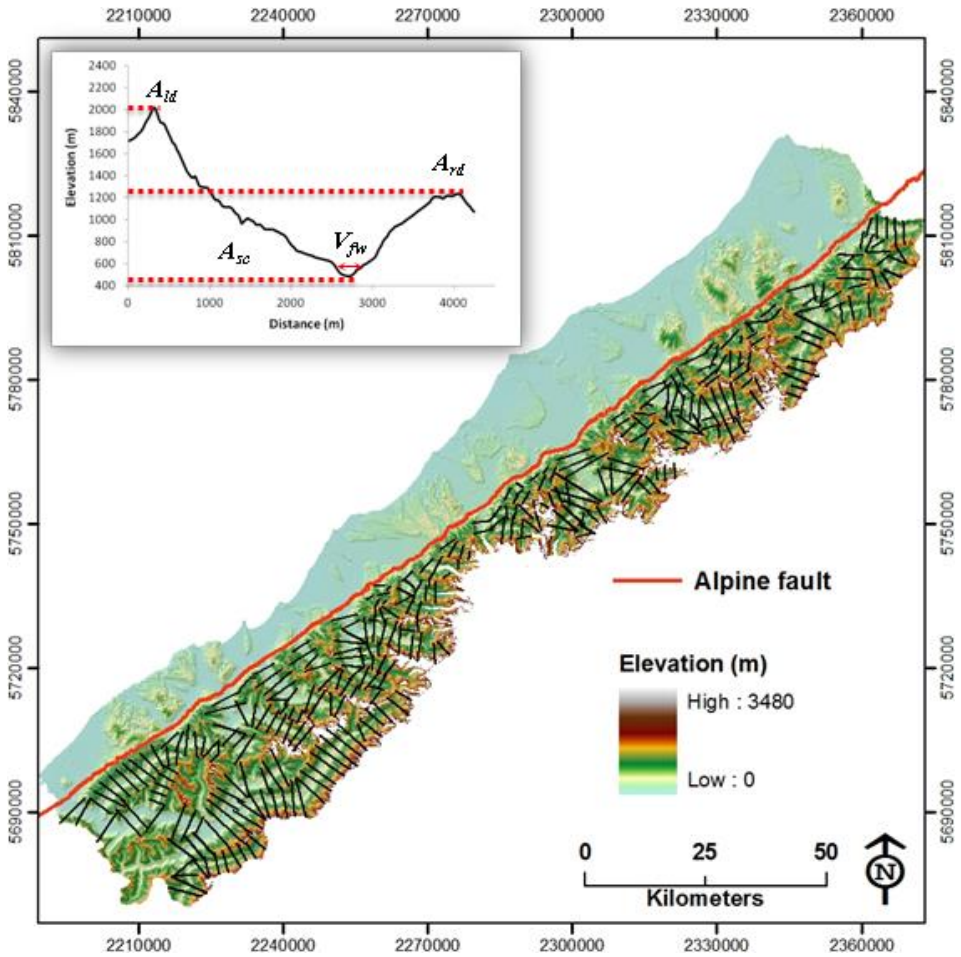

Figure 2.17 Map showing the locations of valley cross-sections used to calculate the Vf ratios (Appendix 3; Table A3.1).

V_f ratio values in the study area range from as low as 1.6 x 10^{-2} at Karangarua catchment (Copland and Douglas rivers) approximately 10 km east of the AF to 1.6 at Haast river catchment, 20 km east of the AF. Figure 2.18 shows the variation of V_f ratio between the AF and the main divide. Based on the variation of V_f ratio three distinct zones were identified: (1) wide flat-bottomed valleys with average V_f = 0.26 at low elevations up to a distance of 5km from the AF, (2) V-shaped deeply incised valleys with avergae V_f = 0.13 at mid-elevations (between 5 and 19 km east from the AF), and (3) a zone with wider, flat valley floors and high V_f ratio values (V_f = 0.34) at high elevations approximately 19 to 30 km from the AF. This latter zone can be further divided in two sections, the first between 19 and 23km where relatively higher values are observed, possibly because of the more prominent glacial geomorphic signature on topography (steep sides that curve in at the base of the valley wall and broad, flat valley floors) and the second from 23 to 30 km with lower values that may reflect the increased frequency of rock falls and rock avalanches closer to the divide as observed by Korup et al. (2005).

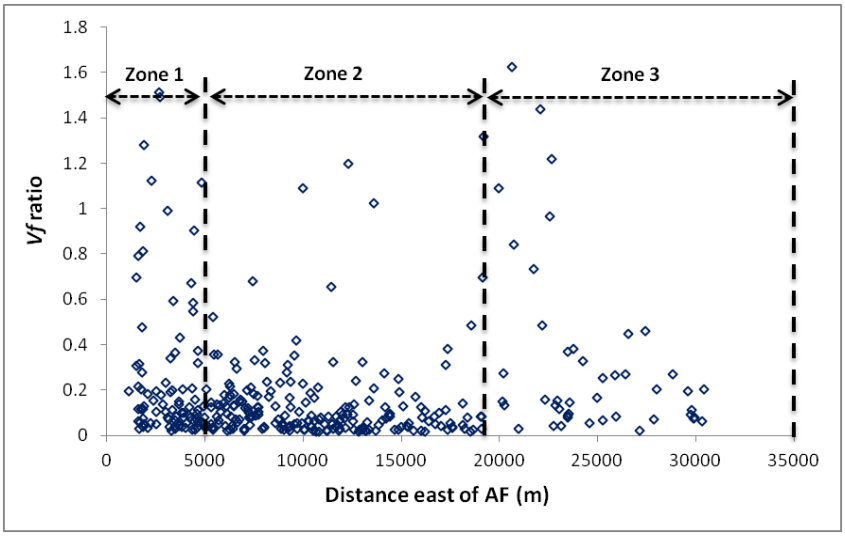

Figure 2.18 Variation of V_f ratio between the Alpine fault and the main Divide. The dashed black lines indicate approximately the distance from the Alpine fault where changes to systematically high or low V_f ratio values occur.

The mean V_f ratio for each catchment was also estimated, demonstrating a very distinct pattern in NE-SW direction. The values are generally low (<0.2) from Hokitika to Makawhio catchment (with exception Ohinematea catchment; V_f mean= 0.24) and increase to the SE (Fig. 2.19). The lowest mean V_f ratio is observed in the Fox-Cook catchment (0.066) suggesting the highest relative tectonic activity in the central region whereas a decreasing trend is observed south of Karangarua. The spatial pattern of mean V_f ratio is also consistent with the inferred variation of uplift rates based on the mean k_{sn}.

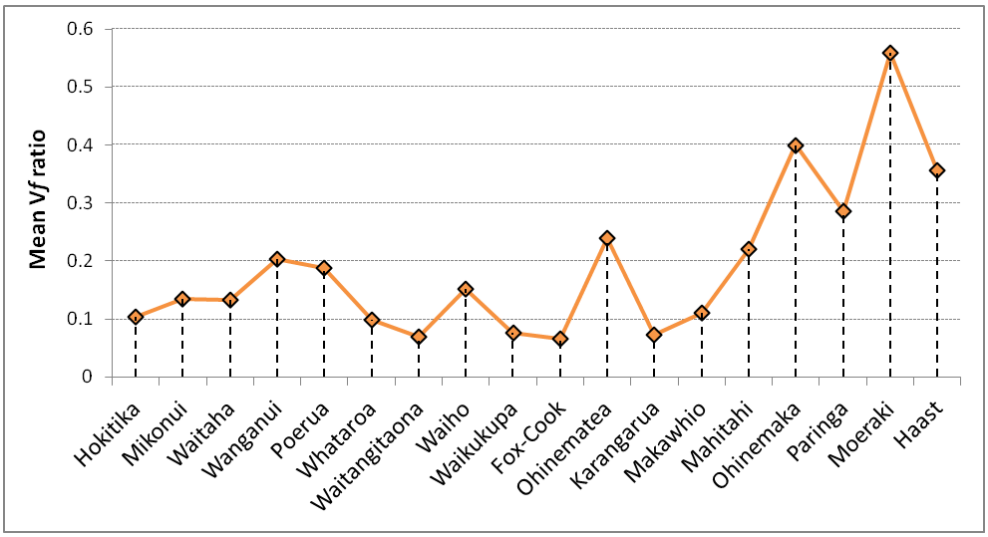

Figure 2.19 Variation of mean catchment V_f ratio in NE-SW direction.

The inferred spatial variation of uplift rates in NE-SW direction based on both the channel gradient and V_f ratio agrees with findings from previous studies on uplift rates in the region (Bull & Cooper 1986; Wllliams 1991; Tippet & Kamp 1993; Norris & Cooper 2000) which also suggest highest uplift rates in the central WSA and lower to the north, south and east respectively.

2.3 Discussion – Conclusions

Geomorphic analysis was performed on 22 catchments in the study area in order to identify the dominant geomorphic processes, their spatial distribution and interrelationships. The findings aim to inform hazard assessment and reveal critical implications in geomorphic hazard modelling. Methods of quantitative geomorphology via GIS have been employed to explore regional patterns of catchment morphometric characteristics which can be related to tectonic, climate and surface processes.

Initially, the extraction of morphometric parameters for each major catchment was performed, followed by drainage network analysis. At regional scale two distinct geomorphic environments on either side of the Alpine Fault are identified. On the NW side, between the mountain front and the coast, a narrow strip of low-slope terrain occupied by large braided rivers, lakes and glacial moraines is predominantly shaped by fluvial processes, the intensity and character (erosional-depositional) of which is largely controlled by the processes taking place in the upstream catchments SE of the Alpine fault. Between the Alpine Fault and the main divide an approximately 22km wide (average width) zone of rugged terrain is shaped by, fluvial processes, orogrpahically-enhanced precipitation,

landslides and high uplift rates and, in the past and presently at high elevations, by glaciers. As a result the major catchments are short, elongated, sub-perpendicular to the Main Divide and occupied in their headwaters by permanent snow and ice. Catchment morphometry as well as the structure of the drainage network show the strong influence and interactions between frequent landslides / debris-flows, glaciers, orographic precipitation and tectonics on landscape evolution.

Analysis of longitudinal channel profiles of major rivers in the study area was also carried out using the software developed by Whipple et al. (2007) and the methods described in Wobus et al. (2006**)**. The shape of the profiles and the results from the *S-A* regression analysis indicate a downstream change of dominant geomorphic processes, with debris-flows, rock avalanches and rock-falls close to the main divide; relic or current glacial topographic signature, bedrock incision and debris flows in the middle section; and fluvial processes in the lower section. A regional scale map illustrating the spatial distribution of stream channel steepness (calculated for every stream channel with contributing catchment ≥ 1 km^2) was also developed. The output demonstrates a characteristic spatial variability in the mean normalized steepness index (k_{sn}) in NE-SW direction, with channel gradients becoming steeper from Hokitika to Callery catchments (highest mean k_{sn}) and then gradually decreasing to the SW. Furthermore, the spatial variation of a simplified spatially distributed stream power index indicates higher fluvial erosion at the central part of the mountain range, where the steepest gradients are observed. The application of the valley floor width-valley height ratio also revealed a spatial pattern of valley geometry in NE-SW direction as well as between the AF and the main divide. In particular, east of the AF, three distinct zones were identified (in upstream direction): (1) a low elevation zone with wide flat-bottomed valleys and high average V_f ratio (2) an approximately 14 km wide region at mid-elevations with V-shaped deeply incised valleys with low V_f ratios and (3) a 11 km wide zone with high V_f ratio, wide U-shaped valleys at high elevations. In NE-SW direction relatively lower V_f ratio values are observed between Hokitika and Karangarua and exhibit an increase south of Makawhio catchment.

The spatial distribution patterns of the mean normalized channel steepness and V_f ratio indicate highest relative tectonic activity, expressed through uplift rates, at the central WSA (Waiho and Fox-Cook catchments) and a decreasing trend south of Karangarua. This observation is consistent with previous studies (Bull & Cooper 1986; Wllliams 1991; Tippet & Kamp 1993; Norris & Cooper 2000) suggesting spatially variable uplift rates along the range-front, with highest uplift rates in the central WSA and lower to the north, south and east.

In addition to providing information on the dominant geomorphic processes and uplift rates in WSA, interpretation of the above findings through the lens of hazard and risk research reveals significant

implications concerning hazard modelling, assessment and effective mitigation. Previous studies (Whitehouse 1988; Hovius et al. 1997; Norris & Cooper 2000; Herman & Braun 2006; Korup et al. 2005) as well as the present study have shown that WSA are affected by landslides, glacial advance-retreat, fluvial processes (erosion-deposition), extreme orographic precipitation and tectonics (through seismic events and aseismic deformation). All these processes control the landscape evolution of the region and are strongly interrelated (Fig. 2.20). Therefore, it is unlikely for a geomorphic event in such a dynamic landscape to not be followed by other potentially hazardous processes even if there is a delay (e.g. river aggradation and consequent flooding following an earthquake).This indicates that a multi-hazard approach incorporating the interactions between geomorphic processes and potential cascade effects, usually neglected in single hazard analysis, is necessary in WSA for realistic hazard assessment and effective mitigation.

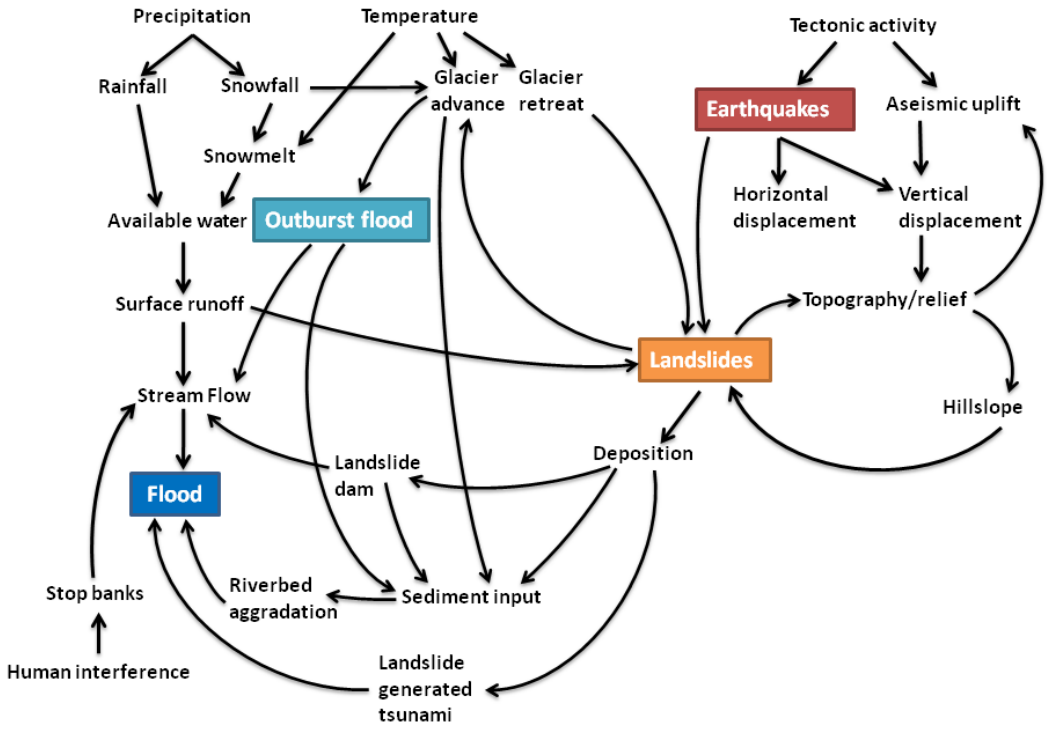

Figure 2.20 Conceptual diagram illustrating the interrelated tectonic, climatic and surface process as well as the consequent geomorphic hazards at the central WSA.

The uniform mode slope of 38° throughout the study area, and the observation that most landslides are observed between 35°-40°, suggest the presence of a regional threshold slope angle in WSA. This hypothesis has further implications in the context of regional landslide hazard. Although earthquakes and intense or prolonged rainfall are considered as the main triggering factors of slope failures in the region, significant landslide events have also occurred without an obvious trigger

mechanism (Benn 2005). This implies that landslides, even those of high magnitude, are fundamental processes of the landscape evolution of the WSA and can occur without an apparent trigger, complicating landslide hazard modelling.

In a highly dynamic landscape such as the WSA, hazard modelling approaches should incorporate the spatial variation as well as the temporal changes of geomorphic processes and landforms in order to provide meaningful outputs for decision-making and land use planning. For example, flood hazard and risk maps are usually derived by combining hydrologic and hydraulic models that require flow cross-section data along a river and high resolution topographic data in order to calculate flow velocity, depth and ultimately flood extent. However, in response to variations in uplift rate in space and time as well as sediment input, river channels constantly adjust their geometry (slope, width, depth, hydraulic radius) in order to maximize their transport capacity (Amos & Burbank 2007), making the output of any model assuming unchanging conditions meaningful only for a short time.

The Western Southern Alps is a very popular attraction for both domestic and international tourists. The central WSA with its low-level glaciers is particularly popular with growing annual visitor numbers and the prospect of further development. Nevertheless, the area is affected by various geomorphic processes, including different types of slope failures (debris-flows, rock fall / avalanching), high intensity fluvial erosion, flooding and riverbed aggradation as well as seismicity (McSaveney & Davies 1998; DTEC 2002) driven by the highest uplift rates observed along the mountain range. Considering risk as a function of hazard (H) impacting on an asset (A) and (C) the consequences of the impact (Schmidt et al. 2011),

$$R \sim H \times A \times C \qquad (2.11)$$

the central part of WSA has the highest total risk and requires the implementation of innovative multi-hazard / risk assessment methods to evaluate the risk from individual and coupled events.

The WSA can be defined as a dynamic open geomorphic system which constantly recovers from various “geomorphic disturbances”. For example, following an earthquake, a rock avalanche or a debris flow a chain reaction of processes will take place in order for the landscape to adjust to the new regime. This strongly implies that any interference with the system will trigger a series of other processes with potentially adverse effects for human developments. However, communities (and governments) seem to favour engineering controls as hazard mitigation measures as they often seem to be cost-effective solutions, rather than investing in more sustainable solutions such as land and property acquisition, change of existing land use or relocation. Engineering controls of geomorphic processes as hazard mitigation options might have obvious short term benefits but they

may interfere with the geomorphic system triggering other potentially hazardous processes. A prominent example in the study area is illustrated by Davies et al. (2003, 2013) who observed that the presence of stopbanks at Waiho River, installed as flood mitigation measure, has induced significant riverbed aggradation which has repeatedly damaged the river-control works and reduced their effectiveness. Therefore, any hazard mitigation approach in order to be effective and sustainable must be seamlessly integrated in the geomorphic system.

2.4 References

Adams J 1980. Contemporary uplift and erosion of the Southern Alps, New Zealand: Summary. Geological Society of America Bulletin, 91, 2-4.

Alcántara-Ayala I 2002. Geomorphology, natural hazards, vulnerability and prevention of natural disasters in developing countries. Geomorphology 47: 107–124.

Alcántara-Ayala I 2010. Geomorphology and coastal hazards. In: Geomorphological hazards and disaster prevention in (eds) I. Alcantara-Ayala and A. Goudie. Cambridge : Cambridge University Press, 2010. pp. 269 - 276.

Amos CB, Burbank DW 2007. Channel width response to differential uplift. J. Geophys. Res., 112, F02010, doi:10.1029/2006JF000672.

Baker VR 1994. Geomorphological understanding of floods. Geomorphology 10: 139–156.

Barringer JRF, Pairman D, McNeill SJ 2002. Development of a high resolution digital elevation model for New Zealand. Landcare Research Contract Report: LC0102/170.

Beaumont C, Fullsack P, Hamilton J 1992. Erosional control of active compressional orogens, in Thrust Tectonics, edited by K. R. McClay, New York: Chapman Hall, pp. 1 – 18.

Beavan J, Denys P, Denham M, Hager B, Herring T, Molnar P 2010. Distribution of present-day vertical deformation across the Southern Alps, New Zealand, from 10 years of GPS data, Geophys. Res. Lett., 37, L16305, doi:10.1029/2010GL044165.

Beaumont C, Jamieson RA, Nguyen MH, Lee B 2001. Himalayan tectonics explained by extrusion of a low-viscosity crustal channel coupled to focused surface denudation, Nature, 414, 738–742.

Bell R, Glade T 2004. Multi-hazard analysis in natural risk assessments.- In: Brebbia C.A. (ed): International Conference on Computer Simulation in Risk Analysis and Hazard Mitigation. WIT Press, 26.-29. September, Rhodes (GR), 197-206.

Benn JL 2005. Landslide events on the West Coast, South Island, 1867-2002. New Zealand Geographer 61: 3-13.

Bishop MP, Shroder JF Jr eds., 2004, Geographic Information Science and Mountain Geomorphology: SpringerPraxis, Chichester, U.K., 486 p.

Brocklehurst SH, Whipple KX 2004. Hypsometry of glaciated landscapes. Earth Surf. Process. Landforms 29, 907–926. DOI: 10.1002/esp.1083

Brocklehurst SH, Whipple KX 2007. Response of glacial landscapes to spatial variations in rock uplift rate. J. Geophys. Res., 112, F02035, doi:10.1029/2006JF000667.

Brozovic N, Burbank DW, Meigs AJ. 1997. Climatic limits on landscape development in the northwestern Himalaya. Science 276: 571–574.

Bull WB, McFadden LD 1977. Tectonic geomorphology north and south of the Garlock Fault, California. In: Geomorphology in Arid Regions (edited by Doehring, D.O.). Proc. 8th. Ann. Geomorph. Symp. State University of New York, Binghamton, 115 - 138.

Bull WB, Cooper AF 1986. Uplifted Marine Terraces along the Alpine Fault, New Zealand. American Association for the Advancement of Science. Science, New Series, Vol. 234, No. 4781, pp. 1225-1228.

Bull WB 2007. Tectonic Geomorphology of Mountains: A New Approach to Paleoseismology. Blackwell Publishing. 316p.

Burbank DW, Leland J, Fielding E, Anderson RS, Brozovic N, Reid MR, Duncan C 1996. Bedrock incision, rock uplift and threshold hillslopes in the northwestern Himalayas. Nature 379, 505-510.

Burbank DW, Anderson RS 2012. Tectonic Geomorphology. 2nd edition, Wiley, 454 pp.

Burrough PA, McDonnell RA 1998. Principles of Geographical Information Systems: Spatial Information Systems and Geostatistics. Oxford Univ. Press, Oxford. 356p.

Church M, Mark DM 1980. On size and scale in geomorphology. Progress in Physical Geography 4, 342– 390.

Cooper RA 1989. Early Paleozoic terranes of New Zealand. Journal of the Royal Society of New Zealand 19: 73–112.

Cooper RA, Tulloch AJ 1992. Early Palaeozoic terranes in New Zealand and their relationship to the Lachlan Fold Belt. Tectonophysics 214(1/4): 129-144.

Davies TR, McSaveney MJ, Clarkson PJ 2003. Anthropic Aggradation of the Waiho River, Westland, New Zealand: Microscale Modelling. Earth Surf. Process. Landforms 28, 209–218.

Davies TR, McSaveney MJ 2006. Geomorphic constraints on the management of bedload dominated rivers. Journal of Hydrology (New Zealand) 45 (2): 69-88.

Davies TRH, Campbell B, Hall RJ, Gomez C (2013 in press). Recent behaviour and sustainable future management of the Waiho River, Westland, New Zealand. Journal of hydrology (New Zealand).

DeMets C, Gordon RG, Argus DF 2010. Geologically current plate motions. Geophys. J. Int. 181, 1–80. doi: 10.1111/j.1365-246X.2009.04491.x

De Scally FA, Owens IF 2004. Morphometric controls and geomorphic response on fans in the Southern Alps, New Zealand. Earth Surf Process Land 29:311–322.

DTec Consulting Ltd 2002: West Coast Regional Council: Natural Hazards Review. Report prepared for West Coast Regional Council by Dtec Consulting Ltd. Client Reference: 1065.136WCRC, Greymouth. 140 p.

Evans SG, Clague JJ 1994. Recent climatic change and catastrophic geomorphic processes in mountain environments. Geomorphology 10, 107–128.

Finlayson DP, Montgomery DR, Hallet B 2002. Spatial coincidence of rapid inferred erosion with young metamorphic massifs in the Himalaya. Geology 30, 219–222.

Finlayson DP, Montgomery DR 2003. Modeling large-scale fluvial erosion in geographic information systems: Geomorphology, v. 53, p. 147–164.

Fitzharris BB, Hay JE, Jones PD 1992. Behaviour of New Zealand glaciers and atmospheric circulation changes over the past 130 years. The Holocene2, 97–106.

Flint JJ 1974. Stream gradient as a function of order, magnitude, and discharge, Water Resour. Res., 10, 969– 973.

Frankel KL, Pazzaglia FJ 2006. Mountain fronts, base level fall, and landscape evolution: Insights from the southern Rocky Mountains, in Willett, S. D., Hovius, N., Brandon, M. T., and Fisher, D. eds., Tectonics, climate, and landscape evolution: Geological Society of America Special Paper 398, p. 419-434.

Gares PA, Sherman DJ, Nordstrom KF 1994. Geomorphology and natural hazards. Geomorphology 10:1– 18.

Glade T, von Elverfeldt K 2005. MultiRISK: An innovative Concept to model Natural Risks. In: Oldrich H, Fell R, Coulture R, Eberhardt E ed. International Conference on Landslide Risk Management.- 31. May - 03. June 2005, Vancouver (CND), Balkemaa: 551-556.

Hack JT 1973. Stream-profile analysis and stream gradinet index. Journ. Res. U.S. Geol. Survey 1. (4): 421-429.

Hancock P, Skinner BJ, 2000. Tectonic geomorphology. The Oxford Companion to the Earth. (http://www.encyclopedia.com)

Harkins NW, Anastasio DJ, Pazzaglia FJ 2005. Tectonic geomorphology of the Red Rock fault, insights into segmentation and landscape evolution of a developing range front normal fault. Journal of Structural Geology 27, 1925-1939.

Hellweger F 1997. AGREE – DEM surface reconditioning system. Center for Research in Water Resources, University of Texas at Austin.

http://www.ce.utexas.edu/prof/maidment/gishydro/ferdi/research/agree/agree.html

Herman F, Braun J 2006. Fluvial response to horizontal shortening and glaciations: A study in the Southern Alps of New Zealand. J. Geophys. Res., 111, F01008, doi:10.1029/2004JF000248.

Hewitt K 2006. Disturbance regime landscapes: mountain drainage systems interrupted by large rockslides. Progress in Physical Geography, Vol. 30, No. 3: 365-393.

Hewitt K, Clague JJ, Orwin JF 2008. Legacies of catastrophic rock slope failures in mountain landscapes. Earth-Science Reviews 87: 1-38.

Horton RE 1945. Erosional development of streams and their drainage basins: hydrophysical approach to quantitative morphology. Bulletin of the Geological Society of America 56, 275-370.

Hovius N, Stark CP, Allen PA 1997. Sediment flux from a mountain belt derived from landslide mapping. Geology 25, 231– 234.

Howard AD, Kerby G 1983. Channel changes in badlands: Geological Society of America Bulletin, v. 94, p. 739–752.

Jackson LE, Kostashuk RA, MacDonald GM 1987. Identification of debris flow hazard on alluvial fans in the Canadian Rocky mountains. Geological Society of America. Reviews in Engineering Geology VII: 155-124.

Jamieson SSR, Sinclair H.D, Kirstein LA, Purves RS 2004. Tectonic forcing of longitudinal valleys in the Himalaya : morphological analysis of the Ladakh Batholith, North India. Geomorphology., 58 (1-4). pp. 49-65.

Kappes M, Keiler M, Glade T 2010. From single- to multi-hazard risk analyses: a concept addressing emerging challenges. In: Malet J.-P., Glade T. & N. Casagli (Editors): Proceedings of the International Conference 'Mountain Risks: Bringing Science to Society', Firenze, 24-26 November 2010, 351-356.

Kirby E, Whipple K 2001. Quantifying differential rock-uplift rates via stream profile analysis, Geology, 29(5), 415– 418.

Kirby E, Whipple KX, Tang W, Chen Z 2003. Distribution of active rock uplift along the eastern margin of the Tibetan Plateau: Inferences from bedrock channel longitudinal profiles: Journal of Geophysical Research, v. 108, no. B4, 2217, doi: 10.1029/2001JB000861.

Kirkby MJ 1980. The stream head as a significant geomorphic threshold, in Coates, D.R., and Vitek, J.D., eds., Thresholds in Geomorphology, Boston, Allen and Unwin, p. 53-73.

Kirkby MJ 1993. Long term interactions between networks and hillslopes, in Beven, K., and Kirkby, M.J., eds., Channel Network Hydrology, New York, John Wiley and Sons, p. 255-293.

Kobor JS, Roering JJ 2004. Systematic variation of bedrock channel gradients in the central Oregon Coast Range: Implications for rock uplift and shallow landsliding: Geomorphology, v. 62, p. 239–256.

Koons PO 1989. The topographic evolution of collisional mountain belts: a numerical look at the Southern Alps, New Zealand. American Journal of Science, Vol. 289, p. 1041-1069.

Koons PO 1990. The two-sided wedge in orogeny. Erosion and collision from the sand box to the Southern Alps, 528 New Zealand. Geology 18, 679–682.

Korup O, McSaveney MJ, Davies TRH 2004. Sediment generation and delivery from large historic landslides in the Southern Alps, New Zealand. Geomorphology 6: 189–207.

Korup O, Schmidt J, McSaveney MJ 2005. Regional relief characteristics and denudation pattern of the western Southern Alps, New Zealand. Geomorphology 71, 402-423.

Korup O 2005a. Geomorphic imprint of landslides on alpine river systems, southwest New Zealand. Earth Surface Processes and Landforms 30: 783-800.

Korup O 2005b. Large landslides and their effect on alpine sediment flux: South Westland, New Zealand. Earth Surface Processes and Landforms 30: 305-323.

Korup O 2005c. Geomorphic hazard assessment of landslide dams in South Westland, New Zealand – fundamental problems and approaches. Geomorphology 66: 167-188.

Korup O 2006a. Rock-slope failure and the river long profile. Geology 34: 45-48.

Korup O 2006b. Effects of deep-seated bedrock landslides on hillslope morphology, Southern Alps, New Zealand. Journal of Geophysical Research 111, F01018, doi:10.1029/2004JF000242.

Korup O, Strom AL, Weidinger JT, 2006. Fluvial response to large rock-slope failures – examples from the Himalayas, the Tien Shan, and the Southern Alps in New Zealand. Geomorphology 78: 3-21.

Korup O, Densmore AL, Schlunegger F 2009. The role of landslides in mountain range evolution. Geomorphology, doi:10.1016/j.geomorph.2009.09.017.

Lague D, Davy P 2003. Constraints on the long-term colluvial erosion law by analyzing slope-area relationships at various tectonic uplift rates in the Siwaliks Hills (Nepal), J. Geophys. Res., 108, B2, 2129, doi:10.1029/2002JB001893.

Larsen IJ, Montgomery DR 2012. Landslide erosion coupled to tectonics and river incision. Nature Geoscience, Vol. 5, 468-473.

McSaveney MJ, Davies TR 1998. Natural hazard assessment for the township of Franz Josef Glacier and its environs. Client Report 43714B.10, Institute of Geological and Nuclear Sciences, Lower Hutt, 58 p.

Melton MA 1965. The geomorphic and paleoclimatic significance of alluvial deposits in southern Arizona. J Geol 73:1–38.

Molnar P, England P 1990. Late Cenozoic uplift of mountain ranges and global climate change: Chicken or egg?, Nature, 346, 29– 34.

Montgomery DR 2001. Slope distributions, threshold hillslopes, and steady-state topography. Am. J. Sci. 301, 432-454.

Montgomery DR, Balco G, Willett SD. 2001. Climate, tectonics and the morphology of the Andes. Geology 29: 579–582.

Montgomery DR, Brandon MT 2002. Topographic controls on erosion rates in tectonically active mountain ranges. Earth Planet. Sc. Lett. 201, 481-489.

Moore ID, Grayson RB, Ladson AR 1991. Digital terrain analysis modelling: a review of hydrological, geomorphological, and biological applications. Hydrological Processes 5, 3– 30.

Mortimer N, Tulloch AJ, Spark RN, Walker NW, Ladley E, Allibone A, Kimbrough DL 1999. Overview of the Median Batholith, New Zealand: a new interpretation of the geology of the Median Tectonic Zone. Journal of African Earth Sciences 29: 257–268.

Norris RJ, Cooper AF 2000. Late Quaternary slip rates and slip partitioning on the Alpine Fault, New Zealand. Journal of Structural Geology 23: 507–520.

Oguchi T, 1997. Drainage density and relative relief in humid steep mountains with frequent slope failure: Earth Surface Processes and Landforms, v. 22, p. 107-120.

Panizza M, Pasuto A, Silvano S, Soldati M 1996. Temporal occurrence and activity of landslides in the area of Cortina d'Ampezzo (Dolomites, Italy). Geomorphology, 15(3–4), 311–326.

Pelletier 2008. Quantitative Modeling of Earth Surface Processes, Cambridge University Press, 304 p.

Robinson TR, Davies TRH 2013. Review Article: Potential geomorphic consequences of a future great (Mw = 8.0+) Alpine Fault earthquake, South Island, New Zealand. Nat. Hazards Earth Syst. Sci., 13, 2279–2299.

Rosenfeld CL 1994. The geomorphological dimensions of natural disasters. Geomorphology 10: 27–36.

Scheidegger AE 1994. Hazards: singularities in geomorphic systems. Geomorphology 10: 19– 25.

Schmidt J, Matchman I, Reese S, King A, Bell R, Henderson R, Smart G, Cousins J, Smith W, Heron D 2011. Quantitative multi-risk analysis for natural hazards: a framework for multi-risk modelling, Nat. Hazards 58, 1169–1192, DOI 10.1007/s11069-011-9721-z.

Schneider B 2001. Phenomenon-based specification of the digital representation of terrain surfaces. Transactions in GIS 5 (1), 39–52.

Schumm SA 1956. Evolution of drainage systems and slopes in badlands at Perth Amboy, New Jersey. Bulletin of the Geological Society, 67, 597–646.

Schumm SA 1988. Geomorphic hazards: problems of prediction. Zeitschrift für Geomorphologie Supplementband, 67, 17–24.

Shulmeister J, Davies TR, Evans DJA, Hyatt OM, Tovar DS 2009. Catastrophic landslides, glacier behaviour and moraine formation – A view from an active plate margin. Quaternary Science Reviews 28: 1085–1096.

Shuster DL, Cuffey KM, Sanders JW, Balco G 2011. Thermochronometry Reveals Headward Propagation of Erosion in an Alpine Landscape. Science 332, 84-88. DOI: 10.1126/science.1198401

Sklar L, Dietrich WE 1998. River longitudinal profiles and bedrock incision models: stream power and the influence of sediment supply. In: Tinkler KJ, Wohl EE (Eds.), Rivers Over Rocks: Fluvial Processes in Bedrock Channels, Geophysical Monograph Series, vol. 107. AGU, Washington, D.C, pp. 237– 260.

Slaymaker O 2010. Mountain hazards. In: Geomorphological hazards and disaster prevention in (eds) I. Alcantara-Ayala and A. Goudie. Cambridge : Cambridge University Press, 2010. pp. 33 - 44.

Snyder NP, Whipple KX, Tucker GE, Merritts DJ 2000. Landscape response to tectonic forcing: Digital elevation model analysis of stream profiles in the Mendocino triple junction region, northern California. GSA Bulletin, v. 112, no. 8, p. 1250–1263.

Stock J, Montgomery DR 1999, Geologic constraints on bedrock river incision using the stream power law: Journal of Geophysical Research, v. 104, p. 4983–4993.

Stock J, Dietrich WE 2003. Valley incision by debris flows: Evidence of a topographic signature, Water Resour. Res., 39(4), 1089, doi:10.1029/2001WR001057.

Strahler AN 1952. Hypsometric (area–altitude) analysis of erosional topography. Geological Society of America Bulletin, 63, 1117–1142.

Strahler AN 1964. Quantitative geomorphology of drainage basins and channel networks. In Chow, V. T. (Ed.) Handbook of Applied Hydrology, McGraw Hill, New York, 4-39–4-76.

Tippett JM, Kamp PJJ 1993. Fission Track Analysis of the Late Cenozoic Vertical Kinematics of Continental Pacific Crust, South Island, New Zealand. Journal of Geophysical Research, Vol. 98, No B9, p. 16,119-16,148.

Tippett JM, Kamp PJJ 1995. Quantitative relationships between uplift and relief parameters for the Southern Alps, New Zealand, as determined by fission track analysis. Earth Surface Processes and Landforms 20, 153– 175.

Tovar DS, Shulmeister J, Davies TR, 2008. A landslide origin of the New Zealand's Waiho Loop Moraine. Nature Geosciences 10.1038/ngeo249.

Tucker GE, Bras RL 1998. Hillslope processes, drainage density, and landscape morphology. Water Resour. Res. 34:2751–64.

United States Geological Service 1997. Standards for digital elevation models. Mid-Continent Mapping Center, Branch of Research, Technology and Applications, 67p.

Verstraeten G, Poesen J 2001. Factors controlling sediment yield from small intensity cultivated catchments in a temperate humid climate. Geomorphology 40, 123–144.

Wallace LM, Beavan RJ, McCaffrey R, Berryman K, Denys P 2007. Balancing the plate motion budget in the South Island, New Zealand using GPS, geological and seismological data. Geophysical Journal International 168, 332-352.

Walsh SJ, Butler DR, Malanson GP 1998. An overview of scale, pattern, process relationships in geomorphology: a remote sensing and GIS perspective. Geomorphology 21, 183-205.

Welsh AJ 2008. Delineating debris-flow hazards on alluvial fans in the Coromandel and Kaimai regions, New Zealand using GIS. MSc thesis, University of Canterbury, New Zealand, 169p + App.

Welsh A, Davies T 2011. Identification of alluvial fans susceptible to debris-flow hazards. Landslides 8:183–194.

Whipple KX, Tucker GE 1999. Dynamics of the stream-power river incision model: implications for height limits of mountain ranges, landscape response timescales, and research needs. Journal of Geophysical Research 104, 17661– 17674.

Whipple KX 2004. Bedrock rivers and the geomorphology of active orogens, Ann. Rev. Earth Planet. Sci., 32, 85–151.

Whipple KX, Wobus CW, Crosby B, Kirby E, Sheehan D 2007. New Tools for Quantitative Geomorphology: Extraction and Interpretation of Stream Profiles from Digital Topographic Data, short course notes, Geological Society of America Annual Meeting, October 28, 2007, http://www.geomorphtools.org/Tools/StPro/StPro.htm.

Whitehouse IE 1983. Distribution of large rock avalanche deposits in the central Southern Alps, New Zealand. New Zealand Journal of Geology and Geophysics 26: 272-279.

Whitehouse IE 1988. Geomorphology of the central Southern Alps, New Zealand: the interaction of plate collision and atmospheric circulation. Zeitschrift fur Geomorphologie Supplement Band N.F 69, 105– 116.

Whittaker AC, Attal M, Cowie PA, Tucker GE, Roberts G 2008. Decoding temporal and spatial patterns of fault uplift using transient river long profiles. Geomorphology 100, 506–526.

Wilford DJ, Sakal ME, Innes JL, Sidle RC, Bergerud WA 2004. Recognition of debrisflow, debris-flood and flood hazard through watershed morphometrics. Landslides 1:61–66.

Willett SD 1999. Orogeny and orography: the effects of erosion on the structure of mountain belts. Journal of Geophysical Research 104, 28,957–81.

Willgoose G, Hancock G 1998. Revisiting the hypsometric curve as an indicator of form and process in transport-limited catchment. Earth Surf. Process. Landforms 23, 611–623.

Williams PW 1991. Tectonic geomorphology, uplift rates and geomorphic response in New Zealand, CATENA, Volume 18, Issue 5, Geomorphology in Unstable Regions, 439-452.

Wobus CW, Hodges KV, Whipple KX 2003. Has focused denudation sustained active thrusting at the Himalayan topographic front?, Geology, 31(10), 861– 864.

Wobus CW, Whipple KX, Kirby E, Snyder NP, Johnson J, Spyropolou K, Crosby B, Sheehan D 2006. Tectonics from topography: Procedures, promise, and pitfalls, in Willett, S.D., Hovius, N., Brandon, M.T., and Fisher, D.M., editors, Tectonics, Climate, and Landscape Evolution, Geological Society of America Special Paper 398, p. 55-74, doi: 10.1130/2006.2398(04).

Wolock DM, Price CV 1994. Effects of digital elevation model map scale and data resolution on a topography-based watershed model. Water Resources Research 30 (11), 3041–3052.

Wood J 1996. Scale-based characterisation of digital elevation models. In: Parker D, Innovations in GIS, vol. 3. Taylor and Francis, London, pp. 163–175.

Zarn B, Davies TR 1994. The significance of processes on alluvial fans to hazard assessment. Zeitschrift fór Geomorphologie 38: 487-500.

Chapter 3: Landslide susceptibility assessment

3.1 Introduction

Landsliding is a very common geomorphic process in the mountainous terrain of the western Southern Alps of New Zealand, due to a combination of high tectonic uplift rates, steep topography, intense and prolonged rainfalls (orographic precipitation) and regular seismic activity. Different types of mass movements occur in the region, ranging in scale from shallow slope failures and rockfalls to catastrophic rock avalanches involving millions of cubic metres of material, frequently causing widespread damage to property and infrastructure, injury, and loss of lives (DTEC 2002). The impact is either direct (burial/destruction) or indirect through the formation and failure of landslide dams inducing catastrophic flooding downstream, or by falling into water bodies potentially creating waves of damaging proportions (Benn 1992).

A recent study on global patterns of loss of life from landslides by Petley (2012) illustrated that landslides are a major hazard particularly in areas with high rates of tectonic processes, high relief, intense rainfall, and high population density. Through a spatiotemporal analysis of a 7 year (2004-2010) global landslide fatality database, Petley (2012) identified 2620 non-seismic fatal landslides that have caused a total of 32,322 recorded deaths, clustering along tectonically active regions.

Research on landslides has a well-established history in New Zealand (Glade & Crozier 1999). The frequency of landslide occurrence, the magnitude of particular historical events and impact on human activity along the West Coast of the South Island has motivated several researchers to study different aspects of landslides such as, their role in landscape evolution of the Southern Alps as primary erosion agents and sources of sediment (Hovius et al. 1997; Korup 2005c, 2005d, Korup 2006b; Hewitt 2006; Hewitt et al. 2008; Korup et al. 2009) and as potential hazards (Whitehouse 1983, Whitehouse & Griffiths 1983; Bell 1994; Davies & Scott 1997; McSaveney & Davies 1998; Benn 2005; Hancox et al. 2005; Korup 2005b; Davies 2002, 2007). These studies have made significant contributions to the understanding of landsliding as a geomorphic process, common triggering and conditioning factors, interactions with other processes and potential impacts on communities.

In 2002, the West Coast Regional Council (WCRC) commissioned DTEC Consulting Ltd to conduct a natural hazard review which would summarize the existing literature on all natural hazards relevant to the region, identify progress and gaps in knowledge and provide recommendations for future research. Regarding landslides, the study defined relationships between mass movements and

common factors (controlling and triggering), presented frequency-magnitude relationships and reported impacts on people and infrastructure as well as effects on other geomorphic processes (e.g. landslide dams and subsequent catastrophic flooding). The development of a landslide inventory and hazard maps were also identified as important steps towards managing the landslide hazard in the region. Benn (2005) compiled a landslide inventory for the West Coast based on literature between 1867 and 2002. For this period, Benn (2005) identified that small-magnitude, high-frequency, rainfall-induced events have caused the most damage to property and infrastructure and at least 36 fatalities in the region. Although earthquakes have triggered deep-seated slides with deposits of the order of > 10^6 m^3, depending on the earthquake's magnitude, distance from the epicentre, soil characteristics and rock types, he concluded that intense or prolonged rainfall is the main trigger of slope failures in the region and argued that more research is required concerning the relationship between landslide occurrence and rainfall. However, landslides have also occurred in several instances without an obvious trigger mechanism. Examples of such events include the Aoraki/Mount Cook summit failure, 1991, Mt Fletcher, 1992 (McSaveney 2002), Mt Adams, 1999 (Hancox et al. 2005) and Mt Vampire, 2003 and 2008 (Cox et al. 2008; Cox & Allen 2009). McCahon et al. (2006) prepared a report on behalf of the West Coast Regional Council aiming to raise issues and make recommendations regarding the required actions that will better prepare the community to withstand the effects of a major earthquake and to recover from it more effectively. Based on an Alpine Fault earthquake scenario they discuss among other seismically induced hazards (shaking, liquefaction and seiches), the potential impact of co-seismic landslides on key lifelines such as the network services of water, sewage, transport, power and communications. England (2011) in an effort to fill the information gaps highlighted in the WCRC Natural Hazards Review (DTEC 2002) and Benn (2005), compiled a historic landslide catalogue, using existing catalogues and other available sources, and applied a GIS-based approach to produce a regional landslide susceptibility map for the West Coast region. Several site-specific geotechnical investigations have been also conducted (Power & Anderson 1992; Metcalf 1993; Yetton 1997; Cooper 2000), which have provided information on landslide-prone developments and infrastructure in populated areas.

Despite progress and available information, landslides still pose a threat to settlements and infrastructure in the area (McSaveney & Davies 1998; Seville & Metcalfe 2005; Benn 2005; Davies 2007). Guzzetti et al. (1999) argue that knowledge of slope processes appears insufficient for a comprehensive and exhaustive evaluation of landslide hazard and stress that landslide phenomena are still poorly understood, particularly at the regional scale. These limitations are reflected in the global patterns of landslide-associated fatalities (Petley 2012) which show that mass movements are still a major threat to human life, property and infrastructure in most tectonically active,

mountainous regions of the world. The relatively low rate of loss of life from landslides in Westland (36 fatalities since 1874; Benn 2005) is primarily due to the low population density. Today the mountainous landscape of the Western Southern Alps is a very popular attraction for both domestic and international tourists. As a result annual visitor numbers have increased and the region is further developing, significantly increasing the likelihood of greater impact from landslides. Mass movements such as the prehistorical Mt Wilberg (Chevalier et al. 2009) Round Top (Dufresne et al. 2009; Wright 1999) and Cascade (Barth 2013) rock avalanches as well as the more recent events of Mt Adams (Hancox et al. 2005) provide an indication of the very high level of hazard in the region.

Slope failures occurring in uninhabited areas such as the mountainous terrain of the western Southern Alps frequently go unnoticed or unreported. These events become hazards only when they impact developed areas and infrastructure or induce other geomorphic hazards (landslide dammed lakes, dambreak flooding, river aggradation). Therefore, in addition to the identification of potential landslide sources, it is crucial to investigate the runout behaviour of landslides and incorporate the findings into the hazard or susceptibility assessments. Considering the current progress and limitations, it is clear that further research is required in order to improve our understanding of landslide conditioning factors and triggering mechanisms as well as their runout behaviour, and to use this information to improve the existing hazard assessment methods.

This study develops a GIS-based approach for shallow landslide and debris flow susceptibility mapping in highly dynamic environments such as the western Southern Alps of New Zealand. A spatial database of landslide-related parameters is developed based on existing literature, statistical analyses and field observations. The application of fuzzy set theory in GIS environments is investigated as a potential regional scale landslide susceptibility assessment method, as it provides a way to deal with uncertainties and non-linear relationships between conditioning factors and landslide occurrence. Finally, a model is developed to identify the potential runout path and distance of the modelled landslide sources. The results have the potential to inform regional-scale land-use planning and to prioritize areas where hazard mitigation measures are required; and, ultimately, to effectively prevent mass movements from becoming disasters.

3.1.1 Landslide hazard and susceptibility assessment

Landslide hazard assessment, according to Varnes (1984), is performed by identifying areas potentially affected by a landslide, quantifying the probability of occurrence and estimating the magnitude (area, volume, rate of movement) of the mass movement (Petley 2010). In order to

establish the temporal frequency of slope failures and quantify the probability of occurrence, accurate and reasonably complete catalogues of historical landslide events are required (Guzzetti et al. 2005). Although an increasing number of studies use landslide inventories and catalogues in order to establish relationships between slope failures and predisposing factors, information on landslide magnitude is usually not available. Determining the volume of a mass movement requires information on the surface and sub-surface geometry of the slope failure and it is an especially challenging task when measurements of a large population of landslides over a large area are necessary (Malamud et al. 2004; Guzzetti et al. 2009). More recently, frequency–area statistics of landslides (Hovius et al. 1997; Stark & Hovius 2001; Guzzetti et al. 2002; Malamud et al. 2004; Korup 2005e; Guzzetti et al. 2009) have been used as a proxy for landslide volume and magnitude (Guzzetti et al. 2005). Although the development of a landslide inventory that includes the location and extent of previous landslides is relatively easy today with the availability of satellite imagery and areal photography (e.g. Google Earth), but to estimate the probability of occurrence within a specific period and conduct meaningful landslide hazard assessments, multi-temporal landslide data are essential but often not available (Dikau et al. 1996; Corominas et al. 1998; Remondo et al. 2003b; Ayalew et al. 2005). Therefore, landslide hazard is often represented by landslide susceptibility, which is the likelihood of a landslide occurring in an area on the basis of local terrain conditions (Brabb, 1984). Landslide susceptibility identifies areas potentially affected without implying the time frame within which a landslide might occur or the magnitude of the expected landslide. Susceptibility models are usually based on statistical relationships between known mass movements and conditioning factors (Remondo et al. 2003a), assuming that slope failures in the future will be more likely to occur under the conditions which led to past and present slope movements (Varnes et al. 1984; Carrara et al. 1991, 1995; Guzzetti et al. 1999; Dai & Lee 2002).

The use of digital spatial information for landslide susceptibility mapping dates back to late 1970s and early 1980s (Van Westen et al 2008) with pioneering studies in the field such as those by Brabb et al. (1978) and Carrara et al. (1977). The study by Carrara et al. (1991) is considered as milestone in the landslide literature, as it introduced the implementation of statistics using GIS for landslide zonation (Gokceoglu & Sezer 2009). Since then numerous GIS-based techniques have been proposed and tested in different environments. Sassa et al. (2009) through a review of literature for the period 2004-2009 found that GIS/remote sensing is the second most frequently cited method after field investigations. Comprehensive reviews and classifications of proposed methods for landslide hazard and susceptibility assessment can be found in Van Westen (1997), Aleotti & Chowdhury (1999), Guzzetti et al. (1999), Huabin et al. (2005), and Crozier & Glade (2005). These studies also provide discussions on the applicability and limitations of the available methods. In general, the existing

methods are classified as either qualitative or quantitative. Qualitative methodologies are mainly based on the expert judgement of the person (s) carrying out the susceptibility or hazard assessment, usually involving descriptive (qualitative) terms to represent the hazard zoning, whereas quantitative methods establish numerical relationships between conditioning factors and landslide occurrence. Qualitative methods include geomorphological hazard mapping (Rupke et al. 1988; Van Westen et al 2003), analysis of landslide inventories (Carrara & Merenda 1976; Chau et al. 2004, Colombo et al 2005; Galli et al 2008) and heuristic or index-based methods (Gupta & Joshi 1989; Dai et al 2002). Among them are also included semi-quantitative methods (Ayalew et al. 2004; Yoshimatsu & Abe 2006; Ladas et al. 2007; Kamp et al. 2008; Kouli et al. 2010; Kritikos & Davies 2011) which involve both expert evaluation and the concept of ranking and weighting factors. Commonly applied quantitative methods are geotechnical or physical-based methods (Montgomery & Dietrich, 1994; Dietrich et al. 1995; Terlien et al. 1995) and statistical analyses such as multivariate logistic regression (Carrara 1983; Carrara et al. 1991; Guzzetti et al. 1999; Dai et al. 2001; Ohlmacher & Davis 2003; Ayalew & Yamagishi 2005; Lee 2005; Duman et al. 2006; Wang et al. 2007; Lee 2007a), bivariate analysis (Van Westen et al. 2003; Lee & Choi 2004; Thiery et al. 2007; Neuhäuser & Terhorst 2007; Dahal et al. 2008a, b; Pradhan et al. 2010a), discriminant analysis (Carrara et al. 1991; Guzzetti et al. 1999; Dhakal et al. 2000; Guzzetti et al. 2005; Guzzetti et al. 2006) and artificial neural networks (ANN) (Ermini et al. 2005; Ercanoglu 2005; Pradhan & lee 2007; Pradhan et al. 2010b; Li et al. 2012).

In particular, statistical methods were developed to overcome the limitation of subjectivity in expert evaluation (Fall et al. 2006) and became very popular as a result of the development of GIS technology in the last few decades. Although there is still no optimum method for landslide hazard/susceptibility mapping, statistical methods are generally considered the most appropriate for landslide susceptibility mapping at regional scales because they are objective, reproducible and easy-to-update (He & Beighley 2008; Naranjo et al. 1994; Soeters & Van Westen 1996; Van Westen et al. 2006). Several studies have applied and compared different methods (Van Westen et al. 1999, Pistocchi et al. 2002; Süzen & Doyuran 2003; Ayalew et al. 2005; Komac 2006; Magliulo et al. 2009; Falaschi et al. 2009; Nandi & Shakoor 2009) providing insights on their predictive capability, technical aspects / applicability and limitations. Despite their popularity and extensive application in landslide susceptibility assessment, statistical approaches have also major limitations. Thiery et al. (2007) discuss a number of drawbacks of bivariate statistical approaches and reveal major limitations that concern all the statistical methods. These are: 1) their significant sensitivity to the quality and accuracy of the input thematic data and particularly to the landslide inventory used to train the model, 2) the absence of expert opinion which may result in a satisfactory statistical output in terms

of degree of fit, but may not be realistic in terms of physical meaning, 3) the number of landslide events to incorporate in the statistical model should be appropriate to the size of the study area, which means increased data requirements in large study areas and 4) the use of over-simplified input thematic data that control or trigger landslides, by only considering information that is relatively easily mapped or derived from a DEM.

The application of fuzzy logic in landslide susceptibility assessment has been proposed by many studies (Lee & Juang 1992; Juang et al. 1992; Ercanoglu & Gockeoglu 2002, 2004; Tangestani 2004; Lee & Lee 2006; Song et al. 2006; Saboya et al. 2006; Kanungo et al. 2006; Lee 2007b; Champati et al 2007; Kanungo et al. 2008; Kanungo et al. 2009; Pradhan 2010, 2011a, 2011b; Ercanoglu & Temiz 2011; Bui et al. 2012) as a way to overcome limitations deriving from inadequate data and insufficient knowledge on the relationship between conditioning factors and landslide occurrence (Thiery et al. 2006). The implementation of fuzzy logic can be either knowledge-driven based on subjective judgement to determine the relative importance of the predictive variables (Bonham-Carter 1994) or data-driven using information from landslide inventories. Herein, the application of fuzzy logic based on both landslide inventory data and user defined membership functions in GIS environment is investigated, to develop a landslide susceptibility index (LSI) suitable for regional scale hazard assessment and land-use planning.

3.2 Methodology

3.2.1 Fuzzy set theory

Fuzzy set theory was introduced by Zadeh (1965) as a method of representing the concept of partial set membership as opposed to the classical binary (two-valued) logic where set membership is represented as either completely true or completely false. It was based on the observation that human reasoning can utilize concepts and knowledge that do not have well-defined, sharp boundaries, as an alternative approach to overcome difficulties in developing and analyzing complex systems encountered by conventional mathematical tools (Yen & Langari 1999). Fuzzy logic has two different meanings in literature; according to Klir et al. (1997) it is viewed as either a system of concepts, principles and methods for dealing with various modes of reasoning which are approximate rather than exact in nature, or as a generalization of the various proposed multi-valued logics. Zadeh (1973), referring to the inability of conventional quantitative techniques of system analysis to deal with complex systems such as humanistic systems (human-centred), introduced the *principle of incompatibility* based on the following reasoning: "*...as the complexity of a system*

increases, our ability to make precise and yet significant statements about its behaviour diminishes until a threshold is reached beyond which precision and significance (or relevance) become almost mutually exclusive characteristics."(Zadeh 1973, p28). This statement implies that the behaviour of complex systems (e.g. human or environmental systems) cannot be quantified with meaningful accuracy using conventional quantitative approaches.

Despite its innovative problem-solving capabilities, it was not until a decade later that fuzzy set theory was successfully applied as control system by Mamdani (1974) and became popular primarily in industrial applications in Europe and Japan. Since then the concept of fuzzy logic has found a wide range of applications in various areas such as, control systems, decision-making, artificial intelligence and spatial analysis.

Fuzzy set theory can be considered as an extension of classical set theory (Ross 1995). In the classical set theory, an element has a clearly defined relationship with a set, which means that the element either belongs (1) or does not belong (0) to the set, therefore its membership degree value can be either 0 or 1.

$$\chi_A(x) = \begin{cases} 1, & x \in A \\ 0, & x \notin A \end{cases} \tag{3.1}$$

where the $\chi_A(x)$ is the indicator or characteristic function of element x representing the membership of element x in the set A.

In the fuzzy set theory, elements have varying degrees of membership in [0, 1] interval.

$$\mu_A(x) \in [0, 1] \tag{3.2}$$

where $\mu_A(x)$ is the degree of membership of the element x in the fuzzy set A; 1 represents full membership and 0 non-membership (Fig. 3.1).

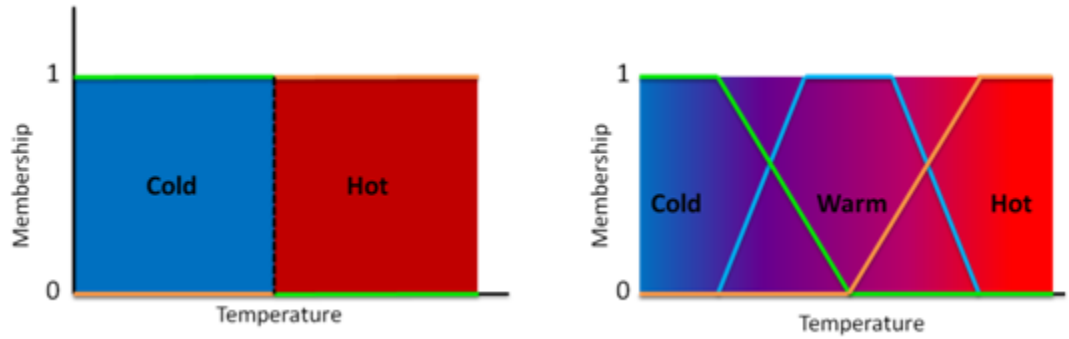

Figure 3.1 Membership functions for "cold" (green), "hot" (orange) and "warm" (blue) temperatures. Boolean logic (left) assumes that temperature is either "cold" below a specific threshold or "hot" above that threshold (never both). Fuzzy logic allows a gradual transition between "cold" and "hot" introducing intermediate values represented by the "warm" membership function.

3.2.1.1 Fuzzy logic in spatial analysis

In spatial analysis concepts like *close to, far from, steep* or *suitable* often do not have clearly defined boundaries, demonstrating a degree of vagueness or uncertainty. To illustrate the application of fuzzy set theory in spatial analysis we consider a hypothetical site suitability analysis problem. The problem involves identifying a suitable location to build a house on the basis of environmental criteria. The criteria to classify a site as suitable could be the following: *low* slope, *favourable* slope aspect, *close to* a State Highway and *not close to* faults. Although the above statements are vague or imprecise compared to precise values (e.g. slope angle ≤ 10^{o}, 135^{o} < slope aspect < 225^{o}, ≤ 1 km distance from State Highway, ≥ 1 km distance from faults), they correspond to the way a human perceives the factors controlling the suitability of a location. Using conventional approaches the above factors would be converted into classes with crisp boundaries. Therefore, if a location falls within the range of the assumed threshold values we would consider it, otherwise, even if it were very close to the class boundaries, it would be excluded from the analysis (e.g. if the distance from faults is 1 km, then we consider the location, but if the distance is 999 m we reject it). As a result neighbouring areas with a slight difference of criteria values may have different suitability. However, by introducing degrees of membership to the classification, locations close to class boundaries will also be included in the analysis by getting an appropriate membership value (e.g. locations with distance 999 m from faults will get a low membership value but they will still be considered), resulting in a more realistic representation of the site suitability (Fig. 3.2). In this sense (Ross 1995), points out that fuzzy systems are useful in two general contexts: in situations involving highly complex systems whose behaviours are not well understood, and in situations where an approximate, but fast solution is required.

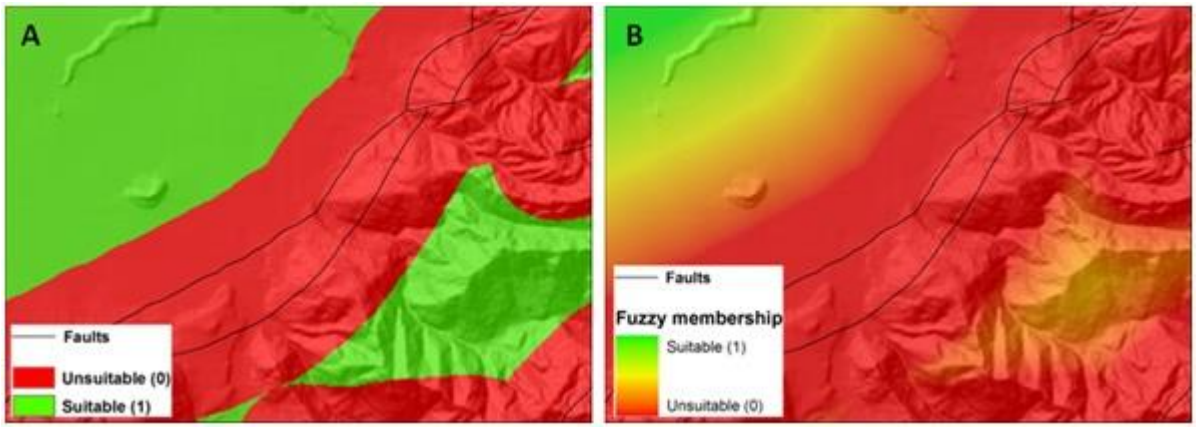

Figure 3.2 Example of site suitability based on distance from faults (≥ 1km) using (A) crisp boundaries and (B) a fuzzy linear membership function. Discrete boundaries are rarely applicable to spatial properties and natural phenomena.

3.2.1.2 Degree of membership vs. probability

Degrees of membership and probabilities may be easily confused as being the same, as they both have values ranging between 0 and 1. However they have a small, yet important difference. The following example illustrates this difference. Assume that we have been asked to identify an area with "very low landslide hazard" in order to build critical infrastructure. According to the available information there are two areas that match this criterion, the area X where there is 0.9 probability of no landslides within the next 100 years and the area Y which has 0.9 membership in the set "very low landslide hazard". Interpreting the above information the X area has 90% chance of having not a single slope failure in the next 100 years and 10% chance of having a landslide, even a catastrophic rock avalanche! On the other hand, the 0.9 membership means that the Y area has "very low landslide hazard" and even if a slope failure occurs it is highly unlikely to be a large magnitude mass movement. Thus, the prior probability 0.9 becomes a posterior probability of 1 or 0 after the 100 years period at the X area, whereas the 0.9 membership value remains the same regardless how many years have passed, as it indicates the relationship between the landscape and the fuzzy concept "very low landslide hazard".

3.2.2 Application of fuzzy logic in landslide susceptibility modelling

As previously described, landslide susceptibility is commonly expressed as the spatial correlation between predisposing factors (terrain, climatic, tectonic, human activity) and the distribution of observed landslides in a region (Brabb 1984; Crozier & Glade 2005; Thiery et al. 2007). Since the parameters involved in landslide susceptibility assessment are fuzzy in nature and are commonly classified by using fuzzy descriptions such as *low, moderate, high, steep, favourable, close to* etc., and the slope failure mechanism is a complex phenomenon not completely understood, particularly

at the regional scale (Guzzetti et al. 1999), the application of fuzzy logic seems appropriate in order to deal with uncertainties and non-linear relationships between conditioning factors and landslide occurrence. Fuzzy logic has been applied for spatial data integration in mineral exploration (Bonham-Carter 1994; Luo & Dimitrakopoulos 2003; Porwal et al. 2006) and landslide susceptibility assessment as either "knowledge-driven" (Juang et al. 1992; Pistocchi et al. 2002; Saboya et al. 2006; Miles & Keefer 2007; Champati et al 2007; Wang et al. 2009) or "data-driven" (Ercanoglu & Gockeoglu 2002, 2004; Lee & Lee 2006; Song et al. 2006; Kanungo et al. 2006; Lee 2007b; Kanungo et al. 2008; Kanungo et al. 2009; Pradhan 2010, 2011a, 2011b; Ercanoglu & Temiz 2011; Bui et al. 2012), based on the assumption that spatial data (i.e. predisposing factors) are members of a set, either mineral favourability or landslide susceptibility.

The fundamental component of any fuzzy logic model lies in deriving the membership function. The membership function essentially associates the fuzzy linguistic terms (*low, moderate, high, steep, favourable, close to* etc.) to degrees of membership, quantifying the "degree of belonging" of a variable to a set. In most of the fuzzy models, membership functions are chosen arbitrarily by the modellers based on their experience and perspectives. Thus, the membership functions given by two modellers could be quite different. Alternatively, membership functions can be derived based on available datasets in order to minimize the subjectivity of knowledge-driven models. In the present study, the membership functions between conditioning factors and landslide occurrence have been derived by applying both knowledge- and data-driven techniques.

3.2.2.1 "Data-driven" fuzzy memberships

Frequency-ratio

Frequency-ratio (FR) is defined as the relative frequency of landslides in a factor category (e.g. landslides within the 20^{o}-25^{o} slope category) to the relative frequency of all landslides in the area or alternatively, as the landslide density within each factor category normalized by the landslide density over the entire area.

$$Frequency\ ratio = \frac{N_{(Li)}/N_{(Ci)}}{N_{(L)}/N_{(A)}} \tag{3.3}$$

where $N_{(Li)}$ is the number of landslide pixels in the category *i*, $N_{(Ci)}$ is the total number of pixels in the category *i*, $N_{(L)}$ is total number of landslide pixels in the study area and $N_{(A)}$ is the total number of pixels of the study area.

The concept of frequency-ratio has been extensively used in statistical approaches such as the weights of evidence method (Bonham-Carter 1994), in order to evaluate the importance of each factor in the occurrence of landslides and calculate the corresponding weights. Frequency-ratio values greater than 1 indicate higher densities of landslides in the category compared to the density of landslides in the entire study area (landslide inventory) and a higher correlation between the category and slope instability, whereas values < 1 indicate lower correlation. It also provides a simple means to derive "data-driven" fuzzy membership functions between factors and landslide occurrence. In order to derive the fuzzy membership function the FR values of the different categories are normalized by the higher FR value within the factor (Lee 2007b; Pradhan 2010, 2011a, 2011b). Therefore, the degrees of membership essentially reflect the landslide density in each factor category (Fig. 3.3).

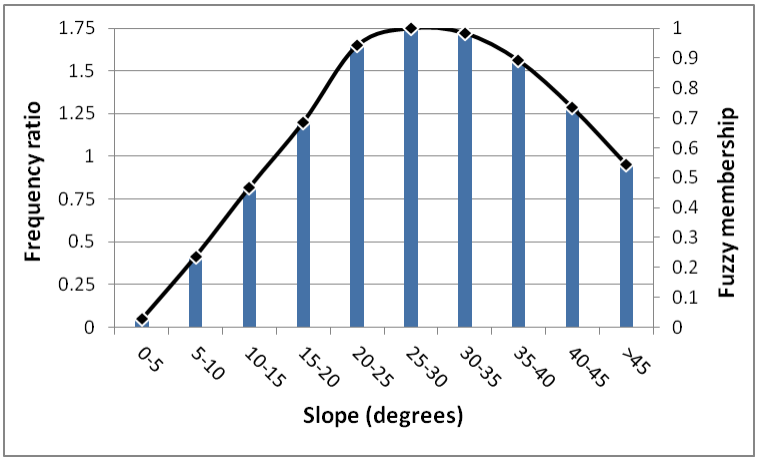

Figure 3.3 Landslide frequency ratio plotted against slope angle (classified in 5° intervals). The shape of the distribution represents the fuzzy membership function (black line) of slope angle.

Cosine amplitude

The cosine amplitude method (Ross 1995) is a widely-applied similarity method (Ercanoglu & Gockeoglu 2004; Song et al. 2006; Kanungo et al. 2006, 2009; Ercanoglu & Temiz 2011) used to establish relationships among elements of two or more data sets. Assuming that n is the number of data samples (categories of a factor used in the analysis) represented as an array X:

$$X = \{x_1, x_2, \ldots, x_n\}, \quad (3.4)$$

and that each of its elements, x_i, is a vector of length m (i.e. the size of the raster image) and can be expressed as:

$$X = \{x_{i1}, x_{i2}, \ldots, x_{im}\} \quad (3.5)$$

then each element of a relation r_{ij}, results from a pair-wise comparison of a factor category x_i with a category of the landslide distribution layer x_j (landslide or non-landslide). According to the cosine amplitude method the strength (degrees of membership) of the relationship or similarity r_{ij} between categories of thematic data layers and the categories of landslide distribution layer are calculated by the following equation with values ranging from 0 to 1 ($0 \leq r_{ij} \leq 1$):

$$r_{ij} = \frac{\left|\sum_{k=1}^{m} x_{ik} x_{jk}\right|}{\sqrt{\left(\sum_{k=1}^{m} x_{ik}^2\right)\left(\sum_{k=1}^{m} x_{jk}^2\right)}} \quad (3.6)$$

Based on the cosine amplitude concept Kanungo et al. (2006) defined the r_{ij} value for any given factor category as the ratio of the total number of landslide pixels in the category to the square root of the product of the total number of pixels in that category and the total number of landslide pixels in the area. Values of r_{ij} close to 1 indicate similarity whereas values close to 0 indicate dissimilarity between the two datasets.

3.2.2.2 "User-defined or knowledge-driven" fuzzy memberships

In knowledge-driven fuzzy models the membership values can be selected based on subjective judgment (Bonham-Carter 1994) using if-then rules (Miles & Keefer 2007), or they can be derived by various functions representing the relationships between factors and the phenomena being studied, such as "J-shaped", "S-shaped", "triangular", "trapezoidal" and "linear" functions.

Recently ESRI incorporated the Fuzzy Membership tool in the Spatial Analyst extension of ArcGIS 10 as an alternative way to transform the input data into membership values ranging from 0 to 1 by selecting a user-specified fuzzy membership function. These functions include:

Fuzzy large

Fuzzy Large is a sigmoid-shaped function used when the larger input values are more likely to be a member of the set, in this case landslide occurrence;

$$\mu(x) = \frac{1}{1 + \left(\frac{x}{f2}\right)^{-f1}} \quad (3.7)$$

where μ(x) is the membership value of category x, f2 is the midpoint and f1 the spread of the function.

The defined midpoint identifies the crossover point (assigned a membership of 0.5) with values greater than the midpoint having a higher possibility of being a member of the set and values below the midpoint having a decreasing membership. The spread parameter defines the shape and character of the transition zone (Fig. 3.4). The spread and midpoint parameters are subjectively determined and reflect the expert opinion. The fuzzy large function is suitable for modelling parameters where increasing the parameter value often results in higher susceptibility (e.g. rainfall, soil drainage).

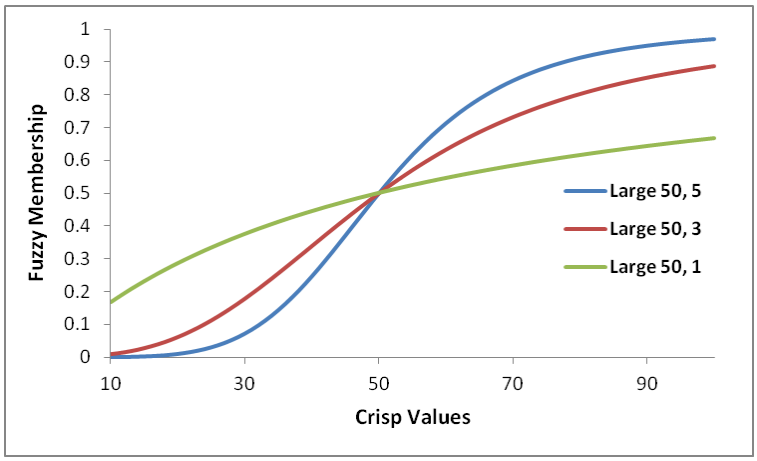

Figure 3.4 Fuzzy Large membership function.

Fuzzy small

Contrary to the Fuzzy Large, the Fuzzy Small function is used when the smaller input values are more likely to be members of the landslide susceptibility set (e.g. proximity to faults and streams).

$$\mu(x) = \frac{1}{1 + \left(\frac{x}{f2}\right)^{f1}} \tag{3.8}$$

where μ(x) is the membership value of category x, f2 is the midpoint and f1 the spread of the function (Fig. 3.5).

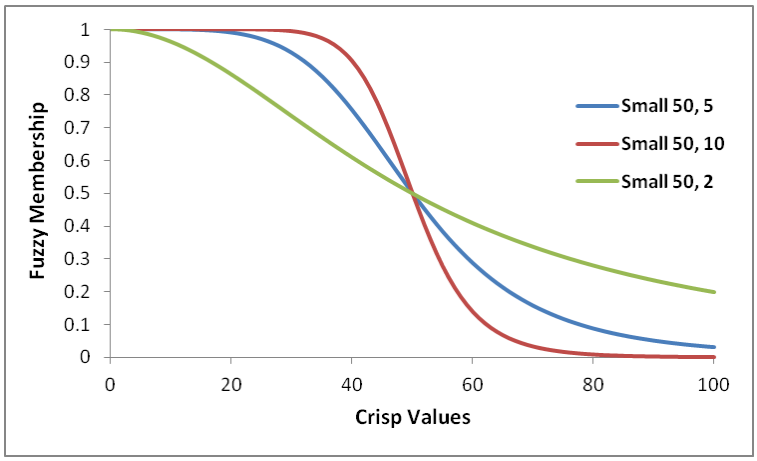

Figure 3.5 Fuzzy Small membership function.

Fuzzy Gaussian

The Fuzzy Gaussian function transforms the original values into a normal distribution. The midpoint here defines the strongest membership with the remaining input values decreasing in membership as they move away from the midpoint in both the positive and negative directions (Fig. 3.6).

$$\mu\,(x) = \; e^{-f1*(x-f2)^2} \qquad (3.9)$$

where μ(x) is the membership value of category x, f2 is the midpoint and f1 the spread of the function.

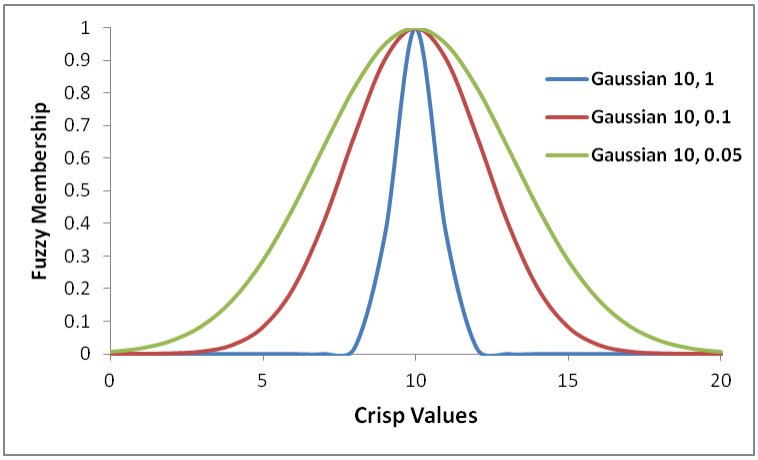

Figure 3.6 Fuzzy Gaussian membership function.

In the present study area the number of rainfall-triggered shallow landslides and debris-flows increases with slope angle up to approximately 35°-40° and then decreases close to the very steep

mountain ridges. Therefore, the slope factor can be approximately represented by a Gaussian fuzzy membership with the midpoint assigned to the class 35°-40° and an appropriate spread.

Fuzzy near

The Fuzzy Near function returns a curved peak of membership over an intermediate value, similar to the fuzzy Gaussian but decreasing at a faster rate, with a narrower spread.

$$\mu(x) = \frac{1}{1 + f1(x - f2)^2} \tag{3.10}$$

It is suitable when a particular intermediate class or classes have significantly more influence compared to the others (Fig. 3.7).

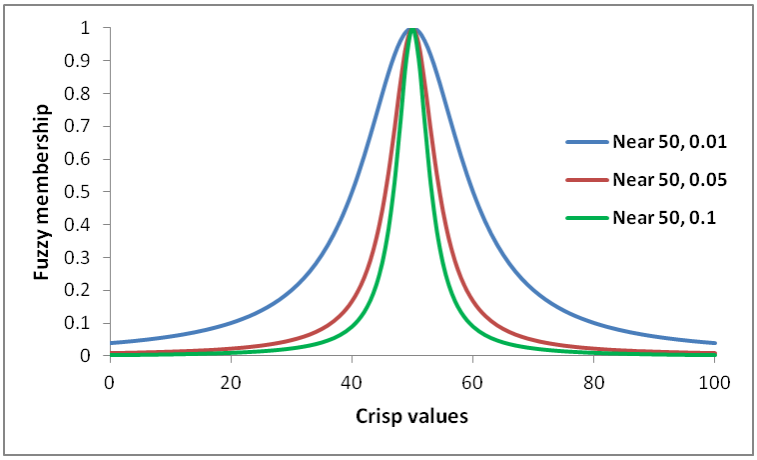

Figure 3.7 Fuzzy Near membership function.

Fuzzy linear

Finally, the Fuzzy Linear function assumes a linear relationship between user-specified minimum and maximum values. Any value below the minimum will be assigned 0 (definitely not a member) and any value above the maximum 1 (definitely a member).

$$\mu(x) = \begin{cases} 0 & x \le a \\ \dfrac{x - a}{b - a} & a < x < b \\ 1 & x \ge b \end{cases} \tag{3.11}$$

where $\mu(x)$ is the membership value of category x and α, b is the minimum and maximum values respectively (Fig. 3.8).

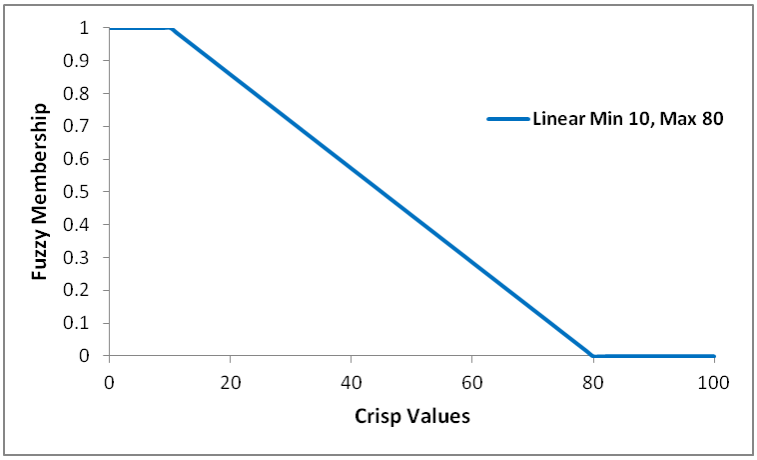

Figure 3.8 Linear fuzzy membership function.

Although its linearized sigmoid shape provides a simplified model, it can be particularly useful when there is no adequate information on the factor - landslide susceptibility relationship and only the effect of the minimum and maximum values is known. For example, provided that no other information exists, the proximity to faults factor can be represented by the linear membership function based only on the observation that within 100 m distance from a fault, landslides have the highest density and significantly decrease up to 3 km distance.

3.2.2.3 Aggregation

To derive the landslide susceptibility index (LSI) map, the "fuzzified" factors represented by information layers in raster format with values ranging from 0 to 1 need to be combined. Aggregation operations on fuzzy sets are used to combine them to a single set (Dubois & Prade 1985; Zimmermann 1991). Bonham-Carter (1994) discusses five operators, the fuzzy AND, fuzzy OR, fuzzy algebraic Product, fuzzy algebraic Sum and fuzzy Gamma operator.

Fuzzy AND

This is equivalent to a Boolean AND (logical intersection) operation on classical set values of (1, 0). It is defined as:

$$\mu_{(x)} = MIN(\mu_A, \mu_B, \mu_C, \dots) \qquad (3.12)$$

where $\mu_{(x)}$ is the combined membership value, μ_A is the membership value for thematic layer A at a particular location, μ_B is the membership value for thematic layer B, and so on. The effect of this

operator is to cause the output map to be controlled by the lowest fuzzy membership value occurring at each location (e.g. if a location has a membership value of 0.9 according to map A and 0.5 according to map B, then the membership for the combination using fuzzy AND is 0.5).

Fuzzy OR

The fuzzy OR operator is similar to the Boolean OR (logical union) in that the output membership values are controlled by the maximum values of any of the input thematic layers, for any particular location. The fuzzy OR is defined as:

$$\mu_{(x)} = MAX(\mu_A, \mu_B, \mu_C, \ldots) \tag{3.13}$$

Using this operator, the combined membership value $\mu_{(x)}$ at a location is influenced only by the most suitable (or susceptible to landsliding) of the thematic layers.

Fuzzy Algebraic Product

This function is defined as:

$$\mu_{(x)} = \prod_{i=1}^{n} \mu_i \tag{3.14}$$

where μ_i is the fuzzy membership function for the i^{th} map, and i = 1, 2, . . . n are the number of thematic layers to be combined. The combined fuzzy membership value using this operator tends to be very small, due to the effect of multiplying several numbers less than 1. The output is always smaller than, or equal to, the smallest contributing membership value.

Fuzzy Algebraic Sum

This operator is complementary to the fuzzy algebraic product, being defined as:

$$\mu_{(x)} = 1 - \prod_{i=1}^{n} (1 - \mu_i) \tag{3.15}$$

The result is always larger than (or equal to) the largest contributing fuzzy membership value. Therefore if two thematic layers both favouring a hypothesis strengthen one another, and their combined result is more supportive than either thematic layer taken individually.

Fuzzy Gamma Operation (γ)

This is defined in terms of the fuzzy algebraic product and the fuzzy algebraic sum by the following formula:

$$\mu_{(x)} = \left(1 - \prod_{i=1}^{n}(1-\mu_i)\right)^{\gamma} * \left(\prod_{i=1}^{n}\mu_i\right)^{1-\gamma} \quad (3.16)$$

where *γ* is a parameter in the range (0, 1). When *γ* is 1, the combination is the same as the fuzzy algebraic sum; and when *γ* is 0 the combination equals the fuzzy algebraic product.

In this study, the fuzzy gamma operator was applied as it establishes the relationships between the multiple input criteria and does not simply return the value of a single membership set as the Fuzzy Or and Fuzzy And do. It also provides a compromise between the increasing tendencies of the fuzzy algebraic sum and the decreasing effect of the fuzzy algebraic product (ESRI 2011). The γ value is a user-defined parameter introducing a degree of subjectivity, even to the data-driven models. In the context of landslide susceptibility the γ value determines how much the favourable and non-favourable factors will affect the overall landslide susceptibility. Similar to the negative and positive factor weights in statistical methods, in fuzzy logic, values close to 0 and 1 tend to decrease or increase respectively the overall landslide susceptibility of a site. The difference however is that the user decides the "importance" of the favourable and non-favourable conditions by adjusting the γ value. Therefore, the selection of the appropriate γ is a critical step in the modelling procedure in order to derive a realistic output.

3.3 Data

The fundamental data layers required in any landslide susceptibility or hazard and risk assessment can be subdivided into four main groups: landslide inventory data, environmental (controlling) factors, triggering factors and elements at risk (Van Westen et al. 2006).

3.3.1 Landslide inventory

Landslide inventory data are critical as they provide insights on the location of mass movements, failure mechanisms (type), causal and triggering factors, frequency of occurrence, volumes and the damage that has been caused (Van Westen et al. 2008). A landslide inventory map should at least indicate the location and extent of previous landslides (Dahal et al. 2008a; He & Beighley 2008). In order to establish the relationships between landslide occurrence and conditioning factors and ultimately produce maps that predict the landslide hazard and risk in their respective areas, several studies (Van Westen et al. 2003; Colombo et al. 2005; Guzzetti et al. 2005; Ayalew & Yamagishi 2005; Thiery et al. 2007; He & Beighley 2008) focus on developing landslide inventories or catalogues during the initial stages of the assessment. As a result, many different techniques have been proposed for landslide data acquisition such as remote sensing techniques, field investigation methods, review of archives and literature as well as landslide deposit dating methods. A comprehensive review of existing techniques can be found in Van Westen et al. (2008).

The landslide inventory map for the present study area was constructed by combining spatial data from various sources. Initially, landslide data were obtained from the Greymouth (Nathan et al. 2002), Aoraki (Cox & Barrell 2007) and Haast (Rattenburry et al. 2010) QMaps developed by GNS. Most of the landslides included in the QMap dataset were mapped primarily using aerial photos, with limited field validation (Nathan et al. 2002, Cox & Barrell 2007) therefore they are not accompanied by specific information about the type, triggering mechanism or age of the slope failure. However, the data are provided as polygons in vector format and can be directly used in the analysis and easily combined with data from other sources. England (2011) compiled a historic landslide catalogue for the West Coast region using various data sources such as the GNS landslide catalogue and the WCRC landslide archives. The catalogue includes 1987 events along the West Coast that occurred between 1900 to 2010. He also constructed a landslide inventory based on aerial photograph interpretation, supplemented by satellite imagery (Google Earth) and field observations. From the catalogue and inventory 106 landslide events located within the study area were obtained. An additional 197 landslide locations were obtained from the New Zealand Land Cover Database 2 (Ministry for the Environment 2004). These were primarily areas of subsoil and parent material exposed due to erosion identified by Landsat 7 satellite imagery analysis, acquired during summer 2001/02. Landslide source areas were also identified using satellite imagery from Google Earth. The identified areas were digitized and transferred into ArcGIS with an accuracy of ± 100 m (Fig. 3.9).

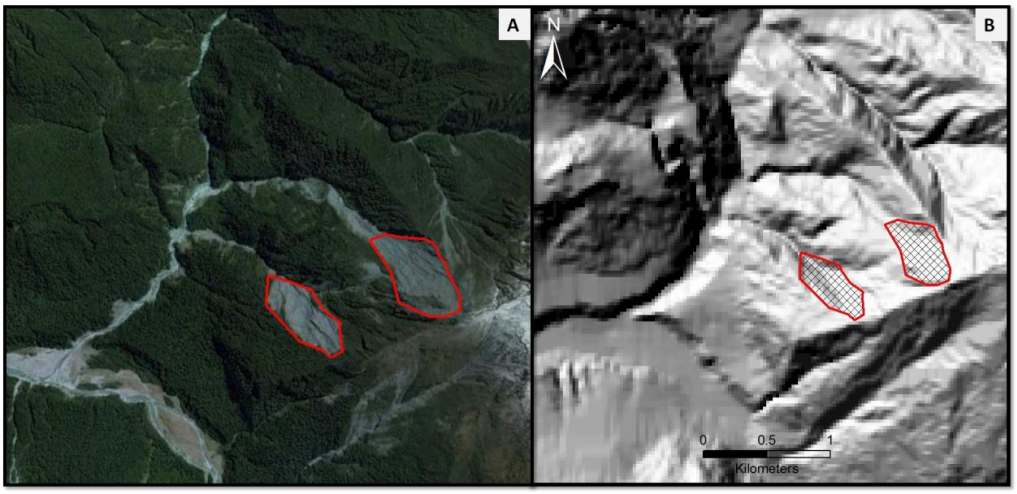

Figure 3.9 A) Digitized shallow landslide sources from Google Earth, B) polygons imported in ArcGIS with variable accuracy (±100m).

Finally all the above data were combined into a single information layer using the Union function resulting in 706 polygons, covering an area of approximately 202 km^2. Figure 3.10 shows the spatial distribution and extent of the landslide events used as landslide inventory.

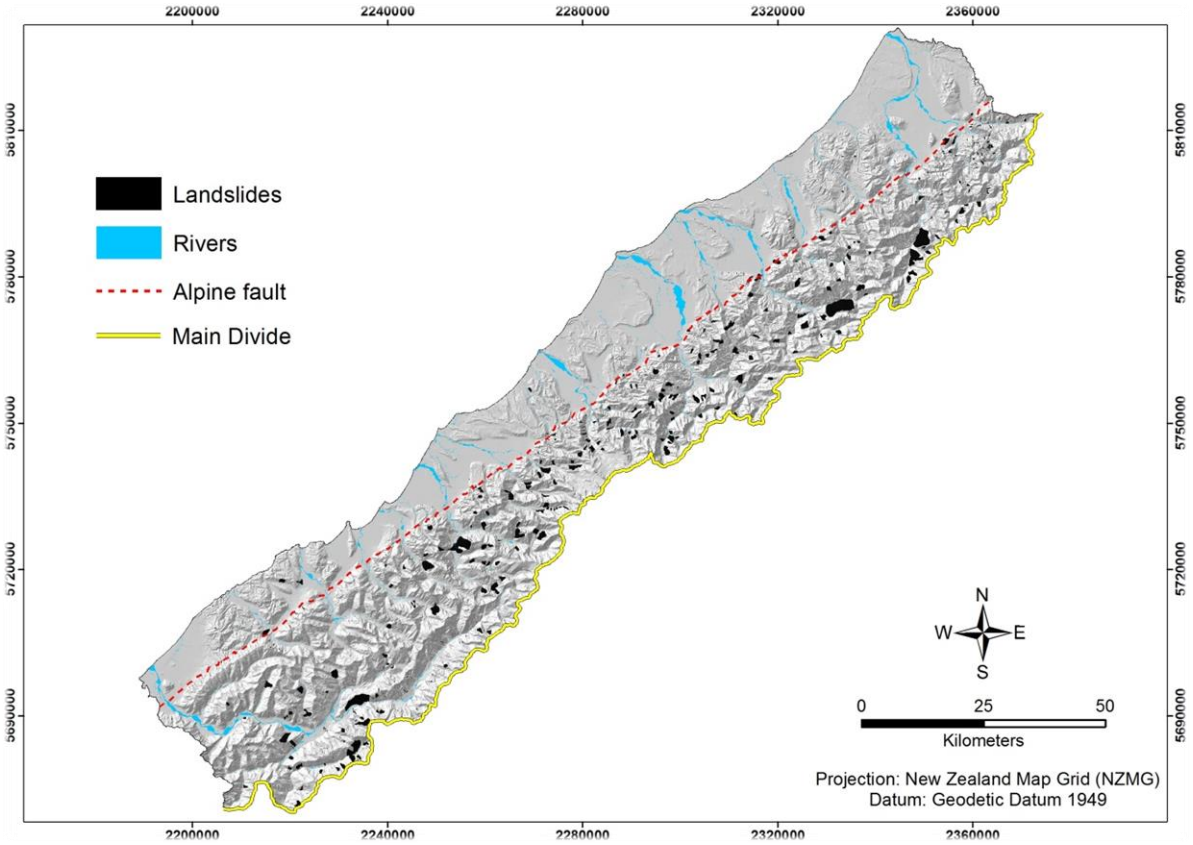

Figure 3.10 Landslide inventory map of the study area.

3.3.2 Landslide controlling and triggering factors

Two general categories of factors are commonly used to determine landslide hazard in an area: controlling (or intrinsic) factors which contribute to, and determine landslide susceptibility as well as triggering (extrinsic) factors which may trigger landslides in a given, already susceptible area. The selection of the most important factors that control landslide susceptibility is a critical step in any assessment and it is based on expert opinion. Therefore, the process is always subject to a degree of uncertainty as to whether the most important parameters have been taken into consideration and whether they have been correctly defined (Voogt 1983, Heywood et al. 1995). Although there is no rule for criteria selection, the following procedure was carried out to ensure that the most important factors are included. Initially, critical factors addressed in relevant literature were identified. From these factors only those important for the study area based on previous research in West Coast, data availability and field observations were selected. The purpose was to include the most significant factors and at the same time avoid over-parameterization of the model. Finally, from the selected datasets only those with appropriate accuracy (resolution) that would produce meaningful results when combined were used. The ten factors considered in the analysis are:

- Slope angle
- Geological formations (lithology)
- Land cover
- Soil drainage
- Soil induration
- Proximity to faults
- Proximity to streams
- Slope aspect
- Curvature
- Rainfall intensity

The first nine thematic layers are the environmental (controlling) factors whereas rainfall intensity is considered as the main triggering factor (this study does not consider coseismic landslides). The role

of each factor in landslide susceptibility and how it was obtained and processed via GIS are described below.

Slope angle

Slope angle is considered to be a critical factor in mass movement initiation and is the most commonly used topographic attribute in landslide susceptibility and hazard assessments (Van Westen et al. 2008). The premise of its importance is that the greater vertical component of gravity (Donati & Turrini 2002) at steeper slopes results in increased gravity-induced shear stress in the soil, rock or other unconsolidated material in the slope, increasing the probability of landslide occurrence (Dai & Lee 2002; Lee & Choi 2004; He & Beighley 2008). Conversely, low gradient slopes are generally associated with lower shear stress and are expected to have a lower frequency of slope failures (Lee & Sambath 2006; Lee & Talib 2005). Furthermore, slope angle controls surface runoff which plays primary role as an erosional agent in mountainous terrain (Korup et al. 2005). However, it has been observed that some steep natural slopes, such as those resulting from outcropping bedrock, may not be susceptible to rainfall triggered shallow landslides (Dai et al. 2001; Dai & Lee 2002; Lee & Sambath 2006; Lee & Talib 2005).

The slope angle map was derived from a 25m DEM prepared for the Foundation for Research, Science and Technology by Landcare Research in 2002. The DEM was generated using digital topographic data (20m contours and spot heights) supplied by Land Information New Zealand (LINZ) following a procedure described in detail by Barringer et al. (2002). Accuracy assessment of the DEM was performed by means of comparison with a very high resolution LIDAR-derived DEM (2m) indicating that its spatial accuracy varies between different landforms (lakes, river channels, riverbeds, floodplains etc.) and the areas of greatest errors are predominantly confined to valley floors (Barringer et al. 2002). However, with overall RMS error of 8.15 m the DEM meets the internationally accepted accuracy standards as set out by US Geological Survey (USGS 1997) and is appropriate for regional scale studies.

To calculate the slope angle from the DEM the Slope function of ArcGIS 9.3 was utilized. The function calculates the maximum rate of change in elevation over the distance between a cell and its eight neighbour cells by identifying the steepest downhill descent from that cell. Conceptually, the slope function fits a plane to the elevation values of a 3 x 3 cell neighbourhood around the processing or centre cell (ESRI 2011). The slope value of this plane is then calculated using the average maximum technique (Burrough & McDonell 1998).

Many variations of slope classes can be found in literature such as equal- or variable-sized intervals. Commonly used intervals are 5^{o} (Lee 2004, 2005; 2007a, 2007b; Lee & Lee 2006; Lee & Talib 2005) and 10^{o} (Dai et al. 2001; van Westen et al. 2003; Ercanoglu & Gökceoglu 2004; Can et al. 2005; Dahal et al. 2008a). The slope grid was reclassified: (1) 0-5°, (2) 5-10°, (3) 10-15°, (4) 15-20°, (5) 20-25°, (6) 25-30°, (7) 30-35°, (8) 35-40°, (9) 40-45°and (10) >45°. The purpose was to take into account the effect of small slope changes on slope stability and at the same time avoid using a large number of classes. Although the > 45^{o} class groups a wide range of slope values into a single category, it was considered appropriate as it includes only the 9.8% of the study area.

Lithology

Lithology is a fundamental factor in slope stability as it is directly related to the rock mass shear strength and permeability which controls the resistance to weathering and erosional processes (Donati & Turrini 2002).

The Alpine Fault divides the study area into two distinct geological provinces, these are: the Torlesse composite terrane mostly comprised by quartzofeldspathic indurated sedimentary rocks, known as greywacke, that have in places been metamorphosed to semischist or schist (Haast Schist) to the southeast; and early Paleozoic metasedimentary rocks of the Buller terrane (Cooper 1989) with mid-Paleozoic igneous intrusions (Cooper & Tulloch 1992; Mortimer et al. 1999) to the northwest. The northwest region is predominantly coastal lowland covered by Quaternary moraines and clastic sediments consisting of unconsolidated gravels, sand and silt. A narrow zone of mylonite has been also mapped immediately southeast of the Alpine Fault (Cox & Barrell 2007).

The required data were obtained by combining the information on geological units (available as polygons in shapefile format) from the Greymouth (Nathan et al. 2002), Aoraki (Cox & Barrell 2007) and Haast (Rattenburry et al. 2010) QMaps. However, directly using the geological unit classifications from the QMaps would result in a large number of geological formations. Therefore, geological formations with similar characteristics were grouped in the same category. An initial classification was made in order to distinguish main rock groups such as sedimentary, metamorphic, and igneous. Then, a second classification followed for each group to distinguish geological formations based on their predominant grain size and metamorphic grade. The resulting categories are: 1) Quaternary sediments (unconsolidated clastic sediments), 2) coarse grained sediments, 3) medium grained sediments, 4) fine grained sediments, 5) low - medium grade metamorphic, 6) high grade metamorphic, 7) granitoids, 8) mafic extrusive, 9) limestones and 10) peat.

Land cover

Land cover (vegetation) is also an important factor affecting slope stability as it influences the surface runoff, infiltration of meteoric water and erosion susceptibility. The extent and type of vegetation is assumed to affect the degree of erosion based on the general observation that bare or sparsely-vegetated slopes are more exposed to erosional processes compare to densely vegetated areas (Dahal et al. 2008a). Additionally, the root systems of trees, often act as a natural anchorage, improving the short-term slope stability (Dahal et al. 2008a; Dai & Lee 2002) (long-term landslide erosion is related to other factors such as uplift rates). Land cover is also directly related to the surface runoff and the infiltration of meteoric water (Donati & Turrini 2002).

Land cover data were obtained from the New Zealand Land Cover Database 2 (MfE 2004). The Land Cover Database 2 (LCDB2) is a thematic classification of 43 land cover and land use classes in New Zealand. It is based on Landsat 7 ETM+ satellite imagery acquired over the summer of 2001/02 with spatial resolution of 15m. The land cover classes were grouped into the following categories: 1) Bare or lightly vegetated surfaces, 2) Forest, 3) Grassland, 4) Scrub and shrubland, 5) Wetland, 6) Cropland and 7) Artificial areas.

Soil drainage

The soil parameters used in landslide hazard and susceptibility assessments usually depend on the method applied and scale of the study. In regional-scale assessments, typical soil parameters include the soil type (Lee 2007a), material and texture (Lee & Choi 2004; Lee et al. 2002; Lee & Lee 2006), drainage and depth or effective thickness (Lee & Choi 2004; Lee et al. 2002); whereas site - specific (large scale) investigations using physically based models usually involve parameters such as soil depth (Gorsevski et al. 2006) cohesion, moisture content, bulk density and unit weight (Gorsevski et al. 2006; Ohlmacher 2007). In this study, two soil parameters are considered, the soil drainage and induration. The drainage reflects the water content of the soil (how fast the water is removed from the soil) and it is related to the ability to generate pore water pressures. Also, it may act as a sliding surface between bedrock and the soil cover increasing its instability.

Soil data were obtained from the Land Environments of New Zealand (LENZ) produced by Landcare Research. LENZ is an environmental classification of New Zealand that is designed to provide a framework for addressing a range of conservation and resource management issues (Leathwick et al. 2002). The information on soil properties is based on data from the New Zealand Land Resource Inventory (NZLRI) and the National Soils Database (NSD) with additional observations from field mapping (Leathwick et al. 2002). However, the accuracy and reliability of the soil thematic layers is

variable mainly due to the wide variation in map scale and quality of the underlying soil surveys (early maps in non-agricultural landscapes were at scales of 1:253440) and the limited measurements of soil chemical and physical attributes. The drainage layer provided by LENZ describes the internal drainage of soils in terms of the soil attributes that develop under different drainage conditions. The classification according to LENZ is: 1) Very poor, 2) Poor, 3) Imperfect, 4) Moderate and 5) Good (well drained). The same classification was applied for the soil drainage information layer used in the landslide susceptibility model.

Soil induration

Soil induration (or soil hardness) is a measure of how hard the soil is and it is quantified by how much force is required to break the soil. Therefore, less indurated soils are more susceptible to erosion compare to strongly indurated. Following the same classification provided by LENZ, the information layer was classified into five categories: 1) Non-indurated, 2) Very weakly indurated, 3) Weakly indurated, 4) Strongly indurated and 5) Very strongly indurated.

Proximity to faults

The spatial correlation between faults and slope failures has been illustrated previously (Eggers 1987; Dramis & Sorriso-Valvo 1994; Korup 2004). Faults generally reduce the strength of the rock mass by breaking and various other weakening mechanisms (Warr & Cox 2001; Brune 2001; Kellog 2001). Based on regional airphoto reconnaissance Korup (2004) argued that tectonic weakening of bedrock along the Alpine Fault Zone (AFZ) in South Westland and northern Fiordland, has favoured erosion of schist-derived mylonite and cataclasite by a variety of slope failures. Petley (2012) stresses the role of seismic activity, in addition to directly triggering mass movements, in weakening slopes allowing the mobilization of material by subsequent rainfall events in tectonically active environments.

Fault lines in the field area were obtained in vector format from the Greymouth (Nathan et al. 2002), Aoraki (Cox & Barrell 2007) and Haast (Rattenburry et al. 2010) QMaps. By applying buffer analysis the study area was divided into a number of zones based on horizontal distance from faults. The task was performed by developing and combining a series of layers of varying buffer distances from the fault lines, into a single spatial dataset. The classes chosen for the study area are: 1) 0-100 m, 2) 100-500 m, 3) 500-1000 m, 4) 1000-2000 m, 5) 2000-3000 m and 6) >3000 m.

Proximity to streams

The effect of river channel incision on hillslope processes and landscape evolution is well established (Snyder et al. 2000; Whipple 2004; Korup 2004; Larsen & Montgomery 2012). Larsen & Montgomery (2012) argue that hillslopes in rapidly uplifting landscapes respond to river incision into bedrock by steepening to a maximum stable (threshold) angle, and observe increased landslide erosion rates as hillslope angles approach and exceed the threshold angle. Korup (2004) identified fluvial undercutting (causing high rates of shear stress due to loss of lateral support) as a key triggering mechanism of aseismic slope instability. Proximity to streams has been used in many landslide hazard and susceptibility assessment studies in order to incorporate localised processes such as terrain modified by gully erosion (Dai & Lee 2002; Dai et al. 2001), stream flow undercutting the banks (Donati & Turrini 2002; Saha et al. 2002; Van Westen et al. 2003), or stream channel erosion (headward and back erosion) initiating slope failure (He & Beighley 2008).

Drainage network data in shapefile format (polygons and polylines) were obtained from the New Zealand topographic maps (Topo50 series) provided by Land Information New Zealand (LINZ). Using buffer analysis the study area was divided into the following classes based on horizontal distance from the drainage network: 1) 0-100 m, 2) 100-200 m, 3) 200-300 m, 4) 300-400 m, 5) 400-500 m, 6) >500 m.

Slope aspect

Slope aspect is essentially the direction of slope. The effect of aspect on slope instability could be direct, as a result of the exposure to drying winds and sunlight (Dai et al. 2001) and the degree of saturation as a result of rainfall (Dai & Lee 2002, Dai et al. 2001); or indirect by affecting vegetation which consequently impacts soil and rock strength through the land cover factor.

To generate the slope aspect map from the DEM, the aspect function of ArcGIS 9.3 fits a plane to the elevation values of a 3 x 3 cell neighbourhood around the processing (or centre) cell and the direction the plane faces is ultimately the aspect of that cell. The aspect value is then converted to compass direction values (0 – 360 degrees) and classified as: 1) Flat, 2) North (which corresponds to 0^{o} - 22.5^{o}), 3) Northeast, 4) East, 5) Southeast, 6) South, 7) Southwest, 8) West 9) Northwest and 10) North (which corresponds to 337.5^{o} - 360^{o}).

Curvature

Surface curvature is another DEM derivative that has been argued to affect slope stability. Curvature is the second order derivative of surface (i.e. the rate of slope change) representing the convexity or

concavity of the surface. It is distinguished in profile curvature which is parallel to the direction of the maximum slope, plan curvature which is perpendicular to the direction of the maximum slope, and a combination of both. From a geomorphic perspective the profile curvature affects the acceleration and deceleration of flow downslope, and as a result influences erosion and deposition; whereas plan curvature influences the convergence and divergence of flow across a surface (ESRI 2011). Finally, their combination (known as curvature) represents more accurately the flow across a surface incorporating both plan and profile curvatures and can be used to describe the physical characteristics of topography reflecting the effect of erosion and runoff processes.

Lee & Talib (2005) point out that the convex and concave slopes are generally more susceptible to rainfall induced slope failures than planar slopes. Ohlmacher (2007) argues that hillslopes with plan curvature are the most susceptible to earth flows and earth slides and that hillslopes with concave plan curvature are slightly more susceptible to landslides than those with convex plan curvature. Although conventional understanding suggests that the convergence of ground and surface water in concave areas should increase landslide susceptibility, Ohlmacher (2007) indicates that the resisting forces between soil particles that result from convergence of material increase the stability of the site and concludes that the relationship between plan curvature and landslide type is complex. Paxton (2010), aiming to develop a methodology to identify slumps (complex rotational slides with deep, spoon-shaped slip surfaces in bedrock) in the western Southern Alps of New Zealand, observed that their longitudinal profiles are characterized by changes of profile curvature from convex to concave to convex both up and down the slope, illustrating a direct relationship between slope failures and curvature.

Curvature is derived from the DEM using the curvature function of ArcGIS by determining the relationship between the elevation of the centroid of a focal cell and its neighbouring 8 cells in a 3x3 surface submatrix, and fitting a fourth-order polynomial to the surface (ESRI 2011). A positive curvature indicates that the surface is upwardly convex, where a negative curvature indicates that the surface is upwardly concave. A value of zero means the surface is planar. The curvature was classified into 5 classes: 1) Concave (-20.7 – -0.5), 2) Less concave (-0.5 – 0), 3) Flat (0), 4) Less convex (0 – 0.4) and 5) Convex (0.4 - 16.3).

Rainfall intensity

Intense or prolonged rainfall has been reported as the most frequent landslide generating mechanism in the West Coast region (Benn 2005). The western Southern Alps are exposed to warm humid westerly air masses from the Tasman Sea resulting in extremely high mean annual

precipitation, up to 14m yr^{-1} near the Main Divide, with frequent storms (Henderson &Thomson 1999). As the intensity and duration of the rainfall are the most important factors in triggering shallow landslides and debris flows in the region, a map of maximum expected rainfall in 24 hours for a specific return period was considered more appropriate than a traditional annual rainfall map.

The data of 24 hour maximum rainfall intensity of a 10 year design rainstorm were supplied by the National Institute of Water and Atmospheric Research (NIWA). The data were generated by the High Intensity Rainfall Design System (HIRDS) version 2 (Thompson 2002). The HIRDS is a web-based programme that can estimate design rainfalls at any location in New Zealand. The map was received in a continuous raster format (Andrew Tait pers. comm.) and reclassified into the following classes: (1) 0-150mm, (2) 150-200mm, (3) 200-250mm, (4) 250-300mm, (5) 300-350mm, (6) 350- 400mm, (7) 400-450mm, (8) 450-500mm, (9) 500-609mm.

3.4 Application of the fuzzy logic model using GIS

By overlaying the landslide inventory map with the factor thematic layers, the number of cells classified as landslides was obtained and the frequency ratio (equation 3.3) was calculated for each factor category. The normalized frequency ratio and “strength of relationship” or “similarity” using the cosine amplitude method (equation 3.6) were also calculated in order to establish the data-driven fuzzy memberships for each factor (Appendix 4; Table A4.1).

The knowledge-driven fuzzy memberships were developed using the fuzzy membership tool in ArcGIS 10. Table A4.2 includes the selected function for each factor and its associated parameters. The selection process was based on existing literature and field observations. Where there was no available information on the relationship between factor categories and landslide occurrence the density of landslides within each category was considered (Fig. 3.11).

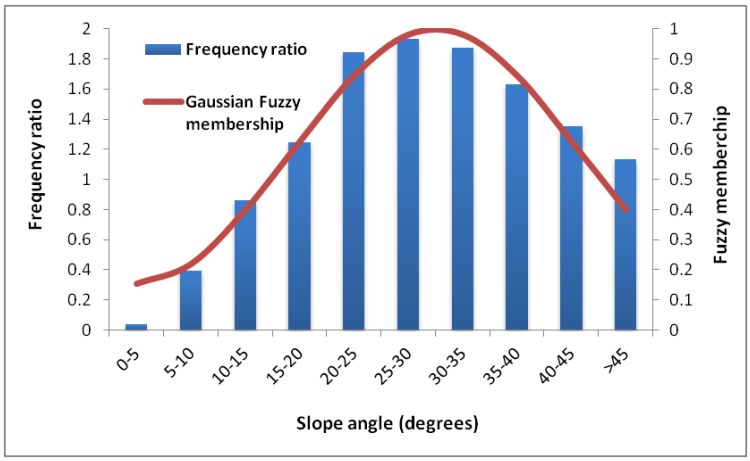

Figure 3.11 The distribution of landslide density can be used to select the appropriate fuzzy membership and its parameters (midpoint, spread). The shape of the fuzzy membership curve approximately fits (r^2 = 0.95) the distribution of landslide frequency ratio.

To aggregate the information layers and calculate the landslide susceptibility index in the study area, the fuzzy Gamma operator (equation 3.16) was applied:

$$LSI = \left(1 - (slope\ angle * lithology * land\ cover * soil\ drainage * soil\ induration * proximity\ to\ streams * proximity\ to\ faults * slope\ aspect * curvature * rainfall\ intensity)\right)^{\gamma} * (Slope\ angle * lithology * land\ cover * soil\ drainage * soil\ induration * proximity\ to\ streams * proximity\ to\ faults * slope\ aspect * curvature * rainfall\ intensity)^{1-\gamma} \quad (3.17)$$

As mentioned above the selection of the appropriate γ value is a critical step in the modelling procedure as it determines the degree to which the favourable and non-favourable landslide susceptibility conditions will affect the output. In a meaningful result the higher susceptibility values should coincide with the observed landslide locations and cover a relatively small area. To achieve this, three pixels coinciding with landslides and three pixels located in the plains (with slopes <5°) were randomly selected. For each pixel the landslide susceptibility index was calculated by applying equation 3.16 using different γ values (Fig. 3.12). Then the landslide susceptibility values for each pixel were plotted against their respective γ values. The curves a, b and c represent the locations where a landslide has occurred whereas the lower three curves d, e, f represent locations in the plains where a landslide is unlikely. It is generally observed that the susceptibility values increase with increasing γ value, as the effect of favourable factors (values close to 1) becomes more important.

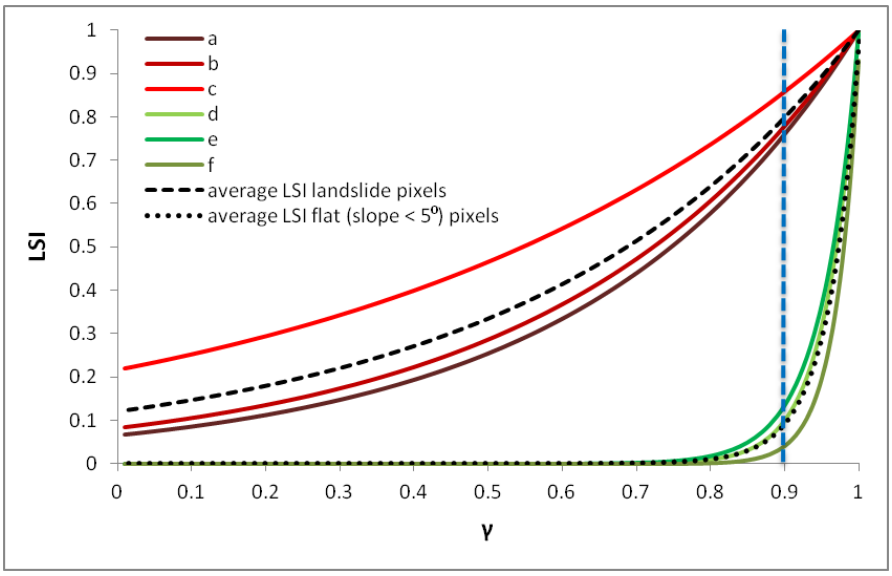

Figure 3.12 Effect of γ value on landslide susceptibility index (LSI). Curves a, b and c correspond to landslide pixels and curves d, e, f correspond to flat slopes where a landslide is unlikely. The greatest distance between the average LSI values for the landslide and flat areas is observed for γ ≈0.9.

Although the high susceptibility values are expected for the pixels coinciding with landslides, those for the pixels representing relatively flat areas are not expected. This means that increasing the value of γ above a threshold value will produce an output that predicts the landslide locations simply because the high susceptibility values cover larger areas. On the other hand, an appropriate γ value will produce an output with the highest possible susceptibility values for the landslide locations and the lowest for the flat areas. This value is estimated by the greatest distance between the average LSI curves of the landslide locations and flat areas.

Three landslide susceptibility index maps (Fig. 3.13) were obtained based on the different methods used to derive the fuzzy memberships (normalized frequency ratio, cosine amplitude and user-defined functions).

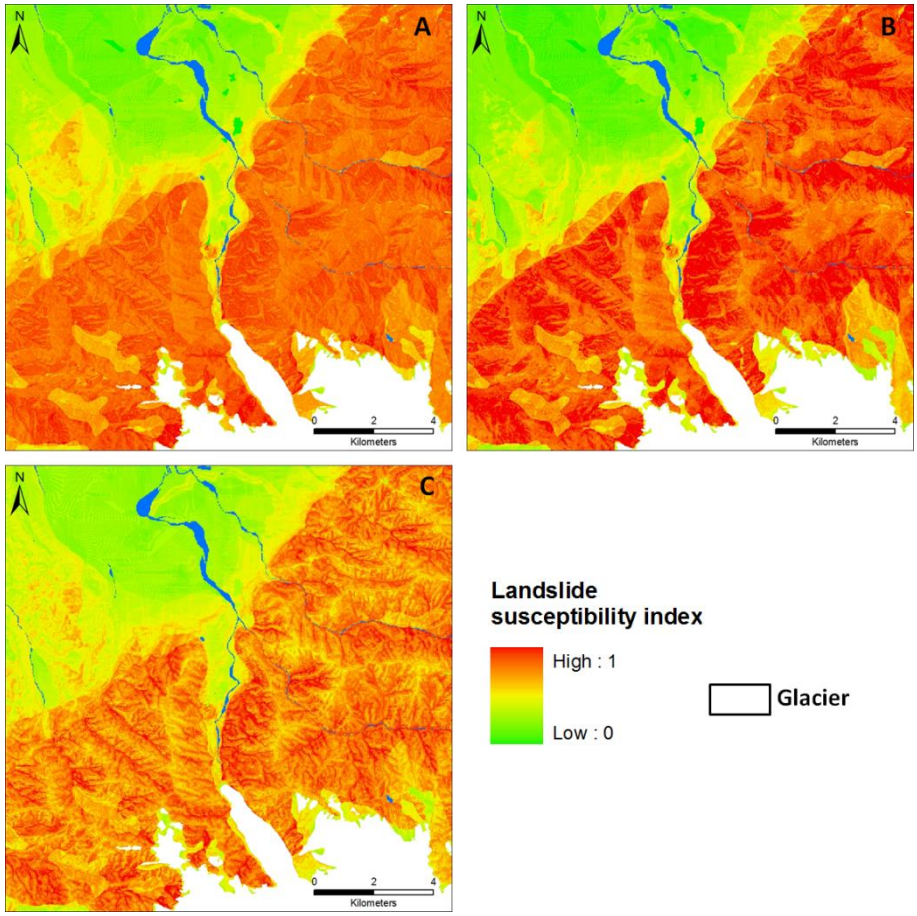

Figure 3.13 LSI maps developed based on A) normalized frequency ratio, B) cosine amplitude, C) user-defined fuzzy membership functions.

3.4.1 Classification

To classify the landslide susceptibility index map into five susceptibility classes from very low to very high, four different methods (equal intervals, geometric intervals, natural breaks and quantile) were implemented and compared. The Equal intervals classification divides the data into classes with equal ranges of values based on the number of classes specified (ESRI 2008). The Natural Breaks classification method is suitable for unevenly distributed data values with distinct breaks. The method groups clustered data values into a single class by identifying breaks where there is a gap between the clusters (ESRI 2008). The Geometrical Interval classification method is designed to accommodate continuous data and produce visually appealing and cartographically comprehensive results. The class ranges are based on intervals that have a geometric sequence based on a multiplier. The intervals are determined by minimizing the square sum of elements per class, ensuring that each interval has an appropriate number of values within it and the intervals are fairly similar (ESRI 2008). With the Quantile classification method, the data are divided into equal proportions, so that each class has the same number of features. It is suitable if the data values are

evenly distributed and the aim is to emphasize the difference in relative position between features (ESRI 2008).

The landslide susceptibility index map (Fig. 3.14) was reclassified using each classification technique generating four slightly different output maps. Summary statistics of the landslide density within each of the susceptibility classes were obtained using the landslide inventory. The criterion for the optimum classification technique is that the higher susceptibility classes should explain a large proportion of the landslides in a relatively small proportion of the total area (Fig. 3.15).

The majority of the landslide events appear in the high to very high susceptibility classes for all four classifications. The map classified by the equal intervals method demonstrates the highest relative landslide frequency for the very high and high susceptibility classes. The natural breaks, quantile and geometric interval methods have similar performances. However, the natural breaks classification can be also considered appropriate as it has similar relative landslide density to the quantile and geometric interval for the very high and high susceptibility classes, and slightly lower at the low and very low susceptibilities. Furthermore, its classes reflect breaks in the data distribution and is more appropriate when data values are neither evenly distributed nor tend to accumulate at one end of the distribution. Figure 3.16 shows the final landslide susceptibility map with five classes using the natural breaks classification method.

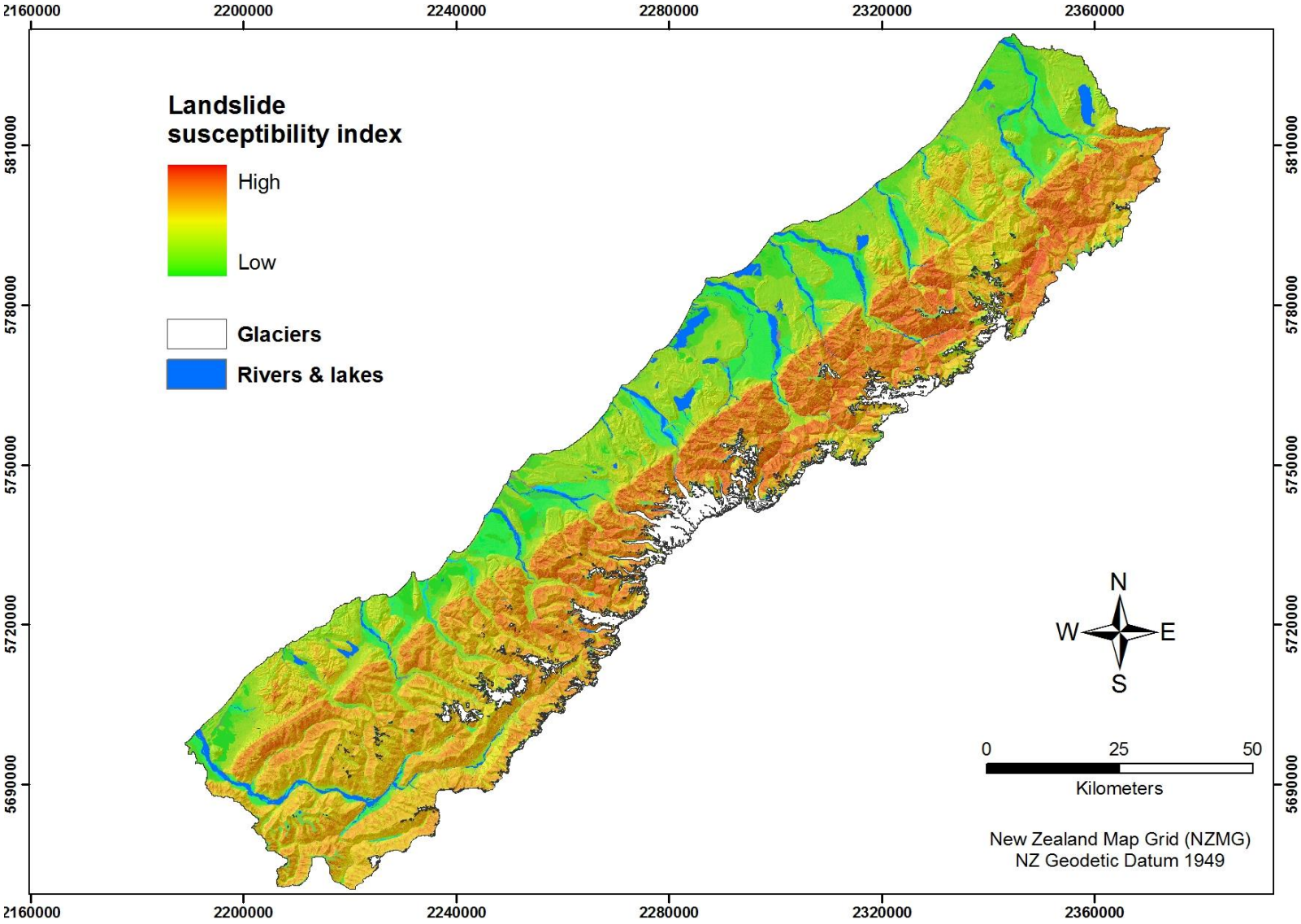

Figure 3.14 Spatial variation of landslide susceptibility index in the study area (cosine amplitude method).

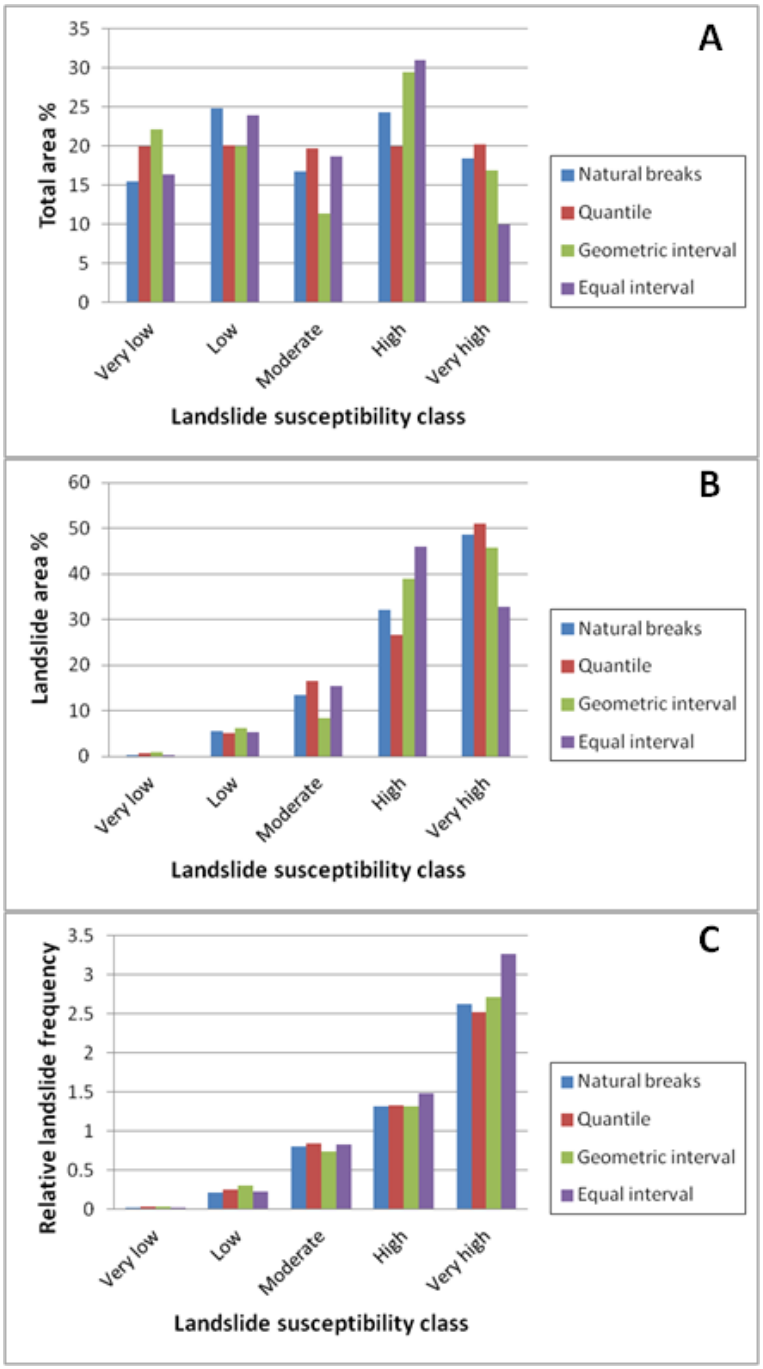

Figure 3.15 Percentage of total area (A), landslide area (B) and relative landslide frequency (C) for each of the five susceptibility classes determined by the four classification techniques (equal interval, geometric interval, natural breaks and quantile). The results concern the ten parameter model based on the cosine amplitude method to derive the fuzzy memberships.

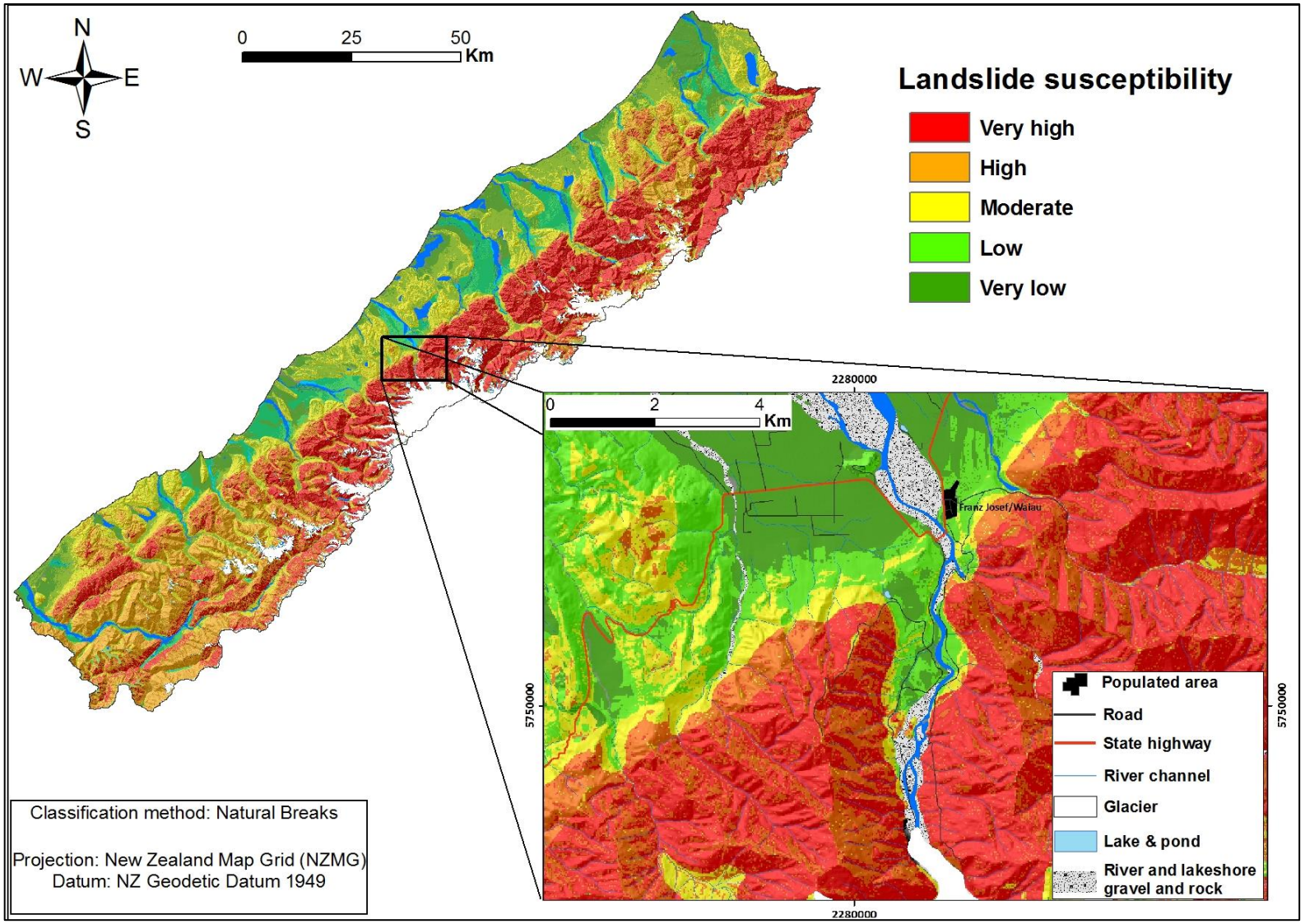

Figure 3.16 Shallow landslide/ debris-flow susceptibility map.

3.4.2 Evaluation

Landslide hazard and susceptibility models aim at providing information on the probability or likelihood of slope failures occurring in an area in order to effectively mitigate their effects. Therefore, their outputs are commonly in the form of maps, explicitly or implicitly representing a prediction of future terrain behaviour (Remondo et al. 2003b). This predictive output requires the application of some form of assessment to test its accuracy and reliability before it is usable in any decision making process. Some studies refer to this process as validation, implying that there is an absolute acceptability as a yes/ no, right/ wrong situation when in fact it is actually an evaluation of the relative degree of acceptability (Oreskes 1998; Carrara & Pike 2008). In this sense true validation of landslide hazard or susceptibility models is only possible using landslides which will occur in the future (Hutchinson 1995; Guzzetti et al. 1999). As the "wait and see" strategy (Neuhäuser & Terhorst 2007) is not an option especially when the result is intended to inform land use management, landslide modellers have turned to numerical testing of their models (Carrara & Pike 2008). In order to evaluate the model output, a landslide population independent to the one used in developing the model is often used and a qualitative or quantitative evaluation is performed (Chung et al. 1995; Remondo et al. 2003b). However, when instead of an independent population the same landslide set is used, what is determined is how well the model fits the data (goodness of fit) and not how good the prediction is (predictive capability). To obtain an independent sample of landslides Remondo et al. (2003b) describe three basic procedures: (a) landslides in the landslide inventory of the study area are randomly split into two groups, one for analysis and one for evaluation, (b) the analysis is carried out in a part of the study area and the final map obtained is tested in another part with a different landslide population or (c) the analysis is carried out using landslides occurred in a certain time period and evaluation is performed by means of landslides occurring in a different period.

Herein, in order to evaluate the predictive capability of the model and not just "the goodness of fit" of the data, the study area was divided into training and test areas (Fig. 3.17). In the selection process of the training and test areas two main criteria were considered. First, both areas should include the same factor categories (e.g. the same rock types or land cover classes should be present in both areas). That is because if the test area includes factor categories that are not present in the training area, the relationship between these categories and landslide occurrence will not be defined and their effect on slope instability will be excluded from the final output. Also, an effort has been made to use the smallest possible area as training area and test if the model is capable of producing satisfactory results using the least possible amount of data. Can et al. (2005) introduce two rules for a meaningful landslide susceptibility map: (i) observed landslide areas should coincide with the areas

having high susceptibility values, and (ii) high susceptibility values should cover only small areas. A commonly-applied technique used to quantitatively assess how well the output from a model predicts the landslides is the construction of validation or success rate curves (Chung & Fabbri 1999; Van Westen et al. 2003; Remondo et al. 2003b; Frattini et al. 2010) based on a comparison between the spatial distribution of landslides and modelled landslide susceptibility.

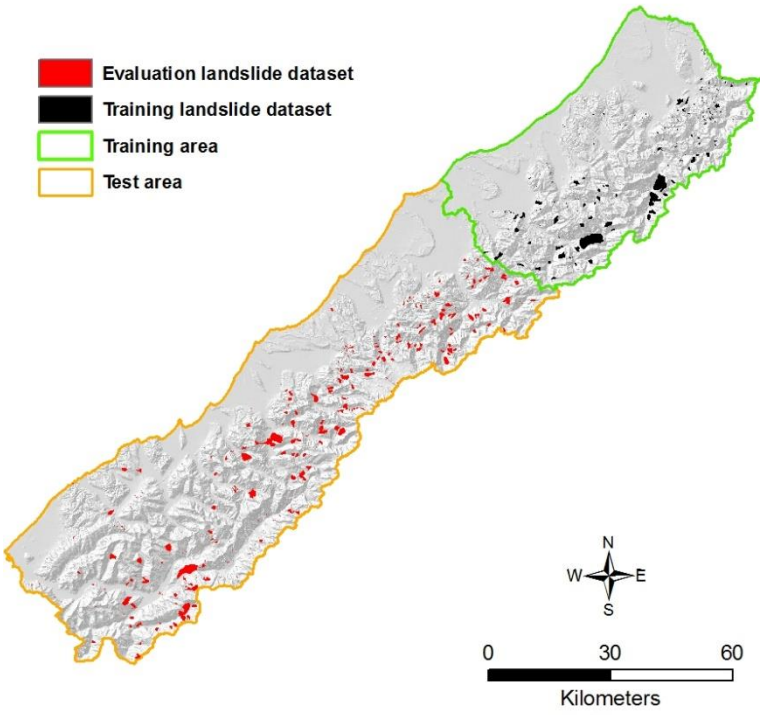

Figure 3.17 Training and test areas covering 34% and 66% of the study area respectively.

The validation or success rate curves can be easily developed using GIS by applying the following procedure. Initially, the pixels of the final LSI map are grouped into a user-specified number of classes, sorted in descending order, using a classification method (e.g. equal interval, quantile etc.) based on their frequency distribution histogram. Then, the landslide inventory is overlayed with the reclassified LSI map and their joint frequency is plotted on a graph generating a curve (Chung & Fabbri 2003). The curve depicts the landslides in the test area as a cumulative percentage (y-axis) with respect to decreasing susceptibility index values (x-axis) also expressed as cumulative percentages of the test area (Remondo et al. 2003b; Guzzetti et al. 2006). A hypothetical success rate curve coinciding with a diagonal from 0 to 100 would be equivalent to a totally random prediction. The further up and away the success rate curve is from that diagonal, the better the predictive value of the model assuming that the majority of landslides should occur in the higher susceptibility zones. Thus, the greater the area under the curve (AUC) the higher its predictive capability (Chung & Fabbri 2003; Bui et al. 2012).

According to the success rate curves (Fig. 3.18), all three models predict the 50% of the mapped landslides in the test area with the 25% of the higher susceptibility values in the same area demonstrating a satisfactory performance with AUC > 0.7.

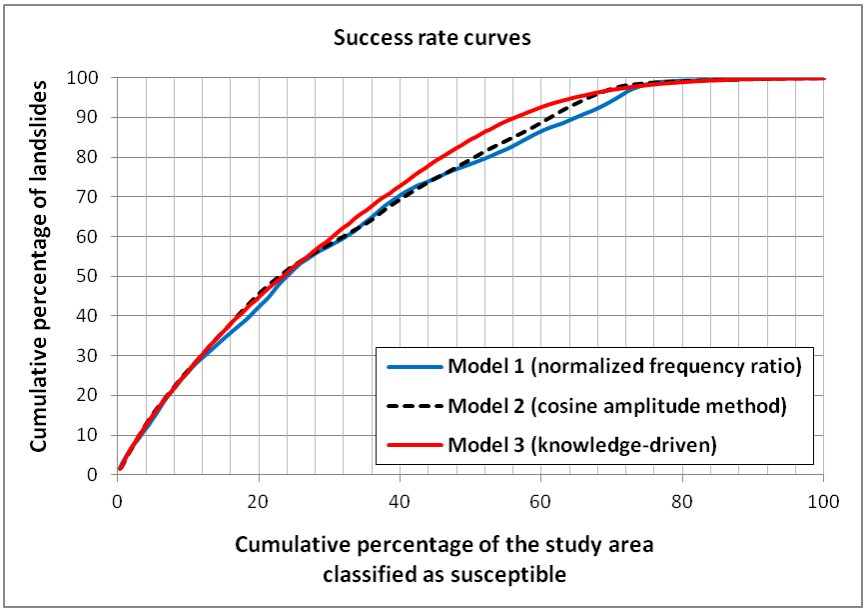

Figure 3.18 Success rate curves and comparison of the predictive performance between the three fuzzy logic models. The model based on the user-defined fuzzy memberships demonstrates slightly better performance (AUC=0.729) compared to the data-driven models using the cosine amplitude (AUC=0.717) and frequency ratio (AUC=0.708) methods.

3.4.3 Sensitivity analysis

Sensitivity analysis was performed in order to assess the sensitivity of the susceptibility model to changes in the input data and investigate the importance of each factor in the model's predictive performance. In general, the output of a robust (least sensitive) statistical model should not change significantly if the input data are changed within a reasonable range (Guzzetti et al. 2006).

The model's sensitivity was assessed by applying variations of equation 3.17 using different factor combinations and evaluating the predictive performance of each model. Ten models were initially tested by excluding one factor in each trial and calculating the area under the prediction curve. If by excluding a factor the model's performance was lower than an all factor model the factor was assumed to be relatively important. Conversely, if the removal of the factor resulted in the same or higher predictive performance the factor was assumed redundant. Four nine-parameter models obtained by removing the curvature, rainfall intensity, land cover or soil drainage factors indicated the same or slightly improved predictive performance compared to the ten-parameter model. The remaining six nine-parameter models obtained by excluding slope, geology, proximity to faults,

proximity to streams, slope aspect and soil induration showed slightly lower performance. An additional 22 other factor combinations were also examined (Appendix 4; Table A4.3).

Of the 31 different factor combinations in total, a six parameter model using the slope, lithology, proximity to faults, proximity to streams, slope aspect and soil induration factors demonstrated the highest performance (0.734) whereas a three parameter model using only the slope, rainfall and curvature demonstrated the worst performance (0.667). The difference in performance of the order of ±0.02, observed by the removal of only one factor in each trial does not necessarily mean that the curvature, rainfall intensity, land cover or soil drainage do not affect landslide susceptibility. It is likely to reflect differences in scale and/or accuracy of the input thematic maps as well. For example, the initial resolution of the rainfall intensity map was 2 km and it was changed to a finer resolution of 25m in order to match the cell size of the other data layers. However this process didn't improve the accuracy of the information (i.e. the spatial distribution of rainfall intensity) as within an area of 4 km^2 the rainfall intensity remained uniform. On the other hand, the 24h maximum rainfall intensity of a 10 year design rainstorm may not be the optimum predictor factor of shallow landslide and debris-flow occurrence, and other characteristics such as the mean and maximum monthly rainfall (Schicker 2010) might be more appropriate. However, it should be noted that the effect of rainfall on slope instability is not completely excluded from the model, even after the rainfall information is removed. That is because its effect is reflected through the slope aspect parameter, as the west and northwest facing slopes that are exposed to the prevailing direction of humid air masses demonstrate higher landslide densities.

3.5 Runout

Estimating the "runout" of mass movements including their velocity and travel distance is an essential component of any landslide hazard or risk assessment (Hungr et al. 2005). It provides information not only on the potential affected area and associated risk, but also allows investigation of how the deposited material interacts with other geomorphic processes and may initiate hazards such as landslide dams and consequent dam-beak floods, river aggradation or tsunami waves. Despite the progress in landslide hazard and susceptibility assessment techniques, modelling the post-failure motion of mass landslides is still a very challenging task, especially in regional-scale studies (Carrara et al. 2008; Hungr et al. 2005). Existing methods for identifying the source area, runout path and deposition zone as well as the kinematic parameters of mass movements are generally classified as empirical approaches, physical-based and dynamic modelling (Chen & Lee 2004).

The empirical approaches are based on relationships between landslide characteristics (e.g. volume), topographic parameters and the distance travelled by the landslide debris. These include geomorphological (Costa 1984; Jackson et al. 1987), geometrical (Hsu 1978; Corominas 1996; Dai & Lee 2002) and volume change methods (Cannon 1993; Fannin & Wise 2001). Although they don't address material rheology or provide any information on kinematic parameters during runout (Chen & Lee 2004) their main advantage is that they are simple and easy to implement in GIS for preliminary runout assessment. In physical-based modelling the parameters are derived from field measurements or laboratory experiments (Davies & McSaveney 1999; Major & Iverson 1999). Dynamic models provide more detailed quantitative estimations of the runout process based on numerical and rheological models including lumped mass (Hutchinson 1986), distinct element (Hart 1993) and continuum mechanics models (Crosta et al. 2003). Hungr et al. (2005) and Chen & Lee (2004) provide comprehensive descriptions of the various methods.

Several parameters such as topography, soil properties, land use, debris volume as well as the water content can affect the runout behaviour of a mass movement (Guinau et al. 2007). Given the difficulty of obtaining and/or predicting these parameters for the entire study area, an empirical approach in GIS environment was developed in this study. The approach assumes that all locations downslope from a source zone are potentially affected until the energy from the mass movement is depleted. Several authors (Michael-Leiba et al. 2003; Jaboyedoff & Labiouse 2003; Hungr et al. 2005; Toyos et al. 2007; Horton et al. 2008; Blahut et al. 2010; Dahl et al. 2010; Jaboyedoff & Labiouse 2011; Kappes et al. 2011) have used the concept of the angle of reach in GIS environment as a simple rule to determine this depletion point and identify where the movement stops. The angle of reach is the angle of a hypothetical line connecting the head of the landslide source to the distal margin of the displaced mass used as an index to express the runout behaviour of landslide mass (Hsu 1978; Corominas 1996; Dai & Lee 2002). Corominas (1996) studied the runout behaviour of different landslide types and observed a continuous reduction of the angle of reach with increasing volume that starts at the smallest volumes. However, for landslide hazard assessments over large areas, the relationship between the angle of reach and the volume of landslide mass may not be a practical method as it is yet very difficult to predict the volume of future landslides (Dai & Lee 2002). Furthermore, Davies & McSaveney (1999) studying the behaviour of small scale granular avalanches under laboratory conditions and comparing their results with well-documented field events, argued that the ratio of fall height to travel distance is not adequate to estimate the runout distance, especially for high mobility material. They also found that granular avalanches in the range from 0.1 L to about 10^5 m^3 show consistent runout behaviour which significantly changes for large volume avalanches greater than about 10^6-10^7 m^3.

Considering the above findings and limitations, and as the landslide susceptibility model developed herein does not provide any information on the volume of potential future slope failures, the application of the angle of reach cannot provide meaningful results in the study area. As an alternative, a different approach is proposed in order to estimate the runout distance of landslides, based on the morphology of debris-flow fan formations, which essentially delineate the runout zones of previous events. Note that this approach specifically excludes consideration of large landslides, whether rainfall- or earthquake-generated.

3.5.1 GIS-based runout modelling

A runout model usually involves two different types of algorithms: flow direction algorithms which calculate the path that the debris flow surge will follow and algorithms that determine its runout distance (Horton et al., 2008). In this study, the multiple flow direction algorithm D-infinity (Tarboton, 1997) and the mean topographic slope of debris-flow fan formations in the study area are used in order to estimate the runout path and maximum distance respectively, of the landslide susceptibility zones identified previously.

3.5.1.1 Flow direction algorithms

Flow direction algorithms based on digital elevation models calculate the direction of the flow from a cell to its eight neighbours and are generally classified as single- and multiple-direction (Erskine et al. 2006). Single-direction algorithms assign the flow from a centre cell to only one downslope neighbour cell. In this category are the widely applied D8 algorithm (O'Callaghan & Mark 1984) that is incorporated in ESRI's ArcGIS software and the Rho8 (Fairfield & Leymarie 1991). Despite its computational efficiency and extensive use the D8 algorithm often produces unrealistic straight and parallel flow paths due to the discretization of flow into only one of eight possible directions (Tarboton 1997; Erskine et al. 2006). Multiple-direction algorithms which partition flow to multiple downslope neighbours have been proposed (Quinn et al. 1991; Freeman 1991) in an effort to overcome the limitations of single-direction methods. Such methods are the MFD (Freeman 1991), the method proposed by Lea (1992), the DEMON (Costa-Cabral & Burges 1994), and the D-infinity (Tarboton 1997).

Several studies have shown differences between single- and multiple-direction algorithms and provide comparisons on the performance of two or more flow-routing algorithms using a variety of criteria such as predicted channel networks or statistical distribution of terrain attributes (Erskine et al. 2006; Wilson et al. 2007; Tarboton 1997). Wilson et al. (2007) illustrate that further work is

required to determine whether one or more of these algorithms should be preferred in specific types of landscapes and/or applications.

The D-infinity algorithm (Tarboton 1997) was implemented in order to track the movement of sediment from a given source pixel, taking into account the flow direction in each downslope pixel. It represents flow direction as a vector along the direction of the steepest downward slope on eight triangular facets formed in a 3 x 3 pixel window centred at the pixel of interest. The flow direction assigned to a pixel, represented as an angle, can take on any value between 0 and 2π (an infinite number of flow directions are possible). Flow from a grid cell is then partitioned between the two, downslope grid cells closest to the vector flow angle (forming the steepest triangle) based on angle proportioning (Fig. 3.19).

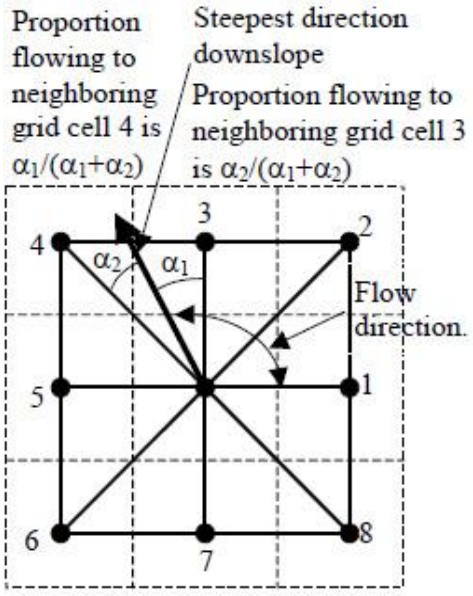

Figure 3.19 D∞ multiple flow direction model (from Tarboton, 1997). Flow direction defined as steepest downwards slope on planar triangular facets on a block centred grid.

3.5.1.2 Runout distance

Fan formations are low-gradient, semi-cone-shaped deposits that form by streams' sediment transport capacity decreasing as they emerge from steep confined mountain valleys, and accumulate on broader, flatter basins, valleys or coastal plains. Fans are usually characterised on the basis of the predominant depositional process responsible for their formation. Davies & McSaveney (2008) classify fan landforms based on the different types of hazard they pose into alluvial, debris-flow, mixed, episodic-aggradation and dynamic equilibrium fans. Debris-flow fans are widespread along the western Southern Alps due to a combination of tectonic uplift, extreme precipitation and steep topography which control the very high rate of erosion that delivers large volumes of sediment to the valley floors. Where they are unconfined and on gentle slopes debris-flows become wide and

shallow and are only able to flow for relatively short distances (McSaveney et al. 2005). Generally, debris-flow surges slow down and eventually stop when they reach a threshold topographic slope (Davies & McSaveney 2008). De Scally & Owens (2004) studying the mountainous catchments in the Aoraki / Mount Cook and Cass areas, Southern Alps, New Zealand indicate a fan gradient of 7.5^{o} as a threshold of separating debris-flow and fluvial dominated fans. Their result is steeper than the 4° fan slope threshold observed for the Rocky Mountains (Jackson et al. 1987) and Cascade Mountains (De Scally et al. 2001) in Canada. Whipple & Dunne (1992) indicated slopes of 4^{o}-6^{o} where debris-flows generally stop in Owens valley, California. However they also argued that variable sediment concentration is the most important controlling factor of flow mobility and observed slopes as low as 1^{o}-2^{o} for debris-flows with relatively low sediment concentrations. Watts & Cox (2010) in addition to contributing catchment morphometry (Melton ratio ≥ 0.4), they identified a threshold fan slope of ≥ 4^{o} to differentiate between debris-flow and fluvial fan formations in Otago, New Zealand. The range of fan slope angles observed in the above studies suggests that the depositional patterns of debris-flows may vary in different environments depending on parameters such as topography and physical characteristics of the moving material. Therefore, data from the study area are critical in identifying the threshold slope angle and estimate the maximum runout distance (Fig. 3.20).

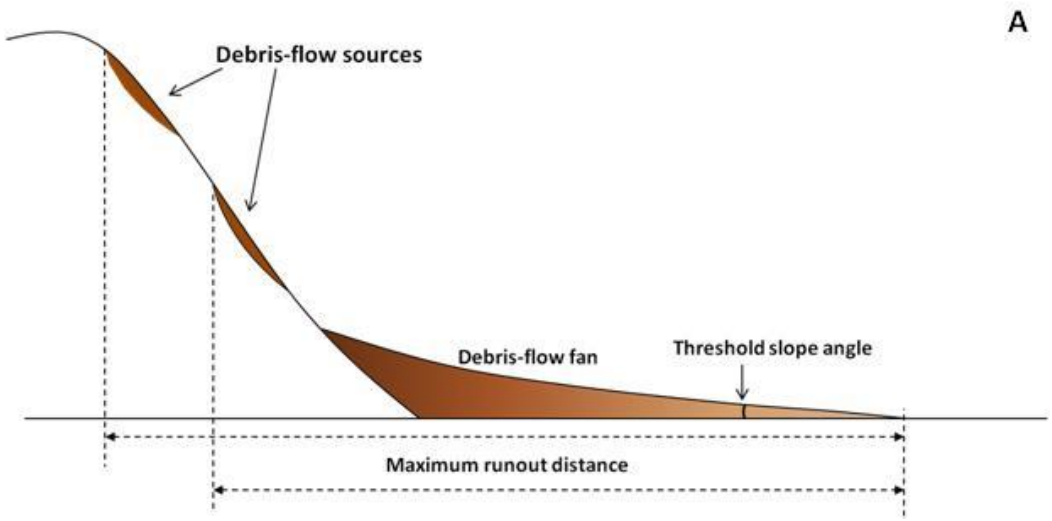

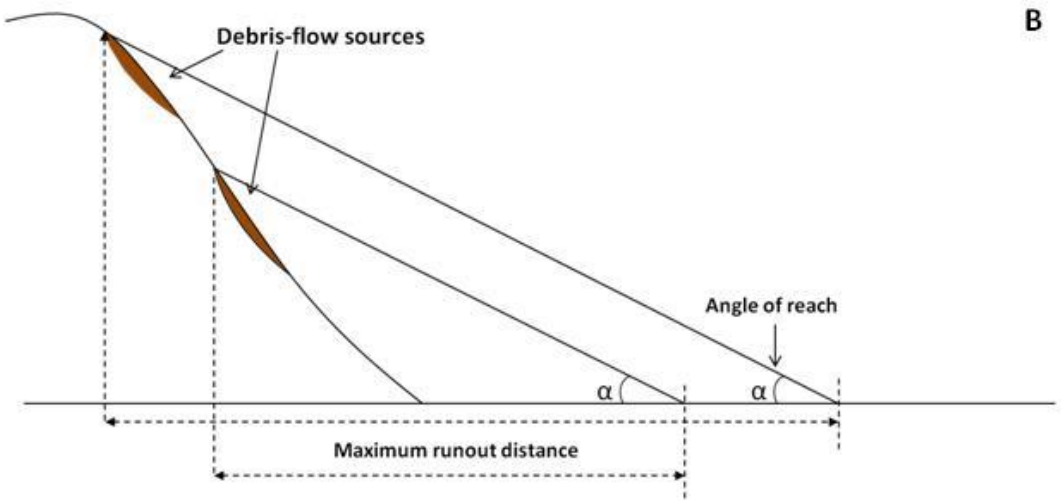

Figure 3.20 Runout distance of shallow landslides and debris flows A) controlled by the surface slope of debris-flow fan deposits (the maximum runout distance is assumed independent from the height of fall) B) based on the angle of reach.

Information on debris-flow fan deposits was extracted from the QMaps (Greymouth, Aoraki and Haast datasets) as polygons. For each polygon the mean slope gradient and Melton ratio of the contributing catchment area were calculated (Fig. 3.21). Melton ratio is an index of basin ruggedness that normalizes basin relief by area (Melton 1965) and it has been applied by several authors (Jackson et al. 1987; De Scally & Owens 2004; Wilford et al. 2004; Welsh 2008; Welsh & Davies 2011) to differentiate between debris-flow and non-debris-flow dominated catchments and their associated fans.

$$Melton\ ratio\ (R) = \frac{H}{\sqrt{A}} \qquad (3.18)$$

where *H* is basin relief (difference between maximum and minimum elevations in the catchment) and *A* is the total catchment area.

Welsh & Davies (2011) proposed Melton ratio > 0.5 as a threshold value for the identification of catchments likely to generate debris flows, based on data from 18 catchments in the Coromandel and Kaimai Ranges, North Island and in 16 catchments in the Southern Alps, South Island of New Zealand, known to generate debris-flows. Based on the following data (Fig. 3.22, 3.23), a slope angle of 4^{o} emerges as a threshold where the energy from the debris-flow movement is depleted and the material is deposited.

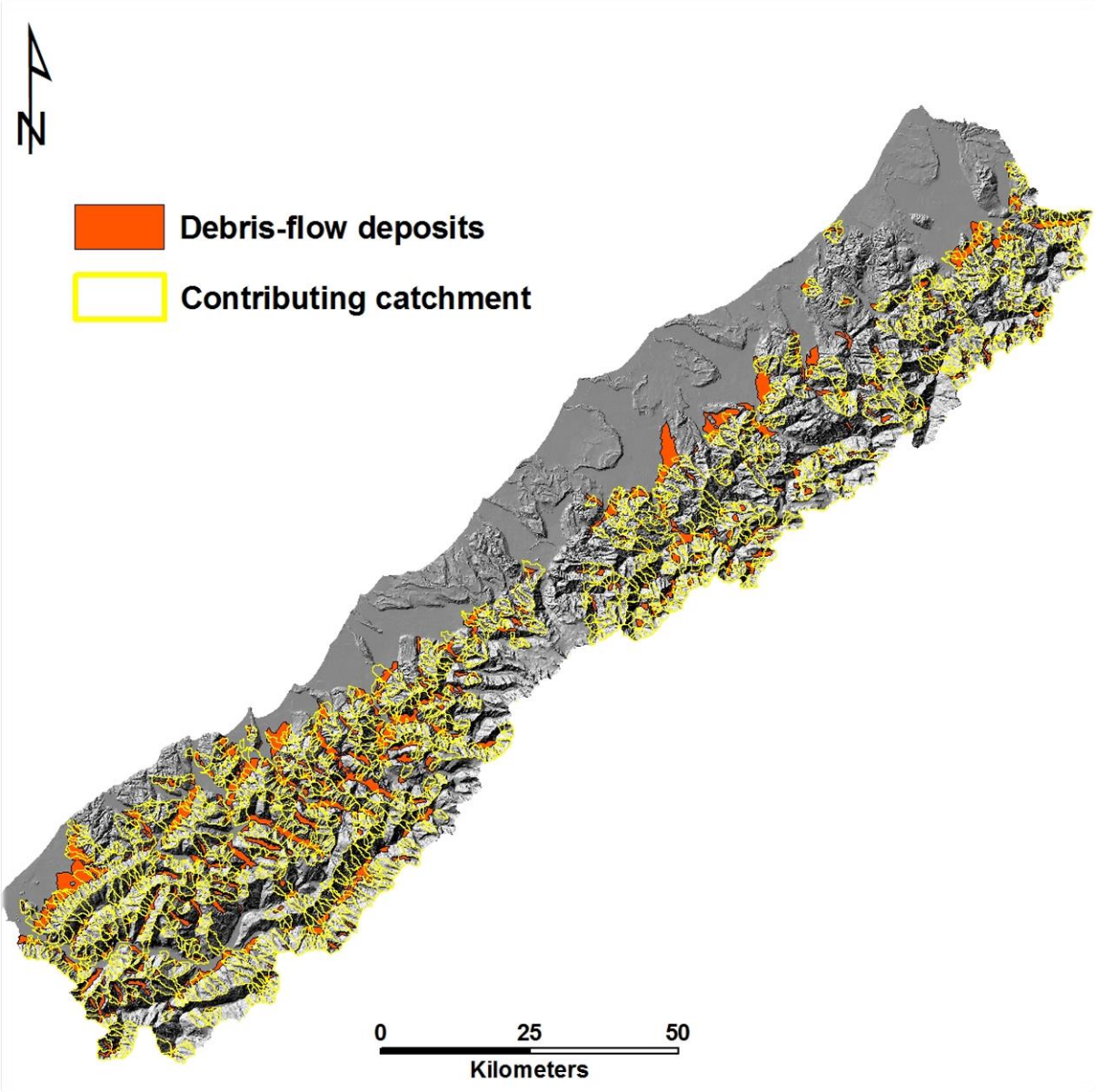

Figure 3.21 Debris-flow fan deposits extracted from the QMaps and their contributing catchment areas identified using the 25m DEM of the study area.

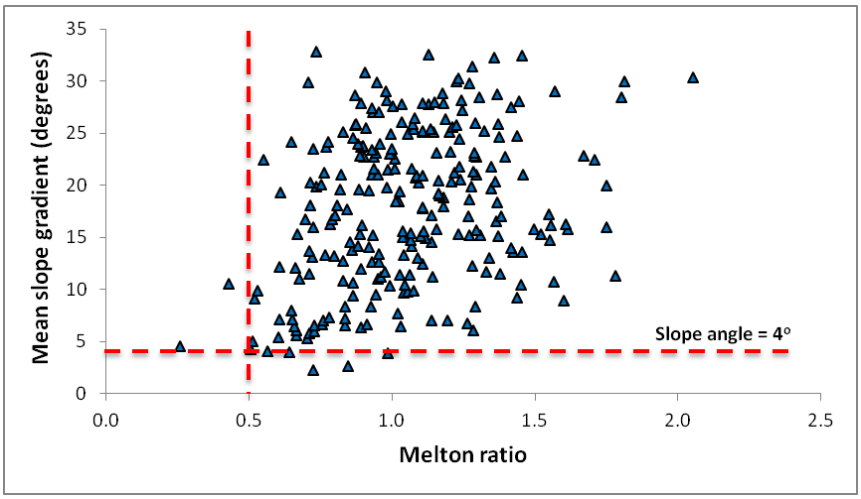

Figure 3.22 Catchment Melton ratio plotted against fan gradient for debris-flow fans. Data based on the 25m DEM of the study area and QMaps.

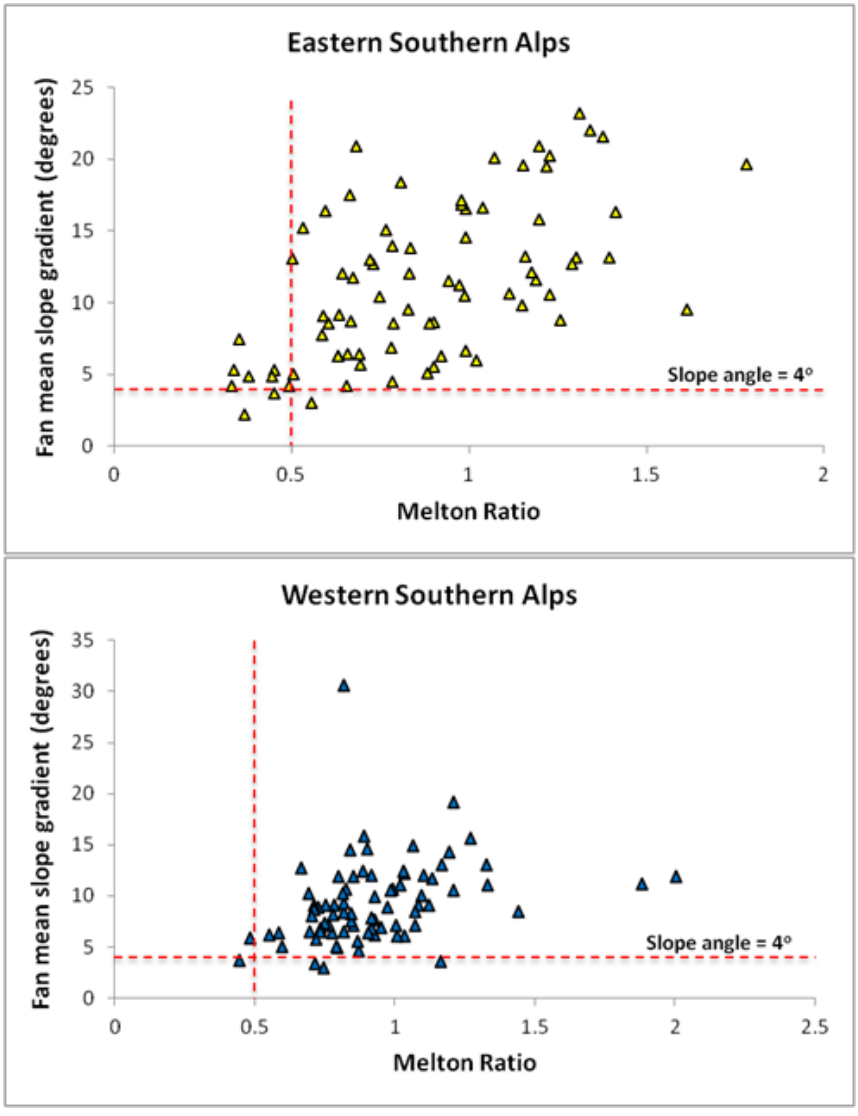

Figure 3.23 Mean slope gradient of fan formations and Melton ratio, based on catchment characteristics extracted from DEM for the eastern and western Southern Alps (Korup O. unpublished data).

The runout susceptibility map was developed using the open source software TauDEM (Terrain Analysis Using Digital Elevation Models) developed by Tarboton (1997). TauDEM is a suite of tools for the extraction and analysis of hydrologic information from topography as represented by a DEM and it can be executed as an ArcGIS extension. The TauDEM software was used to calculate the flow direction (runout path) according to the D-infinity algorithm as well as the runout distance of potential debris-flow sources. The movement of debris flows was assumed to stop when they reach a topographic slope of 4^{o}. The D-infinity algorithm and the assumption of the threshold slope angle were initially evaluated using observed debris-flow sources from the landslide inventory and existing deposits (Fig. 3.24).

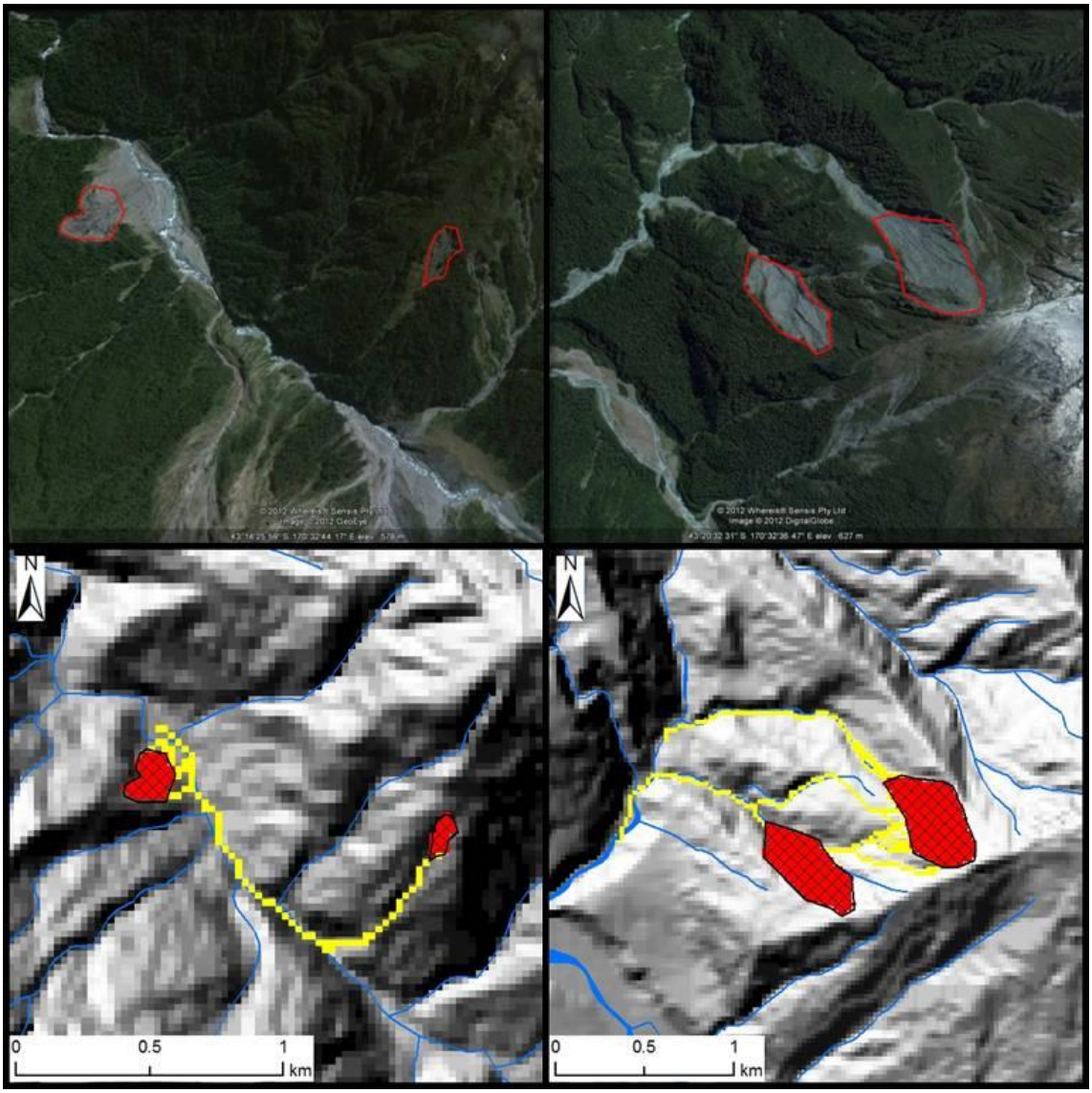

Figure 3.24 Runout path and distance of observed debris flow sources using the D-infinity flow direction algorithm and the slope gradient of previous deposits. The model was initially tested using debris-flow sources from the landslide inventory.

In order to develop the runout susceptibility map for the study area, the very high, high, moderate and low susceptibility zones identified previously using the fuzzy logic models, were used as potential debris-flow sources in the model. The analysis was performed for each susceptibility class separately (Fig. 3.25).

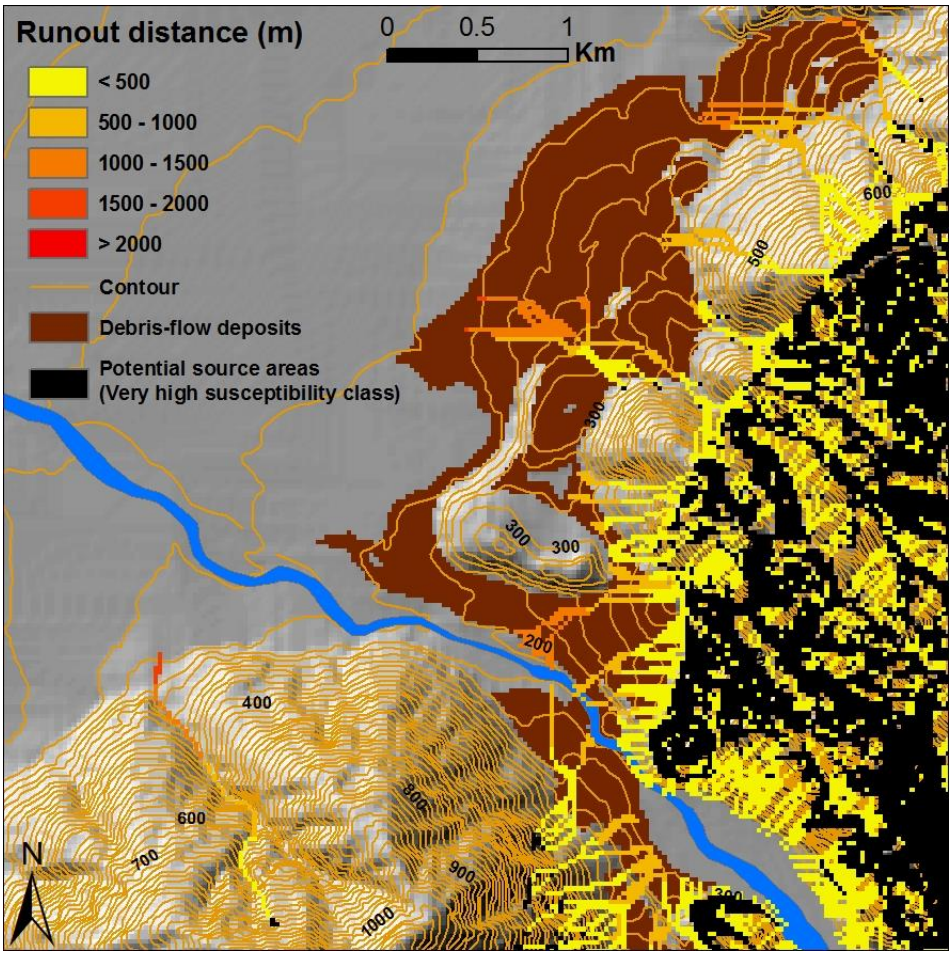

Figure 3.25 Runout path and distance of the very high susceptibility pixels (black). The result was further evaluated by means of visual comparison with debris-flow fan deposits.

Finally, the output runout paths and deposition zones for each class were overlaid to produce the final runout susceptibility map (Fig. 3.26). During the overlay process it was assumed that if a pixel is characterized by two or more different susceptibility values, it is assigned the highest susceptibility. For instance, if a site has moderate landslide susceptibility but it is on the runout path or zone of high and very high susceptible areas, its overall susceptibility is very high.

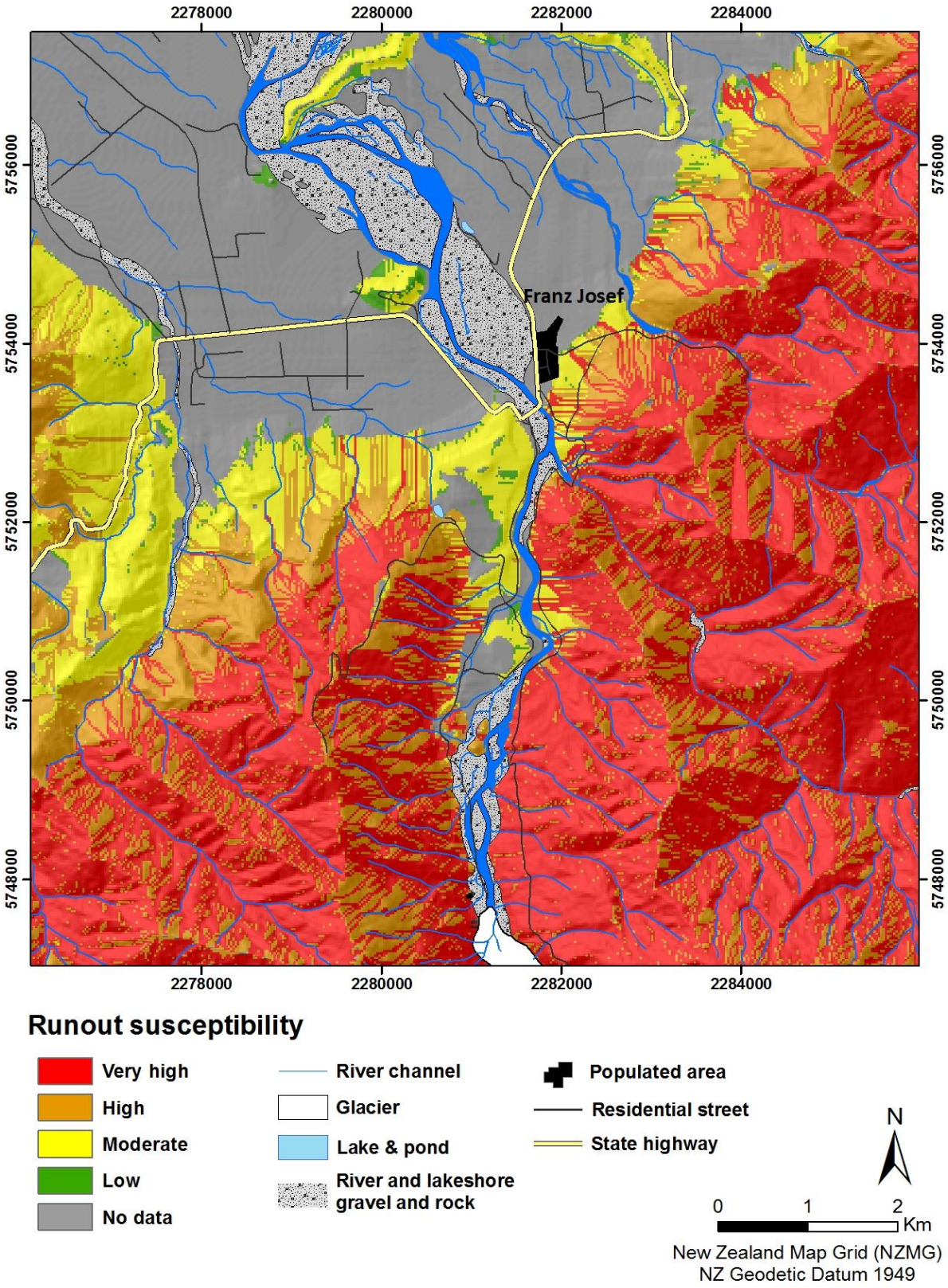

Figure 3.26 Debris-flow runout susceptibility map of Waiho river valley.

3.6 Discussion and conclusions

In the present study an approach based on fuzzy logic in GIS environment is developed, aiming to assess the shallow landslide/debris-flow susceptibility in the western Southern Alps of New Zealand. Preliminary research indicated ten parameters as the most important factors generating shallow slope failures in the study area. Ten thematic maps representing the identified factors were produced and their relationship with the landslide occurrence was established using a landslide inventory.

Since landslide phenomena are complex and any effort to predict their occurrence involves many uncertainties, fuzzy set theory was used in order to deal with these uncertainties and with the non-linear relationships between conditioning factors and slope instability. Three different fuzzy logic models, based on landslide inventory data as well as user-defined fuzzy membership functions were developed, applied and compared in the study area. Their predictive performance was evaluated in a test area using an independent population of landslides that was not considered in establishing the fuzzy relationships between conditioning factors and landslide occurrence. All models demonstrated similar performance predicting approximately 50% of the landslides with the 25% of the higher susceptibility values. However, the overall performance of the "knowledge-driven" fuzzy logic model was slightly better (AUC=0.729) compared to the "data-driven" models based on the cosine amplitude (AUC=0.717) and frequency ratio (AUC=0.708) methods. The observed difference in performance it is likely to reflect spatial inaccuracies between the landslide inventory map and factor categories, as the accuracy of the landslide locations and extent in the inventory is variable, mainly due to the variation in map scale and quality of the data sources used to compile the inventory. Although the "knowledge-driven" model has the limitation of subjectivity and may incorporate simplified factor-landslide occurrence relationships (e.g. fuzzy linear membership function), it is independent of the spatial distribution of previous slope failures within each factor category and therefore independent of potential inaccuracies of landslide locations and extent. Sensitivity analyses illustrate that a six parameter model including slope angle, lithology, slope aspect, proximity to faults, soil induration and proximity to drainage network demonstrates the highest predictive performance (AUC=0.734). The slightly improved performance (+0.0165) compared to the 10 parameter model may be attributed to redundancy of the four excluded factors and/or spatial inaccuracy issues between these information layers and the other input thematic maps that potentially aggravate the prediction of susceptibility. It is also possible that the effect of controlling factors on landslide susceptibility is spatially variable particularly in a regional scale

assessment. Thus, the same factor category (e.g. schist formations or west facing slopes) may affect the susceptibility to a different extent within the study area.

We note with interest that rainfall intensity does not appear to be a significant parameter in the susceptibility of a slope to rainfall-generated failure. This may be because rainfall intensity varies little across the area studied (the entire area is subject to intense and prolonged rainfall), or perhaps because some other rainfall parameter such as mean annual or monthly rainfall, has greater significance.

In addition to the identification of areas susceptible to shallow landslides, a GIS-based approach to estimate the runout path and distance of the potential future slope failures was developed. This utilizes the multiple flow direction algorithm D∞ (Tarboton, 1997) and the topographic slope of debris-flow fan formations in the region to identify potentially affected areas, aiming to provide a more comprehensive evaluation of the landslide susceptibility in the western Southern Alps.

Communicating information about landslide risk is a crucial component of preparedness and hazard mitigation. Therefore, an effort has been made to develop a cost- and time-efficient landslide susceptibility assessment with an acceptable degree of accuracy for regional-scale planning, and contribute in making hazard/susceptibility and risk maps more accessible to individuals and local authorities.

The evolution of GIS-based methods, and modern data availability especially through online databases, significantly contribute towards this aim. However, the challenge lies in producing results with meaningful accuracy for the scale of planning, using the available resources. A number of assumptions are often necessary to overcome data limitations and gaps in knowledge. A fundamental assumption of the proposed approach is that controlling and triggering factors which have induced past landslides will have a similar or equal effect in landslide occurrence in the future (Neuhäuser & Terhorst 2007). This assumption further implies that an adequate number of representative input parameters is considered and combined with a landslide inventory with appropriate spatial distribution of events. Hence, during each stage of the modelling process the evaluation and comparison of the output with field observations and real measurements, if possible, is crucial. For example, the assumption of the 4° slope angle to determine the maximum runout distance of debris-flows does not rule out the possibility that debris flows could travel further on lower slopes. Instead, it only aims to reveal areas susceptible to debris flows on the basis of the morphology of existing deposits observed in the region. The final runout susceptibility map must also be compared with known debris-flow fans to ensure that a realistic result is provided. The

output can be used to inform regional land-use planning and provide critical information on shallow landslide/debris-flow susceptibility to decision makers and stakeholders in the central Westland region. By overlaying the final map with the populated areas, road network and key infrastructure a preliminary evaluation of risk is also feasible in regional scale (Fig. 3.27).

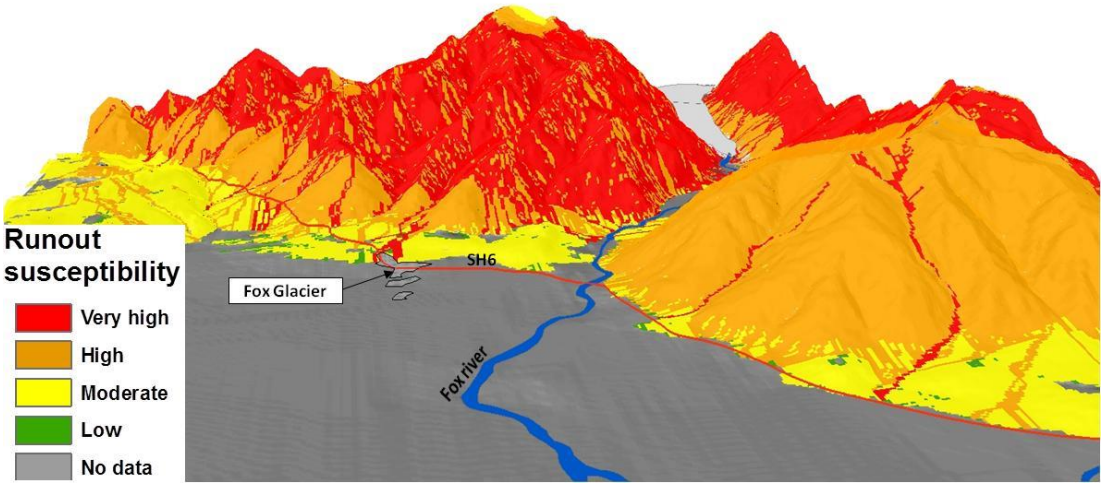

Figure 3.27 The runout susceptibility map reveals several potentially affected locations by debris-flows, which correspond to populated areas and infrastructure.

Previous studies, as well as the present work, highlight that the effectiveness of the final map is directly related to the quality of input data. Updating and improving existing landslide catalogues and inventories including more detailed information for each landslide event is crucial for the development of reliable susceptibility, hazard and risk assessment methods. Updating built environment layers is especially important in a rapidly-developing region. The availability of high quality datasets will also improve the accuracy of the assessments, significantly reducing the time and cost required to produce meaningful outputs making the information more accessible to local authorities, decision makers and key stakeholders. Future research should focus on the development, application and comparison of different landslide hazard and susceptibility methods investigating different landslide types at various scales, as well as on the understanding of the complex relationships between predisposing factors and landslide occurrence.

3.7 References

Aleotti P, Chowdhury R 1999. Landslide hazard assessment: summary review and new perspectives. – Bull. Engng. Geol. Environm., 58: 21–44

Ayalew L, Yamagishi H, Ugawa N 2004. Landslide susceptibility mapping using GIS-based weighted linear combination, the case in Tsugawa area of Agano River, Niigata Prefecture, Japan. Landslides 1:73–81.

Ayalew L, Yamagishi H, Marui H, Kanno T 2005. Landslides in Sado Island of Japan: Part II. GIS-based susceptibility mapping with comparisons of results from two methods and verifications. Engineering Geology 81(4): 432-445.

Ayalew L, Yamagishi H 2005. The application of GIS-based logistic regression for landslide susceptibility mapping in the Kakuda-Yahiko Mountains, Central Japan. Geomorphology, 65(1-2), 15-31.

Barringer JRF, Pairman D, McNeill SJ 2002. Development of a high resolution digital elevation model for New Zealand. Landcare Research Contract Report: LC0102/170.

Barth NC 2013. A tectono-geomorphic study of the Alpine Fault, New Zealand. PhD thesis, University of Otago, New Zealand. 303p.

Bell DH 1994. Landslide hazards. In: Canterbury Regional Council Report 94 (19), Natural hazards in Canterbury, 55–76.

Benn JL 1992. Review of Earthquake Hazards on the West Coast. The West Coast Regional Council, Greymouth. 62p.

Benn JL 2005. Landslide events on the West Coast, South Island, 1867-2002. New Zealand Geographer 61: 3-13.

Blahut J, Horton P, Sterlacchini S, Jaboyedoff M 2010. Debris flow hazard modelling on medium scale: Valtellina di Tirano, Italy. Nat. Hazards Earth Syst. Sci., 10, 2379–2390.

Bonham-Carter GF 1994. Geographic information systems for geoscientists. Ottawa, Pergamon.

Brabb EE, Pampeyan EH, Bonilla MG 1978. Landslide susceptibility in San Mateo County, California. US Geological Survey Miscellaneous Field Studies Map, MF-360, Map at 1: 62,500 scale.

Brabb EE 1984. Innovative approaches to landslide hazard and risk mapping, Proceedings of the 4th International Symposium on Landslides, 16–21 September, Toronto, Ontario, Canada (Canadian Geotechnical Society, Toronto, Ontario, Canada), 1:307–324.

Brune JN 2001. Shattered rock and precarious rock evidence for strong asymmetry in ground motions during thrust faulting. Seismological Society of America Bulletin 91: 441– 447.

Bui DT, Pradhan B, Lofman O, Revhaug I, Dick OB. 2012. Landslide susceptibility mapping at Hoa Binh province (Vietnam) using an adaptive neuro-fuzzy inference system and GIS. Computers & Geosciences 45:199–211.

Burrough PA, McDonell RA 1998. Principles of Geographical Information Systems. Oxford University Press, New York, p. 190.

Can T, Nefeslioglu HA , Gokceoglu C, Sonmez H, Duman TY 2005. Susceptibility assessments of shallow earthflows triggered by heavy rainfall at three catchments by logistic regression analyses. Geomorphology, 72(1-4), 250-271.

Cannon SH 1993. An empirical model for the volume-change behavior of debris flows. Proc. ASCE National Conference on Hydraulic Engineering, San Francisco, CA, pp. 1768–1773.

Carrara A, Merenda L (1976) Landslide inventory in northern Calabria, southern Italy. Geol Soc Am Bull, 87: 1153–1162.

Carrara A, Carratelli EP, Merenda L 1977. Computer-based data bank and statistical analysis of slope instability phenomena. Zeitschrift für Geomorphologie 21, 187–222.

Carrara A 1983. A multivariate model for landslide hazard evaluation. Mathematical Geology 15, 403–426.

Carrara A, Cardinali M, Detti R, Guzzetti F, Pasqui V, Reichenbach P 1991. GIS Techniques and statistical models in evaluating landslide hazard. Earth Surface Processes and Landform 16, 427–445.

Carrara A, Cardinali M, Guzzetti F, Reichenbach P 1995. GIS technology in mapping landslide hazard. In: Carrara A, Guzzetti F ed. Geographical Information Systems in Assessing Natural Hazards. Kluwer Academic Publisher, Dordrecht, The Netherlands, pp. 135–175.

Carrara A, Pike RJ 2008. GIS technology and models for assessing landslide hazard and risk. Geomorphology, 94(3-4), 257-260.

Carrara A, Crosta G, Frattini P 2008. Comparing models of debris-flow susceptibility in the alpine environment. Geomorphology 94, 353–378.

Champati ray PK, Dimri S, Lakhera RC, Sati S 2007. Fuzzy-based method for landslide hazard assessment in active seismic zone of Himalaya. Landslides 4:101–111.

Chau KT, Sze YL, Fung MK, Wong WY, Fong EL, Chan LCP 2004. Landslide hazard analysis for Hong Kong using landslide inventory and GIS. Computers & Geosciences 30:429–443.

Chen H, Lee CF 2004. Geohazards of slope mass movement and its prevention in Hong Kong. Engineering Geology 76: 3-25.

Chevalier G, Davies T, McSaveney M 2009. The prehistoric Mt Wilberg rock avalanche, Westland, New Zealand, Landslides 6: 253–262.

Chung CF, Fabbri AG 1999. Probabilistic prediction models for landslide hazard mapping, Photogrammetric Engineering & Remote Sensing 65(12), 1389–1399.

Chung CF, Fabbri A, Van Westen CJ 1995. Multivariate regression analysis for landslide hazard zonation, In: A. Carrara and F. Guzzetti (eds.), Geographical Information Systems in Assessing Natural Hazards, Kluwer Academic Publishers, the Netherlands, pp. 107–133.

Chung C-JF, Fabbri AG 2003. Validation of Spatial Prediction Models for Landslide Hazard Mapping. Natural Hazards 30(3): 451-472.

Colombo A, Lanteri L, Ramasco M, Troisi C 2005. Systematic GIS-based landslide inventory as the first step for effective landslide-hazard management. Landslides 2: 291–301.

Cooper LL 2000. Geotechnical hazard analysis, management and the development of Hazreg for the Buller District. Unpublished MSc Thesis (Engineering Geology). Department of Geological Sciences, University of Canterbury, Christchurch, Vol. 1, 205 pp; Vol. 2, Appendices.

Cooper RA 1989. Early Paleozoic terranes of New Zealand. Journal of the Royal Society of New Zealand 19: 73–112.

Cooper RA, Tulloch AJ 1992. Early Palaeozoic terranes in New Zealand and their relationship to the Lachlan Fold Belt. Tectonophysics 214(1/4): 129-144.

Corominas J 1996. The angle of reach as a mobility index for small and large landslides. Canadian Geotechnical Journal 33, 260–271.

Corominas J, Moya J, Ledesma A, Gili JA, Lloret A, Rius J 1998. New Technologies for Landslide Hazard Assessment and Management in Europe (NEWTECH), European Commission.

Costa JE 1984. Physical geomorphology of debris flows. In Costa & Fleisher (eds.). Developments and Applications of Geomorphology. Springer Verlag. pp. 268-317.

Costa-Cabral M, Burges SJ 1994. Digital elevation model networks (DEMON): A model of flow over hillslopes for computation of contributing and dispersal areas, Water Resour. Res., 30(6), 1681– 1692.

Cox SC, Barrell DJA (compilers) 2007. Geology of the Aoraki area. Institute of Geological & Nuclear Sciences 1:250 000 geological map 15. 1 sheet + 71 p. Lower Hutt, New Zealand. GNS Science.

Cox SC, Allen SK, Ferris BG 2008. Vampire rock avalanches, Aoraki/Mount Cook National Park, New Zealand. Science Report 2008/10, GNS Science, Lower Hutt, New Zealand, p. 34.

Cox SC, Allen SK 2009. Vampire rock avalanches of January 2008 and 2003, Southern Alps, New Zealand. Landslides 6:161–166.

Crosta GB, Imposimato S, Roddeman DG 2003. Numerical modelling of large landslides stability and runout. Natural Hazards and Earth System Sciences 3: 523–538.

Crozier MJ, Glade T 2005. Landslide hazard and risk: issues, concepts and approach. In: Glade T, Anderson MG, Crozier MJ ed. Landslide risk assessment. John Wiley, 1-40.

Dahal RK, Hasegawa S, Nonomura A, Yamanaka M, Masuda T, Nishino K 2008a. GIS-based weights-of-evidence modelling of rainfall induced landslides in small catchments for landslide susceptibility mapping. Environmental Geology, 54(2), 311-324.

Dahal RK, Hasegawa S, Nonomura A, Yamanaka M, Dhakal S, Paudyal P 2008b. Predictive modelling of rainfall-induced landslide hazard in the Lesser Himalaya of Nepal based on weights-of-evidence. Geomorphology, 102(3-4), 496-510.

Dahl M-PJ, Mortensen LE, Veihe A, Jensen NH 2010. A simple qualitative approach for mapping regional landslide susceptibility in the Faroe Islands. Nat. Hazards Earth Syst. Sci., 10, 159–170.

Dai FC, Lee CF, Li J, Xu ZW 2001. Assessment of landslide susceptibility on the natural terrain of Lantau Island, Hong Kong. Environmental Geology, 40(3), 381-391.

Dai FC, Lee, CF 2002. Landslide characteristics and, slope instability modeling using GIS, Lantau Island, Hong Kong. Geomorphology, 42(3-4), 213-228.

Dai FC, Lee CF, Ngai YY. 2002. Landslide risk assessment and management: an overview. Eng Geol 64: 65–87.

Davies TR, Scott BK 1997. Dambreak Flood Hazard from the Callery River, Westland New Zealand. New Zealand Journal of Hydrology, Vol. 36 (1), pp 1-13.

Davies TR, McSaveney 1999. Runout of dry granular avalanches. Canadian Geotechnical Journal 36: 2, 313-320.

Davies TRH 2002. Landslide dambreak flood hazards at Franz Josef Glacier township, NewZealand: a risk assessment. Journal of Hydrology (New Zealand) 41: 1-17.

Davies T 2007. Potential for rock avalanche hazard at Franz Josef glacier village, Westland. Confidential report to west coast regional council. Natural Hazards Research Centre Dept of Geological Sciences University of Canterbury, New Zealand, 14p.

Davies TR, McSaveney MJ 2008. Principles of sustainable development on fans. Journal of Hydrology (NZ) 47 (1): 43-65.

De Scally FA, Slaymaker O, Owens IF 2001. Morphometric controls and basin response in the Cascade Mountains. Geogr Ann 83A:117–130.

De Scally FA, Owens IF 2004. Morphometric controls and geomorphic response on fans in the Southern Alps, New Zealand. Earth Surf Process Land 29:311–322.

Dietrich EW, Reiss R, Hsu M-L, Montgomery DR 1995. A process-based model for colluvial soil depth and shallow landsliding using digital elevation data. Hydrological Process 9, 383–400.

Dhakal SA, Amada T, Aniya M 2000. Landslide Hazard Mapping and its Evaluation Using GIs: An Investigation of Sampling Schemes for a Grid-Cell Based Quantitative Method. Photogrammetric Engineering & Remote Sensing, Vol. 66, No. 8., 981-989.

Dikau R, Schrott L, Dehn M, Hennrich K, Rasemann S 1996. The Temporal Stability and Activity of Landslides in Europe with respect to Climatic Change (TESLEC), European Commission.

Donati L, Turrini MC 2002. An objective method to rank, the importance of the factors predisposing to landslides with the GIS methodology: application to an area of the Apennines, (Valnerina; Perugia, Italy). Engineering Geology, 63(3-4), 277-289.

Dramis F, Sorriso-Valvo M 1994. Deep-seated gravitational slope deformation, related landslides and tectonics. Engineering Geology 38: 231–243.

DTec Consulting Ltd 2002. West Coast Regional Council: Natural Hazards Review. Report prepared for West Coast Regional Council by Dtec Consulting Ltd. Client Reference: 1065.136WCRC, Greymouth. 140 p.

Dubois D, Prade H 1985. A review of fuzzy set aggregation connectives. Information Sciences 36, 85–121.

Dufresne A, Davies TR, McSaveney MJ 2009. Influence of runout-path material on emplacement of the Round Top rock avalanche, New Zealand. Earth Surface Processes and Landforms. DOI: 10.1002/esp.1900.

Duman TY, Can T, Gokceoglu C, Nefeslioglu HA, Sonmez H 2006. Application of logistic regression for landslide susceptibility zoning of Cekmece Area, Istanbul, Turkey. Environ Geol (2006) 51: 241–256 DOI 10.1007/s00254-006-0322-1

Eggers MJ 1987. Engineering geology assessment of slope instability on forest lands in South Westland. Unpublished MSc thesis, University of Canterbury, Christchurch, New Zealand. 345p.

England K 2011. A GIS approach to landslide hazard management for the West Coast region, New Zealand. Unpublished MSc thesis, University of Canterbury, Christchurch, New Zealand.

Ercanoglu M 2005. Landslide susceptibility assessment of SE Bartin (West Black Sea region, Turkey) by artificial neural networks. Natural Hazards and Earth System Sciences, 5, 979–992.

Ercanoglu M, Gokceoglu C 2002. Assessment of landslide susceptibility for a landslide-prone area (north of Yenice, NW Turkey) by fuzzy approach. Environmental Geology 41:720–730.

Ercanoglu M, Gokceoglu C 2004. Use of fuzzy relations to produce landslide susceptibility map of a landslide prone area (West Black Sea Region, Turkey). Engineering Geology 75, 229–250.

Ercanoglu M, Temiz FA 2011. Application of logistic regression and fuzzy operators to landslide susceptibility assessment in Azdavay (Kastamonu, Turkey). Environ Earth Sci 64:949–964.

Ermini L, Catani F, Casagli N 2005. Artificial Neural Networks applied to landslide susceptibility assessment. Geomorphology, 66(1-4), 327-343.

Erskine R, Green T, Ramirez J, MacDonald L 2006. Comparison of grid-based algorithms for computing upslope contributing area. Water Resources Research, Vol. 42, W09416, doi:10.1029/2005WR004648.

ESRI 2008. ArcGIS Desktop Help 9.2 – Classification methods. Available at: http://webhelp.esri.com/arcgisdesktop/9.2/index.cfm?TopicName=Classification_methods Accessed on 9/30/2011

ESRI 2011. ArcGIS Desktop Help 9.3 – About updating statistics. Available at: http://webhelp.esri.com/arcgisdesktop/9.3/index.cfm?TopicName=How%20Slope%20works Accessed on 9/30/2011

Fairfield J, Leymarie P 1991. Drainage networks from grid digital elevation models, Water Resour. Res., 27(5), 709–717.

Falaschi F, Giacomelli F, Federici PR, Puccinelli A, D'Amato Avanzi G, Pochini A, Ribolini A 2009. Logistic regression versus artificial neural networks: landslide susceptibility evaluation in a sample area of the Serchio River valley, Italy. Nat Hazards 50:551–569. DOI 10.1007/s11069-009-9356-5.

Fall M, Azzam R, Noubactep C 2006. A multi-method approach to study the stability of natural slopes and landslide susceptibility mapping. Engineering Geology 82: 241–263.

Fannin RJ, Wise MP 2001. An empirical-statistical model for debris flow travel distance. Canadian Geotechnical Journal, 38: 982-994

Frattini P, Crosta G, Carrara A 2010. Techniques for evaluating the performance of landslide susceptibility models. Engineering Geology 111(1-4): 62-72.

Freeman TG 1991. Calculating catchment area with divergent flow based on a regular grid, Comput. Geosci., 17(3), 413–422.

Galli M, Ardizzone F, Cardinali M, Guzzetti F, Reichenbach P 2008. Comparing landslide inventory maps. Geomorphology 94:268–289.

Glade T , Crozier MJ 1999. Landslides in New Zealand - a selected bibliography.- Research Report No. 1, School of Earth Sciences, Victoria University of Wellington, New Zealand, 103 pp.

Gokceoglu C, Sezer E 2009. A statistical assessment on international landslide literature (1945–2008). Landslides 6:345–351.

Gorsevski PV, Gessler PE, Boll J, Elliot WJ, Foltz RB 2006. Spatially and temporally distributed modeling of landslide susceptibility. Geomorphology, 80(3-4), 178-198.

Guinau M, Vilajosana I, Vilaplana JM 2007. GIS-based debris flow source and runout susceptibility assessment from DEM data – a case study in NW Nicaragua. Nat. Hazards Earth Syst. Sci., 7, 703–716.

Gupta RP, Joshi BC 1989. Landslide hazard zoning using the GIS approach – a case study from the Ramganga catchment, Himalayas. Engineering Geology 28: 119–131.

Guzzetti F, Carrara A, Cardinali M, Reichenbach P 1999. Landslide hazard evaluation: a review of current techniques and their application in a multi-scale study, central Italy. Geomorphology 31, 181–216.

Guzzetti F, Malamud BD, Turcotte DL, Reichenbach P 2002. Power-law correlations of landslide areas in Central Italy. Earth and Planetary Science Letters 195, 169– 183.

Guzzetti F, Reichenbach P, Cardinali M, Galli M, Ardizzone F 2005. Probabilistic landslide hazard assessment at the basin scale. Geomorphology 72: 272-299.

Guzzetti F, Reichenbach P, Ardizzone F, Cardinali M, Galli M 2006. Estimating the quality of landslide susceptibility models. Geomorphology 81(1-2): 166-184.

Guzzetti F, Ardizzone F, Cardinali M, Rossi M, Valigi D 2009. Landslide volumes and landslide mobilization rates in Umbria, central Italy. Earth and Planetary Science Letters, 279, 222–229.

Hancox GT, McSaveney MJ, Manville VR, Davies TRH 2005. The October 1999 Mt Adams rock avalanche and subsequent landslide dam-break flood and effects in Poerua River, Westland, New Zealand. New Zealand Journal of Geology & Geophysics 48: 683-705.

Hart RD 1993. An introduction to distinct element modelling for rock engineering. In Hudson (ed.), Comprehensive Rock Engineering: Principles, Practice & Projects. Oxford: Pergamon Press, v.2, 245-261.

He YP, Beighley RE 2008. GIS-based regional landslide susceptibility mapping: a case study in southern California. Earth Surface Processes and Landforms, 33(3), 380-393.

Henderson RD, Thompson SM 1999. Extreme rainfalls in the Southern Alps of New Zealand. Journal of Hydrology (New Zealand) 38: 309-330.

Hewitt K 2006. Disturbance regime landscapes: mountain drainage systems interrupted by large rockslides. Progress in Physical Geography, Vol. 30, No. 3, 365-393.

Hewitt K, Clague JJ, Orwin JF 2008. Legacies of catastrophic rock slope failures in mountain landscapes. Earth-Science Reviews 87, 1-38.

Heywood I, Oliver J, Tomlinson S 1995. Building an exploratory multi-criteria modeling environment for spatial decision support. In: Fisher, P. (ed.): Innovations in GIS 2: 127-136, Bristol (Taylor & Francis).

Horton P, Jaboyedoff M, Bardou, E 2008. Debris flow susceptibility mapping at a regional scale, 4th Canadian Conference on Geohazards, Quebec, Canada, May 20–24, 2008.

Hovius N, Stark CP, Allen PA 1997. Sediment flux from a mountain belt derived from landslide mapping. Geology 25, 231– 234.

Hsu KJ 1978. Albert Heim: observations on landslides and relevance to modern interpretations. In: Voight, B. (Ed.), Rockslides and Avalanches, vol. 1, Elsevier, Amsterdam, pp. 71– 93.

Huabin W, Gangjun L, Weiya X, Gonghui W 2005. GIS based landslide hazard assessment: an overview. – Progr. Phys. Geogr., 29 (4): 548–567.

Hungr O, Corominas J, Eberhardt E 2005. Estimating landslide motion mechanisms, travel distance and velocity. Proceed. Int. conf. on Landslide Risk Management, O. Hungr, R. Fell, R. Couture and E. Eberhardt eds.: 99-128, Taylor and Francis, London.

Hutchinson JN 1986. A sliding-consolidation model for flow slides. Canadian Geotechnical Journal 23: 115-126.

Hutchinson JN 1995. Keynote paper: landslide hazard assess- ment. In: Bell (Ed.), Landslides. Balkema, Rotterdam, pp. 1805–1841.

Jaboyedoff M, Labiouse V 2003. Preliminary assessment of rockfall hazard based on GIS data, in: 10th International Congress on Rock Mechanics ISRM 2003. Technology roadmap for rock mechanics, South African Institute of Mining and Metallurgy, Johannesburg, South Africa, 575–578, 2003.

Jaboyedoff M, Labiouse V 2011. Technical Note: Preliminary estimation of rockfall runout zones. Nat. Hazards Earth Syst. Sci., 11, 819–828.

Jackson LE, Kostashuk RA, MacDonald GM 1987. Identification of debris flow hazard on alluvial fans in the Canadian Rocky mountains. Geological Society of America. Reviews in Engineering Geology VII: 155-124.

Juang CH, Lee DH, Sheu C 1992. Mapping slope failure potential using fuzzy sets. Journal of Geotechnical Engineering, ASCE 118, 475–494.

Kamp U, Growley BJ, Khattak GA, Owen LA 2008. GIS-based landslide susceptibility mapping for the 2005 Kashmir earthquake region. Geomorphology 101, 631–642.

Kanungo DP, Arora MK, Sarkar S, Gupta RP 2006. A comparative study of conventional, ANN black box, fuzzy and combined neural and fuzzy weighting procedures for landslide susceptibility zonation in Darjeeling Himalayas. Engineering Geology 85, 347–366.

Kanungo DP, Arora MK, Gupta RP, Sarkar S 2008. Landslide risk assessment using concepts of danger pixels and fuzzy set theory in Darjeeling Himalayas. Landslides 5:407-416.

Kanungo DP, Arora MK, Sarkar S, Gupta RP 2009. A fuzzy set based approach for integration of thematic maps for landslide susceptibility zonation. Georisk: Assessment and Management of Risk for Engineered Systems and Geohazards, 3:1, 30-43.

Kappes MS, Malet JP, Remaître A, Horton P, Jaboyedoff M, Bell R 2011. Assessment of debris-flow susceptibility at medium-scale in the Barcelonnette Basin, France, Nat. Hazards Earth Syst. Sci., 11, 627–641.

Kellogg, K. S. 2001: Tectonic controls on a large landslide complex: Williams Fork Mountains near Dillon, Colorado. Geomorphology 41: 355–368.

Klir GJ, Clair UHS, Yuan B 1997. Fuzzy set theory. Foundations and applications. Prentice-Hall, 245pp

Komac M 2006. A landslide susceptibility model using the Analytical Hierarchy Process method and multivariate statistics in perialpine Slovenia. Geomorphology 74: 17–28.

Korup O 2004. Geomorphic implications of fault zone weakening: slope instability along the Alpine Fault, South Westland to Fiordland. New Zealand Journal of Geology and Geophysics 47, 257-267.

Korup O, Schmidt J, McSaveney MJ 2005. Regional relief characteristics and denudation pattern of the western Southern Alps, New Zealand. Geomorphology 71, 402-423.

Korup O 2005b. Geomorphic hazard assessment of landslide dams in South Westland, New Zealand – fundamental problems and approaches. Geomorphology 66, 167-188.

Korup O 2005c. Large landslides and their effect on alpine sediment flux: South Westland, New Zealand. Earth Surface Processes and Landforms 30, 305-323.

Korup O 2005d. Geomorphic imprint of landslides on alpine river systems, southwest New Zealand. Earth Surface Processes and Landforms 30, 783-800.

Korup O 2005e. Distribution of landslides in southwest New Zealand. Landslides 2, 43–51.

Korup O 2006b. Effects of deep-seated bedrock landslides on hillslope morphology, Southern Alps, New Zealand. Journal of Geophysical Research 111, F01018, doi:10.1029/2004JF000242.

Korup O, Densmore AL, Schlunegger F 2009. The role of landslides in mountain range evolution. Geomorphology, doi:10.1016/j.geomorph.2009.09.017.

Kouli M, Loupasakis C, Pantelis Soupios P, Vallianatos F 2010. Landslide hazard zonation in high risk areas of Rethymno Prefecture, Crete Island, Greece. Nat Hazards (2010) 52:599–621 DOI 10.1007/s11069-009-9403-2

Kritikos T, Davies TRH 2011. GIS-based multi-criteria decision analysis for landslide susceptibility mapping at northern Evia, Greece. Z. dt. Ges. Geowiss., 162/4, p. 421–434.

Ladas I, Fountoulis I, Mariolakos I 2007. Using GIS & Multicriteria Decision Analysis in landslide susceptibility mapping a case study in Messinia prefecture area (SW Peloponnesus, Greece). Proc. of the 11th Nat. Congress / Bull. Geol. Soc. Greece, 40 (4): 1973–1985.

Larsen IJ, Montgomery DR 2012. Landslide erosion coupled to tectonics and river incision. Nature Geoscience, Vol. 5, 468-473.

Lea NL 1992. An aspect driven kinematic routing algorithm, in Overland Flow: Hydraulics and Erosion Mechanics, edited by A. J. Parsons and A. D. Abrahams, Chapman & Hall, New York.

Leathwick JR, Morgan F, Wilson G, Rutledge D, McLeod M, Johnston K 2002. LENZ technical guide. Ministry for the Environment, Wellington.

Lee DH, Juang CH 1992. Evaluation of failure potential in mudstone slopes using fuzzy sets. ASCE Geotechnical Special Publication 31, Stability and Performance of Slopes and Embankment- II, vol. 2, pp. 1137–1151.

Lee S 2004. Application of likelihood ratio and logistic regression models to landslide susceptibility mapping using GIS. Environmental Management, 34(2), 223-232.

Lee S, Choi J, Min K 2002. Landslide susceptibility analysis and verification using the Bayesian probability model. Environmental Geology, 43(1-2), 120-131.

Lee S, Choi J 2004. Landslide susceptibility mapping using GIS and the weight-of-evidence model. International Journal of Geographical Information Science, 18(8), 789-814.

Lee S, Talib JA 2005. Probabilistic landslide susceptibility and factor effect analysis. Environmental Geology, 47(7), 982-990.

Lee S 2005. Application of logistic regression model and its validation for landslide susceptibility mapping using GIS and remote sensing data, International Journal of Remote Sensing, 26:7, 1477-1491.

Lee GS, Lee KH 2006. Application of fuzzy representation of geographic boundary to the soil loss model. Hydrol. Earth Syst. Sci. Discuss., 3, 115–133.

Lee S, Sambath T 2006. Landslide susceptibility mapping in the Damrei Romel area, Cambodia using frequency ratio and logistic regression models. Environmental Geology, 50(6), 847-855.

Lee S 2007a. Comparison of landslide susceptibility maps generated through multiple logistic regression for three test areas in Korea. Earth Surf. Process. Landforms 32, 2133–2148.

Lee S 2007b. Application and verification of fuzzy algebraic operators to landslide susceptibility mapping. Environ Geol 52:615–623.

Li Y, Chen G, Tang C, Zhou G, Zheng L 2012. Rainfall and earthquake-induced landslide susceptibility assessment using GIS and Artificial Neural Network. Nat. Hazards Earth Syst. Sci., 12, 2719–2729.

Luo X, Dimitrakopoulos R 2003. Data-driven fuzzy analysis in quantitative mineral resource assessment. Computers & Geosciences 29, 3–13.

Magliulo P, Di Lisio A, Russo F 2009. Comparison of GIS-based methodologies for the landslide susceptibility assessment. Geoinformatica 13:253–265

Major JJ, Iverson RM 1999. Debris-flow deposition: Effects of pore-fluid pressure and friction concentrated at flow margins. GSA Bulletin, v. 111, no. 10, p. 1424–1434.

Malamud BD, Turcotte DL, Guzzetti F, Reichenbach P 2004. Landslide inventories and their statistical properties. Earth Surface Processes and Landforms 29 (6), 687– 711.

Mamdani EM 1974. Applications of Fuzzy Algorithms for Simple Dynamic Plants; Proc. IEEE, vol. 21, no. 12, pp.1585-1588.

McCahon I, Elms D, Dewhirst R 2006. West Coast Engineering Lifelines Group Study: Alpine fault earthquake scenario. A report prepared for the West Coast Engineering Lifelines Group and the West Coast Regional Council. Greymouth, 204 p.

McSaveney MJ, Davies TR 1998. Natural Hazard Assessment for the township of Franz Josef Glacier and its Environs. Client Report 43714B.10, Institute of Geological and Nuclear Sciences, Lower Hutt, 58 p.

McSaveney MJ 2002. Recent rock falls and rock avalanches in Mount Cook National Park, New Zealand. Geological Society of America Reviews in Engineering Geology XV: 35-70.

McSaveney MJ, Beetham RD, Leonard GS 2005. The 18 May 2005 debris flow disaster at Matata: Causes and mitigation suggestions. GNS Science client report 2005/71. Prepared for Whakatane District Council, 51p.

Melton MA 1965. The geomorphic and paleoclimatic significance of alluvial deposits in southern Arizona. J Geol 73:1–38.

Metcalf PL 1993. Landslide investigation and hazard zonation in the Greymouth urban area. Unpublished MSc Thesis (Engineering Geology). Geology Department, University of Canterbury, Christchurch, 184 pp.

Michael-Leiba M, Baynes F, Scott G, Granger K 2003. Regional Landslide Risk to the Cairns Community. Natural Hazards 30: 233–249.

Miles SB, Keefer DK 2007. Comprehensive areal model of earthquake-induced landslides: technical specification and user guide. U.S. Geological Survey Open File Report 2007-p1072, 69pp.

Ministry for the Environment (MfE) 2004. New Zealand Land Cover Database 2 (LCDB2).

Montgomery DR, Dietrich WE 1994. A physically based model for the topographic control of shallow landsliding. Water Resources Research 30:4, 1153–1171.

Mortimer N, Tulloch AJ, Spark RN, Walker NW, Ladley E, Allibone A, Kimbrough DL 1999. Overview of the Median Batholith, New Zealand: a new interpretation of the geology of the Median Tectonic Zone. Journal of African Earth Sciences 29: 257–268.

Nandi A, Shakoor A 2009. A GIS-based landslide susceptibility evaluation using bivariate and multivariate statistical analyses. Engineering Geology, 110(1-2), 11-20.

Naranjo JL, VanWesten CJ, Soeters R. 1994. Evaluating the use of training areas in bivariate statistical landslide hazard analysis: a case study in Colombia, ITC Journal 1994-3, 292–300.

Nathan S, Rattenbury MS, Suggate RP (compilers) 2002. Geology of the Greymouth area. Institute of Geological & Nuclear Sciences 1:250 000 geological map 12. 1 sheet + 58 p. Lower Hutt, New Zealand. GNS Science.

Neuhäuser B, Terhorst B 2007. Landslide susceptibility assessment using “weights-of-evidence” applied to a study area at the Jurassic escarpment (SW-Germany). Geomorphology, 86(1-2), 12-24.

O’Callaghan JF, Mark DM 1984. The extraction of drainage networks from digital elevation data, Comput. Vision Graphics Image Process., 28, 328–344.

Ohlmacher GC, Davis JC 2003. Using multiple logistic regression and GIS technology to predict landslide hazard in northeast Kansas, USA. Engineering Geology 69: 331–343.

Ohlmacher GC 2007. Plan curvature and landslide probability in regions dominated by earth flows and earth slides. Engineering Geology, 91(2-4), 117-134.

Oreskes N 1998. Evaluation (not validation) of quantitative models. Environ. Health Perspect. 106 (suppl. 6), 1453–1460.

http://ehp.niehs.nih.gov/members/1998/Suppl-6/1453 1460oreskes/oreskesfull.html.

Paxton R 2010. Method for the extraction and analysis of hillslope profiles for the detection of slumps in Westland, New Zealand. Unpublished BSc thesis. University of Canterbury, Christchurch, New Zealand.

Petley D 2010. Landslide hazards. In: Alcantara-Ayala I, Goudie A ed. Geomorphological hazards and disaster prevention. Cambridge, Cambridge University Press, 2010. pp. 13 – 28.

Petley D 2012. Global patterns of loss of life from landslides. Geology, v. 40; no. 10; p. 927–930.

Pistocchi A, Luzi L, Napolitano P 2002. The use of predictive modelling techniques for optimal exploitation of spatial databases: a case study in landslide hazard mapping with expert system-like methods. Environmental Geology 41:765–775.

Porwal A, Carranza EJM, Hale M 2006. A Hybrid Fuzzy Weights-of-Evidence Model for Mineral Potential Mapping**.** Natural Resources Research, Vol. 15, No. 1, 1-14.

Power J, Anderson C 1992. Geotechnical report; Assessment of hazard and risk to the Little Wanganui subdivision. Report prepared by Barrett, Fuller and Partners for the Buller District Council, Westport: 8 pp.

Pradhan B, Lee S 2007. Utilization of Optical Remote Sensing Data and GIS Tools for Regional Landslide Hazard Analysis Using an Artificial Neural Network Model. Earth Science Frontiers 14(6): 143–152.

Pradhan B 2010. Landslide Susceptibility mapping of a catchment area using frequency ratio, fuzzy logic and multivariate logistic regression approaches. J. Indian Soc. Remote Sens. 38:301– 320.

Pradhan B, Oh H-J, Buchroithner M 2010a. Weights-of-evidence model applied to landslide susceptibility mapping in a tropical hilly area. Geomatics, Natural Hazards and Risk, Vol. 1, No. 3, 199–223.

Pradhan B, Lee S, Buchroithner MF 2010b. A GIS-based back-propagation neural network model and its cross-application and validation for landslide susceptibility analyses. Computers, Environment and Urban Systems (2010), doi:10.1016/j.compenvurbsys.2009.12.004.

Pradhan B 2011a. Manifestation of an advanced fuzzy logic model coupled with Geo-information techniques to landslide susceptibility mapping and their comparison with logistic regression modelling. Environ Ecol Stat 18:471–493.

Pradhan B 2011b. Use of GIS-based fuzzy logic relations and its cross application to produce landslide susceptibility maps in three test areas in Malaysia. Environ Earth Sci 63:329–349.

Quinn P, Beven K, Chevallier P, Planchon O 1991. The prediction of hillslope flow paths for distributed hydrological modeling using digital terrain models, Hydrol. Proc., 5, 59–80.

Rattenbury MS, Jongens R, Cox SC (compilers) 2010. Geology of the Haast area. Institute of Geological & Nuclear Sciences 1:250 000 geological map 14. 1 sheet + 58 p. Lower Hutt, New Zealand. GNS Science.

Remondo J, González-Díez A, Diaz De Terán JR, Cendrero A 2003a. Landslide Susceptibility Models Utilising Spatial Data Analysis Techniques. A Case Study from the Lower Deba Valley, Guipúzcoa (Spain). Natural Hazards, 30:3 267-279.

Remondo J, Gonzalez A, De Teran JRD, Cendrero A, Fabbri A, Chung CJF 2003b. Validation of landslide susceptibility maps; Examples and applications from a case study in northern Spain. Natural Hazards, 30(3), 437-449.

Ross T 1995. Fuzzy logic with engineering applications. McGraw-Hill, New York.

Rupke J, Cammeraat E, Seijmonsbergen AC, van Westen CJ 1988. Engineering geomorphology of Widentobel Catchment, Appenzell and Sankt Gallen, Switzerland: a geomorphological inventory system applied to geotechnical appraisal of slope stability. Engineering Geology, 26:33–68.

Saboya Jr. F Alves MDG, Pinto WD 2006. Assessment of failure susceptibility of soil slopes using fuzzy logic. Engineering Geology 86, 211–224.

Saha AK, Gupta RP, Arora MK 2002. GIS-based Landslide Hazard Zonation in the Bhagirathi (Ganga) Valley, Himalayas. International Journal of Remote Sensing, 23(2), 357-369.

Sassa K, Tsuchiya S, Ugai K, Wakai A, Uchimura T 2009. Landslides: a review of achievements in the first 5 years (2004–2009). Landslides 6:275–286.

Schicker RD 2010. Quantitative landslide susceptibility assessment of the Waikato region using GIS. Unpublished MSc thesis, University of Waikato, Hamilton, New Zealand.

Seville E, Metcalfe J 2005. Developing a hazard risk assessment framework for the New Zealand State Highway network. Land Transport New Zealand Research Report 276. 80pp.

Snyder NP, Whipple KX, Tucker GE, Merritts DJ 2000. Landscape response to tectonic forcing: Digital elevation model analysis of stream profiles in the Mendocino triple junction region, northern California. Geological Society of America Bulletin, 112:1250-1263.

Soeters R, Van Westen CJ. 1996. Slope stability: recognition, analysis and zonation. In Landslides: Investigation and Mitigation, Transportation Research Board, National Research Council Special Report 247, Turner AK, Shuster RL (eds); 129 –177.

Song S, Zhang B, Feng W, Zhou W 2006. Using Fuzzy Relations and GIS Method to Evaluate Debris Flow Hazard. Whuan Journal of Natural Sciences. Vol. 11, No. 4, 875-881.

Stark CP, Hovius N 2001. The characterization of landslide size distributions. Geophysics Research Letters 28 (6), 1091– 1094.

Süzen ML, Doyuran V 2003. A comparison of the GIS based landslide susceptibility assessment methods: multivariate versus bivariate. Environmental Geology 45:665–679. DOI 10.1007/s00254-003-0917-8.

Tangestani MH 2004. Landslide susceptibility mapping using the fuzzy gamma approach in a GIS, Kakan catchment area, southwest Iran. Australian Journal of Earth Sciences, 51(3), 439-450.

Tarboton DG (1997) A new method for the determination of flow directions and upslope areas in grid digital elevation models. Water Resour Res 33: 309–319.

Terlien MTJ, Van Westen CJ, Van Asch ThWJ 1995. Deterministic modelling in GIS-based landslide hazard assessment. In: Carrara, A., Guzzetti, F. (Eds.), Geographical Information Systems in Assessing Natural Hazards. Kluwer Academic Publisher, Dordrecht, The Netherlands, pp. 57–77.

Thiery Y, Malet J-P. Maquaire O 2006. Test of Fuzzy Logic Rules for landslide susceptibility assessment. In Weber C. and Gancarski P. (Eds): SAGEO 2006, Proceedings International

Conference on Spatial Analysis and Geomatics, Strasbourg, France, CD-Rom Support Proceedings, 18p.

Thiery Y, Malet JP, Sterlacchini S, Puissant A, Maquaire O 2007. Landslide susceptibility assessment by bivariate methods at large scales: Application to a complex mountainous environment. Geomorphology, 92(1-2), 38-59.

Thompson CR 2002. The High Intensity Rainfall Design System: HIRDS. In: NIWA ed. Wellington

Toyos G, Oramas Dorta D, Oppenheimer C, Pareschi MT, Sulpizio R, Zanchetta G 2007. GIS-assisted modelling for debris flow hazard assessment based on the events of May 1998 in the area of Sarno, Southern Italy: Part I. Maximum run-out. Earth Surface Processes and Landforms, 32(10): 1491-1502.

United States Geological Service 1997. Standards for digital elevation models. Mid-Continent Mapping Center, Branch of Research, Technology and Applications, 67p.

Van Westen CJ, Rengers N, Terlien MTJ, Soeters R 1997. Prediction of the occurrence of slope instability phenomena through GIS-based hazard zonation. Geologische Rundschau, 86: 404-414.

Van Westen CJ, Seijmonsbergen AC, Mantovani F 1999. Comparing Landslide Hazard Maps. Natural Hazards 20: 137–158.

Van Westen CJ, Rengers N, Soeters R 2003. Use of geomorphological information in indirect landslide susceptibility assessment. Natural Hazards, 30(3), 399-419.

Van Westen CJ, Van Asch Th W J, Soeters R 2006. Landslide hazard and risk zonation: why is it still so difficult? Bulletin of Engineering Geology and the Environment 65, 167–184.

Van Westen CJ, Castellanos E, Kuriakose SL 2008. Spatial data for landslide susceptibility, hazard, and vulnerability assessment: An overview. Engineering Geology 102(3-4): 112-131.

Varnes DJ 1984. Landslide Hazard Zonation: a review of principles and practice. Commission on landslides of the IAEG, UNESCO, Nat Hazards 3:61.

Voogd H 1983. Multicriteria evaluation for urban and regional planning. London (Pion), 367 p.

Wang HB, Sassa K, Hu WY 2007. Assessment of Landslide Susceptibility Using Multivariate Logistic Regression: A Case Study in Southern Japan. Environmental & Engineering Geoscience, Vol. XIII, No. 2, pp. 183–192.

Wang WD, Xie CM, Du XG 2009. Landslides susceptibility mapping based on geographical information system, GuiZhou, south-west China. Environ Geol 58:33–43.

Warr LN, Cox S 2001. Clay mineral transformations and weakening mechanisms along the Alpine Fault, New Zealand. In: Holdsworth, R. E.; Strachan, R. A.; Magloughlin, J. F.; Knipe, R. J. ed. The nature and tectonic significance of fault zone weakening. Geological Society London Special Publication 186: 85–101.

Watts JK, Cox SC 2010. Assessment of debris flow potential on alluvial fans in Otago, New Zealand, using morphometry. GNS Science Consultancy Report 2010/144. Prepared for Otago Regional Council. 27p.

Welsh AJ 2008. Delineating debris-flow hazards on alluvial fans in the Coromandel and Kaimai regions, New Zealand using GIS. MSc thesis, University of Canterbury, New Zealand, 169p + App.

Welsh A, Davies T 2011. Identification of alluvial fans susceptible to debris-flow hazards. Landslides 8:183–194.

Whipple KX, Dunne T 1992. The influence of debris-flow rheology on fan morphology, Owens Valley, California. Geological Society of America Bulletin, v.104, p. 887-900.

Whipple KX 2004. Bedrock rivers and the geomorphology of active orogens, Ann. Rev. Earth Planet. Sci., 32, 85–151.

Whitehouse IE 1983. Distribution of large rock avalanche deposits in the central Southern Alps, New Zealand. New Zealand Journal of Geology and Geophysics 26: 272-279.

Whitehouse IE, Griffiths GA 1983. Frequency and Hazard of Large Rock Avalanches in the Central Southern Alps, New Zealand. Geology, Vol. 11, pp 331-334.

Wilford DJ, Sakal ME, Innes JL, Sidle RC, Bergerud WA (2004) Recognition of debrisflow, debris-flood and flood hazard through watershed morphometrics. Landslides 1:61–66.

Wilson JP, Lam CS, Deng Y 2007. Comparison of the performance of flow-routing algorithms used in GIS-based hydrologic analysis. Hydrological Processes. 21:1026-1044.

Wright CA 1999. The AD 930 long-runout Round Top debris avalanche, Westland, New Zealand. New Zealand Journal of Geology and Geophysics 41: 493–497.

Yoshimatsu H, Abe S 2006. A review of landslide hazards in Japan and assessment of their susceptibility using an analytical hierarchic process (AHP) method. Landslides 3: 149–158.

Yen J, Langari R 1999. Fuzzy Logic: Intelligent Control and Information, Prentice Hall. 532p.

Yetton MD 1997. Draft of evidence (Little Wanganui) by Geotech Consulting Ltd. in the case of Smaill and Ors v. Buller District Council and Ors: 14 pp.

Zadeh LA 1965. Fuzzy sets. Information and control, 8:338:353.

Zadeh LA 1973. Outline of a New Approach to the Analysis of Complex Systems and Decision Processes; IEEE Trans. Syst. Man. Cybern., vol. 3, no. 1, pp. 28-44.

Zimmermann HJ 1991. Fuzzy Set Theory and Its Applications. Kluwer Academic Publishers, Boston, 399pp.

Chapter 4: Flood susceptibility assessment

4.1 Introduction

Flooding is a recurring hazard in the West Coast of New Zealand's South Island, often with disastrous impact on local communities. Although the extremely high orographically-enhanced precipitation (up to 14m/yr close to the Main Divide; Henderson & Thomson 1999) combined with the steep topography have been recognized as the main factors for river floods in West Coast region (Griffiths & McSaveney 1983), a number of other geomorphic processes have been also identified as very important factors such as, river aggradation (McSaveney & Davies 1998; Davies et al 2003a; Korup 2005c; Davies & McSaveney 2006; Davies & Korup 2007) landslide dam break floods (Davies & Scott 1997; Davies 2002; Korup 2005b; Hancox et al 2005) and glacier bursts (Davies et al. 2003b; Goodsell et al. 2005; Korup & Tweed 2007). Nevertheless, floods - even those of high magnitude - are natural and expected phenomena of rivers and they become hazards only when the floodplain is occupied by settlements and infrastructure (Gupta 2010). The fact that most settlements are located in active floodplains is the main factor underlying the high flood risk in the region. Benn (1990) compiled 405 flood events occurring between 1846 and March 1990 and further 69 events between April 1990 and June 2002 were added as part of the Natural Hazard Review (DTEC 2002). Both records together provide information on 471 events in a 156 year period that indicate the frequency of floods and the level of hazard in West Coast region.

4.1.1 Flood hazard mapping

To mitigate the impact of flooding, flood hazard mapping has been considered a vital component in guiding land use planning and in communicating critical information such as the spatial extent of inundation, flood depth, flow velocity and probability of occurrence to decision makers, stakeholders and the general public. The growing demand for more reliable maps in flood hazard and risk assessment spurred the development of flood modelling based on different approaches such as: hydrological, which include several rainfall-runoff and statistical models used to simulate a flood providing information on flow discharge, time and return periods (e.g. HEC-HMS; TOPKAPI; TOPMODEL); hydraulic, which allow the simulation of flood propagation in a watercourse through the implementation of 1D, 2D and 3D hydrodynamic models (e.g. MIKE11; HEC-RAS; FLO-2D; SOBEK); geomorphological , which include the modification of the landscape by the river flow (Rodriguez-Iturbe & Valdes 1979; Baker 1976; Baker 2008; Lastra et al. 2008; Benito & Hudson 2010)

and various combinations of the above approaches. Although the principles of hydrological modelling predate GIS by more than a century (Maidment 1993a), the integration of GIS with hydrological modelling did not take place until the late 1980s as a result of the rapidly improving analytical capabilities of GIS and the increased demand for accurate representations of terrain by hydrologists (Sui & Maggio 1999). The mutual benefits from this integration have been illustrated by many previous researchers (DeVantier & Feldman 1993; Maidment 1993a; McDonnell 1996; Moore 1996), while others have identified the limitations of GIS in hydrological modelling (Maidment 1993a; Bennett 1997; Clark 1998; Sui & Maggio 1999) and the need for further improvement. A number of integration examples exist ranging from "tight integration" (or coupling) where the modelling process occurs within the GIS environment, to less integrated (loose) approaches where GIS is used in the pre-processing, model parameterisation and post-processing (display) stages (Zerger & Wealands 2004). Today, GIS in hydrology has moved beyond just being a mapping and visualization tool and is able to conduct sophisticated modelling, data analysis and simulation (Sui & Maggio 1999).

Traditionally, flood hazard assessment is performed by identifying parameters such as peak flow rate, rate of rise, depth of flood, inundation extent, velocity, sediment load, duration and frequency of the flood with an associated probability of exceedence. Liu & De Smedt (2005) highlight that the prediction of peak flow and the simulation of flood hydrographs in a river is a very complex process, as the hydrological variables vary both in space and time as a function of the meteorological inputs, spatial variability of topography, land use and soil types. In particular, modelling the response of a catchment to rainfall input is particularly challenging when the region is subject to highly dynamic geomorphic processes as well as glaciers. In this case several critical limitations arise which complicate the implementation and usefulness of many available models. Flood hazard and risk maps are usually derived by combining hydrologic and hydraulic models (e.g. HEC series) that require flow cross-section data along a river and / or high resolution topographic data. Flow cross-section data allow the models to calculate flow velocity, depth and eventually flood extend when combined with floodplain topography in case of overbank flows, provided that channel geometry is unchanging and known with corresponding accuracy (Davies & McSaveney 2006). In Westland the riverbed aggradation/degradation and braiding channels make channel geometry highly variable and extremely difficult to obtain with meaningful accuracy (Fig. 4.1). Sediment input from the steep slopes of the Western Southern Alps locally exceeds the transport capacity of the drainage systems resulting in deposition, particularly where sediment carried by streams leaves the steep, narrow mountain valleys and accumulates on broader, flatter areas (Davies & McSaveney 2008). This process creates a network of small channels separated by small, temporary islands (braid bars)

instead of a single main channel (Fig. 4.2). Covered by Quaternary moraines and clastic sediments consisting primarily of unconsolidated gravels, sand and silt, floodplain topography is also dynamic and rapidly changing as new layers of sediments are deposited or eroded during high flows. In addition to the changing landscape, the costs associated with the acquisition of high-resolution topographic data, appropriate for hydrological applications, are often very high especially when assessment over a large area is required. In view of the above limitations, a conceptually simple and computationally efficient GIS-based approach is developed that does not require detailed field data. It is important to note that the proposed approach it is not intended to replace existing hydraulic models in terms of accuracy, instead, it aims to provide an alternative option when detailed high resolution data are not available or when the study area is too large.

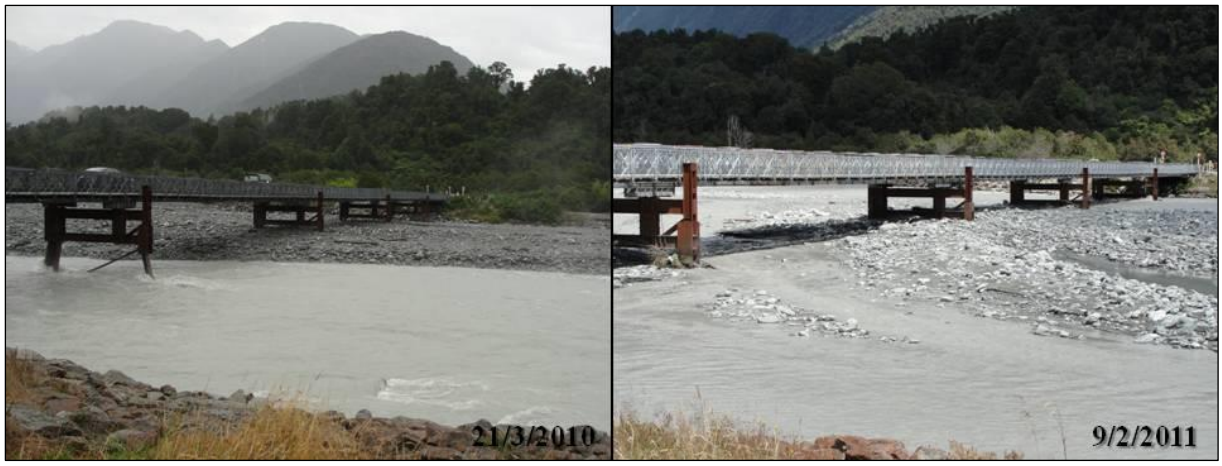

Figure 4.1 Riverbed aggradation. SH6 bridge at Waiho-Callery rivers' confluence.

Figure 4.2 Major braided rivers in the study area (the arrows denote the flow direction).

The present study is divided in two parts. First a GIS-based approach is developed based on the time-area method and the concept of spatially distributed unit hydrographs, in order to investigate the hydrologic response of major ungauged river catchments in the study area based on their

morphometry, land cover and soil characteristics. The underlying hypothesis is that flood hazard at any location is directly related to the hydrological response of the upstream catchment area. In other words, the upstream catchment area may produce different amounts of run-off for a given rainfall based on its specific morphometric, soil and land cover characteristics. The unit hydrograph (UH) captures this hydrologic response providing a standardized way to compare the intrinsic tendencies of different catchments to produce high peak irrespective of rainfall. Runoff hydrographs are also generated combining the UH with rainfall intensity data. The model's predictive performance and its potential as a tool to inform preparedness and emergency response activities are evaluated by comparing the output with observed hydrographs from two gauging sites.

Additionally, a regional flood susceptibility map is developed combining five parameters identified as critical conditioning factors for flooding in the study area. Fuzzy memberships are established between each factor and flood occurrence based on historical flood events in the region. The approach aims to identify flood-prone areas and provide a cost- and time-efficient flood susceptibility assessment tool for regional scale planning, suitable for highly dynamic environments such as glaciated, tectonically active mountainous landscapes. While we recognise the impact of geomorphic processes and glaciers on flood hazard, this approach specifically excludes consideration of flooding due to processes such as landslide dambreak floods, landslide induced tsunamis, river aggradation and glacier bursts.

4.2 Methodology

4.2.1 Spatially distributed unit hydrograph model

4.2.1.1 Unit hydrograph

A unit hydrograph (UH) is defined as the direct runoff hydrograph of a catchment, resulting from one unit (1 inch or 1 mm) of effective rainfall with constant intensity uniformly distributed over the drainage area (Fig. 4.3). It is essentially a theoretical hydrograph which describes the response of a catchment (in terms of runoff volume and timing) at a particular point to one unit of rainfall input, and can in turn be used to infer how the catchment will respond to any amount of rainfall input. Although the UH of a catchment as suggested by Sherman (1932) is derived from observed runoff and rainfall records, different synthetic methods have been proposed (Clark 1945; Rodriguez-Iturbe & Valdes 1979; Jin 1992; Maidment 1993b; Saghafian & Julien 1995; Kull & Feldman 1998; Olivera & Maidment 1999; Lee & Yen 1997) to infer the unit hydrograph for ungauged catchments. These

methods vary in how catchments' geomorphic characteristics are combined to predict the unit hydrograph (Cleveland et al. 2008). However, a number of assumptions in UH theory do not correspond with reality and must be understood before any implementation. These assumptions as summarized by Ramirez (2000) are:

- The UH assumes that catchments respond as linear systems. This implies that effective rainfall intensities of different magnitudes produce catchment responses that are scaled in proportion to the inputs. Furthermore, it implies that responses of several different storms can be superimposed to obtain the composite response of the catchment,
- The rainfall excess (i.e. the volume of rainfall available for direct runoff) has a constant intensity throughout the rainfall duration,
- The effective rainfall intensity is uniformly distributed throughout the entire drainage area,
- The base time of the direct runoff hydrograph is constant based on a given rainfall duration. This implies that the unit hydrograph model does not account for differences in the watershed response related to different rainfall intensities.

Furthermore, the UH does not reflect variations in the catchment response due to land use, channel characteristics or seasonal changes. However, despite its inherent assumptions and hence limitations the UH has been widely applied in hydrologic modelling for estimating the runoff hydrograph of a catchment corresponding to a rainfall hyetograph, primarily because of its simplicity. The UH method can be applied as either a "lumped" model, where catchment parameters and variables used as input represent average values over the entire catchment, or a "distributed" model where input catchment parameters such as morphometric, soil and land cover characteristics vary spatially. Herein a spatially-distributed UH model is developed in GIS environment using a 25m DEM and available soil and land cover data.

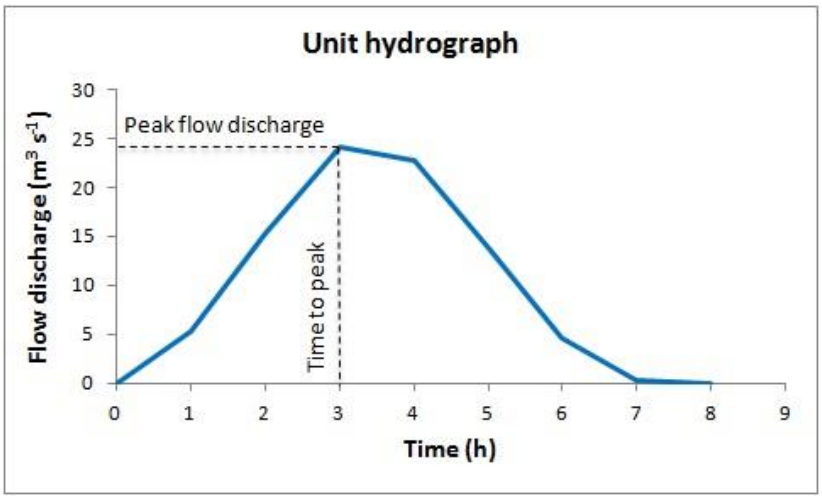

Figure 4.3 Example of unit hydrograph derived from 1mm of rainfall uniformly distributed over the catchment area.

4.2.1.2 Time-area method

The time-area method is a widely applied hydrologic watershed routing technique that is used to derive a discharge hydrograph from an effective rainfall hyetograph. Since Ross (1921) suggested that a hydrograph can be predicted using the time-area-concentration diagram combined with a hypothetical storm event derived from a rainfall intensity– duration curve (Dooge 1973), many time-area methods have been proposed (Clark 1945; Rodriguez-Iturbe et al. 1979; Maidment 1993a, 1993b; Maidment et al. 1996; Muzik 1996; Ajward & Music 2000; Saghafian et al. 2000, 2002; Martinez et al. 2002; Melesse & Graham 2004; Noto & Loggia 2007; Du et al. 2009).

The fundamental component of the time-area method is the time-area histogram, which represents the distribution of watershed's sub-areas contributing to runoff at the outlet as a function of travel time (Ajward & Musik 2000). The sub-areas are bounded by isochrones, which are essentially contour lines enclosing areas that require the same time to reach the outlet (Fig. 4.4). The time-area histogram is used to generate the time-area curve and the resulting unit hydrograph, by applying the standard S-curve technique (Chow et al. 1988). Finally, in order to produce a runoff hydrograph, the time-area histogram is convolved with a precipitation hyetograph, and the resulting discrete convolution equation (Chow et al. 1988) yields the direct runoff volume.

$$Q_n = \sum_{m=1}^{n \le m} P_m \, U_{n-m+1} \qquad (4.1)$$

where Q_n is the direct runoff, P_m is rainfall excess, $U_{n-m+1}$are the unit hydrograph's ordinates, *n* represents the direct hydrograph time interval and *m* is the precipitation time interval (*m*=1,2,...*n*)

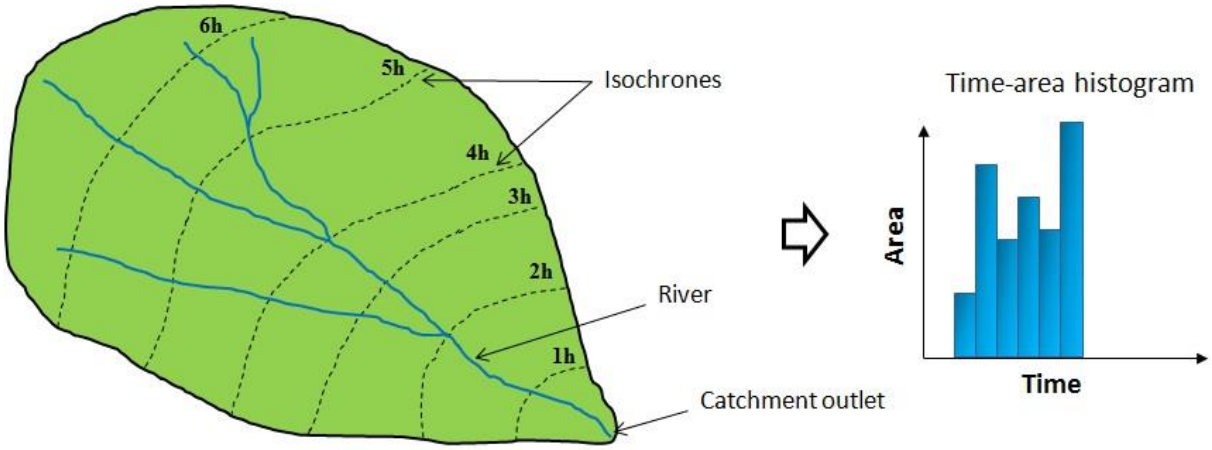

Figure 4.4 Time-area method.

Maidment (1993b) introduced a new method combining the time-area concept with GIS to derive a Spatially Distributed Unit Hydrograph (SDUH). The innovation of the method lies in the process to generate the isochrones in GIS environment, incorporating the spatially distributed rainfall characteristics and flow patterns of the catchment. The proposed GIS-based method in order to generate the isochrones, in addition to the distance from the catchment outlet, accounts for differences in runoff velocity due to slope, land use, and surface elevation changes. However, the method does not account for storage or backwater effects because it assumes equilibrium conditions; flow volume at the outlet in any time interval is equal to rainfall volume falling on the contributing area in the same time interval. Although Maidment's initial result was inconclusive, as he used a very small hypothetical watershed to evaluate his model (Kilgore 1997), later attempts to enhance the method produced more reliable results. Muzik (1996) modified the spatially distributed unit hydrograph (SDUH) approach through distinguishing overland and channel flows and estimating travel time for each flow type as well as accounting for channel storage. Also, Maidment et al. (1996) improved the SDUH approach by considering not only the slope of a cell but also its upstream catchment area in estimating the average flow velocity and introduced a lagged linear reservoir to account for storage effects.

4.2.1.3 Time of concentration

The most critical step of the SDUH modelling approach is to estimate the runoff travel time from each cell in the watershed to the outlet by determining the flow path and velocity through each cell

along the path. The travel time (t_t) through each individual cell along the flow path is then summed to estimate the cumulative travel time to the outlet, known as time of concentration (T_c):

$$T_c = t_{t1} + t_{t2} + t_{t3} + \cdots + t_{tn} = \sum_{i=1}^{n} \frac{L_i}{V_i} \quad (4.2)$$

where, t_t is the travel time through the cell, L_i is the i^{th} cell's flow length and V_i is the flow velocity through the i^{th} cell along the flow path.

The "time of concentration" concept describes the time required for runoff to travel from the hydraulically most distant point of the watershed to a point of interest within the watershed (SCS 1986). It is a critical input parameter in widely applied rainfall-runoff models (HEC-HMS; USACE 2001; TR-20; SCS 1975; TR-55; SCS 1986) as it directly affects peak discharge and time to peak.

Numerous empirical formulae with varying accuracy have been proposed in literature to estimate the time of concentration (Giandotti 1934; Kirpich 1940; Izzard 1946; USACE 1954; Kerby 1959; Morgali & Linsley 1965; FAA 1970; SCS 1972, 1986; Simas-Hawkins 2002). These equations usually relate various catchment characteristics such as slope, drainage area, flow length and land use with time of concentration or lag time parameters. Fang et al. (2005) provide a comprehensive review of several commonly used empirical formulae and their development. Wong (2005) evaluated and compared the performance of nine formulae intended for overland flow (subject to uniform rain) and concluded that formulas which account for rainfall intensity generally give better results. Nevertheless, Shafiri & Hosseini (2011), recognizing that there is no optimum method to estimate the T_c, propose a methodology for identifying the most suitable equations for watersheds located in a specific geographic region, by modification of available equations in order to minimize their bias for this particular region.

In this study, four different methods / formulae were applied to estimate the T_c of western Southern Alps catchments. Each method incorporates different catchment parameters such as watershed area, main channel length, basin slope, soil and land cover types, demonstrating variable sensitivity to each parameter. Although a comparative assessment of the available methods is beyond the scope of this study, the application of different empirical formulae and their effect on the model's performance reveals the most critical catchment parameters affecting the rainfall – runoff transformation in the study area, and provides insight into the model's sensitivity to different

combinations of these parameters. The methods used include Kirpich's formula, the NRCS velocity method, the NRCS watershed lag time equation and a combination of kinematic wave approximation with Manning's equation (Muzik 1995; Melesse & Graham 2004). Following is a brief description of each method. The empirical formulas presented below are in their original form (as they first appeared in literature), however all calculations in this study have been carried out using metric units.

Kirpich's formula

Kirpich (1940) studied the hydrographs of small agricultural watersheds in Tennessee with drainage areas from 0.005 to 0.453 km^2 and slopes from 0.03 to 0.1, and presented a graph relating the time of concentration with the main channel length and catchment slope. The best fit regression equation to his data (McCuen 1998) known as Kirpich Tc formula is:

$$t_c = 0.0078 \left(\frac{L^{0.77}}{S^{0.385}} \right) \tag{4.3}$$

where t_c = time of concentration (min), L = length of main channel (ft), and S = catchment slope.

NRCS watershed lag method

The Natural Resources Conservation Service (NRCS) of the U.S Department of Agriculture, formerly known as Soil Conservation Service (SCS), has developed two methods for calculating the time of concentration, the watershed lag and velocity methods.

The watershed lag method was developed by Mockus (1961) from regression analysis using data from 24 gauged catchments ranging from 1.3 acres (5.26 * 10^{-3} km^2) to 9.2 mi^2 (23.8 km^2)(NRCS 2010). Folmar et al (2007) provide a concise documentation of the equation's development over the years and discuss its theoretical background and assumptions. According to the U.S. National Engineering Handbook (NRCS 2010) the method is suitable "for a broad set of conditions from heavily forested watersheds with steep channels and a high percent of runoff resulting from subsurface flow, to meadows providing a high retardance to surface runoff, to smooth land surfaces and large paved areas."

$$t_{lag} = \frac{L^{0.8}(S+1)^{0.7}}{1900\,Y^{0.5}} \tag{4.4}$$

$$S = \frac{1000}{cn'} - 10 \tag{4.5}$$

where T_{lag} = time lag in h, L = flow length in ft ,Y = average watershed land slope in percent (%), S = maximum potential retention and cn' = the retardance factor, which is approximately the same as the curve number (CN).

The curve number ($0 \leq CN \leq 100$) is a dimensionless parameter used as a surrogate for potential retention, a conceptual parameter varying in the range $0 \leq S \leq \infty$ (Ponce & Hawkins 1996). The CN of a catchment is estimated considering a combination of land cover, soil type and antecedent moisture condition (AMC). The AMC, also known as antecedent runoff condition (ARC), is determined by the total rainfall in the 5-day period prior to the storm of interest and is divided into three classes: dry (AMC I), average (AMC II) and wet conditions (AMC III) (NRCS 2004b).

In a graphical plot of runoff depth Q as a function of rainfall depth P, the actual retention (P - Q) asymptotically approaches a constant value (S) as rainfall depth P increases. The S value, known as "potential maximum retention", is used to describe the catchment's potential for abstracting and retaining rainfall moisture and, therefore, its direct runoff potential (Ponce & Hawkins 1996). A CN value of 100 represents a condition of zero potential retention (S = 0), that is, impermeable ground conditions. Conversely, CN = 0 represents a theoretical upper bound to the potential retention ($S = \infty$), that is, infinitely permeable ground conditions.

According to NRCS (2010), for average natural watershed conditions and an approximately uniform distribution of runoff the time of concentration is related to lag time:

$$t_{lag} = 0.6\,t_c \tag{4.6}$$

By combining equations 4, 5 and 6 the time of concentration is estimated as a function of lag time:

$$t_c = \frac{L^{0.8}\left(\frac{1000}{CN} - 9\right)^{0.7}}{1140\,Y^{0.5}} \tag{4.7}$$

Herein the CN values (Table 4.1) were obtained based on the tables provided by the Hydrologic Soil-Cover Complexes (NRCS 2004a) and the Hydrologic Soil Groups (NRCS 2007) for land cover types and soil hydrologic conditions in the study area.

Table 4.1 Curve numbers based on land cover type and soil hydrologic soil groups (NRCS).

Land cover class (Level2)	Land cover class (Level1)	NRCS soil groups			
		A	B	C	D
Alpine Grass-/Herbfield	Bare or lightly vegetated surfaces	68	79	86	89
River and Lakeshore Gravel and Rock		98	98	98	98
Alpine Gravel and Rock					
Coastal Sand and Gravel		50	50	50	50
Permanent Snow and Ice		-	-	-	-
Landslide		98	98	98	98
Deciduous Hardwoods	Forest	30	55	70	77
Forest Harvested					
Indigenous Forest					
Other Exotic Forest					
Pine Forest - Closed Canopy					
Pine Forest - Open Canopy					
Major Shelterbelts					
Low Producing Grassland	Grassland	68	79	86	89
High Producing Exotic Grassland		39	61	74	80
Tall Tussock Grassland					
Fernland	Scrub and shrubland	30	48	65	73
Gorse and Broom					
Grey Scrub					
Manuka and or Kanuka					
Mixed Exotic Shrubland					
Broadleaved Indigenous Hardwoods					
Sub Alpine Shrubland					
Flaxland	Wetland	30	58	71	78
Herbaceous Freshwater Vegetation					
Herbaceous Saline Vegetation					
Short-rotation Cropland	Cropland	49	69	79	84
Built-up Area	Artificial areas	89	92	94	95
Transport Infrastructure		83	89	92	93
Urban Parkland/ Open Space		49	69	79	84
Surface Mine		77	86	91	94
Dump					
Estuarine Open Water	Water bodies	-	-	-	-
Lake and Pond		-	-	-	-
Rivers		-	-	-	-

NRCS velocity method

The NRCS velocity method divides the flow path into segments of different types of flow and determines the travel time through each segment, using hydraulic equations to calculate the time of concentration. The procedure divides the flow path into sheet, shallow concentrated, channelized and/or pipe flow. Sheet flow usually occurs in the headwaters of a stream near the ridgeline that defines the watershed boundary, typically over short distances (30 m). After this short distance, due topographic changes, the sheet flow becomes shallow concentrated flow collecting in swales, small rills, and gullies. Finally, runoff enters the main drainage system as channelized or pipe flow. The following simplified form of Manning's kinematic solution developed by Welle & Woodward (1986) is applied to estimate the travel time of sheet flow:

$$t_t = \frac{0.007(nl)^{0.8}}{\sqrt{P}\, S^{0.4}} \tag{4.8}$$

where t_t travel time (h), n Manning's roughness coefficient, l sheet flow length (ft), P 2-year, 24-hour rainfall (in) and S slope of land surface

Shallow concentrated flow velocity is estimated as function of slope and type of channel according to NRCS (2010). To estimate the average open channel flow velocity Manning's equation is proposed by the method as the most appropriate:

$$V = \frac{1}{n} * Rh^{2/3} * S^{1/2} \tag{4.9}$$

where n = Manning's n coefficient, Rh = hydraulic radius, S = slope

Overland and open channel flow

The combination of different flow types is increasingly used in estimating travel times and ultimately T_c at the catchment outlet. According to this technique, the velocity for each grid cell can be estimated differently depending on whether the cell represents an area of overland or concentrated channel flow (Muzik 1995; Melesse & Graham 2004).

The river channel cells were delineated based on the upstream catchment area above each cell, assuming that only upstream contributing areas larger than a threshold value can create and maintain a stream channel. This threshold value depends on regional and watershed characteristics such as climatic conditions, soil properties, land cover and topography (Martz & Garbrecht 1992), therefore it significantly varies within different areas. The threshold value used for the catchments in the study area was A=0.156 km^2 after comparison with the drainage network available by the River Environment Classification system (REC) developed by the National Institute of Water and Atmospheric Research (NIWA) and 1:50000 topographic maps. Any cells that were not classified as stream channels were classified as overland flow cells.

Overland flow travel time was estimated by applying a combination of a steady state kinematic wave approximation with Manning's equation (Eq. 4.10) (Chow et al. 1988; Muzik 1995, 1996; Melesse & Graham 2004; Kilgore 1997; Diakakis 2010):

$$t_c = \frac{L^{0.6} * n^{0.6}}{{i_e}^{0.4} * S^{0.3}} \quad (4.10)$$

where, t_c is in seconds, L is the length of flow in the grid cell (m), n is the Manning's n coefficient, i_e is the average excess rainfall intensity estimated using the NRCS curve number method (SCS 1986) and S is the slope.

Manning's n coefficients for different land cover types were determined using the method proposed by Arcement & Schneider (1989) (Table 4.2). By altering Cowan's (1956) procedure that was developed for estimating n values for river channels, Arcement & Schneider (1989) developed the following equation for estimating n values for floodplains:

$$n = (n_b + n_1 + n_2 + n_3 + n_4)\, m \quad (4.11)$$

where: n_b = a base value of n for the flood plain's natural bare soil surface, n_1 = a correction factor for the effect of surface irregularities on the floodplain, n_2 = a value for variations in shape and size of the floodplain cross section, n_3 = a value for obstructions on the flood plain, n_4 = a value for vegetation on the flood plain and m = a correction factor for sinuosity of the flood plain, equal to 1.

Table 4.2 Manning's n coefficients for land cover types in the study area.

Land cover class (Level2)	Land cover class (Level1)	Manning's n values
Alpine Grass-/Herbfield	Bare or lightly vegetated surfaces	0.08
River and Lakeshore Gravel and Rock		0.047
Alpine Gravel and Rock		0.076
Coastal Sand and Gravel		0.037
Permanent Snow and Ice		-
Landslide		0.055
Deciduous Hardwoods	Forest	0.23
Forest Harvested		
Indigenous Forest		
Other Exotic Forest		
Pine Forest - Closed Canopy		
Pine Forest - Open Canopy		
Major Shelterbelts		
Low Producing Grassland	Grassland	0.056
High Producing Exotic Grassland		0.071
Tall Tussock Grassland		
Fernland	Scrub and shrubland	0.18
Gorse and Broom		
Grey Scrub		
Manuka and or Kanuka		
Mixed Exotic Shrubland		
Broadleaved Indigenous Hardwoods		
Sub Alpine Shrubland		
Flaxland	Wetland	0.08
Herbaceous Freshwater Vegetation		0.068
Herbaceous Saline Vegetation		
Short-rotation Cropland	Cropland	0.042
Built-up Area	Artificial areas	0.02
Transport Infrastructure		
Urban Parkland/ Open Space		0.046
Surface Mine		0.066
Dump		
Estuarine Open Water	Water bodies	-
Lake and Pond		
Rivers		

The channel flow velocity, V_{str} (m s^{-1}), was estimated using Manning's equation combined with the steady state continuity equation for a wide channel (Eq. 4.13) (Muzik 1995):

$$Q = VWy \tag{4.12}$$

$$V_{str} = \left[\frac{S^{1/2}}{n}\left(\frac{Q}{W}\right)^{2/3}\right]^{3/5} \quad (4.13)$$

where Q is the mean annual discharge through each cell, W = is the channel width (m), S is the slope and n is Manning's n coefficient.

A critical limitation however, as already discussed above, is that channel geometry is highly variable due to the high sediment flux through the drainage systems and cannot be easily obtained for braided rivers in the study area. Therefore, equation 4.13 was considered more appropriate instead of directly applying Manning's formula as width can be obtained more efficiently compared to hydraulic radius, by using satellite images or air photos. However the size of the study area makes the direct measurement of channel widths an extremely time-consuming process. Molnar & Ramirez (1998) substituted the hydraulic radius parameter with a power law relationship with an exceedence probability, which relates the hydraulic radius to the contributing catchment area, as a representation of the average channel geometry at each cell. Herein a similar concept was used, in order to estimate the downstream change of channel width, the power law relationship proposed by Leopold & Maddock (1953) which relates channel width to the bankfull flow discharge was applied:

$$W = aQ^b \quad (4.14)$$

where W is channel width (m), Q is mean annual discharge ($m^3\ s^{-1}$) and α, b are constants.

Previous researchers (Griffiths 1980; Ibbit 1997; McKerchar et al 1998; Henderson et al. 1999; Jowett 1998; Wohl & Wilcox 2005) have investigated the downstream changes in channel geometry of New Zealand rivers providing a range of different values for the α and b constants depending on the specific characteristics of the rivers they studied. For example, Wohl & Wilcox (2005) studying single-thread channels at bankfull flow, both on the eastern and western sides of South Island, obtain an exponent b of 0.52 for western rivers, whereas Griffiths (1980) using data from wide gravel bed New Zealand rivers, obtains an exponent b of 0.48. The following table indicates the different values for the b exponent as they were estimated for various rivers (Table 4.3).

Table 4.3 Variation of b exponent for New Zealand rivers (after Wohl & Wilcox 2005).

River (data source)	Channel width (b exponent)
Camp creek (Wohl & Wilcox, 2005)	0.52
*(Griffiths, 1980)	0.48
Cropp River (Henderson et al., 1999)	0.47
Ashley River (McKerchar et al., 1998)	0.44
Taieri River (Ibbitt et al., 1998)	0.52
Hutt River (Ibbitt, 1997)	0.52
Buller River above Te Kuha (Ibbitt, 1997)	0.45

(* Buller, Ngaruroro, Rangitaiki, Wairau, Wanganui and Whakatane rivers)

The mean annual flood for catchments in the WSA was estimated as a function of catchment area A as given by McKerchar & Pearson (1989):

$$Q = 15\,A^{0.808} \tag{4.15}$$

However, as the proposed relationships and exponent values are subject to uncertainties depending on the method applied, the specific geomorphic characteristics of the river channels from which the data were obtained and the highly dynamic geomorphic processes in the study area, they only provide an approximate estimation of the channel width. They essentially reflect the downstream changes in channel width due to increasing discharge. The relationship proposed by Wohl & Wilcox (2005) was applied for low-order (1-3) (Strahler's stream order method; Strahler 1957) single-thread mountain stream channels and the relationship by Griffiths (1980) was applied for higher-order (>3) wide river channels.

4.2.1.4 Glacier cover and hydrology

Approximately 395 km^2 (5%) of the study area is covered by glaciers which flow westwards from the Main Divide and through steep valleys; two of them to elevations of about 300 m. The ice and snow forming the glaciers are produced and maintained by New Zealand's humid maritime climate and the orientation of the main axial range across the dominant Southern Hemisphere westerlies (Fitzharris et al. 1992). As a result several catchments, especially those located at the central part of WSA, have up to 20-25% of the total catchment area covered by ice (e.g. Waiho, Fox-Cook river catchments).

The presence of glaciers in a watershed, even at a few percent of areal cover, affects the lag time between rainfall and runoff and modifies the variability of annual and seasonal discharge (Lawson 1993), so the hydrograph is not directly related only to rainfall and catchment characteristics. This significant impact on the hydrology of a catchment takes place primarily through storage and release of water from the glacier. Water can be stored in a variety of ways such as in surface snow and firn, crevasses, surface pools, englacial pockets, subglacial cavities, englacial and subglacial drainage network, and in basal sediments (Jansson et al. 2003). Additionally, water is released through ice- and snowmelt or by sudden, discrete events such as glacial outburst floods (Jokulhaups).

The lack of glacio-hydrologic data and the regional scale of the study did not allow the modelling of the above water storage - release mechanisms. Extrapolating data concerning glacial storage and release seasonal patterns obtained from one glacierized catchment to other catchments would involve major assumptions, as there is significant spatial variability of glacier cover, precipitation and geomorphic processes along the western Southern Alps. On the other hand, data acquisition for each individual catchment was not possible given the available resources. Nevertheless, the contribution of the glacier covered areas to the flow rate at the catchment outlet cannot be ignored.

In general, the routing of rainfall and melt water through a glacial system is controlled by three interlinked drainage systems; supraglacial, englacial, and subglacial. According to the GIS-based time area method, as it is applied for the non-glacierized catchment parts, the travel time through glacier cells is required in order to incorporate the contribution of these areas to the total flow rate at the catchment outlet.

Initially, glacier surface area was divided into accumulation (snow cells) and ablation (ice cells) areas based on the equilibrium-line altitude (ELA) (Fig. 4.5A). The mean elevation of glacial cover at each catchment was taken as an approximation of ELA (Haeberli & Hoezle 1995).

Routing of water through snow and firn (accumulation zone) is typically slow (10^{-4} -10^{-5} m s^{-1}) significantly delaying runoff at the glacier terminus, whereas flow across exposed ice surfaces (ablation zone) is typically 3–5 orders of magnitude faster (Nienow & Hubbard 2005). Therefore, it is assumed that precipitation in the accumulation zone only affects the total annual runoff and seasonal regulation of flow and does not significantly contribute to direct runoff at the catchment outlet, considering the time scale of a storm event, due to its very low flow velocity.

In general, supraglacial flow tends to concentrate into discrete rills or channels (Moore 1991), however the geometry of these channels, required to estimate the flow velocity, is highly variable due to the rapidly changing glacier surface. Therefore, in order to estimate the flow travel time

through the ice cells a combination of a steady state kinematic wave approximation with Manning's equation (Eq. 4.10) was applied, assuming that runoff generated by ice-melt reduces the travel time of rainfall excess through the cell. This implies that rainfall generated runoff occurs as surface (overland) flow on an already wet ice surface due to ice-melt with low flow resistance.

$$t_{ice} = \frac{L^{0.6} * n^{0.6}}{R^{0.4} * S^{0.3}} \tag{4.16}$$

where t_{ice} is the travel time (seconds), L is the length of flow in the grid cell (meters), n is the Manning's roughness coefficient, S is the slope, and R is the total ice surface runoff generated by excess rainfall intensity (i_e) and ice-melt rate (M); $R = (i_e + M)$.

Ice melt (Fig. 4.5B) was estimated by applying the distributed temperature-index ice-and snowmelt model including potential direct solar radiation developed by Hock (1999):

$$M = \begin{cases} \left(\frac{1}{n} MF + \alpha_{snow/ice} I\right) T, & T > 0 \\ 0 \quad , & T < 0 \end{cases} \tag{4.17}$$

where M is melt rate (mm day^{-1}), MF is a melt factor (7.17 mm $^0C^{-1}$ day^{-1}; Anderson et al. 2006), $\alpha_{snow/ice}$ is a radiation coefficient different for snow and ice surfaces (α_{ice} = 0.001; Hock 1999), I is potential clear-sky direct solar radiation at the ice or snow surface (W m^{-2}), T is air temperature (^oC) and n is the number of time steps per day. Average daily temperature and daily solar radiation data were provided by Landcare Research (Leathwick et al. 2002).

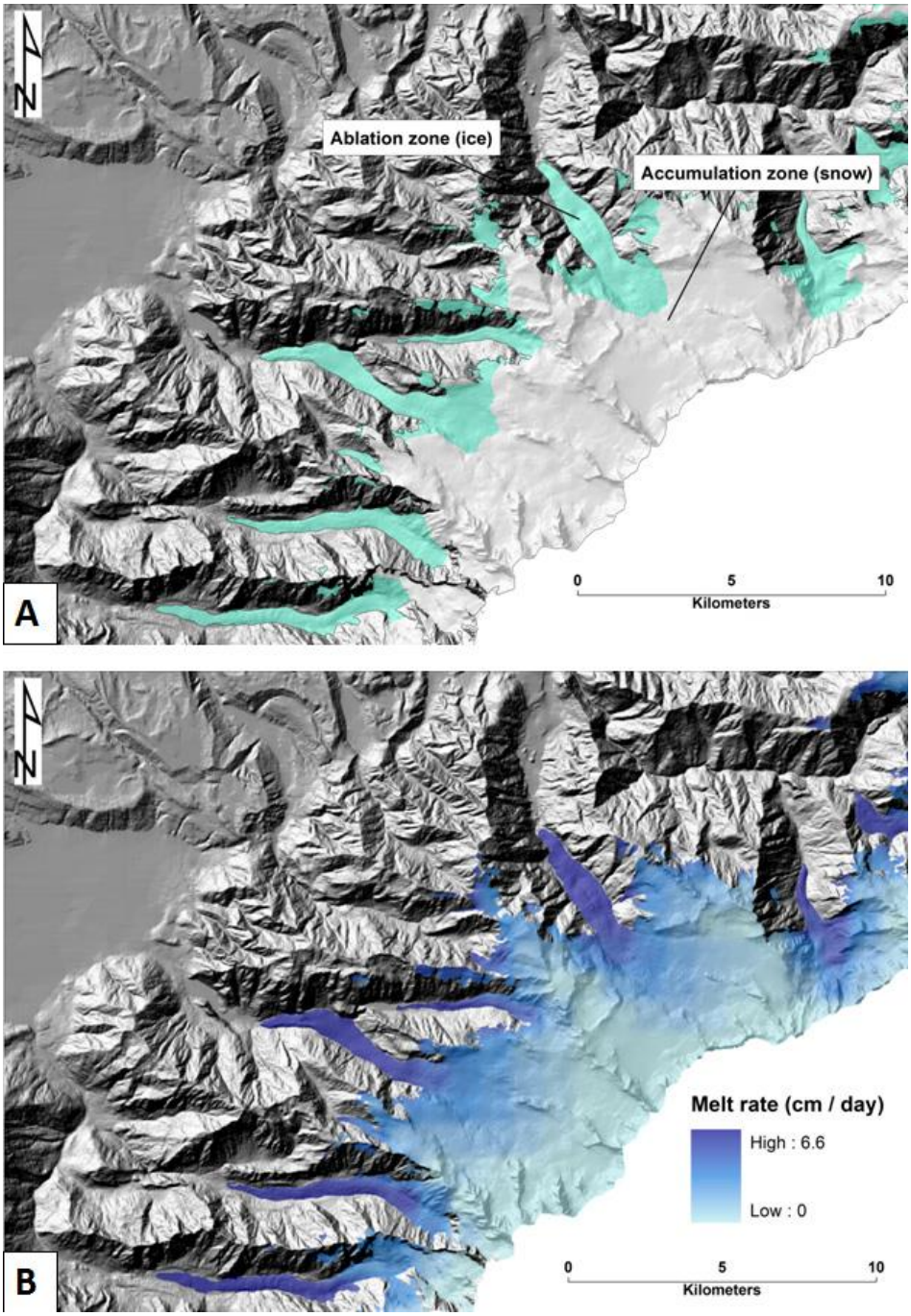

Figure 4.5 A) Accumulation and ablation zones based on the Equilibrium Line altitude (ELA), B) Melt rate on the ablation zone using the distributed temperature-index model was estimated up to 6.6 cm d^{-1}.

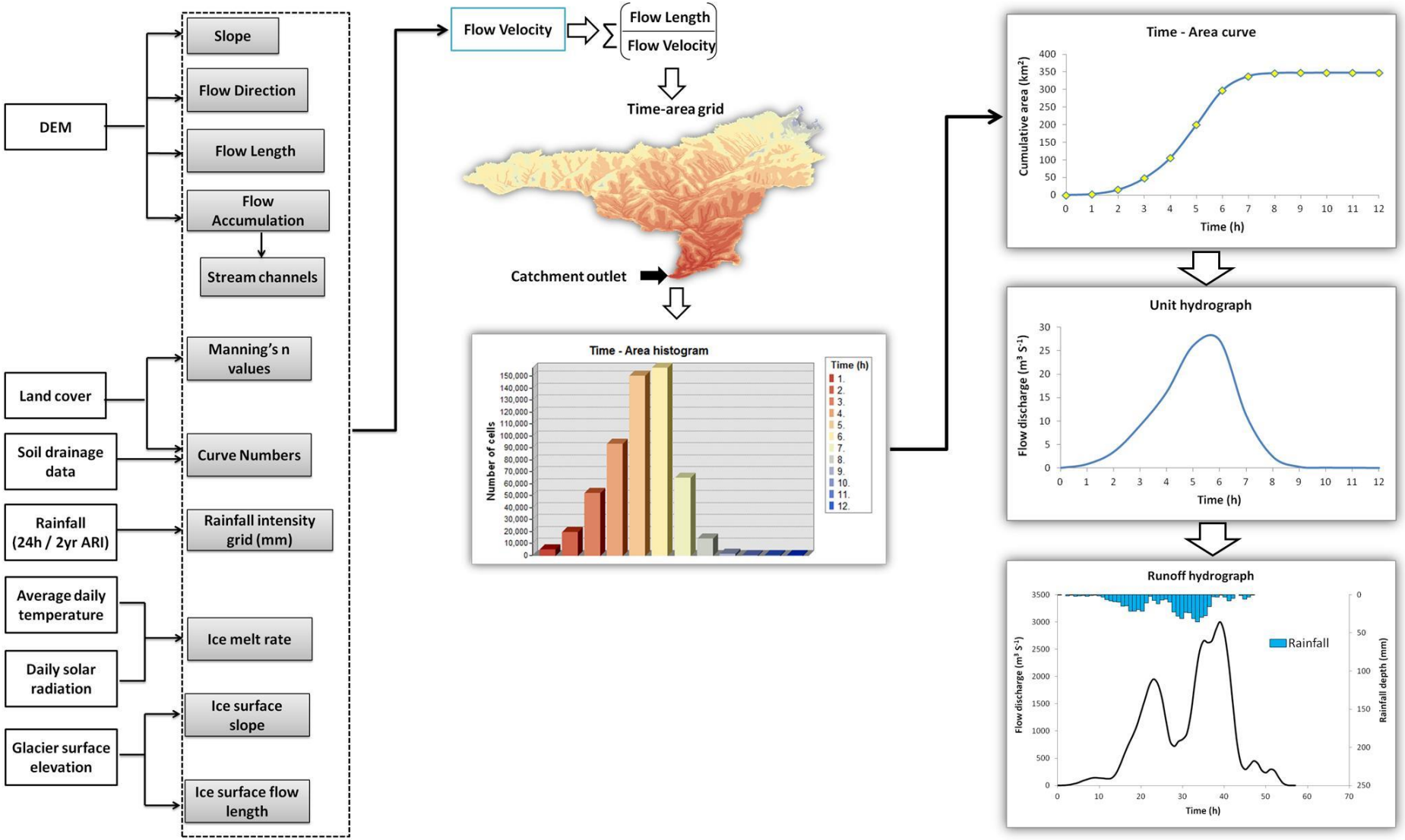

Figure 4.6 GIS-based spatially distributed unit hydrograph (SDHU) model.

4.2.2 Runoff hydrographs and evaluation

The GIS-based SDUH model (Fig. 4.6) was applied to generate the runoff hydrographs (i.e. the response of a given catchment to a specific rainfall input) for ungauged catchments in the WSA using observed rainfall intensity data. In order to evaluate the performance of the modelling approach in predicting the runoff hydrographs of real rainfall events, the results are compared with observed hydrograph data by applying different evaluation measures. Although a wide range of measures for the evaluation of hydrologic model performance have been proposed in literature (Krause et al. 2005; Dawson et al. 2007), inherent limitations in each method suggest that a combination of different efficiency criteria is required to adequately validate a model. Therefore, the modelled hydrographs were evaluated based on visual comparison, calculation of the Coefficient of Efficiency (CE), Relative Volume Error (RVE), and Percent Error in Peak (PEP).

Two different catchments (Fig. 4.7) in the study area with available rainfall and hydrograph data were used in the evaluation process, in order to observe how the specific morphometric, climatic and land cover characteristics of each catchment influence the model's predictive performance. The flow discharge and rainfall intensity data were accessed through NIWA's extensive automated monitoring network archive data (Environmental Data Explorer - http://edenz.niwa.co.nz/).

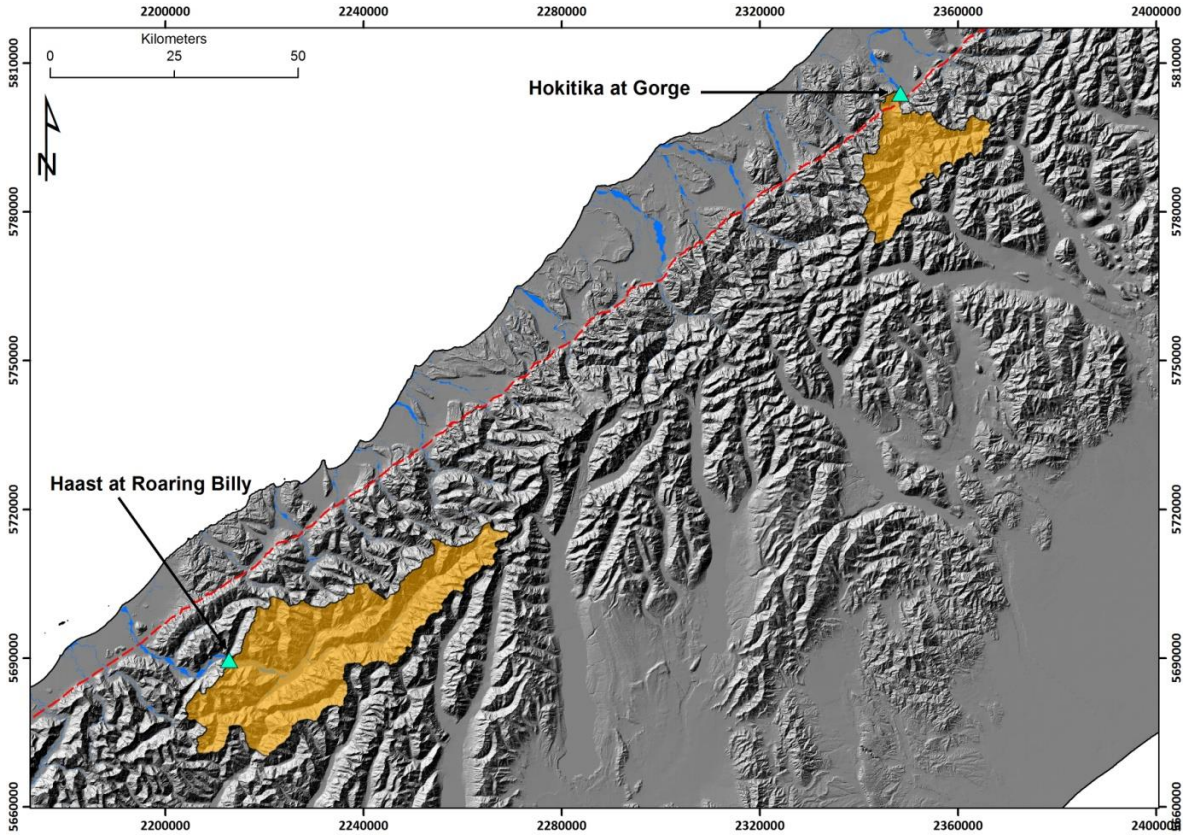

Figure 4.7 Evaluation catchments and gauging stations.

4.2.2.1 Evaluation measures

The Coefficient of Efficiency (CE) evaluates the level of overall agreement between the observed and modelled datasets and it is calculated by:

$$CE = 1 - \frac{\sum_{i=1}^{n}(Q_{obs} - Q_{mod})^2}{\sum_{i=1}^{n}(Q_{obs} - \bar{Q}_{obs})^2} \quad (4.18)$$

where Q_{obs} is the observed flow rate, Q_{mod} is the modelled flow rate and $\bar{Q}_{obs}$ is the mean observed flow rate.

The coefficient of efficiency (CE) proposed by Nash & Sutcliffe (1970) is a widely applied measure that is defined as one minus the ratio of sum square error (SSE) to the statistical variance of the observed dataset about the mean of the observed dataset. It ranges from zero to one but negative scores are also permitted. The maximum positive score of one represents a perfect model whereas a value of zero indicates that the model is no better than a one parameter ‘‘no knowledge’’ model in which the forecast is the mean of the observed series at all time steps (Dawson et al. 2007). Negative values indicate that the mean value of the observed data series is a better predictor than the model.

Relative Volume Error (RVE) is a popular relative measure of overall volume error that is used to provide an indication of the overall water balance of the model.

$$RVE = \frac{\sum_{i=1}^{n}(Q_{obs} - Q_{mod})}{\sum_{i=1}^{n} Q_{obs}} \quad (4.19)$$

where Q_{obs} is the observed flow rate and Q_{mod} is the modelled flow rate

RVE was considered to be an ‘‘adequate measure’’ for the volumetric assessment of single event models (Green & Stephenson 1986), but, conversely, it has been also recommended for the evaluation of continuous hydrographs (ASCE 1993). It is an unbounded measure and for a perfect model the result would be zero. However, low score does not necessarily indicate a good model, in

terms of forecast accuracy, since positive and negative errors will tend to cancel each other out (Dawson et al. 2007).

Percent Error in Peak (PEP) is defined as the difference between the highest value in the modelled dataset and the highest value in the observed dataset, normalized by the highest value in the observed dataset and expressed as percentage.

$$PEP = \frac{Q_{obs\ max} - Q_{mod\ max}}{Q_{obs\ max}} \times 100 \tag{4.20}$$

where $Q_{obs\ max}$ is the observed peak flow rate and $Q_{mod\ max}$ is the modelled peak flow rate.

It can be either positive or negative and for a perfect model the result would be zero. PEP is considered appropriate for single-event modelling as opposed to continuous modelling (Dawson et al. 2007). Positive values indicate that the model underestimates the peak discharge and negative values indicate the opposite.

Baseflow separation

Direct runoff hydrographs derived from unit hydrographs do not account for baseflow. Baseflow can be described as the longer-term delayed flow from natural storages, in contrast to quickflow which is the direct response to a rainfall event. Therefore, in order to allow the comparison between the observed and modelled hydrographs, the observed hydrographs are usually separated into base and direct runoff. Baseflow analysis has long history of development (Brodie & Hostetler 2005) and many different techniques have been proposed and evolved over the years.

However, herein we assume that baseflow is insignificant compared to the peak flow discharge (approximately 2% of the maximum flow rate) as the modelled catchments are steep with thin soil cover. Thus no separation technique is applied.

Hokitika at Gorge

The Hokitika at Gorge site is located on the Hokitika River approximately 37 km upstream of the township of Hokitika and it has a contributing catchment area of 357 km^2. It includes the upper branch of Hokitika River, its main tributary Whitcombe River and other smaller rivers such as Cropp, Price and Mungo Rivers. The main geological units are schist and semischist. The soils are

predominantly podzol soils, with slow permeability and limited root depth, typical in areas of high rainfall and usually associated with forests (Hewitt 1993). The catchment at lower and mid- altitudes is covered by indigenous forests (41%), scrub and shrubland (15%) and at higher altitudes the main land cover types are tall tussock grasslands (17%), alpine grass-/herbfields and alpine gravel and rock (24%) as well as glaciers (3%). Rainfall data are available from five different NIWA climate/weather stations in the catchment (Table 4.4).

Table 4.4 Altitude (m) and mean annual rainfall (mm) of climatic stations in Hokitika and Haast river catchments.

Climatic station	Altitude (m)	Mean annual rainfall (mm)
Hokitika at Colliers ck	95	7202
Hokitika at Rapid ck	152	7506
Hokitika at Prices Flat	427	7540
Cropp at Cropp Hut	860	10510
Cropp at Waterfall	975	11516
Haast at Roaring Billy	60	5341
Haast at Moa ck	105	3969

Haast at Roaring Billy

The Haast at Roaring Billy gauging site is situated on the Haast River about 47 km upstream of the township of Haast. The 1024 km^2 contributing catchment includes the upper Haast River, its main tributary Landsborough River and the smaller Wills, Burke, Macfarlane and Clarke Rivers. The main geological formations are schists, semischists and quaternary sediments (gravel, sand and landslide deposits) on valley floors. The dominant soil types are podzols (54%), raw soils (23%) which are very young soils lacking distinct topsoil as a result of active erosion, and brown soils (12%) which characterize soils that remain relatively wet throughout the year. Land cover consists of indigenous forests (44%), scrub and shrubland (6%), grasslands (25%), alpine grass-/herbfields and alpine gravel and rock (19%) as well as glaciers (5%). Available rainfall data come from two NIWA climate/weather stations (Table 4.4). Using rainfall records from different stations to generate the hydrographs allows us to observe the model's sensitivity to spatially variable rainfall intensity within the catchment. Tables 4.5 and 4.6 summarize the morphometric and hydrologic characteristics for each catchment.

Table 4.5 Evaluation catchments' morphometric parameters

	Hokitika at Gorge	Haast at Roaring Billy
Area (km)	357	1024.2
Min elevation (m)	79	75
Max elevation (m)	2600	2730
Mean elevation (m)	1111.2	1060.8
Relief (m)	2521	2655
Mean slope (deg)	31.6	29.8
Glaciers %	3.64	5.46
Basin order	6	6
Mean Rb	3.82	4.67
Mean Rl	1.63	1.96
Total steam length (km)	486.95	1423.15
Total streams	645	1780
Drainage density	1.36	1.39
Drainage frequency	1.8	1.73
Perimeter (m)	156.8	292.15
Basin length (m)	30	62
Form factor	0.396	0.267
Relief ratio	84	42.89
Ruggedness number	3438.27	3689.14
Elongation ratio	0.71	0.58
Circularity ratio	0.182	0.15

Table 4.6 Evaluation catchments' hydrologic parameters (source: Environmental Data Explorer - http://edenz.niwa.co.nz/)

	Hokitika at Gorge	Haast at Roaring Billy
Max flow ($m^3 s^{-1}$)	2820	6330
Min flow ($m^3 s^{-1}$)	18.39	25.9
Mean flow ($m^3 s^{-1}$)	102.4	192.2
Median flow ($m^3 s^{-1}$)	63.74	122.9
Min stage (m)	1174	604
Max stage (m)	5903	7580
Mean annual rainfall (mm)	7202	5341
Altitude (m)	95	60

Rainfall event 27 & 28 Dec 2010

Data from the 27-28 December 2010 rainfall event were used to develop and evaluate the runoff hydrographs in Hokitika and Haast river catchments. The heavy rainfall-induced flooding affecting

the entire region from Haast to Karamea, ranging between a 1 in 5 year and 1 in 50 year event depending on the catchment (WCRC 2010). Smaller rainfall events prior to the 27/28 storm resulted in increased antecedent ground moisture that contributed in higher runoff. This specific storm was selected as it was well recorded event that did not just affect a localised part of the West Coast but instead had an impact on the entire region inducing surface flooding, generating landslides and damaging bridges. The following figures (4.8 - 4.14) and tables (4.7 - 4.13) illustrate the simulated runoff hydrographs using the SDUH model and allow the comparison with observed flow rates for the Hokitika and Haast river catchments.

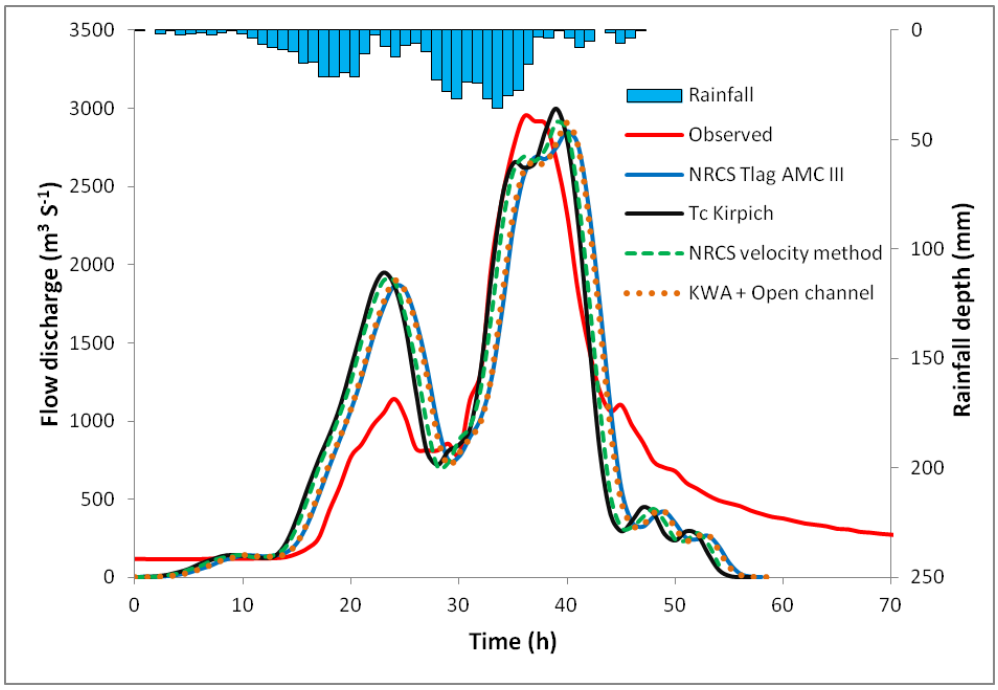

Figure 4.8 Rainfall data from Colliers ck station

Table 4.7 Evaluation results (Colliers ck station).

Method	Rainfall (26 - 28 Dec 2010)				
	Qp	Tp	CE	RVE	PEP
Observed	2947.4	36	-	-	-
Tlag AMC I	2563.8	44	0.197	0.056	13
Tlag AMC II	2699.3	40	0.542	0.032	8.41
Tlag AMC III	2852.3	40	0.742	0.011	3.22
Tc Kirpich	2998.6	39	0.775	0.004	-1.74
NRCS velocity method	2912	39	0.781	0.003	1.2
KWA + open channel	2906.3	40	0.738	0.042	1.39

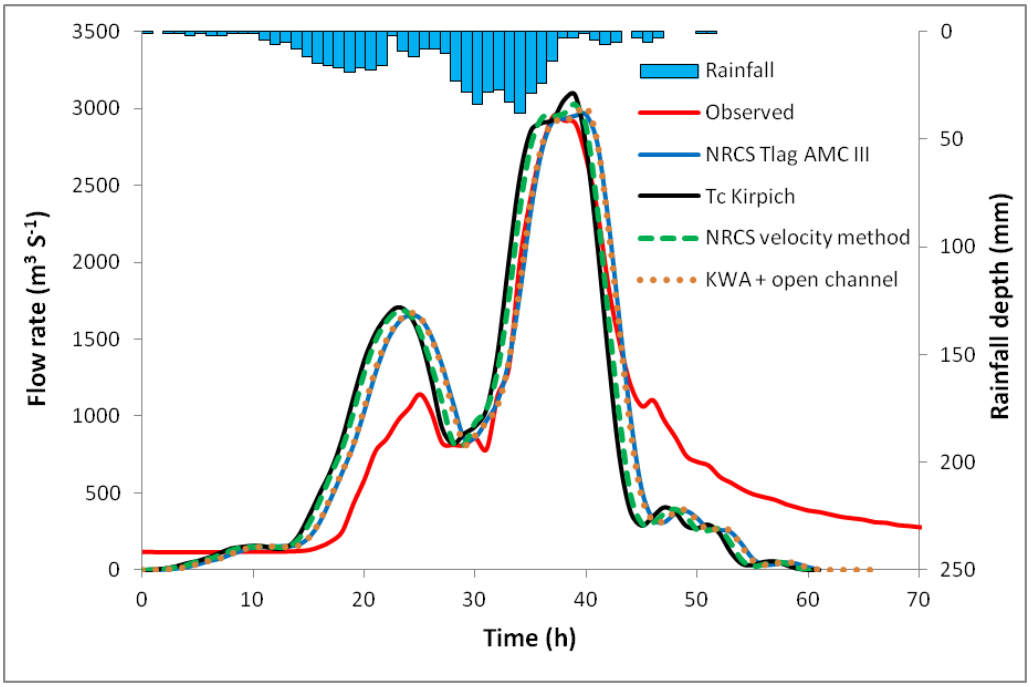

Figure 4.9 Rainfall data from Rapid ck station

Table 4.8 Evaluation results (Rapid ck station)

Method	Rainfall (26 - 28 Dec 2010)				
	Qp	Tp	CE	RVE	PEP
Observed	2947.4	37	-	-	-
Tlag AMC I	2709.8	44	0.311	0.043	8.06
Tlag AMC II	2915.1	40	0.713	0.043	1.1
Tlag AMC III	2960	40	0.82	0.018	-0.43
Tc Kirpich	3086.2	39	0.724	0.011	-4.71
NRCS velocity method	3023.1	39	0.767	0.01	-2.57
KWA + open channel	3004.6	40	0.809	0.046	-1.94

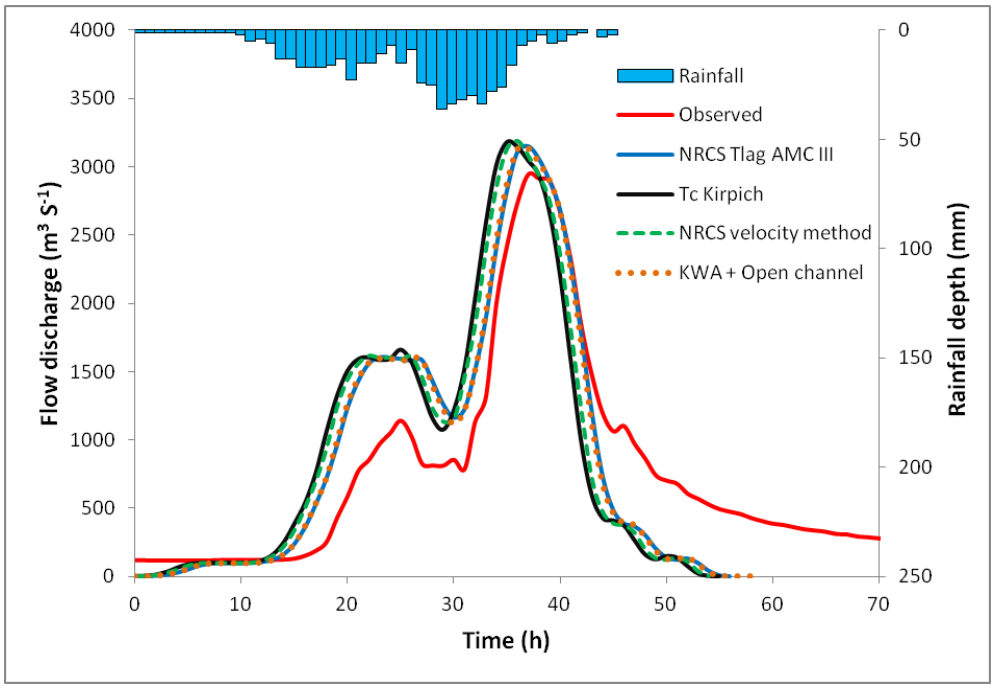

Figure 4.10 Rainfall data from Prices Flat station.

Table 4.9 Evaluation results (Prices Flat station)

Method	Rainfall (26 - 28 Dec 2010)				
	Qp	Tp	CE	PVE	PEP
Observed	2947.4	37	-	-	-
Tlag AMC I	2806.5	43	0.458	-0.002	4.78
Tlag AMC II	3071.9	39	0.783	-0.03	-4.22
Tlag AMC III	3147.9	37	0.752	-0.056	-6.8
Tc Kirpich	3180.6	35	0.54	-0.066	-7.9
NRCS velocity method	3187.4	36	0.612	-0.067	-8.14
KWA + open channel	3137.5	37	0.728	-0.019	-6.45

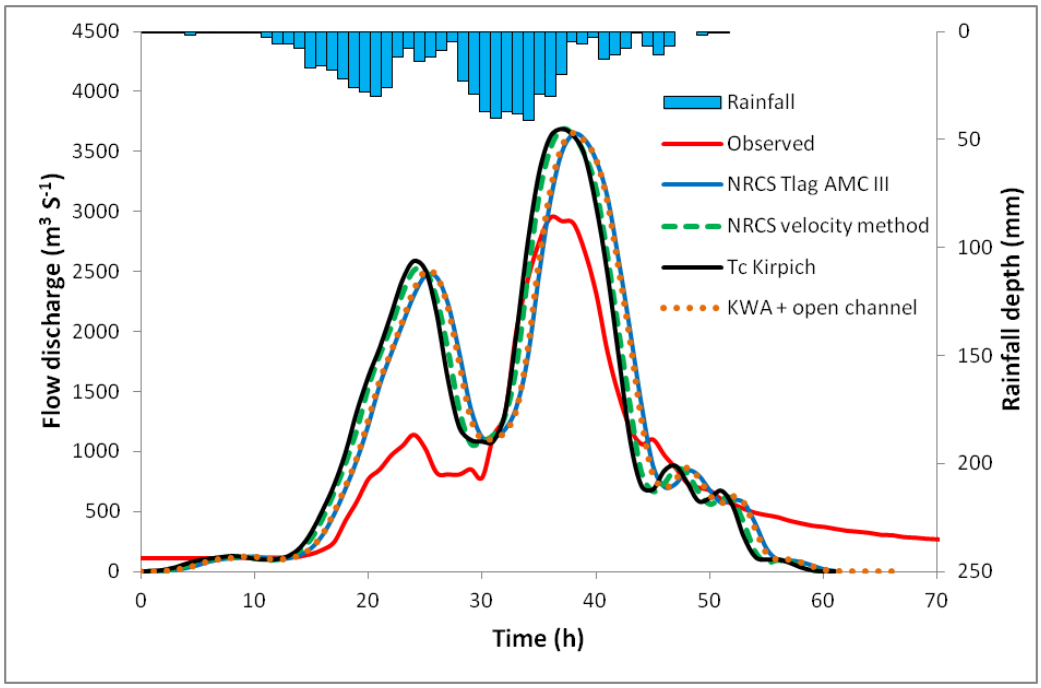

Figure 4.11 Rainfall data from Cropp Hut station.

Table 4.10 Evaluation results (Cropp Hut station)

Method	Rainfall (26 - 28 Dec 2010)				
	Qp	Tp	CE	PVE	PEP
Observed	2947.4	36	-	-	-
Tlag AMC I	-	-	-	-	-
Tlag AMC II	3521.3	40	0.226	-0.234	-19.5
Tlag AMC III	3643.85	38	0.471	-0.257	-23.6
Tc Kirpich	3685.1	37	0.532	-0.264	-25
NRCS velocity method	3686.73	37	0.532	-0.267	-25.1
KWA + open channel	3650.63	38	0.48	-0.223	-23.8

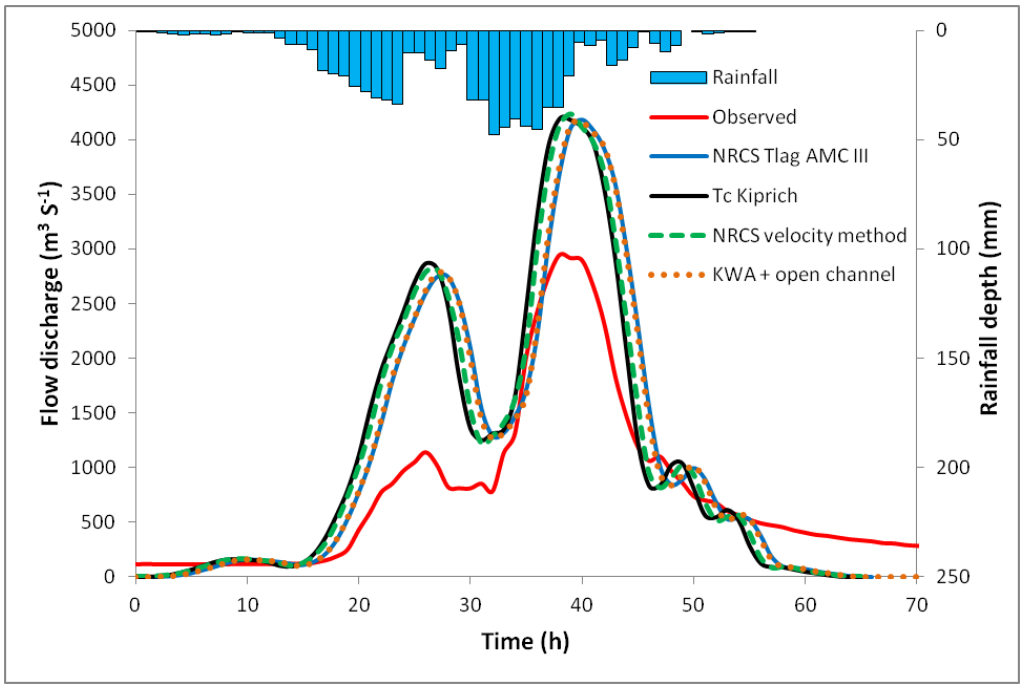

Figure4.12 Rainfall data from Cropp at Waterfall station.

Table 4.11 Evaluation results (Cropp at Waterfall station).

Method	Rainfall (26 - 28 Dec 2010)				
	Qp	Tp	CE	PVE	PEP
Observed	2947.4	38	-	-	-
Tlag AMC I	-	-	-	-	-
Tlag AMC II	4074.8	42	-0.117	-0.397	-38.2
Tlag AMC III	4178.1	40	0.12	-0.421	-41.7
Tc Kirpich	4195.9	38	0.155	-0.43	-42.3
NRCS velocity method	4233.2	39	0.164	-0.432	-43.6
KWA + open channel	4161	40	0.138	-0.385	-41.2

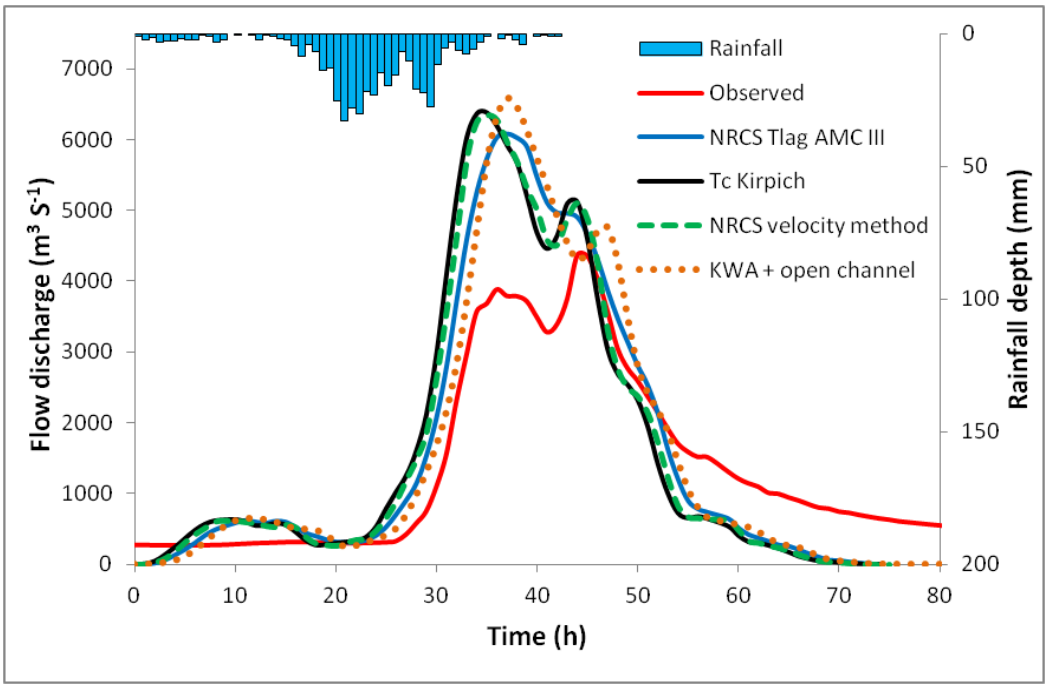

Figure 4.13 Rainfall data from Haast at Roaring Billy station.

Table 4.12 Evaluation results (Haast at Roaring Billy station)

Method	Rainfall 26 - 28 Dec 2010				
	Qp	Tp	CE	RVE	PEP
Observed	4370.3	44	-	-	-
Tlag AMC I	-	-	-	-	-
Tlag AMC II	5640.2	39	0.686	-0.163	-29
Tlag AMC III	6078.6	37	0.568	-0.186	-39
Tc Kirpich	6377.3	35	0.359	-0.186	-45.9
NRCS velocity method	6344.3	35	0.436	-0.18	-45.1
KWA + open channel	6582.2	37	0.55	-0.136	-50.6

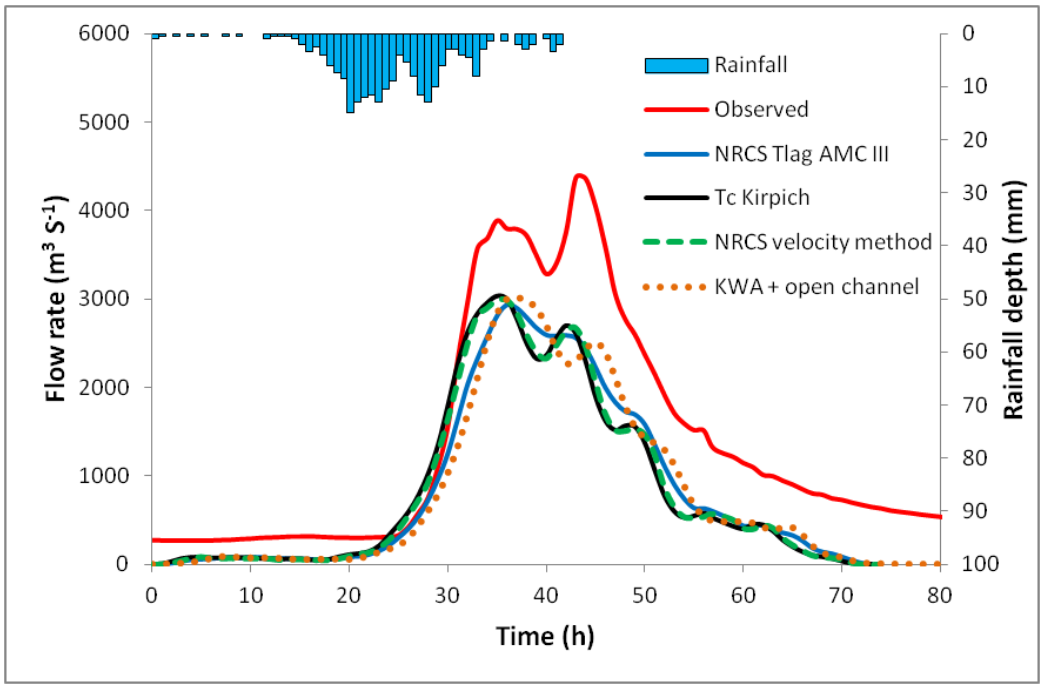

Figure 4.14 Rainfall data from Haast at Moa ck station.

Table 4.13 Evaluation results (Haast at Moa ck station)

Method	Rainfall 26 – 28 Dec 2010				
	Qp	Tp	CE	PVE	PEP
Observed	4370.3	43	-	-	-
Tlag AMC I	-	-	-	-	-
Tlag AMC II	2779.7	42	0.689	0.412	36.4
Tlag AMC III	2933.3	36	0.667	0.4	32.8
Tc Kirpich	3034.1	35	0.57	0.4	30.6
NRCS velocity method	2983.4	36	0.678	0.39	31.7
KWA + open channel	3016.6	37	0.686	0.426	30.9

The shapes of the predicted hydrographs correspond to the input hyetographs and generally match with the shapes of the observed hydrographs. The predictive performance of the simulated hydrographs, however, varies significantly from poor to satisfactory, primarily depending on the method applied to estimate flow velocity and input rainfall data. All models seem to over-predict the first peak as they assume a constant rainfall excess intensity throughout the rainfall duration and do not account for initial losses of rainfall volume available for direct runoff due to interception, depression storage, and absorption processes. Nevertheless, the evaluation results show that the GIS-based SDUH is capable to predict the peak discharge and time to peak with reasonable accuracy.

4.2.3 Flood susceptibility assessment

As mentioned above, flood hazard assessment requires the estimation of parameters such as peak flow rate, flood depth and extent with associated probabilities of exceedence. To determine the frequency and ultimately estimate the probability of flood events with reasonable accuracy, hydro-meteorological data obtained for extended periods of time are required. However, such records are often insufficient or absent. Records of historical flood events are also necessary in order to calibrate and evaluate the models. Furthermore, high resolution topographic data are critical to determine flood depth and extent, but often not easy to obtain especially in regional-scale studies. To overcome these limitations flood hazard can be represented through flood susceptibility, which identifies areas prone to inundation based on terrain characteristics. The concept of susceptibility has been extensively used in landslide hazard studies to overcome data constraints, implying the likelihood of a landslide occurring in an area on the basis of local terrain conditions (Brabb 1984). Susceptibility assessments are usually based on statistical relationships between known geomorphic events (landslides, floods etc.) and conditioning factors and identify areas potentially affected without providing any information on the time frame within which the event might occur or the magnitude of the expected event. The fundamental assumption of this approach is that future geomorphic events will be more likely to occur under the conditions which led to past and present events. A common approach to susceptibility assessment is through GIS-based overlay analysis where different layers of information (factors) are combined to identify locations meeting specific criteria, in this case areas prone to inundation.

Nevertheless, quantifying the influence of different factors in determining flood susceptibility is subject to uncertainty as it usually involves "fuzzy" descriptions such as *low, moderate, high, favourable, close to* etc. For example, *low* elevation areas with *low* slope, *close to* rivers are generally more susceptible to inundation than *steep*, *higher* elevation areas *away* from stream channels. Although the previous description is useful when describing the factors that make an area prone to flooding, it is also quite imprecise as it is very difficult to accurately quantify the above linguistic terms. In addition, the relative importance of each factor and how they affect one another when combined are also very difficult to determine. As discussed in Chapter 3 (section 3.2.1) fuzzy logic, introduced by Zadeh (1965) as a methodology to model highly complex systems, offers an alternative approach to deal with uncertainties related to insufficient knowledge, data limitations and ambiguous or imprecise input information. Therefore it can be applied to quantify the relationships between conditioning factors and flood occurrence especially over large areas with limited and/or imprecise input data.

The most crucial part of any fuzzy logic model is deriving the membership function which associates the fuzzy semantic descriptions (*low, moderate, high, steep, favourable, close to* etc.) to degrees of membership, quantifying the "degree of belonging" of a variable to a set. Membership functions can be determined by the modellers based on their experience and perspectives (knowledge-driven) or they can be derived based on data (data-driven). In the present study, a series of knowledge-driven fuzzy memberships between factors and flood susceptibility have been developed using the fuzzy membership tool incorporated in the Spatial Analyst extension of ArcGIS 10. The fuzzy membership tool transforms input data to a 0 to 1 scale based on the possibility of being a member of a specified set (in this case flood susceptibility) using a series of specific functions. The functions used in the analysis were selected and modified to fit the distribution of flood occurrence frequency ratio (i.e. flood occurrence within each factor category normalized by the flood occurrence over the entire study area). The fuzzy membership functions used in developing the flood susceptibility model and selected input parameters are shown in Fig. 4.15 and Table 4.14 respectively.

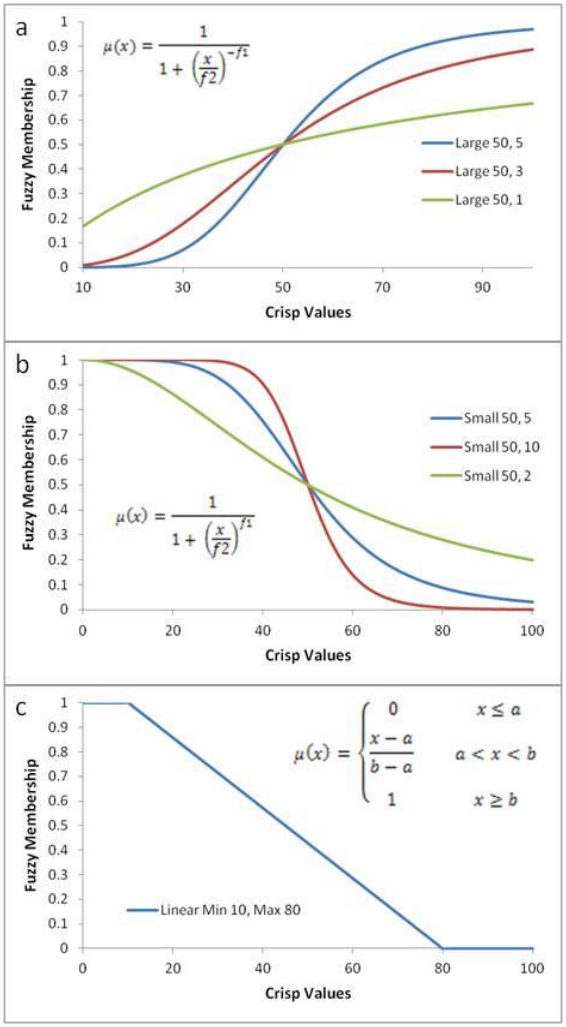

Figure 4.15 A) Fuzzy Large; μ(x) is the membership value of category x, f2 is the midpoint and f1 the spread of the function. The defined midpoint identifies the crossover point (assigned a membership of 0.5) with

values greater than the midpoint having a higher possibility of being a member of the set and values below the midpoint having a decreasing membership. The spread parameter defines the shape and character of the transition zone. The spread and midpoint parameters are subjectively determined by the modeller B) Fuzzy Small; it is suitable when the smaller input values are more likely to be members of the flood susceptibility set (e.g. slope), C) Fuzzy Linear; μ(x) is the membership value of category x and α, b is the minimum and maximum values respectively. It assumes a linear relationship between user-specified minimum and maximum values.

Table 4.14 Selected fuzzy membership functions and associated input parameters.

Factors	Function	Function parameters			
		Minimum	Maximum	Midpoint	Spread
Height above nearest drainage	Small	-	-	7	7.5
Slope gradient	Small	-	-	2.75	4
Soil drainage	Large	-	-	2.5	4.5
Land cover	Large	-	-	4.5	8
Proximity to stream channels	Linear	>1500 m	< 50 m	-	-

4.2.3.1 Flood event inventory

Information on historical flood events is critical for quantifying the spatial and temporal distribution of floods as well as the development of prediction models, thus it is a fundamental component of any effective flood hazard assessment. A flood event catalogue or inventory, in order to be useful in inundation modelling and hazard assessment studies, should at least include the specific geospatial information (i.e., latitude and longitude) and any available flood characteristics such as flow discharge, depth, extent, damage, flow velocity etc. No detailed database exists for the study area hence an effort has been made to develop an inventory by combining information from various available data sources.

Information was initially obtained from Benn (1990) who recorded details of 405 flood events that occurred between 1845 and 1990 in the West Coast region. Additionally the New Zealand historic weather events catalogue provided by NIWA was used. This has been developed from newspaper reports, journals, books and databases provided by various organisations and individuals including information on major weather events in New Zealand over the last 200 years. Finally, data were obtained from the Natural Hazard Review (DTEC 2002) that includes flood events between 1990 and 2002. However most of the above records lack spatial reference, only providing the date and general descriptions of the wider affected area as well as consequent impacts. As such the locations were inferred based on these descriptions and represented by points with variable accuracy, accompanied by information on discharge, flood depth, rainfall intensity and damage when these were available (Fig. 4.16).

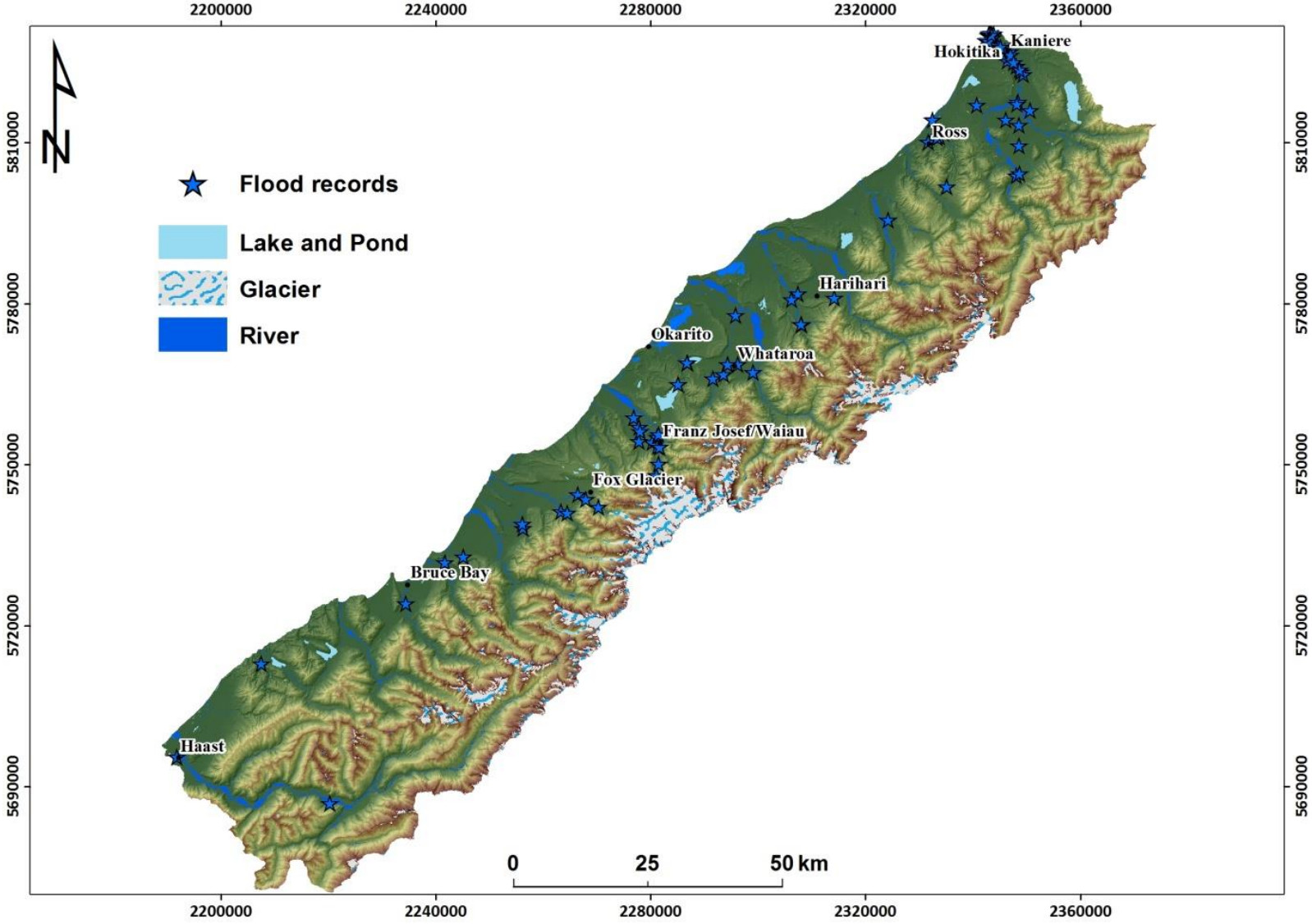

Figure 4.16 Locations of historical flood events.

The majority of records concern populated areas whereas uninhabited flooded areas are often excluded from the descriptions, underestimating the number of affected locations and extent of inundation during an event. Despite the above limitations these records provide the best available information on flood hazard in the study area and herein are used to identify the most important factors controlling the flood susceptibility in the area as well as to derive the fuzzy membership functions. Finally, the spatial distribution of historically affected locations is used to evaluate the model's performance.

4.2.3.2 Flood susceptibility factors

Floodplain topography, land use, vegetation and flood controls (e.g. stop banks, roads, buildings), all have a significant influence on the routing of flood flows and therefore significantly affect flood hazard to people and property. In the present research the terrain factors that contribute to making an area susceptible to flooding were identified based on previously inundated areas. Five parameters were identified at the regional scale as the most important as they are related to critical flood characteristics such as flood water velocity, inundation extent, flood duration and flood depth. The five parameters considered in the analysis are the height above nearest drainage, slope gradient, land cover, soil permeability and distance from river channels. We note that other factors may be also important, depending on the scale and data availability.

Height above nearest drainage (HAND)

Depending on the peak flow discharge in the case of overbank flow (design flood event) the height above river channels controls the extent and depth of flood water on the floodplain. Thus, areas with a continuous surface flow path (hydrologically connected) to the river channel, of the same or lower elevation, are susceptible to inundation. Bock & Köthe (2008), in order to predict the depth of hydromorphic soil characteristics determined by groundwater, introduced the "vertical distance to channel network" by subtracting an interpolated surface (representing base level) from the DEM. Dilts & Yang (2010) proposed the "height above a river" (HAR) which is the elevation of a non-stream grid cell minus the weighted average of the stream cells within a user-specified neighbourhood, as a surrogate for important abiotic variables, such as depth to groundwater. Rennò et al. (2008) developed the "height above nearest drainage" (HAND) in order to classify the ecological zones in Amazonia. HAND normalizes a DEM according to distributed vertical distances relative to the drainage channels, in other words it is the relative height of any point (classified as non-stream cell) to the nearest stream cell following the steepest path. In the present study it was deemed appropriate to use the HAND model as it delineates low elevation areas hydrologically connected to the rivers that are more susceptible to inundation. The HAND thematic layer was developed using

the 25m DEM according to the methodology described in Rennò et al. (2008). The calculations were performed using Terraview GIS (Fig. 4.17).

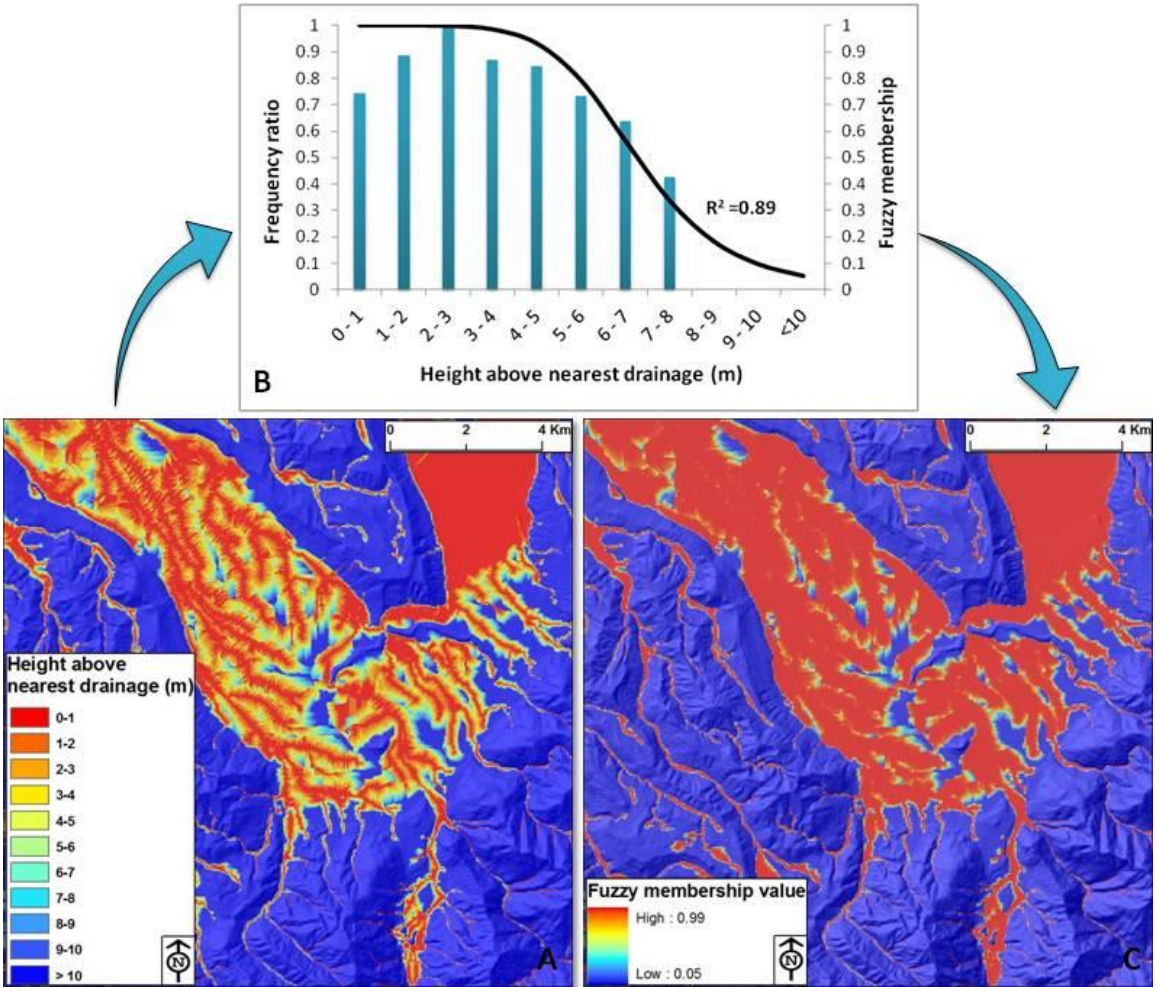

Figure 4.17 A) Height above nearest drainage B) flood occurence frequency ratio and corresponding fuzzy membership, C) "fuzzified" height above nearest drainage. The map essentially delineates the spatial variation of flood susceptibility based on the HAND factor.

Slope gradient

Slope gradient is a commonly used topographic parameter in hydrology and a critical flood susceptibility factor. It determines the water velocity as well as indicating flat surfaces where the surface runoff may be temporarily retained (ponding). According to the flood records low elevation, relatively flat areas and valley floors have been repeatedly subject to inundation in the study area. The slope gradient map was derived from a 25m DEM developed by Landcare Research in 2002 (Barringer et al. 2002). The slope grid was reclassified into 7 classes: (1) 0-1°, (2) 1-2°, (3) 2-3°, (4) 3-4°, (5) 4-5°, (6) 5-10° and (7) >10° (Fig. 4.18).

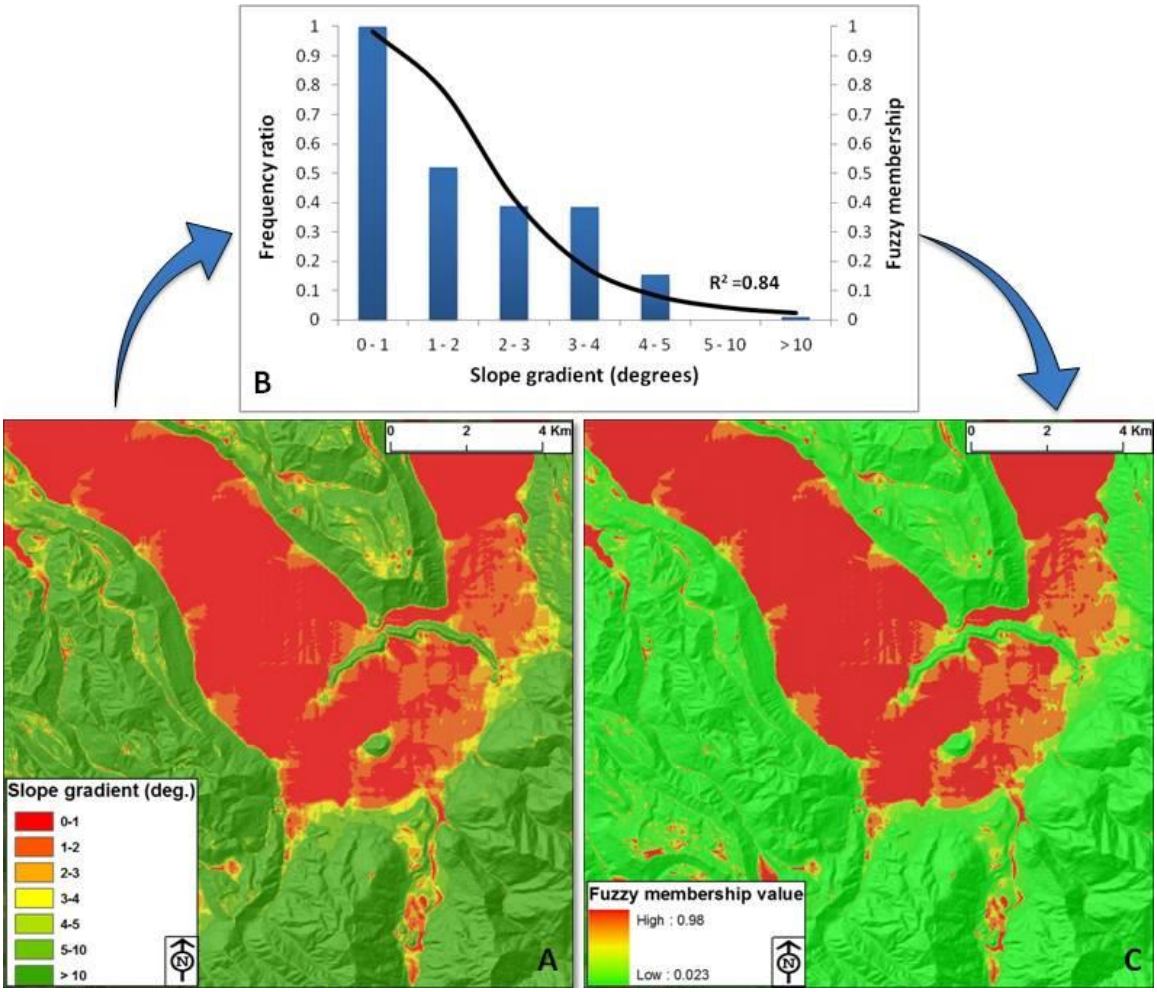

Figure 4.18 A) Classified slope gradient map B) flood occurrence frequency ratio and corresponding fuzzy membership function, C) fuzzy slope gradient map.

Land cover

Land cover is considered to have significant influence on the hydrologic response of a catchment (Mahe et al. 2004; Sriwongsitanon & Taesombat 2011). The impact of land cover on flooding has been recently illustrated by different authors (Bradshaw et al. 2007; Lin & Wei 2008) who conclude that deforestation is strongly correlated with flood occurrence and severity. The land cover type and density influence the total amount of runoff mainly by affecting rainfall water retention and soil infiltration capacity. Bare soil or bedrock surfaces have higher runoff potential compared to dense forested areas, and therefore higher flood susceptibility. Land cover data were obtained from the New Zealand Land Cover Database 2 (MfE 2004). The Land Cover Database 2 (LCDB2) is a thematic classification of 43 land cover and land use classes in New Zealand. It is based on Landsat 7 ETM+ satellite imagery acquired over the summer of 2001/02 with spatial resolution of 15m. The land cover grid was reclassified into 8 classes: (1) Bare or lightly vegetated area, (2) Forest, (3) Grassland,

(4) Scrub and shrubland, (5) Wetland, (6) Cropland, (7) Artificial areas and 8) River and lakeshore gravel and rock (Fig. 4.19, 4.20).

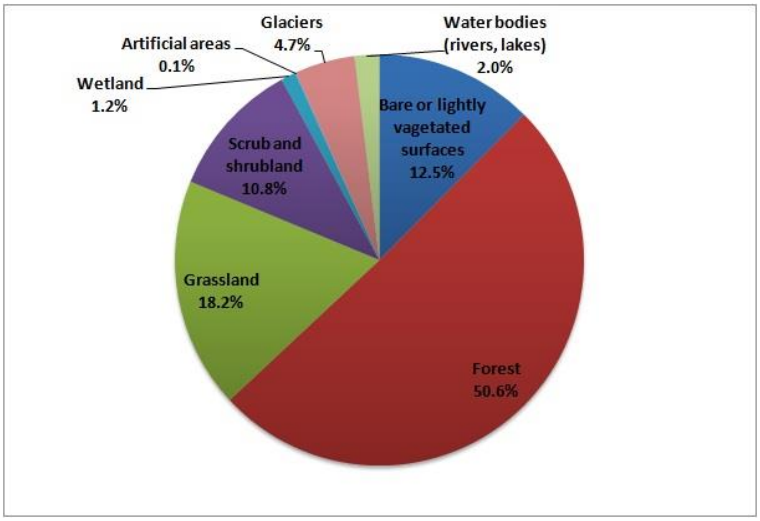

Figure 4.19 Approximately 50 % of the study area is covered by forests. The floodplains of major rivers are predominately covered by grasslands.

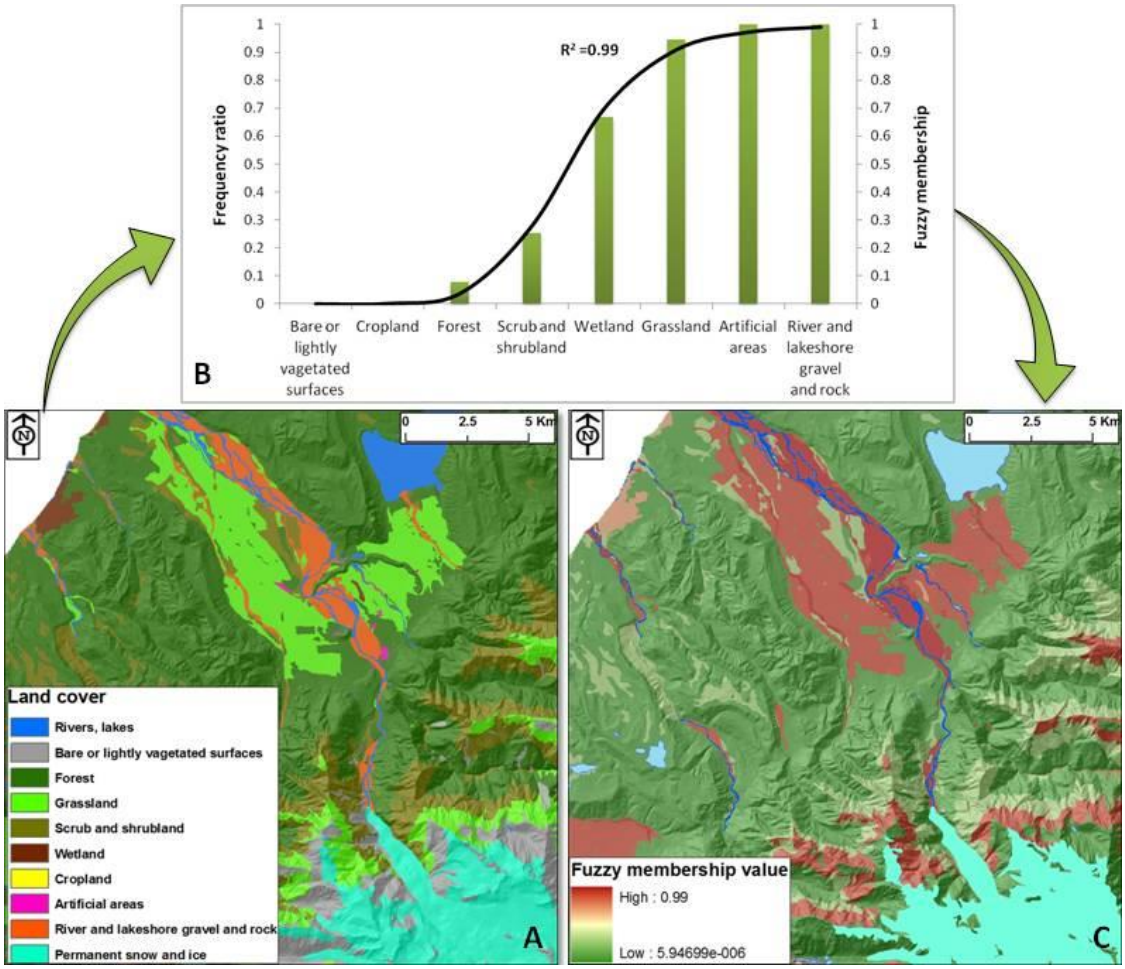

Figure 4.20 A) Land cover map B) flood occurrence frequency ratio and corresponding fuzzy membership function, C) fuzzy land cover map.

Soil permeability

In addition to land cover, soil permeability is also considered an important factor in regulating runoff. Soil characteristics such as the grain size, the structure of the soil matrix, and the relative amount of saturation control the soil infiltration capacity and can substantially affect the total runoff. Soil that allows water to permeate easily (where there are many macropores) is less vulnerable to flooding than less permeable soil types (clayey soils). Antecedent moisture conditions are also influenced by soil permeability as the soil types that retain water for a longer period after a rainfall event require less rainfall to produce runoff during the next event. Permeability classes representing the rate that water moves through saturated soil are given from Clayden & Webb (1994) as follows: 1) Rapid, 2) Rapid/Moderate, 3) Rapid/Slow, 4) Moderate/Rapid, 5) Moderate, 6) Moderate/Slow, 7) Slow/Moderate, 8) Slow, 9) Bedrock, 10) Paved areas (Fig. 4.21). Soil permeability data were obtained from the Land Resource Information System, a spatial archive of New Zealand's physical resource information, developed by Landcare Research.

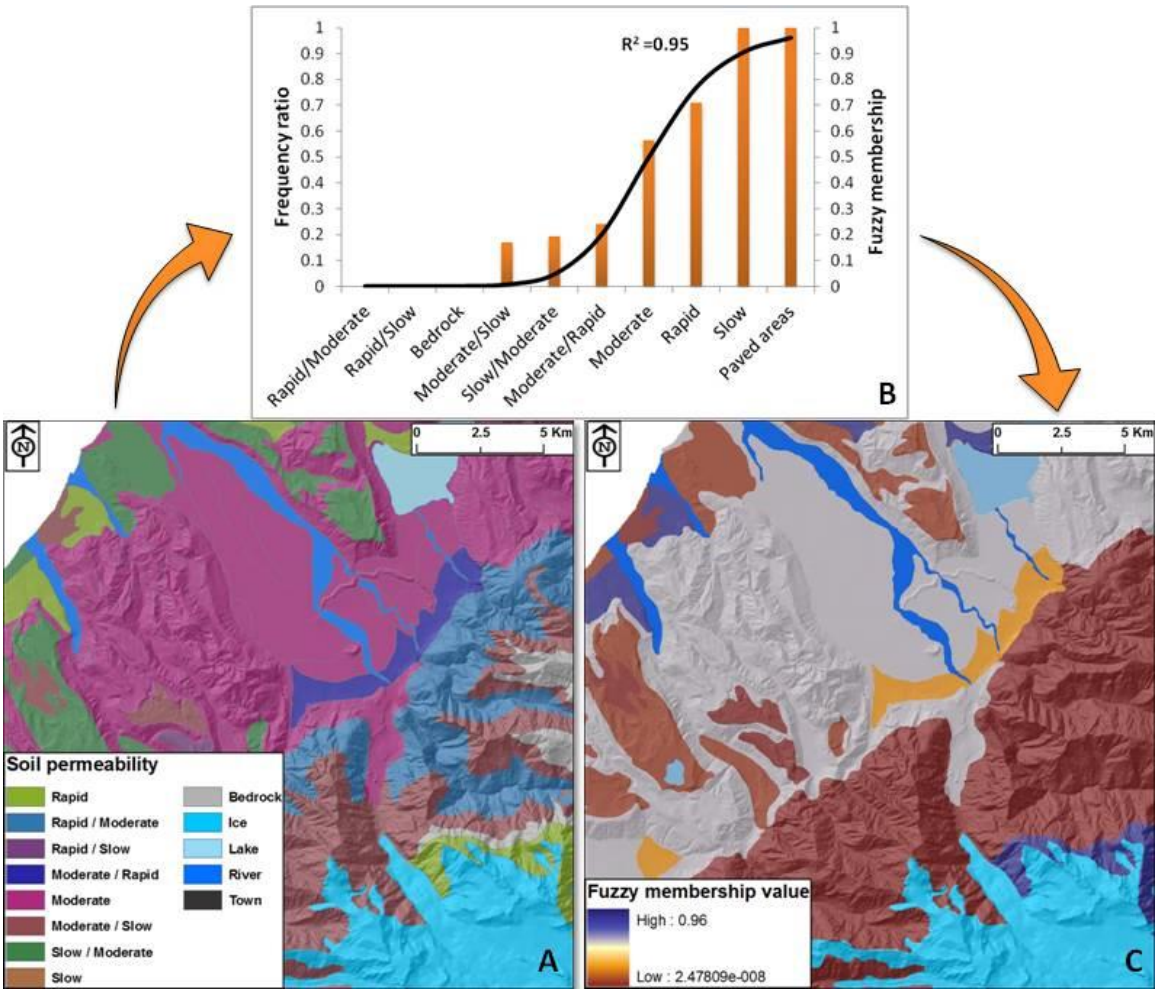

Figure 4.21 A) Soil permeability map B) flood occurrence frequency ratio and corresponding fuzzy membership function, C) fuzzy soil permeability map.

Distance from river channels

Based on the flood event inventory the most affected areas as a consequence of overflow during river flood events are those in close proximity to river channels and streams. Drainage network data in shapefile format (polygons and polylines) were obtained from the New Zealand topographic maps (Topo50 series) provided by Land Information New Zealand (LINZ). Using buffer analysis the study area was divided into the following classes based on horizontal distance from the drainage network: 1) 0-50 m, 2) 50-100 m, 3) 100-200 m, 4) 200-300 m, 5) 300-400 m, 6) 400-500 m, 7) 500-1000 m, 8) 1000-1500 m and 9) > 1500 m (Fig. 4.22).

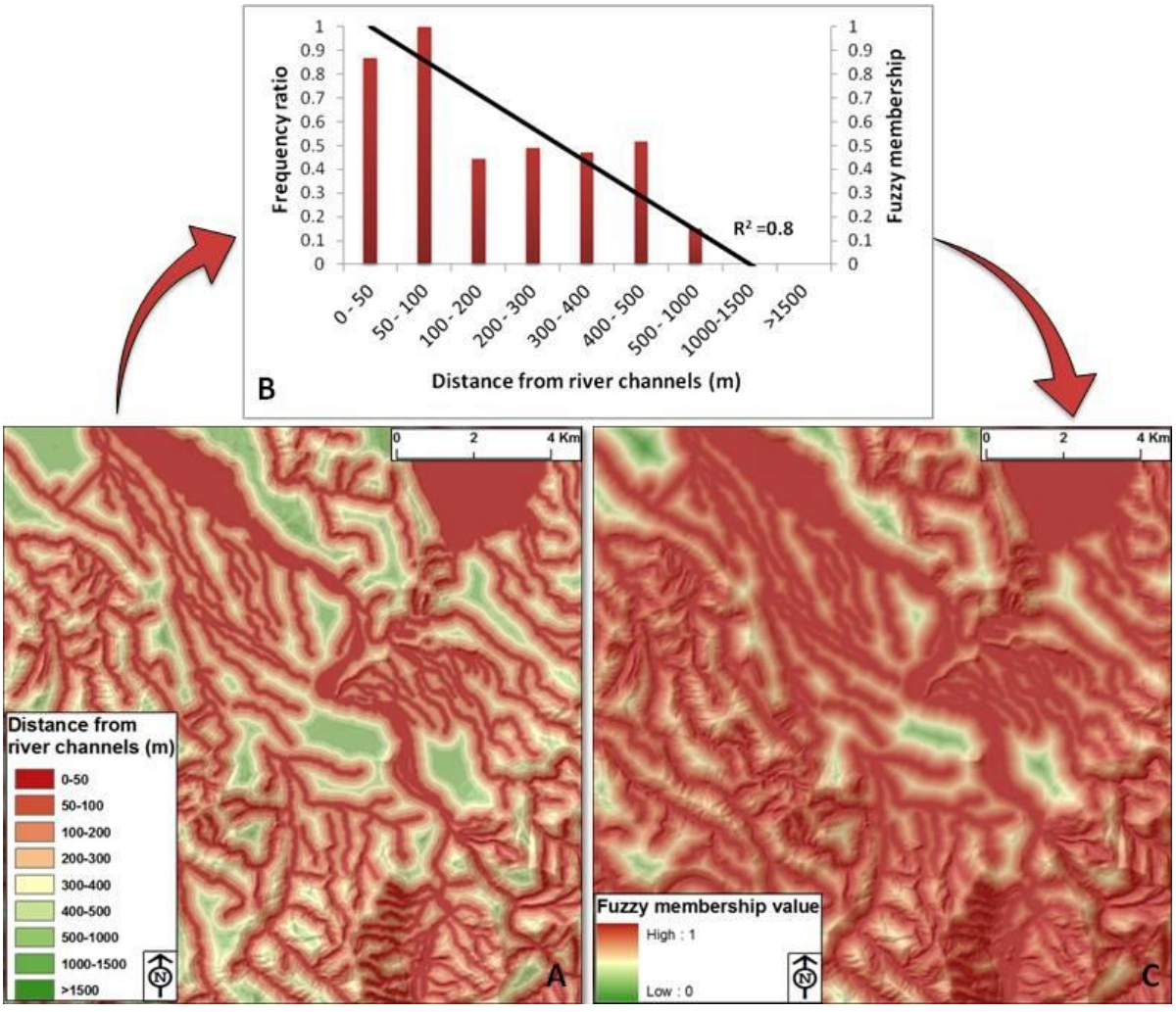

Figure 4.22 A) Classified distance from river channels map B) flood occurrence frequency ratio and corresponding fuzzy membership function, C) fuzzy distance from river channels.

4.2.3.3 Flood susceptibility index map

In order to develop the flood susceptibility index (FSI) map the above five parameters, represented by the "fuzzified" information layers in raster format with values ranging from 0 to 1, need to be combined. Different operators are available such as the fuzzy AND, fuzzy OR, fuzzy algebraic Product,

fuzzy algebraic Sum and fuzzy gamma operator (Bonham-Carter 1994). Herein, the criteria were combined by applying the fuzzy gamma operator (eq. 4.21), as it provides a way to overcome the increasing tendencies of the fuzzy algebraic sum and the decreasing effect of the fuzzy algebraic product, establishing the relationships between the multiple input criteria and not simply returning the value of a single membership set as the Fuzzy Or and Fuzzy And do.

$$\mu_{(x)} = \left(1 - \prod_{i=1}^{n}(1-\mu_i)\right)^{\gamma} * \left(\prod_{i=1}^{n}\mu_i\right)^{1-\gamma} \quad (4.21)$$

where $\mu_{(x)}$ is the combined membership value, $\prod_{i=1}^{n}\mu_i$ is the algebraic product, $1 - \prod_{i=1}^{n}(1-\mu_i)$ is the algebraic sum and γ is a parameter ranging between 0 and 1 (when γ is 1, the combination is the same as the fuzzy algebraic sum; and when γ is 0 the combination equals the fuzzy algebraic product).

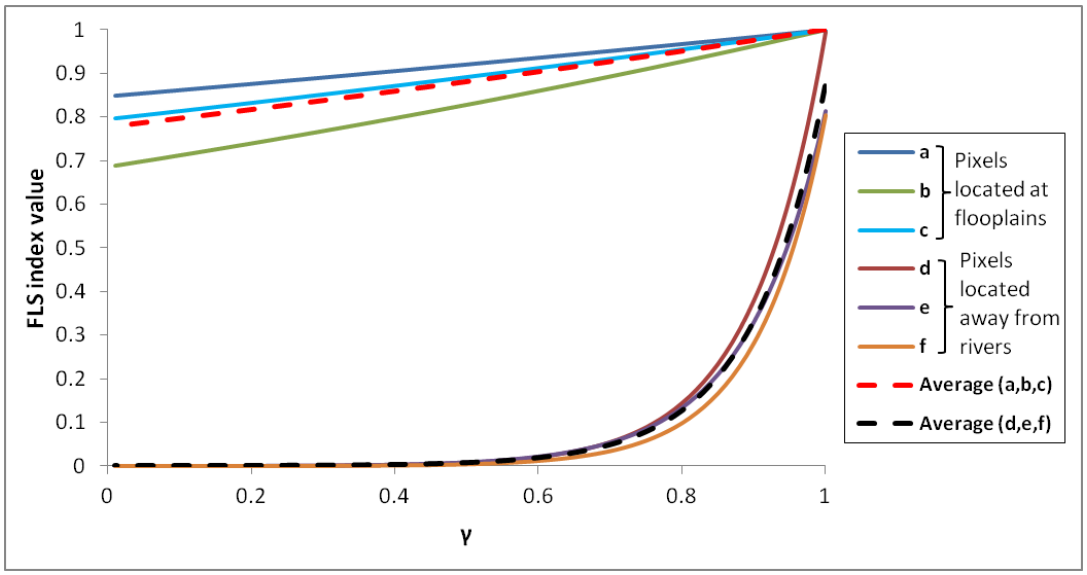

Figure 4.23 Effect of γ value on flood susceptibility index. The optimum gamma value (γ≈0.8) was estimated based on the distance between the curves that correspond to floodplain pixels and the curves from the higher elevation areas away from rivers.

The γ value is a user-defined parameter that determines the degree to which the favourable and non-favourable flood susceptibility conditioning factors will affect the output. A meaningful output is the one where most if not all the observed flood locations coincide with the higher susceptibility values which should cover a relatively small area. This requires an optimum γ value. To accomplish this all possible γ values in the range 0 to 1 were tested and their effect on the flood susceptibility

index was observed for different pixels in the study area. Half of the pixels were randomly obtained from the floodplains close to rivers and the remaining from locations with very low or no flood susceptibility (high elevation areas away from rivers). Flood susceptibility values generally increase with increasing γ value, as the effect of favourable factors (with membership values close to 1) becomes more important. However, increasing the γ value above a certain threshold, even cells that are supposed to have low to very low susceptibility (hills, steep slopes, mountain ridges and areas away from rivers) will eventually have higher susceptibility values. This would yield a result that doesn't correspond to reality and can't be used to inform planning. Therefore, the optimum γ value was defined based on the distance between the curves that represent the floodplain pixels and the curves from the higher elevation areas away from rivers (Fig. 4.23). By applying equation 4.22 in GIS environment, using the five factors discussed above, the flood susceptibility index (FSI) was estimated (Fig. 4.24).

$$FSI = \big(1 - (Height\ above\ nearest\ drainage * slope\ gradient * land\ cover * soil\ permeability * proximity\ to\ river\ channels)\big)^{\gamma} * (Height\ above\ nearest\ drainage * slope\ gradient * land\ cover * soil\ permeability * proximity\ to\ river\ channels)^{1-\gamma} \quad (4.22)$$

4.2.3.4 Evaluation

To evaluate the predictive capability of the flood susceptibility index map, data from the flood inventory were used. Unfortunately the number of events and their spatial distribution don't allow separating the data into training and test subsets, with the risk that the evaluation process is not indicative of the predictive performance of the model but of the goodness of fit of the historical records with the susceptibility values. However, the historical records have not directly been used to derive the fuzzy memberships; instead they were utilized to derive a best fit membership function that approximately follows the pattern of the frequency ratio between flood occurrence and factor classes. The evaluation was performed by constructing the success rate curve between flood events and susceptibility zones (Fig. 4.25). The derivation of success rate curves is a commonly-applied technique in landslide susceptibility assessment studies that allows comparing the spatial distribution of landslides and modelled landslide susceptibility classes (Chung & Fabbri 1999; Van Westen et al. 2003; Remondo et al. 2003; Frattini et al. 2010). In order to derive a meaningful output the majority of the historical floods should coincide with the higher susceptibility zones, which should cover relatively small area on the map.

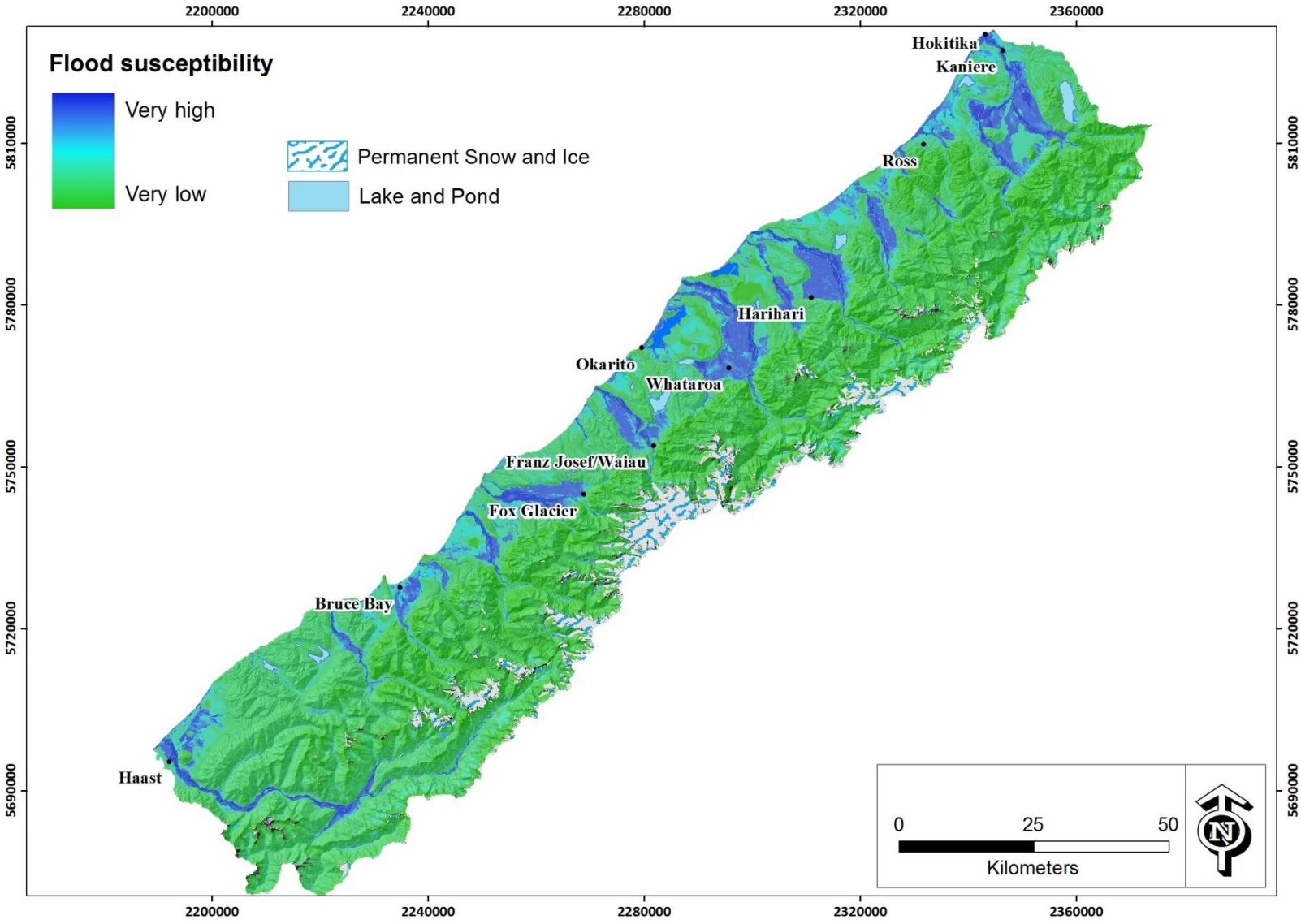

Figure 4.24 Regional flood susceptibility index map.

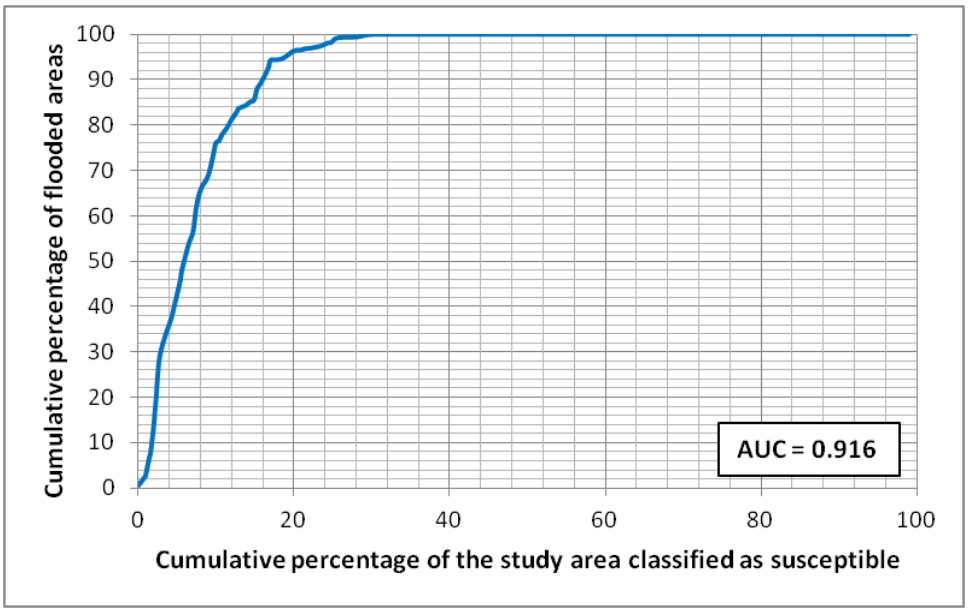

Figure 4.25 Success rate curve of the flood susceptibility index map.

4.3 Discussion – Flood hazard

In the present study a GIS-based spatially distributed unit hydrograph model is developed in order to investigate the hydrologic response of major ungauged catchments in the study area based on their morphometry, land cover and soil characteristics. The purpose of the model is twofold. First, the model aims to simulate the hydrologic response of the catchments and compare the intrinsic tendency of different catchments to produce runoff, and second, to generate runoff hydrographs that correspond to real rainfall intensity data.

A number of climatic and physiographic factors have been identified to affect the shape of a hydrograph (Subramanya 1984) such as: drainage basin characteristics (area, slope, shape, elevation, drainage density), infiltration characteristics (land use and cover, soil type and geological formations, lakes, swamps and other storage), river channel characteristics (cross-section, roughness and storage capacity) and rainfall characteristics (intensity, duration, storm movement). Additionally, when glacier cover is present it affects the shape of the hydrograph, especially in heavily glaciated catchments. As it is not possible to consider all the above factors and their temporal variability and spatial heterogeneity, even in a spatially distributed model, a number of assumptions are inevitable in order to develop a model that would incorporate as many critical factors as possible and produce an output with reasonable accuracy. The most important of these factors, which emerged from the development and implementation of the SDUH model, are discussed below.

Flow velocity and time of concentration (T_c) are fundamental components of the model determining the shape of the hydrograph and ultimately its peak discharge (Q_p) and time to peak (T_p). The empirical formulas used to estimate the flow travel times, incorporate different combinations of catchment parameters (morphometric, soil, land cover) demonstrating variable sensitivity to each parameter and reflect the characteristics of the specific environment in which they were developed. For example, formulas derived from data obtained from arid relatively flat catchments assign different weights on slope and land cover compared to those derived from humid steep catchments. Similarly relationships derived using data from rural catchments might demonstrate different sensitivity to land use from those developed using urban catchment data. Therefore, it is very important to state that there is no optimum method to calculate the time of concentration and flow velocity and all the available empirical formulas provide only an estimate, which has to be further evaluated with real measurements before its application for a specific area.

Another critical issue concerns the implementation of the empirical formulas using GIS. Although it is generally accepted that high resolution data produce better results, the cell's small area might have the opposite effect when calculating the time of concentration in a cell-based approach. The problem stems from the fact all the above formulas were originally developed and applied to calculate the time of concentration in much coarser flow path segments (sub-catchments) than the cells of a DEM. Calculating the T_c in each cell assuming it is a sub-catchment, although it allows for more detailed spatial distribution of catchment parameters, it also uses the slope value of the cell. Cell slopes generated by DEM processing often yield very small or zero values, especially in valley floors and flat areas, resulting in unusually high travel times and very low flow velocities. Conversely, cells with very high slope values yield low travel times and consequently very high velocities. The presence of a large number of high flow velocity cells in the catchment will ultimately generate a hydrograph overestimating the Q_p and T_p, whereas many low flow velocity cells will result in an underestimation of Q_p and T_p.

Antecedent runoff conditions also significantly affect runoff generation as they regulate water retention and storage. As mentioned above the rainfall event used to develop and evaluate the runoff hydrographs occurred in already increased antecedent moisture conditions due to smaller rainfall events the previous days. This implies that water retention and storage was limited, enabling models using empirical formulas that do not take into account storage (e.g. Kirpich's formula) to perform well. The best performance in terms of overall agreement with the measured hydrograph (CE=0.82) and predicted peak flow rate (PEP=-0.43) was observed by applying the NRCS watershed

lag method using AMCIII (wet conditions), whereas the input of AMCII (average) and AMCI (dry) conditions generally resulted in lower predictive capability.

The variability of the models' predictive performance using data from different rainfall gauging stations suggests that the spatial variation of rainfall characteristics within the catchment is a key factor in this modelling approach. As can be seen from the evaluation results in Hokitika at Gorge catchment the peak flow rate was overpredicted using rainfall data from the Colliers ck station (95m altitude) and it was consistently underpredicted using data from higher altitude stations. However the opposite is observed in Haast river catchment. Although the Moa ck station is located at higher altitude compared to the Roaring Billy station the orientation of the station in conjunction with the storm movement (a warm moist north-easterly flow followed by a large cold frontal system caused heavy rain with a south to north direction) resulted in receiving less amount of rainfall (Station $_{\text{Moa ck}}$ = 220mm, Station $_{\text{Roaring Billy}}$ = 414.5 mm). The sensitivity of the modelling output to the spatial variation of rainfall within the catchment indicates that the unit hydrograph approach may not be appropriate for relatively large watersheds where the spatial variation in rainfall tends to be high or where there is a strong orographic effect. To overcome this issue stations with a good spatial distribution over the catchment area are necessary.

Despite the limitations discussed above, the SDUH model is able to predict the peak flow rate and time to peak of ungauged river catchments for any rainfall event with reasonable accuracy. Generating the UHs for major catchments and river confluences in the study area have been also used to investigate the hydrologic response of different catchments based on their morphometry.

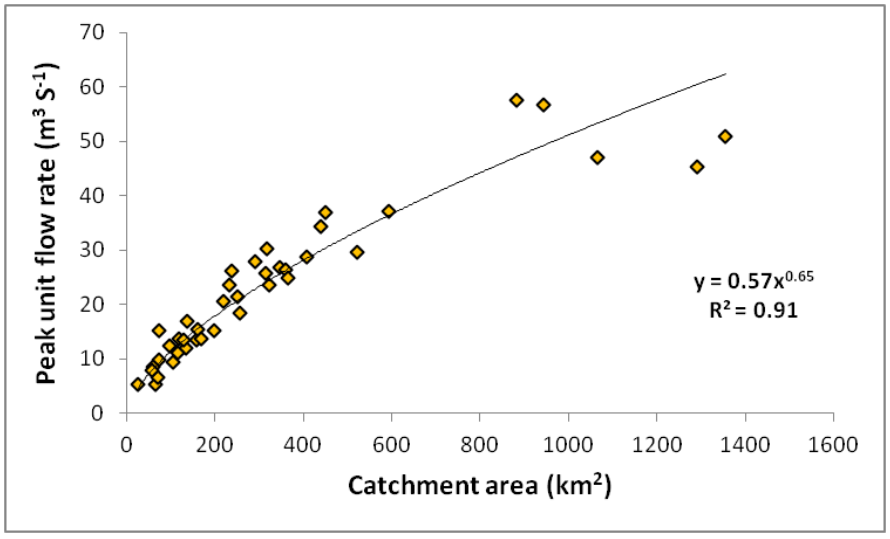

Figure 4.26 UH peak flow rate plotted against catchment area.

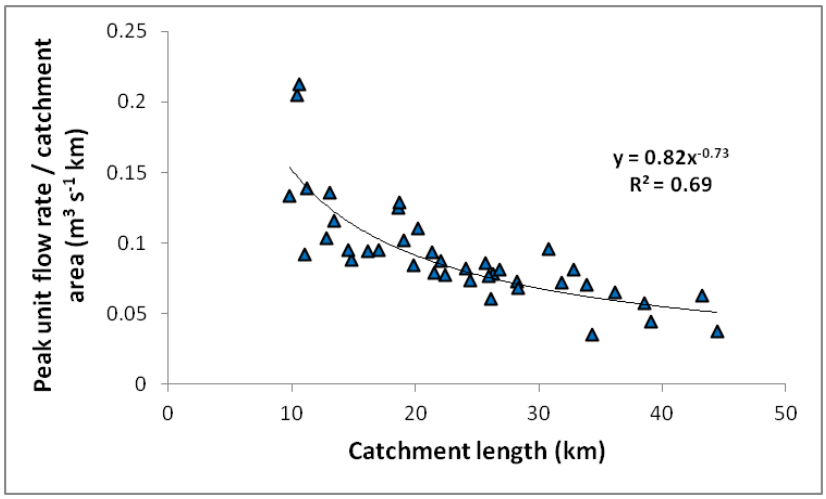

Figure 4.27 Negative correlation between catchment length and Q A^{-1}.

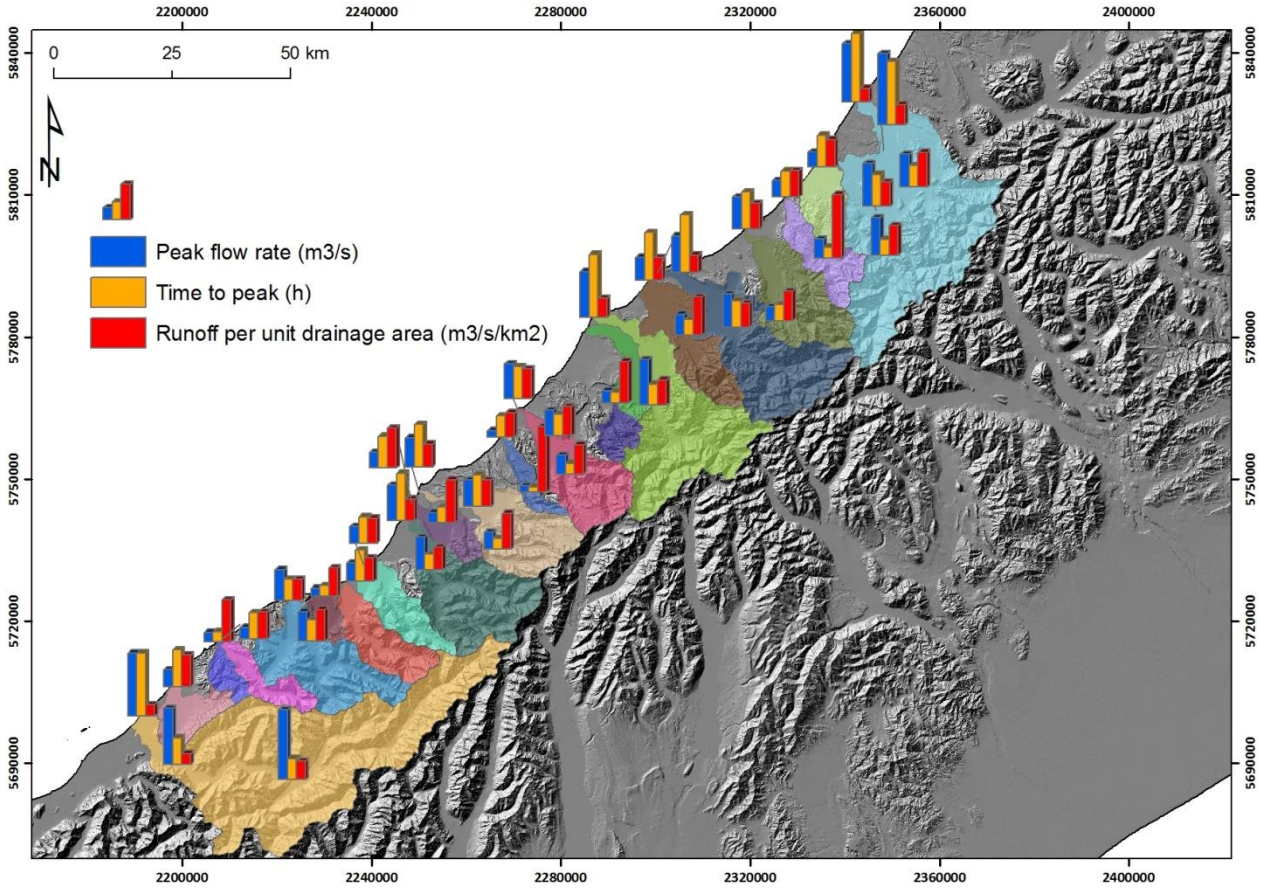

Figure 4.28 Spatial distribution of UH peak flow rate, time to peak and runoff per unit area. Analysis performed at major river confluences and major catchment outlets.

The peak flow rate demonstrates strong correlation with catchment area (Fig. 4.26) however, normalizing the Q_p with the contributing catchment area (A), allows comparing the intrinsic tendency of different catchments to produce runoff (runoff per unit area) without the influence of

climate and drainage area. According to the spatial distribution of the Q_p / A ratio steep, relatively short mountainous catchments generate more runoff per unit area compared to larger catchments (Figs. 4.27, 4.28). Due to their increased runoff efficiency (greater amounts of precipitation become surface runoff) these catchments have greater potential to induce flooding downstream, especially where the rivers exit from the confined steep valleys close to the mountain front.

In addition to the SDUH model, an approach based on fuzzy logic in GIS environment was developed, aiming to assess the flood susceptibility in the study area. The proposed approach provides a simple method to identify areas susceptible to flooding at regional scale using terrain, land cover and soil parameters. Five factors were identified and their relationship with flood occurrence was established based on fuzzy set theory and historical flood events. The implementation of fuzzy logic allows a more realistic representation of the predisposing factors as it takes into account uncertainties related to insufficient knowledge, data limitations and non-linear relationships between conditioning factors and flood susceptibility.

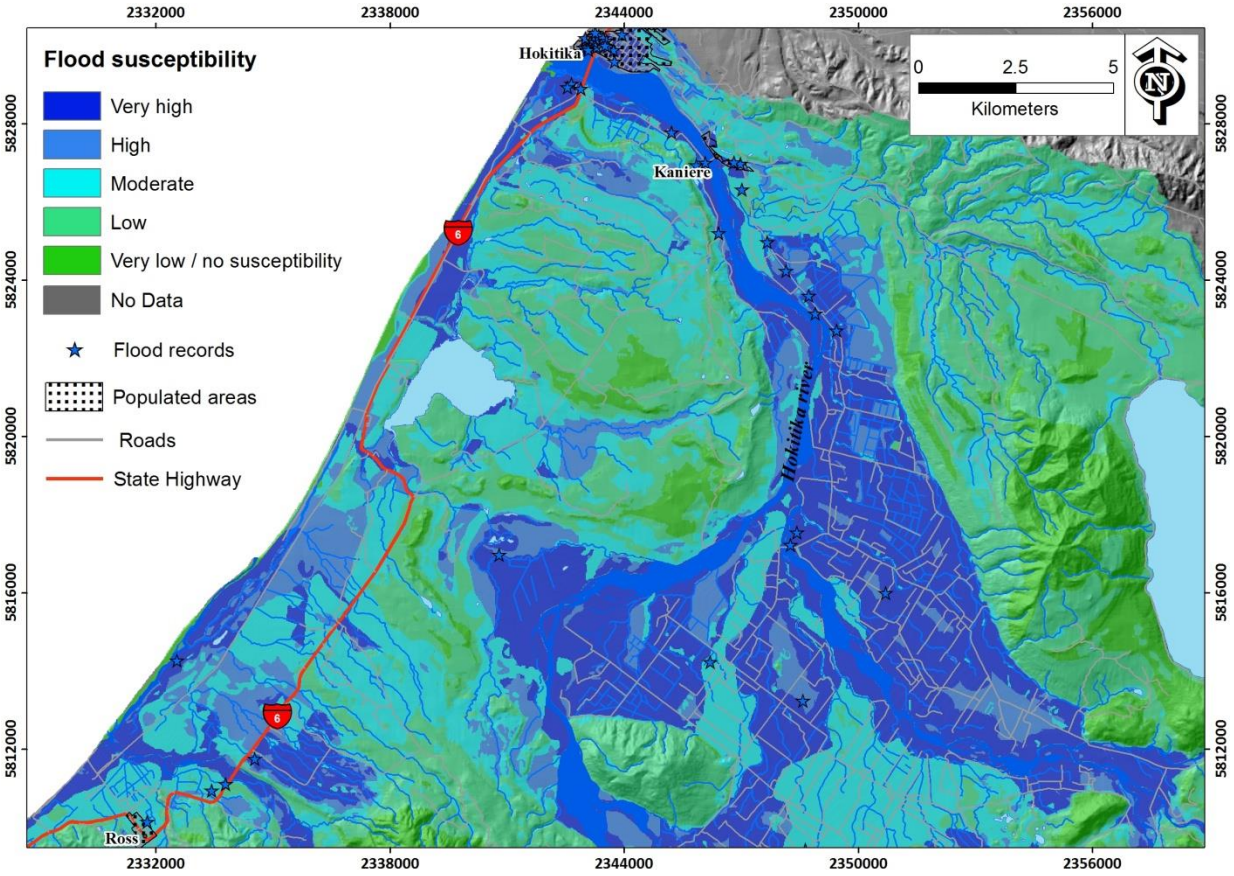

Figure 4.29 Flood susceptibility classified in five categories in the lower Hokitika river catchment.

The final flood susceptibility map reveals several locations where populated areas and road network coincide with very high flood susceptibility zones (Fig. 4.29). Predicting the peak flow rate and time to peak of ungauged river catchments as well as identify areas susceptible to flooding is a vital component of regional scale flood hazard assessment in Western Southern Alps. The two models combined provide a useful tool to inform land use planning and guide the development of critical infrastructure and lifelines in the region. Based on the output different flood susceptibility zones can be identified and placed under land-use regulations aiming to minimize the flood damage potential in those areas.

4.4 Conclusions

Considering the findings from the development and application of the SDUH and flood susceptibility models a number of conclusions can be drawn concerning the flood hazard in the study area.

1. The extremely high orographically-enhanced precipitation, and the fact that most settlements are located on active floodplains close to rivers that source from steep mountain catchments, significantly increase the flood hazard in the region.

2. The high denudation rates due frequent landsliding (Hovius et al. 1997; Korup et al. 2005) in WSA, generate very high sediment input and flux through the drainage network constantly altering the channels' geometry (width, depth, radius) and their position on the flood plains (braided rivers). Additionally, glacier cover significantly affects catchment hydrological response altering the annual and seasonal flow discharge patterns through the storage and release of precipitation water. These processes make flood hazard assessment in WSA extremely difficult using available modelling approaches. Despite these complexities the proposed approach offers a simple way to predict the peak flow rate and time to peak of ungauged river catchments using real rainfall scenarios as well as to identify areas susceptible to flooding at regional scale with reasonable accuracy. Nevertheless future effort should focus on incorporating other critical geomorphic processes such as landslide dam break floods, glacier bursts and river aggradation as well as the impact of large magnitude earthquakes that can induce both landslide dams and river aggradation in flood hazard assessment modelling.

3. The development of a comprehensive flood catalogue or inventory that includes the specific geospatial information (i.e., latitude and longitude) of flood events accompanied by parameters such as peak flow discharge and velocity, flood depth, extent and damage, is

critical for quantifying the spatial and temporal distribution of flood occurrence as well as in the development of effective flood hazard assessment models.

4. Finally, as the flood hazard in the region is controlled by tectonic, climatic and surface processes as well as their interrelationships, flood hazard mitigation activities either through engineering works, flood proofing of buildings and infrastructure or relocation of existing developments, should consider the catchment as a geomorphic system (not only the drainage system) in order to effectively mitigate the impact of flooding in the context of sustainability.

4.5 References

Ajward MH, Muzik I 2000. A spatially varied unit hydrograph model. Journal of Environmental Hydrology 8: Paper 7.

Anderson B, Lawson W, Owens I, Goodsell B 2006. Past and future mass balance of Ka Roimata o Hine Hukatere (Franz Josef Glacier). Journal of Glaciology 52 (179), 597–607.

Arcement, Jr. GH, Schneider VR 1989. Guide for selecting manning's roughness coefficients for natural channels and flood plains. Water supply paper 2339, U.S. Geol. Survey, Washington D.C. http://www.fhwa.dot.gov/bridge/wsp2339.pdf

ASCE, 1993. Criteria for evaluation of watershed models. Journal of Irrigation and Drainage Engineering 119 (3), 429-442.

Baker VR 1976. Hydrogeomorphic methods for the regional evaluation of hazards. Environmental Gelogy, 1, 261-281.

Baker VR 2008. Paleoflood hydrology: origin, progress, prospects. Geomorphology, 101(1-2), 1-13.

Barringer JRF, Pairman D, McNeill SJ 2002. Development of a high resolution digital elevation model for New Zealand. Landcare Research Contract Report: LC0102/170.

Benito G, Hudson PF 2010. Flood hazards: the context of fluvial geomorphology. In: Geomorphological hazards and disaster prevention in (eds) I. Alcantara-Ayala and A. Goudie. Cambridge : Cambridge University Press, 2010. pp. 111-128

Benn JL 1990. A Chronology of Flooding on the West Coast, South Island, New Zealand: 1846 – 1990. The West Coast Regional Council, Greymouth. 159p

Bennett DA 1997. A framework for the integration of geographical information systems and model base management, International Journal of Geographical Information Science, 11(4): 337–357.

Bock M, Köthe R 2008. Predicting the depth of hydromorphic soil characteristics influenced by ground water. Hamburger Beiträge zur Physischen Geographie und Landschaftsökologie, Heft 19, pp 13-22.

Bonham-Carter GF 1994. Geographic information systems for geoscientists. Ottawa, Pergamon.

Brabb EE 1984. Innovative approaches to landslide hazard and risk mapping, Proceedings of the 4th International Symposium on Landslides, 16–21 September, Toronto, Ontario, Canada (Canadian Geotechnical Society, Toronto, Ontario, Canada), 1:307–324.

Bradshaw CJA, Sodi NS, Peh KSH, Brook BW 2007. Global evidence that deforestation amplifies flood risk and severity in the developing world. Global Change Biol. 13, 2379–2395.

Brodie RS, Hostetler S 2005. A review of techniques for analysing baseflow from streamflow hydrographs. Proceedings of the NZHS-International Association of Hydrogeologists-NZSSS 2005 Conference, 28 Nov-2 Dec, 2005, Auckland, New Zealand.

Brunner GW, United States Army Corps of Engineers, Institute for Water Resources (U.S.), Hydrologic Engineering Center (U.S.) 2001b. HEC-RAS river analysis system: user's manual, US Army Corps of Engineers Institute for Water Resources Hydrologic Engineering Center, Davis, CA.

Chow VT, Maidment DR, and Mays LW 1988, Applied Hydrology, McGraw-Hill, New York.

Chung CF, Fabbri AG 1999. Probabilistic prediction models for landslide hazard mapping, Photogrammetric Engineering & Remote Sensing **65**(12), 1389–1399.

Clark CO 1945. Storage and the unit hydrograph. Trans. ASCE 110:1419-1446.

Clark MJ 1998. Putting water in its place: a perspective on GIS in hydrology and water management. Hydrological Processes 12, 823-834.

Clayden B, Webb TH 1994. Criteria for defining the soil form – the fourth category of the New Zealand Soil Classification. Landcare Research Science Series 3. Lincoln, New Zealand, Manaaki Whenua Press. 36p.

Cleveland TG, Thompson DB, Fang X, He X 2008. Synthesis of Unit Hydrographs from a Digital Elevation Model. Journal of Irrigation and Drainage Engineering 134:2 (212).

Cowan WL 1956. Estimating hydraulic roughness coefficients. Agricultural Engineering, 37(7), 473-475.

Davies TR, Scott BK 1997. Dambreak Flood Hazard from the Callery River, Westland New Zealand. New Zealand Journal of Hydrology, Vol. 36 (1), pp 1-13.

Davies TRH 2002. Landslide dambreak flood hazards at Franz Josef Glacier township, NewZealand: a risk assessment. Journal of Hydrology (New Zealand) 41: 1-17.

Davies TR, McSaveney MJ, Clarkson PJ 2003a. Anthropic Aggradation of the Waiho River, Westland, New Zealand: Microscale Modelling. Earth Surf. Process. Landforms 28, 209–218.

Davies TR, Smart CC, Turnbull JM 2003b. Water and Sediment Outbursts from Advanced Franz Josef Glacier, New Zealand. Earth Surface Processes and Landforms, 28, 1081–1096.

Davies TR, McSaveney MJ 2006. Geomorphic constraints on the management of bedloaddominated rivers. Journal of Hydrology (New Zealand) 45 (2): 69-88.

Davies TR, Korup O 2007. Alluvial fanhead trenching resulting from catastrophic sediment inputs. Earth Surface Processes and Landforms 32: 725-742.

Davies TR, McSaveney MJ 2008. Principles of sustainable development on fans. Journal of Hydrology (NZ) 47 (1): 43-65.

Dawson CW, Abrahart RJ, See LM 2007. HydroTest: A web-based toolbox of evaluation metrics for the standardised assessment of hydrological forecasts. Environmental Modelling & Software 22, 1034-1052.

DeVantier BA, Feldman AD 1993. Review of GIS applications in hydrologic modeling. J. Water Resources Planning and Management 119(2): 246-261

Diakakis M 2010. A method for flood hazard mapping based on basin morphometry: application in two catchments in Greece. Nat Hazards, DOI 10.1007/s11069-010-9592-8

Dilts TE, Yang J 2010. Riparian Topography Toolbox for ArcGIS 9.3. University of Nevada Reno. Available at: http://www.cabnr.unr.edu/weisberg/downloads

Dooge JCI 1973. Linear theory of hydrologic systems. Technical bulletin no. 1468, Agricultural Research Service, U.S. Department of Agriculture, Washington D.C.

DTec Consulting Ltd 2002. West Coast Regional Council: Natural Hazards Review. Report prepared for West Coast Regional Council by Dtec Consulting Ltd. Client Reference: 1065.136WCRC, Greymouth. 140 p.

Du J, Xie H, Hu Y, Xu Y, Xu C 2009. Development and testing of a new storm runoff routing approach based on time variant spatially distributed travel time method. Journal of Hydrology 369: 44-54.

Fang X, Cleveland TG, Garcia CA, Thompson DB, Malla R 2005. Literature review on time parameters for hydrographs: Texas Department of Transportation Research Report 0–4696–1, Lamar University, 82 p.

Federal Aviation Administration (FAA) 1970. Airport drainage. *Advisory Circular No. 150/5320-5B*, Dept. of Transportation, Washington, D.C.

Fitzharris BB, Hay JE, Jones PD 1992. Behaviour of New Zealand glaciers and atmospheric circulation changes over the past 130 years. The Holocene2, 97–106.

Folmar ND, Miller AC, Woodward DE 2007. History and development of the NRCS lag time equation. J. Am. Water Resour. Assoc., 43(3), 829–838.

Frattini P, Crosta G, Carrara A 2010. Techniques for evaluating the performance of landslide susceptibility models. Engineering Geology 111(1-4): 62-72.

Giandotti M 1934. Previsione delle piene e delle magre dei corsi d' acqua. Ministero LL.PP., Memorie e studi idrografici, Vol. 8, Rep. No. 2, Servizio Idrografico Italiano, Rome (in Italian).

Goodsell B, Anderson B, Lawson WJ, Owens IF 2005. Outburst flooding at Franz Josef Glacier, South Westland, New Zealand', New Zealand Journal of Geology and Geophysics, 48: 1, 95-104

Green IRA, Stephenson D 1986. Criteria for comparison of single event models. Hydrological Sciences Journal 31 (3), 395-411.

Griffiths GA 1980. Hydraulic geometry relationships of some New Zealand gravel bed rivers. J. Hydrol. (NZ), 19(2): 106–118.

Griffiths GA, McSaveney MJ 1983. Distribution of mean annual precipitation across some steepland regions of New Zealand: New Zealand Journal of Science, v. 26, p. 197–209.

Gupta A 2010.The hazardousness of high-magnitude floods. In: Geomorphological hazards and disaster prevention in (eds) I. Alcantara-Ayala and A. Goudie. Cambridge : Cambridge University Press, 2010. pp. 97-109.

Haeberli W, Hoelzle M 1995. Application of inventory data for estimating characteristics of and regional climate-change effects on mountain glaciers: a pilot study with the European Alps. Annals of Glaciology 21, 206-212.

Hancox GT, McSaveney MJ, Manville VR, Davies TRH 2005. The October 1999 Mt Adams rock avalanche and subsequent landslide dam-break flood and effects in Poerua River, Westland, New Zealand. New Zealand Journal of Geology & Geophysics 48: 683-705.

Havnø K, Madsen MN, Dørge J 1995. MIKE 11 - A generalised river modelling package, in Computer Models of Watershed Hydrology, Singh, V.P., Ed., Water Resources Publications, Colorado, USA, 1995, p809-846.

Henderson RD, Thompson SM 1999. Extreme rainfalls in the Southern Alps of New Zealand. Journal of Hydrology (New Zealand) 38: 309-330.

Henderson RD, Ibbitt RP, Duncan MJ 1999. Cropp River: data to test concepts of channel network and river basin heterogeneity - data note. Journal of Hydrology (NZ) 38, 331–339.

Hewitt AE 1993. Methods and rationale of the New Zealand Soil Classification. Landcare Research Science Series 2. Lincoln, New Zealand. Manaaki Whenua Press. 71p.

Hock R 1999. A distributed temperature-index ice- and snowmelt model including potential direct solar radiation. J. Glaciol. 45 (149), 101–111.

Hovius N, Stark CP, Allen PA 1997. Sediment flux from a mountain belt derived from landslide mapping. Geology 25, 231– 234.

Ibbitt RP 1997. Evaluation of optimal channel network and river basin heterogeneity concepts using measured flow and channel properties. Journal of Hydrology 196, 119–138.

Izzard CF 1946. Hydraulics of runoff from developed surfaces. 26th Annual Meetings of the Highway Research Board. Vol. 26. pp. 129-146.

Jansson P, Hock R, Schneider T 2003. The concept of glacier storage: a review. Journal of Hydrology 282, 116–129

Jin C 1992. A deterministic gamma-type geomorphologic instantaneous unit hydrograph based on path types. Water Resour. Res., 28, 2, 479–486.

Jowett IG 1998. Hydraulic geometry of New Zealand Rivers and its use as a preliminary method of habitat assessment. *Regulated Rivers: Research and Management*, 14, 451-466.

Kerby WS 1959. Time of concentration for overland flow. *Civil Engineering*. 29(3), pp. 174.

Kilgore JL 1997. Developent and evauation of a GIS-based spatially distributed unit hydrograph model. Unpublished MSc thesis in Biological Systems Engineering, Faculty of Virginia Polytechnic Institute, State University

Kirpich ZP 1940. Time of concentration of small agricultural watersheds. *Civil Engineering*. 10(6), pp. 362.

Korup O 2004b. Geomorphic implications of fault zone weakening: slope instability along the Alpine Fault, South Westland to Fiordland. *New Zealand Journal of Geology and Geophysics 47*, 257-267.

Korup O, Schmidt J, McSaveney MJ 2005. Regional relief characteristics and denudation pattern of the western Southern Alps, New Zealand. Geomorphology 71, 402-423.

Korup O 2005b. Geomorphic hazard assessment of landslide dams in South Westland, New Zealand – fundamental problems and approaches. Geomorphology 66, 167-188.(doi:10.1016/j.geomorph.2004.09.013)

Korup O 2005c. Large landslides and their effect on alpine sediment flux: South Westland, New Zealand. Earth Surface Processes and Landforms 30, 305-323.

Korup O, Tweed F 2007. Ice, moraine, and landslide dams in mountainous terrain. Quaternary Science Reviews 26, 3406–3422

Krause P, Boyle DP, Bäse F 2005. Comparison of different efficiency criteria for hydrological model assessment. In: Krause, P., Bongartz, K., Flügel, W.-A. (Eds.), Proceedings of the 8th Workshop for Large Scale Hydrological Modelling-Oppurg 2004. Advances in Geosciences, vol. 5, pp. 89-97.

Kull DW, Feldman AD 1998. Evolution of Clarks unit graph method to spatially distributed runoff. J. Hydrol. Eng., 3(1), 9–19.

Lastra J, Fernadez E, Diez-Herrero A, Marquinez J 2008. Flood hazard delineation combining geomorphological and hydrological methods: an example in the Northern Iberian Peninsula. Nat Hazards 45:277–293.

Lawson DE 1993. Glaciohydrologic and glaciohydraulic effects on runoff and sediment yield in glacierized basins, Monogr. 93 – 2, 123 pp., US Army Corps of Eng., Cold Regions Res. and Eng Lab., Hanover, N.H., 1993.

Leathwick JR, Wilson G, Stephens RTT 2002. Climate Surfaces for New Zealand. Landcare Research Contract Report: LC9798/126.

Lee KT, Yen BC 1997. Hydrograph derivation. J. Hydraul. Eng., 123 (1), 73–80.

Leopold LB, Maddock T 1953. The hydraulic geometry of stream channels and some physiographic implications. U.S. Geological Survey Professional Paper 252, 56 p.

Lin Y, Wei X 2008. The impact of large-scale forest harvesting on hydrology in the Willow watershed of Central British Columbia. J. Hydrol. 359, 141–149.

Liu YB, De Smedt F 2005. Flood Modeling for Complex Terrain Using GIS and Remote Sensed Information. Water Resources Management 19, 605–624.

Mahe G, Paturela JE, Servatb E, Conwayc D, Dezetter A 2004. The impact of land use change on soil water holding capacity and river flow modelling in the Nakambe River, Burkina-Faso. J. Hydrol. 300, 33–43.

Maidment DR 1993a. GIS and hydrologic modeling. In Environmental Modeling with GIS. eds. M. F. Goodchild, B. O. Parks, L. Steyaert, New York: Oxford University Press.

Maidment DR 1993b. Developing a spatially distributed unit hydrograph by using GIS. In HydroGIS 93: Application of Geographic Information Systems in Hydrology and Water Resources, Proceedings of the Vienna Conference, eds. K. Dovar and H. P. Natchnebel, 181 - 192. Vienna: Int. Assoc. of Hydrological Sci. Publ. no 211.

Maidment DR, Olivera F, Calver A, Eatherall A, Fraczek W 1996. Unit hydrograph derived from a spatially distributed velocity field. Hydrological Processes 10: 831-844.

Martinez V, Garcia AI, Ayuga F 2002. Distributed routing techniques developed on GIS for generating synthetic unit hydrograph. Trans ASAE 45(6):1825–1834.

Martz LW, Garbrecht J 1992. Numerical Definition of Drainage Network and Subcatch-ment Areas from Digital Elevation Models. Computers and Geosciences, 18(6):747-761.

McCuen RH 1998. Hydrologic Analysis and Design. 2nd edition, Prentice-Hall, Inc. 814 p.

McDonnell RA 1996. Including the spatial dimension: Using geographical information systems in hydrology. Progress in Physical Geography, 20, 159-177.

McKerchar AI, Pearson CP 1989. Flood frequency in New Zealand. Hydrology Centre, Christchurch, Publ. No. 20, Division of Water Sciences, Department of Scientific and Industrial Research, Christchurch, NZ, 87 p.

McKerchar AI, Ibbitt RP, Brown SLR, Duncan MJ 1998. Data for Ashley River to test channel network and river basin heterogeneity concepts. Water Resources Research 34, 139–142.

McSaveney MJ, Davies TR 1998. Natural Hazard Assessment for the township of Franz Josef Glacier and its Environs. Client Report 43714B.10, Institute of Geological and Nuclear Sciences, Lower Hutt, 58 p.

Melesse AM, Graham WD 2004. Storm runoff prediction based on a spatially distributed travel time method utilizing remote sensing and GIS. *Journal of American Water Resources Association* 40(4): 863-879.

Ministry for the Environment (MfE) 2004. New Zealand Land Cover Database 2 (LCDB2).

Mockus V 1961. Watershed lag. U.S. Dept. of Agriculture, Soil Conservation Service, ES–1015, Washington, DC.

Molnar P, Ramirez JA 1998, Energy dissipation theories and optimal channel characteristics of river networks, Water Resour. Res. 34, 1809–1818.

Moore RD 1991. A numerical simulation of supraglacial heat advection and its influence on ice melt. Journal of Glaciology, Vol. 37, No. 126.

Moore ID 1996. Hydrologic modeling and GIS. In M. F. Goodchild, B. O. Parks, & L. T. Steyaert (Eds.), GIS and environmental modeling: Progress and research issues (pp. 143-148). Fort Collins, CO: GIS World Books.

Morgali JR, Linsley RK 1965. Computer analysis of overland flow. *Journal of Hydraulics Division.* (HY3).

Muzik I 1995. GIS derived distributed unit hydrograph, a new tool for flood modeling. In *Developments in Computer Aided Design and Modeling for Civil Engineering*, ed. B. H. V. Topping, 243-247. Edinburgh, UK: Civil-Comp Press.

Muzik I 1996. Flooding modelling with GIS-derived distributed unit hydrographs. *Hydrological Processes* 10: 1401-1409.

Nash JE, Sutcliffe JV 1970. River flow forecasting through conceptual models 1: a discussion of principles. Journal of Hydrology 10 (3), 282-290.

Natural Resources Conservation Service (NRCS) 2004a. National Engineering Handbook, Part 630, Chapter 9, Hydrologic Soil-Cover Complexes, U.S. Department of Agriculture, Washington, DC.

Natural Resources Conservation Service (NRCS) 2004b. National Engineering Handbook, Part 630, Chapter 10, Estimation of direct runoff from storm rainfall, U.S. Department of Agriculture, Washington, DC.

Natural Resources Conservation Service (NRCS) 2007. National Engineering Handbook, Part 630, Chapter 7, Hydrologic Soil Groups, U.S. Department of Agriculture, Washington, DC.

Natural Resources Conservation Service (NRCS) 2010. National Engineering Handbook, Part 630, Chapter 15, Time of Concentration, U.S. Department of Agriculture, Washington, DC.

Nienow P, Hubbard B 2005. Surface and Englacial Drainage of Glaciers and Ice Sheets. Encyclopedia of Hydrological Sciences. Ed. Malcolm G. Anderson and Jeffrey J. McDonnell. Vol. 4: Parts 12-14. West Sussex, England: Wiley, 2005. [2575]-2586. Gale Virtual Reference Library. Web. 8 Apr. 2012.

Noto LV, Loggia GL 2007. Derivation of a distributed unit hydrograph integrating GIS and remote sensing. Journal of Hydrologic Engineering 12(6): 639-650.

Olivera F, Maidment D 1999. Geographic information systems GIS-based spatially distributed model for runoff routing. Water Resour. Res., 35(4), 1135–1164.

Ponce VM, Hawkins RH 1996. Runoff Curve Number: Has it Reached Maturity? Journal of Hydrologic Engineering, Vol. 1, No.1, 11-19.

Ramírez JA 2000. Prediction and Modeling of Flood Hydrology and Hydraulics. Chapter 11 of Inland Flood Hazards: Human, Riparian and Aquatic Communities Eds. Ellen Wohl; Cambridge University Press.

Remondo J, Gonzalez A, De Teran JRD, Cendrero A, Fabbri A, Chung CJF 2003. Validation of landslide susceptibility maps; Examples and applications from a case study in northern Spain. Natural Hazards, 30(3), 437-449.

Rennó CD, Nobre AD, Cuartas LA, Soares JV, Hodnett MG, Tomasella J, Waterloo M 2008. HAND, a new terrain descriptor using SRTM-DEM; mapping terra-firme rainforest environments in Amazonia. Remote Sensing of Environment 112, 3469–3481.

Rodriguez-Iturbe I, Valdes JB 1979. The geomorphological structure of hydrologic response. Water Resources Res. 15(6):1409-1420.

Ross CN 1921. The calculation of flood discharges by the use of a time contour plan, Transactions of the Institution of Engineers Australia, 2:85-92.

Saghafian B, Julien PY 1995. Time to equilibrium for spatially variable watersheds. J. Hydrol., 172, 231–245.

Saghafian B, van Lieshout AM, Rajaei HM 2000. Distributed catchment simulation using a raster GIS. International Journal of Applied Earth Observation and Geoinformation 2(3-4): 199-203.

Saghafian B, Julien PY, Rajaei H 2002. Runoff hydrograph simulation based on time variable isochrone technique. *Journal of Hydrology* 261: 193-203.

Safiri S, Hosseini SM 2011. Methodology for Identifying the Best Equations for Estimating the Time of Concentration of Watersheds in a Particular Region. Journal of Irrigation and Drainage Engineering, Vol. 137, No. 11. 712-719.

Scharffenberg WA, Fleming MJ, and Hydrologic Engineering Center (U.S.) 2006. Hydrologic modeling system HEC-HMS : user's manual, US Army Corps of Engineers Hydrologic Engineering Center, Davis, CA.

Sherman LK 1932. Streamflow from rainfall by the unit-graph method. Eng. News Record 108:501-505.

Simas MJ, Hawkins RH. 2002. Lag time characteristics in small watersheds in the United States. Proceeding of the Second Federal Interagency Hydrologic Modeling Conference, Las Vegas, Nevada.

Snyder FF 1938. Synthetic unit-graphs: Transactions, American Geophysical Union, vol. 19, p. 447-454.

Soil Conservation Service (SCS, currently Natural Resource Conservation Service -NRCS), 1972. National Engineering Handbook, Section 4, Hydrology. U.S. Department of Agriculture, Washington, D.C.

Soil Conservation Service (SCS, currently Natural Resource Conservation Service –NRCS) 1975. Computer program for project formulation. Hydrology. Technical Release 20, U.S. Department of Agriculture, Washington, D.C

Soil Conservation Service (SCS, currently Natural Resource Conservation Service -NRCS) 1986. Urban hydrology for small watersheds. Technical Release 55, U.S. Department of Agriculture, Washington, D.C.

Sriwongsitanon N, Taesombat W 2011. Effects of land cover on runoff coefficient. Journal of Hydrology 410: 226–238.

Strahler AN 1957. Quantitative analysis of watershed geomorphology. Trans. Amer. Geophys. Un. 38,913-920.

Subramanya K 1984. Engineering Hydrology. 2nd edition, Tata McGraw-Hill, 391 p.

Sui DZ, Maggio RC 1999. Integrating GIS with hydrological modeling: practices, problems, and prospects. Computers, Environment and Urban Systems 23, 33-51.

United States Army Corps of Engineers (USACE) 1954. Data report, airfield drainage investigation. *Rep. Prepared for Los Angeles District for the Office of the Chief of Engineers*, Washington, D.C.

U.S. Army Corps of Engineers (USACE) 2001. HEC-HMS hydrologic modeling system. User's manual Version 2.2.1.

U.S. Army Corps of Engineers (USACE) 2008. Hydrologic Engineering Centers River Analysis System (HEC-RAS) software, United States Army Corps of Engineers. Available at: http://www.hec.usace.army.mil/software/hec-ras/

Van Westen CJ, Rengers N, Soeters, R. 2003. Use of geomorphological information in indirect landslide susceptibility assessment. Natural Hazards, 30(3), 399-419.

Welle PJ, Woodward DE. 1986. Time of concentration. Hydrology, Technical Note No. N4. U.S. Department of Agriculture, Soil Conservation Service, NENTC, Chester, PA.

West Coast Regional Council (WCRC) 2010. Report on West Coast Weather Event 27 & 28 December 2010. 43p.

WL/Delft Hydraulics 2008. SOBEK-Rural: Hydrodynamics

Wohl EE, Wilcox A 2005. Channel geometry of mountain streams in New Zealand. Journal of Hydrology 300, 252–266.

Wong TSW 2005. Assessment of Time of Concentration Formulas for Overland Flow. Journal of Irrigation and Drainage Engineering, Vol. 131, No. 4, pp. 383–387.

Zadeh LA 1965. Fuzzy sets. Information and control, 8:338:353.

Zerger A, Wealands S 2004. Beyond Modelling: Linking Models with GIS for Flood Risk Management. Natural Hazards 33: 191–208, 2004.

Chapter 5: Regional multi-hazard analysis

5.1 Introduction

Increased demand for land development as a result of on-going population growth and urbanization increasingly forces people to occupy environments where natural processes intensely affect the landscape, by way of potentially hazardous natural events. Plate boundaries, active volcanic regions and rapidly uplifting mountain ranges are examples of areas threatened by geomorphic hazards that have hosted entire civilizations for centuries (with occasional catastrophes) and today accommodate some of the world's largest cities. These areas are often affected by more than one hazard such as volcanic eruptions, earthquakes, landslides, tsunamis, floods, storms and wildfires which frequently interact with each other increasing the total impact on communities. Disaster losses however are the result of interaction among the earth's physical system with human and constructed systems (Mileti 1999). Therefore, over the past few decades fatalities and economic losses due to natural catastrophic events have substantially increased, not only a direct result of the growth of population density in hazard-prone areas, but also due to the consequent increase of possible cascade effects that derive from the interactions between various natural and human systems (Marzocchi et al. 2009). Recent disasters such as the 2011 Tohoku earthquake in Japan, as well as causing significant economic losses, highlight the interplay among different natural and technological hazards, causing catastrophic cascading effects, with severe consequences to communities and the environment (Dunbar et al. 2011). Cascading hazards in highly dynamic environments (e.g. tectonically active mountains) are also generated from the interactions between tectonic, climatic and surface processes. The 2008 Wenchuan earthquake, China, induced an unprecedented number of co- and post-seismic geomorphic hazards. Among other factors the combination of strong, long duration ground shaking and steep topography generated tens of thousands co-seismic landslides blocking rivers and inducing consequent dam-break floods (Huang & Fan 2013).

Independent assessments of multiple single processes might lead to an underestimation of the total risk in highly dynamic landscapes, as the possible interactions between hazards, and their cascade effects, are often neglected (Bell & Glade 2004; Marzocchi et al. 2012). Therefore meaningful hazard assessment and effective mitigation in these environments require approaches incorporating the interrelationships between different processes and accounting for all the possible consequent events. Although well-established hazard and risk analysis methods exist for many natural processes, their combined analysis under a common framework still poses a variety of challenges and

limitations (Kappes et al. 2010). These limitations derive mainly from the diverse characteristics of the single processes such as magnitude, intensity, duration, extent, recurrence interval and impacts, as well as from the different existing procedures used to model each hazard and the different units to quantify them, which further complicate multi-hazard analyses (Kappes et al. 2010; Marzocchi et al. 2009, 2012). Additionally, since data requirements are very demanding for modelling multiple processes compared to single process analysis, communities often lack the technology, expertise and time to perform multi-hazard assessment due to resource constraints (Tate et al. 2011). Comprehensive multi-risk analysis is a widely interdisciplinary field, where specialists investigating different types of natural and technological hazards need to closely collaborate with stakeholders in order to understand the long-term co-evolution of the natural, human and constructed systems, the various hazard triggering mechanisms and their cascade effects. However, communication barriers due to different terminologies often make the dissemination of knowledge very difficult and impede the simultaneous investigation of multiple-processes.

Therefore, a holistic approach to natural hazard and risk research is required, which includes determining interactions between hazards, and understanding cascade effects as well as incorporating comparable hazard and risk analysis methods for different potentially damaging phenomena. These are essential prerequisites for reducing risk in highly dynamic environments and require not only innovative modelling tools but also close co-operation between different disciplines of the hazards research field. Considering the above challenges this study develops an approach for integrated analysis of different geomorphic processes in an effort to establish the basic principles for multi-hazard and -risk assessment in highly dynamic environments such as tectonically active mountains.

5.1.1 Multi-hazard analyses

A generally accepted definition of the term “multi-hazard” has yet to be determined in the academic literature. As a result the term has different meanings according to the purpose of the study in which it is used. Most commonly multi-hazard is perceived as referring to different independent hazards affecting a given (common) area, whereas another interpretation considers multi-hazard as the various hazards affecting a given area taking into account all possible interactions and/or cascade effects between them (Garcia-Aristizabal & Marzocchi 2011). No common terminology exists to describe the relations between hazards. For instance some authors refer to these relations as interactions (Kappes et al. 2010; Selva 2013) while others describe them as cascades (Carpignano et al. 2009). Other commonly used terms are domino effects (Delmonaco et al. 2006), compound hazards (Alexander 2001) and coupled events (Marzocchi et al. 2009; Van Westen et al. 2014).

Multi- hazard and risk analyses generally aim at the consideration of multiple hazards in a specified administrative or geographical unit. According to the two different interpretations mentioned above, the focus of a multi-hazard assessment can be on identifying multiple independent hazards in a given area, or on incorporating their interactions and/or their potential cascade effects. Several different approaches and initiatives to integrate independent hazard assessment processes in a multi-hazard/risk framework have been proposed. A comparative assessment of the existing approaches is beyond of the scope of this study, however a brief review of some important initiatives and projects sheds light on the current state of multi-hazard/risk assessment and highlights advances and limitations to date. Comprehensive reviews and comparison of existing methodologies can be found in Delmonaco et al. (2006) and Garcia-Aristizabal & Marzocchi (2011).

A well-known initiative on multi-hazard assessment is the "Multi-hazard identification and risk assessment" of the Federal Emergency Management Agency in U.S (FEMA 1997). The initiative is based on the loss estimation tool HAZUS developed by FEMA in collaboration with the National Institute of Building Sciences (NIBS). First released in 1997, HAZUS is a software compatible with ArcGIS, focusing primarily on estimating earthquake losses and more recently extended to multi-hazard losses (incorporating models for floods and hurricane winds: FEMA 2004). Secondary effects from earthquakes, floods and hurricanes (e.g. debris generation and fires following an earthquake) are also considered, however the losses from individual hazards are analyzed separately.

The Integrated Geological Risk Assessment project (TIGRA) (Del Monaco et al. 1999) is an approach considering climate-related (e.g. floods, landslides, coastal erosion) and geophysical hazards (e.g. earthquakes, volcanic eruptions), the state of human system (exposure and related vulnerability), and their mutual relationships, as well as potential mitigation strategies. The aim of the project was to homogenise the existing methodologies on individual natural events within a unified approach. A specific summary of the assessment methodology for any type of hazard has been provided, demonstrating how different natural phenomena may be constrained in a process grid. The assessment of each process is divided into specific steps such as identifying the event typology (hazard characteristics), the input information (e.g. scale, data inventory, predisposing areas, triggering events, long term evaluation, monitoring and geo-indicators), the modelling procedure, and the type of assessment. An interesting finding was that it is not possible to define a multi-hazard approach simply by overlapping the individual hazard procedures, however it is possible to define a multi-hazard risk assessment by means of economic indexes reporting the expected economic losses resulting from each individual procedure applied to single hazards.

The European Multi-Hazard Risk Assessment Project (TEMRAP) (European Commission 2000) has been focused to underline a common strategy among different natural hazards based on a comprehensive investigation on the environment and human structures in order to define the most suitable mitigation strategy. It is stated that the most reliable models (for multi-hazards) can be implemented for climate-related hazards (i.e. floods, landslides, strong winds), whereas 'geophysical' hazards need to be investigated individually. The primary step of the proposed methodology is related to the definition of hazard, that is the event probability (at a local scale) or susceptibility (at a regional scale), by associating magnitude (or intensity) with probability. The output is the probability of occurrence of certain events over time or the susceptibility that an area may be affected by a specific natural event. However, all hazards are discussed separately, even following the same chain of events. According to the project's findings, multi-hazard analysis is possible only for disasters triggered by common factors and multi-hazard mapping is heavily constrained by typical dimensions of the natural event, data availability and format, methods of analysis and scales of representation.

Within the framework of the ESPON Hazards project (Schmith-Thomé 2005) a method to create an integrated map showing the spatial patterns of natural and technological hazards in Europe was developed. The aim was to use existing results of hazard research and combine them in such a way that the obtained information is comparable over the European Union countries. However, not all hazards are equally relevant for the entire region, as the importance of hazards and risk differ spatially, therefore a weighting system, the Delphi method, was applied to derive an integrated map of aggregated hazards in Europe hazard. An important result of the ESPON Hazards project is the development of a typology of regions In Europe that clusters areas threatened by similar hazards in space and time.

The research project ARMONIA (Applied multi Risk Mapping of Natural Hazards for Impact Assessment), funded by the European Union as a part of the Sixth EU Framework Programme for Research and Technological Development, aims to develop a new approach to producing integrated multi- risk maps in order to achieve more effective spatial planning procedures in areas prone to natural disasters in Europe (Delmonaco et al. 2006). Amongst other things, the output of the ARMONIA project was to harmonise the methodologies for hazard and risk assessment for different types of potentially disastrous events and the different processes of risk mapping in order to standardise data collection, data analysis, monitoring, outputs and terminology in a form useful to end users.

The Central American Probabilistic Risk Assessment (CAPRA) is an ongoing initiative that aims to develop an online open platform for disaster risk assessment based on Geographic Information Systems, which would allow users from the Central American countries to analyze the risk in their areas, and be able to take informed decisions on disaster risk reduction (CAPRA 2013). The approach focuses on the development of probabilistic hazard assessment modules, for different types of hazards such as earthquakes, hurricanes, extreme rainfall, and volcanic hazards as well as consequent hazards such as flooding, windstorms, landslides and tsunamis. The hazard analysis is based on the frequencies and magnitudes of historical events. The output is then combined with elements-at-risk with particular focus on buildings and population. Under the CAPRA project a software tool (CAPRA-GIS) for probabilistic risk calculations is developed.

In New Zealand, RiskScape is a regional multi-hazard tool, currently in a development phase, that models potential losses from climate- and geological-driven hazards aiming to support decision-making for the management of natural hazard events (Reese et al. 2007; Schmidt et al. 2011). RiskScape is built on three main modules, 1) the inventories of all assets that may be impacted by a hazard, 2) hazard models and 3) the fragility / loss module; and runs through a sequence of steps, from hazards and exposure through to vulnerability and potential losses, before determining risk. However, the system does not allow modelling the interaction between multiple hazards and assets in a risk scenario. If a scenario with multiple hazards occurs, the relative impact of each hazard on the asset needs to be considered separately.

Although a growing number of studies separately investigate various types of hazards in mountainous areas, using diverse methods and at different scales (Wilford et al. 2004; Korup 2005; Remondo et al. 2005, 2008; Gude & Barsch 2005; Arnaud-Fassetta et al. 2005; Luino 2005), relatively few studies attempt to evaluate hazard and risk from multiple hazards while looking into their interactions (Van Westen et al. 2002; Bell & Glade 2004; Kappes et al. 2012; Van Westen et al. 2014). MultiRisk is a GIS-based software for multi-hazard risk analyses developed in the framework of the Mountain Risks project (Kappes et al. 2012). It is designed to allow the combined examination of multiple mountain hazards (e.g. debris flows, rock falls, shallow landslides, avalanches and river floods) according to a top-down concept (a first simple and fast analysis at a small scale provides an approximation, followed by a more detailed analysis at a larger scale). Currently, the MultiRisk platform allows only for regional scale analyses using relatively simple empirical models with low data requirements.

In spite of their apparent different approaches, all the above projects highlight the need for bringing together and linking diverse hazard assessment methodologies. This task involves many disciplines,

collaboration and sharing of knowledge, data and findings. Therefore it is crucial to develop a common framework to improve the communication between scientists with different backgrounds and practitioners/decision makers. In an effort to address some of the critical challenges of multi-hazard analysis illustrated by international initiatives and projects, an approach for multi-hazard and risk assessment suitable for highly dynamic environments is developed and applied in the western Southern Alps of New Zealand. The proposed approach aims to provide a conceptual framework for comprehensive multi-hazard/risk assessment and the means to communicate the complexity of multi-hazard assessment to non-experts, decision makers, emergency managers and other stakeholders.

5.2 Methodology

Perceiving the geomorphic processes shaping the western Southern Alps as interrelated components that compose a broader "hazardscape", the implementation of a systems approach was considered appropriate in order to link the various components and identify interactions between them. The proposed framework follows the concept of systems theory. Systems theory was originally introduced by the biologist Ludwig von Bertalanffy in 1940s, who illustrated that the behaviour of a system is not defined only by the individual functions of its isolated components, but the relationships between these components have also to be considered (von Bertalanffy 1968). Systems theory is closely related to cybernetics (Wiener 1954; Ashby 1956), an interdisciplinary approach examining the system organization and feedback relationships between its components, as well as system dynamics (Forester 1961, 1969), an approach focusing on understanding the behaviour of complex systems over time employing feedback loops and time delays to model the interactions between the various components.

Although the concept of systems has been widely recognized in almost all fields of science (physical, social, engineering etc.), a commonly accepted definition for the term "system" doesn't exist. Laszlo & Krippner (1988) define a system "as a complex of interacting components, together with the relationships between them, which permits the identification of a boundary-maintaining entity or process" (p. 51), while Kim (1994) views a system as a group of interacting, interrelated, or interdependent elements forming a complex whole which is almost always defined with respect to a specific purpose. The essential idea, however, common in the various definitions, is that systems are complex with their many interrelated components embedded in a larger context.

Hazard modelling focuses on developing reliable methods to predict the behaviour of natural processes (e.g. climatic, tectonic, surface) with potentially adverse effects on human systems in both

space and time. The inherent complexity of systems often inhibits some forms of predictability and limits the range of forecasts, however Phillips (2003), investigating the sources of nonlinearity and complexity in geomorphic systems, argued that analysis of the nonlinear complexities in geomorphic (or other systems) may enhance some modes of understanding and predictability. Therefore it is clear that understanding the complexity of geomorphic systems and being able to predict their behaviour, focusing on the ways that the various components interact, is a priority.

In the field of hazard and disaster management, the idea of "systems" has been used with particular emphasis on three main system types involved in disasters: natural (Buchanan 1996; Kanaori 1997; Li & Simonovic 2002), infrastructure (Ambrose & Vergun 1995; Schiff 1995) and social systems (Drabek 1986). Other aspects of disaster management approached through systems perspective are the stages of disaster (Gillespie & Banerjee 1993), emergency management planning systems (Patterson & Boehm 1992), emergency response systems (Comfort 1994), early warning systems (Schmeidl & Jenkins 1998), information systems (Clinton et al. 1995), health care systems (Axelrod et al. 1994), decision support systems (Wallace & De Balogh 1985), public policy systems (Platt 1999), hazard mitigation (Mileti 1999) and designing safe social systems (Gillespie et al. 2004).

The approach developed herein is composed of seven stages. The results from each stage are used as input for the next; therefore caution is required with respect to the propagation of uncertainties through the stages to the final output. An effort has been made to create a relatively simple procedure to analyse a highly complex phenomenon that can be applied at various scales. The main stages of the proposed multi-hazard framework are shown in the following scheme (Fig. 5.1). Each stage is separately discussed below with examples from the WSA.

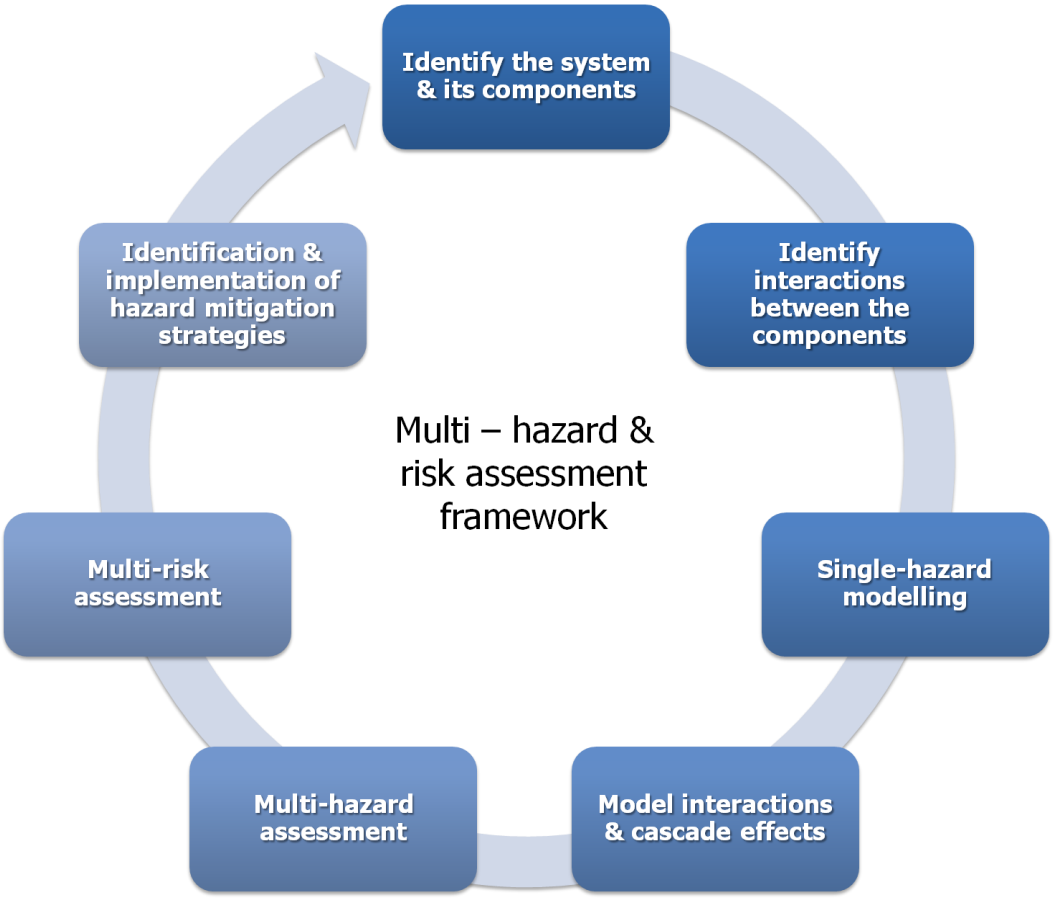

Figure 5.1 The seven consecutive stages of the multi-hazard & risk assessment framework. The circular arrow denotes that the procedure is iterative. Integration of mitigation measures into the system and re-evaluating the response of the other components is essential to ensure that the new processes or interactions introduced to the system will not increase the total risk.

5.2.1 Identify the system and its components

The fundamental step of the proposed framework includes the identification of the geomorphic system and its various components (sub-systems). Systems, in general, are characterized as closed or open. Closed systems are those which possess clearly defined closed boundaries, across which no transfer of materials or energy occurs (Von Bertalanffy 1951). This view of systems immediately excludes a large number, perhaps all, natural systems, and particularly geomorphic systems (Chorley 1962). Conversely, an open system requires an energy supply for its maintenance and preservation (Reiner & Spiegelman 1945), and is in effect maintained by a constant supply and removal of material and energy (Von Bertalanffy 1952, p. 125).

Determining the system's boundaries is the first critical task that essentially defines the complexity of the model, the number of processes involved, data requirements, time and expertise needed. The mountainous landscape of WSA is an open geomorphic system that exchanges material and energy

with its surrounding environment and constantly interacts with other systems. Although the concept of boundaries clearly contradicts with the definition of an open system, for modelling purposes it is often necessary to define hypothetical boundaries and assume that the system does not interact or has limited interaction with other systems outside of these boundaries.

In WSA the main divide and the coast can be used as hypothetical geomorphic boundaries, outside of which there is only limited interaction with other systems (Fig. 5.2). For example, a tsunami generated by a large offshore earthquake, or volcanic ash from a major volcanic eruption from the Taupo Volcanic Zone (New Zealand) that can potentially affect the region and trigger other processes are not considered in the modelling procedure. However, weather systems and other climatic factors (solar radiation, temperature), tectonic plate movement, water and sediment transport from the mountains to the nearby ocean are vital interactions for the system's function and cannot be excluded. The boundaries can be also defined using specific processes (e.g. seismicity, landslides and floods), assuming that interactions are taking place only between them and their triggering processes (e.g. tectonics, climate) and they are not influenced by other processes.

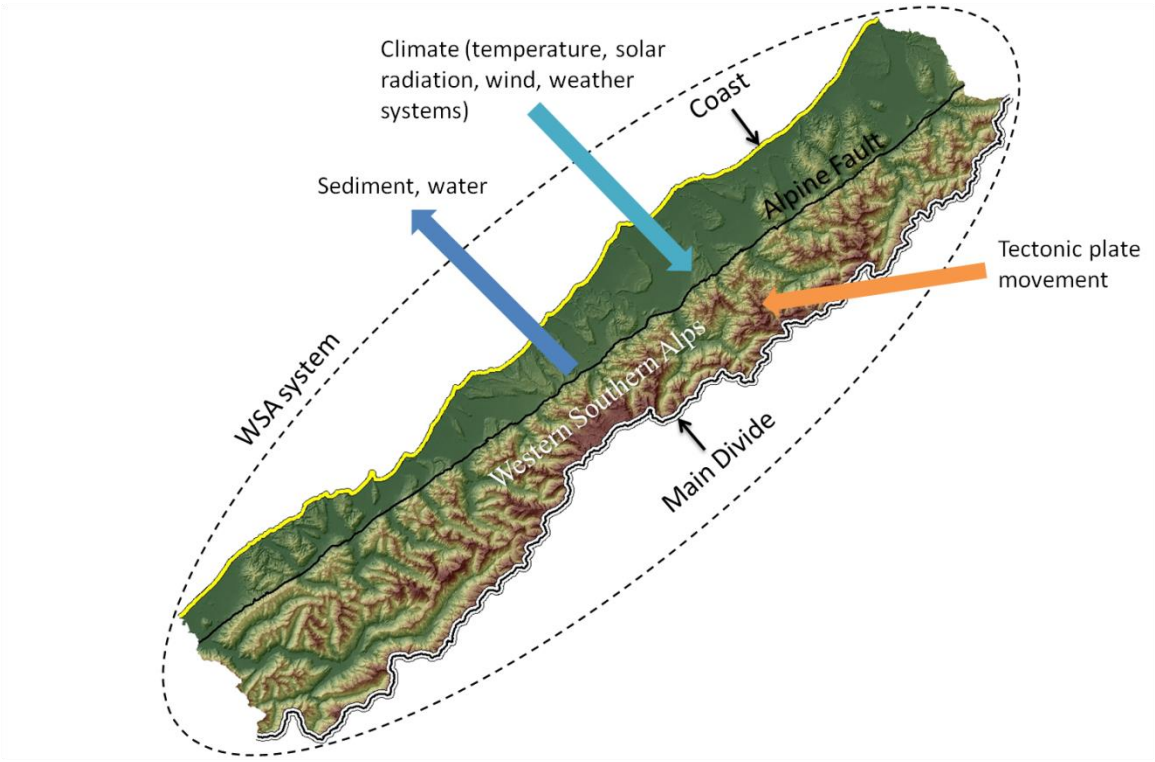

Figure 5.2 Hypothetical geomorphic boundaries of the WSA system outside of which it is assumed that there is only limited interaction with other systems.

Following the identification of the system and its boundaries the next important task at this stage is to determine its various components. These are essentially the geomorphic processes/potential hazards that compose the hazardscape being studied. Debris flows, tectonics (aseismic uplift and

earthquakes), precipitation, rock avalanches, rockfalls, sediment cascades, glacial debutressing are all common components of mountain systems. These processes are effectively sub-systems composed by other components - and so on. Therefore according to scale of the study the level of detail must be determined in order to avoid over-parameterization and associated uncertainties. It is important to note that all system models, even the most realistic ones, are only representations of reality, including only the most important elements that describe the phenomenon of interest, especially if it is a complex one. A degree of simplification inherent in modelling, however, is necessary in order to identify the core of a complex problem and understand it (Waddington 1977). Thus, a good balance between realism and simplicity focusing on the most essential parameters and relationships is the ultimate goal of an effective modelling approach. The contribution of geomorphology at this stage is invaluable as it provides the means to identify tectonic, climate and surface processes driving the landscape evolution of dynamic environments, and their various interactions, and ultimately defines the geomorphic system (Shroder & Bishop 2004).

5.2.2 Identify interactions

The second critical step is to identify how the previously determined processes/hazards interact. Van Westen et al. (2014) identify three main relationships between hazards. First, different hazard types are triggered by the same triggering event (coupled events). The temporal probability of occurrence of such coupled events is the same, as it is linked to the probability of occurrence of the triggering mechanism. A second type of interrelation is the influence one hazard exerts on the disposition of a second peril, though without triggering it (Kappes et al. 2010). This implies that as long as no direct triggering between hazards or temporally simultaneous occurrence exists, one process may alter the disposition of another towards a potential trigger event. The third type of hazard relationships consists of those that occur in chains (one hazard triggers the next).

In this study five interaction types are indentified based on regional geomorphic analysis in WSA carried out in the context of this project (Chapter 2) and previous research on interrelated geomorphic processes and hazards (Zarn & Davies 1994; DTec 2002; McSaveney & Davies 1998; Korup 2005; Davies & McSaveney 2006; McCahon et al. 2006; Welsh & Davies 2011; Robinson & Davies 2013) in the region. The interactions are classified into the following five types:

Spatial coincidence

This is the most simple interaction type where different types of hazards occur in the same area. A cause-effect relationship or common trigger is not necessary. For example, a coastal region can be subject to coastal hazards (e.g. shoreline erosion) and volcanism or windstorms and earthquakes.

These processes can spatially overlap without significantly interacting; in this case multi-hazard assessment can be performed by combining the results from single-process analyses.

Temporal coincidence (common trigger)

According to this interaction type various processes occur at the same time. This often occurs when the processes have a common trigger. In WSA heavy rainfall often triggers shallow landslides/debris flows and flooding (river and flash floods). Temporal coincidence generally increases the probability of spatial overlapping between processes. Thus, two hazards triggered by the same process frequently overlap in space and time (spatio-temporal coincidence).

Amplification of magnitude or intensity

The spatio-temporal coincidence of processes, not necessarily resulting from the same process, may increase their magnitude or intensity resulting in greater impact. This interaction type corresponds to the worst case scenario, where the occurrence of a process amplifies another. For example, during heavy rainfall on a catchment a landslide dam-break flood occurs which significantly increases the already high runoff, amplifying the flood magnitude.

Susceptibility change during consecutive hazards

Following the definition of landslide susceptibility by Brabb (1984), as the likelihood of a landslide occurring in an area on the basis of local terrain conditions, we view susceptibility as the proneness of an area to a process due to specific factors, without implying the time frame within which the process might occur or its magnitude. It is common during a geomorphic event for one or more conditioning factors to be altered, changing the area's susceptibility towards another process without directly triggering it.

De Graff et al. (2007) mention the fire-flood chain of hazards which describes the relation of forest fires and subsequent floods and debris flows due to the loss of vegetation, rapid runoff and increased sediment washout. In New Zealand after the 2011 Christchurch earthquake, as a result of extensive lateral spreading that affected the geometry of stream channels, there was increased flood hazard in areas close to these rivers. This occurred as smaller amount of water that hitherto was required to induce flooding due to higher river bed and narrower channel width. Another example of this interaction type involving man-made structures is the damage to buildings during an earthquake which may increase their susceptibility to subsequent hazards (e.g. aftershocks, windstorms or tsunamis).

Cascade effect (dependent probability)

Albeit with different terminologies (cascade, domino or coupled events), a growing number of studies examine the case where one hazard triggers another (Delmonaco et al. 2006; De Pippo et al. 2008; Marzocchi et al. 2009; Carpignano et al. 2009; Kappes et al. 2010, 2012; Van Westen 2010; Selva 2013). The triggering may be direct (earthquake-rock avalanche) or have a delay (earthquake-river aggradation) but the processes are directly linked or related through other intermediate processes. The main characteristic of this type of interaction is that the trigger is the result of the preceding hazard. The most prominent example of cascading hazards in mountains is the earthquake triggered landslides (Miles & Keefer 2009) and subsequent landslide dams dam break floods and river aggradation (Davies 2002; Davies et al. 2007; Korup 2005; Korup & Tweed 2007). An important aspect of this interaction type is that the temporal probability of each consequent hazard depends on the temporal probability of the hazard causing it. Thus, dam break and river aggradation flooding have the same or lower probability as the earthquake inducing the landslide dams and sediment input. Assuming two hazard events A and B, and that the occurrence of A depends somehow on the occurrence of B, Marzocchi et al. (2012) define the probability of occurrence of *A* as:

$$p_{(A)} = p(A|B)\, p\,(B) + \; p(A|\bar{B}) p\,(\bar{B})$$

where *p* represents the probability or a distribution of probability of A and B events and $\bar{B}$ means that the event *B* does not occur**.**

Nevertheless in real geomorphic systems it is common for two or more processes/hazards to interact in more than one of the above ways. For instance, the chain of processes that involves landslides triggered by rainfall and consequent river aggradation following a large earthquake (Tang et al. 2011) involves spatio-temporal coincidence, change of susceptibility and cascading processes.

To more easily identify, organize and present the hazard interactions we adapted the method by De Pippo et al. (2008) and Kappes et al. (2010) and used a matrix relating all the identified processes/hazards to each other (Table 5.1).

Table 5.1 Matrix for the identification of interactions between processes, relating all identified hazards with the range of identified triggers and consequent processes. According to this example flooding is the most common process triggered by all the other hazards, whereas earthquake is the hazard with the most significant consequences due to direct impact and cascade effects.

		Consequent process / hazard					
Triggering process / hazard		Earthquake	Debris flow	Rock fall / landslide	Rock avalanche	Flood	Heavy rainfall
	Earthquake	Initiate aftershock sequence	Ground shaking	Ground shaking	Ground shaking	Landslide dams and consequent dam-break	-
	Debris flow	-	-	-	-	River aggradation	-
	Rock fall / landslide	-	Increased sediment availability	-	-	Landslide dam-break	-
	Rock avalanche	Ground shaking	-	-	-	Landslide dam-break / river aggradation	-
	Flood	-	-	Slope undercutting	-	-	-
	Heavy rainfall	-	Runoff	Pore water pressure	Pore water pressure*	Runoff	-

* Co-seismically preconditioned slope failure triggered by rainfall

5.2.3 Single hazard analysis

Single process analysis and modelling is an essential pre-requisite of a comprehensive multi-hazard analysis. Each process is essentially a sub-system composed of various components and requires in-depth understanding before it's interaction with other processes is studied.

Remarkable progress has been made in hazard and risk analysis methods for many geomorphic processes. The evolution of GIS and remote sensing form means to visualize geographic information

in advanced analysis tools, as well as the availability of high-quality digital data and online sharing, have significantly contributed in the development of an increasing number of qualitative or quantitative methods to assess hazards and estimate their probabilities. Hazard assessment involves the estimation of magnitude and probability, which require accurate and reasonably complete catalogues or inventories of historical events. When this information is not available, the hazard can be represented by susceptibility, which involves the identification of locations where potentially damaging processes may occur on the basis of various controlling and triggering factors. Susceptibility models are based on statistical relationships between known geomorphic events and conditioning factors, assuming that in the future these events will be likely to occur under the conditions which led to past and present hazards. This means that historical or geomorphic records are still required indicating at least the locations and extent of previous events. In the present study the outputs from two GIS-based susceptibility models are utilized to assess the occurrence of rainfall-induced shallow landslides and river flooding. Combining two single-susceptibility assessments of spatially and temporally overlapping processes is the simplest case of multi-hazard analysis and it is used as an example to outline the steps required as well as to demonstrate the inherent challenges of a regional scale multi-hazard and risk assessment.

5.2.4 Interaction modelling

Based on the identified interaction types, this step aims to model the links between processes/hazards. Considering the common event chain in mountainous environments, where a landslide dams a river and consequent failure of the dam causes flooding downstream, the link between landsliding and dam-break river flooding requires estimating the volume, and hence the runout path and distance, of the mass movement. Therefore, delineating the runout path and distance of future slope failures combined with the drainage network will reveal all the potentially affected river reaches. Then estimating the landslide volumes and the transport capacities of stream channels will indicate the most likely landslide dam locations. In the fire-flood chain mentioned above, the link is the changed land cover after the fire that can be used to estimate the runoff. Modelling the links may involve additional processes (e.g. runout path and distance) or it can directly use the output of the preceding hazard (e.g. ground shaking).

5.2.5 Multi-hazard assessment

European Commission (2010) defines the concept of multi-hazard assessment as the process *"to determine the likelihood of occurrence of different hazards either occurring at the same time or shortly following each other, because they are dependent from (sic) one another or because they are*

caused by the same triggering event or hazard, or merely threatening the same elements at risk without chronological coincidence" (p.11). The output of hazard analysis is usually a hazard map which delineates the spatial distribution of hazards and their associated temporal probabilities. Following the well-established concept of single-hazard mapping, a multi-hazard map is expected to illustrate the spatial distribution of multiple potentially damaging processes and their consequent effects; or alternatively to classify areas according to their susceptibility to multiple processes (interacting or not). However the diversity in hazard characteristics such as magnitude, intensity, duration, extend, recurrence interval and units often don't allow the coupling between processes in a single output. Additionally, using many different overlapping symbols can make the result difficult to communicate and impractical to use. In an effort to address these issues two approaches to combining multiple hazards are proposed based on the type of interaction between the processes being analysed (Fig. 5.3).

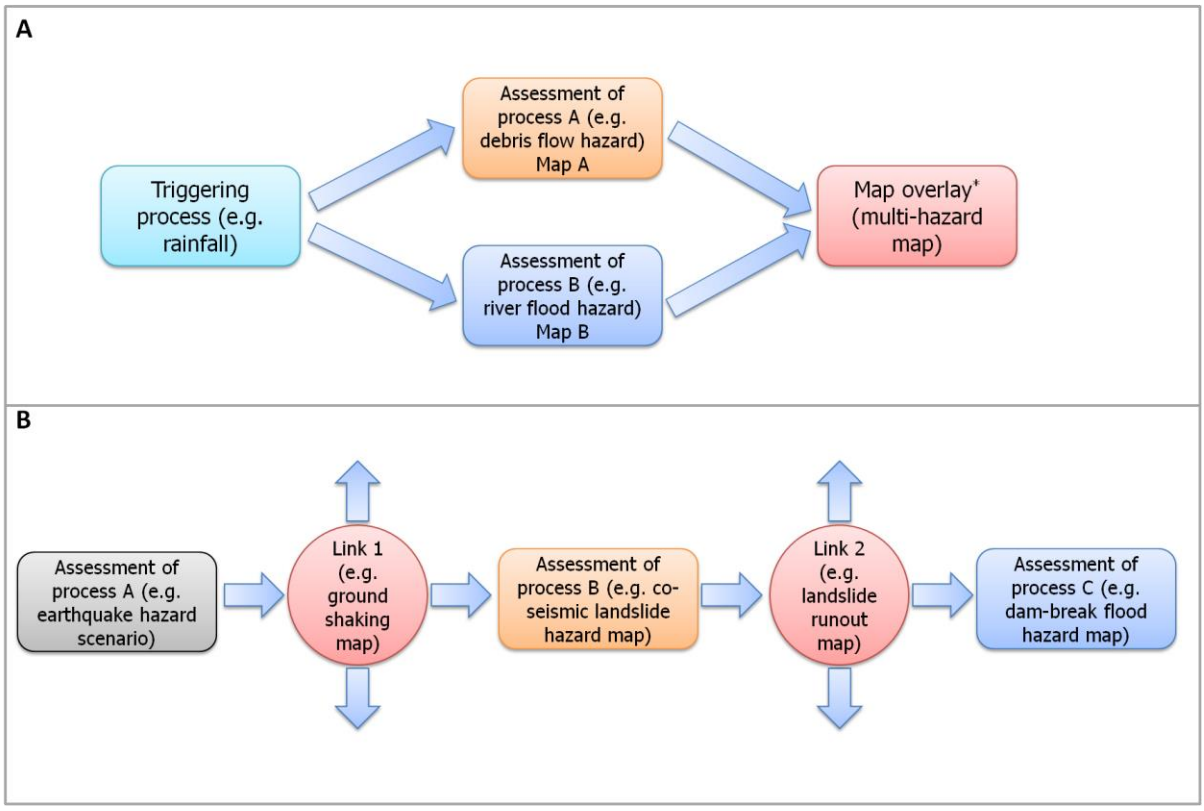

Figure 5.3 Mapping approaches based on the dominant type of interaction between the processes. A) This is used when there is spatial and/or temporal coincidence between the processes (*the combination is performed using the matrix shown in Table 2). B) This is used when the hazards are related through change of susceptibility or cause-effect interaction. The upward and downward arrows on the links indicate that other chains of events can be attached, e.g. Ground shaking triggers co-seismic landslides as well as lateral spreading and liquefaction that may induce different cascade effects.

If two processes are spatially overlapped regardless of having a common trigger, without a cause-effect relationship, the output of their joint analysis can be represented by a simple map overlay.

However the problem of different hazard characteristics still remains (e.g. flood depth in meters and debris flow occurrence). This can be achieved by classifying the overlapped hazards using a common hazard or susceptibility scale. Assuming that a region is subject to both floods and debris flows triggered by rainfall, each location is susceptible to a different degree to either flood, debris flow or both. Classifying the processes using the same susceptibility of hazard classes (e.g. very high to very low) allows their combination using a matrix relating all classes to each other (Table 5.2). The matrix allows estimating a combined (total) susceptibility for each cell. The rationale is that, if a cell is characterized by two different susceptibility classes, its total susceptibility depends on the highest class. For example, a location with moderate flood and debris flow susceptibilities will be overall less susceptible compared to a location with very high flood and low landslide susceptibilities.

Table 5.2 Matrix where the susceptibility classes of hazard A (rows) and the susceptibility classes of hazard B (on the columns) are combined in order to define the total susceptibility for the multi-process susceptibility zonation. The different colours indicate the combined susceptibility varying from very high (dark red) to very low (dark green).

		Hazard (B)				
		Very high (B)	High (B)	Moderate (B)	Low (B)	Very low (B)
Hazard (A)	Very high (A)	Vh (A, B)	Vh (A), H (B)	Vh (A), M (B)	Vh (A), L (B)	Vh (A), Vl (B)
	High (A)	H (A), Vh (B)	H (A, B)	H (A), M (B)	H (A), L (B)	H (A), Vl (B)
	Moderate (A)	M (A), Vh (B)	M (A), H (B)	M (A, B)	M (A), L (B)	M (A), Vl (B)
	Low (A)	L (A) , Vh (B)	L (A), H (B)	L (A), M (B)	L (A, B)	L (A), Vl (B)
	Very low (A)	Vl (A), Vh (B)	Vl (A), H (B)	Vl (A), M (B)	Vl (A), L (B)	Vl (A, B)

Nevertheless if the hazards interact through either change of susceptibility or cascade effects, and since each hazard assessment uses the result of the preceding hazard analysis as the main triggering factor, the final output is represented by a series of interlinked maps. The intermediate outputs are essentially the links between the cascading events. A link however can simultaneously trigger two or more processes and lead to other chain of events involving other interaction types.

5.2.6 Exposure analysis and multi-risk assessment

According to Varnes (1984) the specific risk for a given element (Rs) is defined as the product of the hazard (H) and vulnerability (V) of the element at risk. From this he defined the total risk as the product of specific risk (Rs) and the exposed elements at risk or asset (E). The three fundamental components in risk analysis, hazard, vulnerability and elements-at-risk are characterized by both non-spatial and spatial attributes (Van Westen et al. 2014). For describing a hazard, the location of the source and affected area (spatial attribute) as well as the probability of occurrence (non-spatial

attribute) are both required. Likewise assets also have spatial (location and extent) and non-spatial (economic value, number of floors and use for buildings, material type etc.) characteristics. Vulnerability, considered as the expected loss resulting from a hazard of given magnitude impacting on a specific asset with specific attributes (Schmidt et al. 2011), is determined by the spatial correlation between assets and hazards. Therefore, combining the assets with the output of the multi-hazard assessment using a GIS allows estimation of their spatial correlation (exposure) and effectively the total risk from different hazards and their cascade effects. To generate meaningful results, in addition to reasonably accurate multi-hazard analysis outputs, updated asset information layers accompanied by databases that include their non-spatial attributes are especially important in rapidly-developing regions.

5.2.7 Mitigation strategy

The final stage of the framework aims to identify the most appropriate mitigation strategy in the context of the overall geomorphic system. In an effort to mitigate the impact from a hazard, society often interferes with the geomorphic system by introducing a new component/sub-system. This interference can induce unpredictable consequences that can potentially exceed the initial hazard. The notion to 'control the hazard process' through, for example, engineering controls such as stopbanks for flood protection has been a common practice to protect communities in highly dynamic environments. However, several studies (Burby 1998; Mileti 1999; Ericksen et al. 2000; MfE 2008) have indicated that protective works, which provide protection against events that are within design parameters, tend to increase the risk of a disaster occurring, and the magnitude of the disaster, when an event eventually exceeds the estimated design parameters.

Recently increasing attention is being focused on hazard risk reduction through land-use planning (Mileti 1999; Burby et al. 2000; Saunders et al. 2007; Becker et al. 2008; Glavovic et al. 2010). Current planning options in New Zealand are based on historical land-use decisions that are often prone to a variety of hazards such as floods, earthquakes and landslides. Further development or relocation requires novel land use planning that will promote risk reduction. Therefore, whether hazard mitigation is approached through land use or engineering controls, these have to be analysed in conjunction with the other system components. This task will ensure that the new processes or interactions which will be potentially introduced to the system from the implementation of protection works or land-use options will not have adverse consequent effects on the communities.

5.3 Regional scale multi-hazard assessment in the WSA

The western Southern Alps of New Zealand's South Island are located along an actively deforming plate boundary and are subject to high rates of uplift, erosion and extreme precipitation totals that drive a range of geomorphic processes and consequent hazards. Furthermore, the mountainous landscape of WSA with its low-level glaciers and rain forest is an increasingly popular tourist attraction with growing domestic and international visitor numbers and demand for further development. Therefore the region is an ideal place for studying the interactions between hazards and their impacts on the human environment, offering a unique opportunity to apply and evaluate a multi-hazard/risk assessment methodology. Previous research (Whitehouse 1988; Hovius et al. 1997; Norris & Cooper 2000; Herman & Braun 2006; Korup et al. 2005; Hancox et al. 2005; Jacobson et al. 2003; Larsen & Davies 2005; Korup & Tweed 2007; Shulmeister et al. 2009; Tovar et al. 2008) as well as regional geomorphic analysis carried out in the context of this research (chapter 2) have illustrated that the mountain range is subject to interrelated climatic, surface and tectonic processes expressed through various types of slope failures (debris flows/ rock avalanches), glacial advance-retreat, fluvial processes (erosion-deposition), extreme orographic precipitation, high uplift rates and seismicity. Given the complexity of the environment and the potential for future tourism growth and development, a multi-hazard approach is required to inform land-use planning and enhance sustainable hazard mitigation in local communities. The methodology applied in WSA follows the framework for multi-hazard/risk assessment discussed in the previous section. This case study aims to demonstrate the key stages for a regional hazard/risk assessment in a tectonically-active mountainous environment. However mitigation strategies are not considered in the assessment primarily due to the regional scale of the study and data constraints. Additionally the limited number of geomorphic hazards considered in the analysis doesn't allow exploring the full extent of interactions between potential mitigation measures and other components of the geomorphic system.

Initially, regional geomorphic analysis using quantitative geomorphology via GIS was carried out in order to identify the dominant geomorphic processes, their spatial distribution and inter-dependent effects. The main focus of the analysis was on the drainage network as it is directly linked to tectonic forcing and therefore contains potentially useful information on differential rock uplift rates across the landscape as well as, reflects critical relationships between tectonic, climatic and surface processes (Wobus et al. 2006; Tucker & Bras 1998). From interpretation of the findings, the geomorphic system with its major components, at regional scale, was emerged (Chapter 2, Fig. 2.20). The processes considered in the multi-hazard assessment were shallow landslides / debris

flows, river floods and earthquakes. Further hazards threatening the study area are coastal hazards (e.g. coastal erosion, storm surge, tsunami, sea level rise), climatic hazards (e.g. strong wind, tornadoes, hail, snow, ice, droughts, wildfires), lake tsunamis and glacier outburst floods (DTec 2002), which are at this point not included into the analysis. Interactions between identified processes / hazards are given in Table 5.1. Shallow landslide / debris flow and river flood susceptibilities are assessed by means of GIS-based models using regional scale input data. Seismic hazard is based on findings from previous studies (Benn 1992; McCahon et al 2006; Sutherland et al. 2007; Robinson & Davies 2013) that have indicated a likely earthquake scenario for the Alpine Fault and a corresponding spatial distribution of Modified Mercalli shaking intensity.

5.3.1 Rainfall-triggered shallow landslide / debris-flow and river flood susceptibility

Prolonged or high intensity rainfall combined with the steep topography of WSA frequently induces river floods as well as triggers shallow landslides and debris flows (Griffiths & McSaveney 1983; Benn 1990, 2005; DTec 2002; WCRC 2010). The impacts on local communities are often severe with road closures, bridge collapses, destroyed buildings and farmland and loss of lives. The shallow landslide /debris flow and river flood susceptibility assessments were separately carried out at regional scales using GIS-based models (Chapters 3 and 4). In particular, an approach based on fuzzy logic in GIS environment was developed to assess the shallow landslide/debris-flow susceptibility in the study area. Since slope failures are complex phenomena and prediction of their spatio-temporal occurrence involves many uncertainties, fuzzy logic was implemented in order to minimize these uncertainties and model the non-linear relationships between conditioning factors and slope instability (Chapter 3, sections 3.2.1, 3.2.2). Ten parameters were initially identified as the most important conditioning factors for rainfall-generated shallow landslides in WSA and fuzzy memberships were established between each parameter and landslide occurrence based on landslide inventory data and used-defined functions. Evaluation of the output in a test area using an independent population of landslides, demonstrated satisfactory performance (up to AUC = 0.734). Figure 5.4 shows the spatial distribution of shallow landslide susceptibility in the study area. The potential runout path and distance of landslides from the susceptible areas were also assessed based on a multiple flow direction algorithm and the topographic slope of existing debris-flow deposits. Detailed description of the shallow landslide susceptibility and runout models as well as discussion on their strengths and limitations are given in Chapter 3.

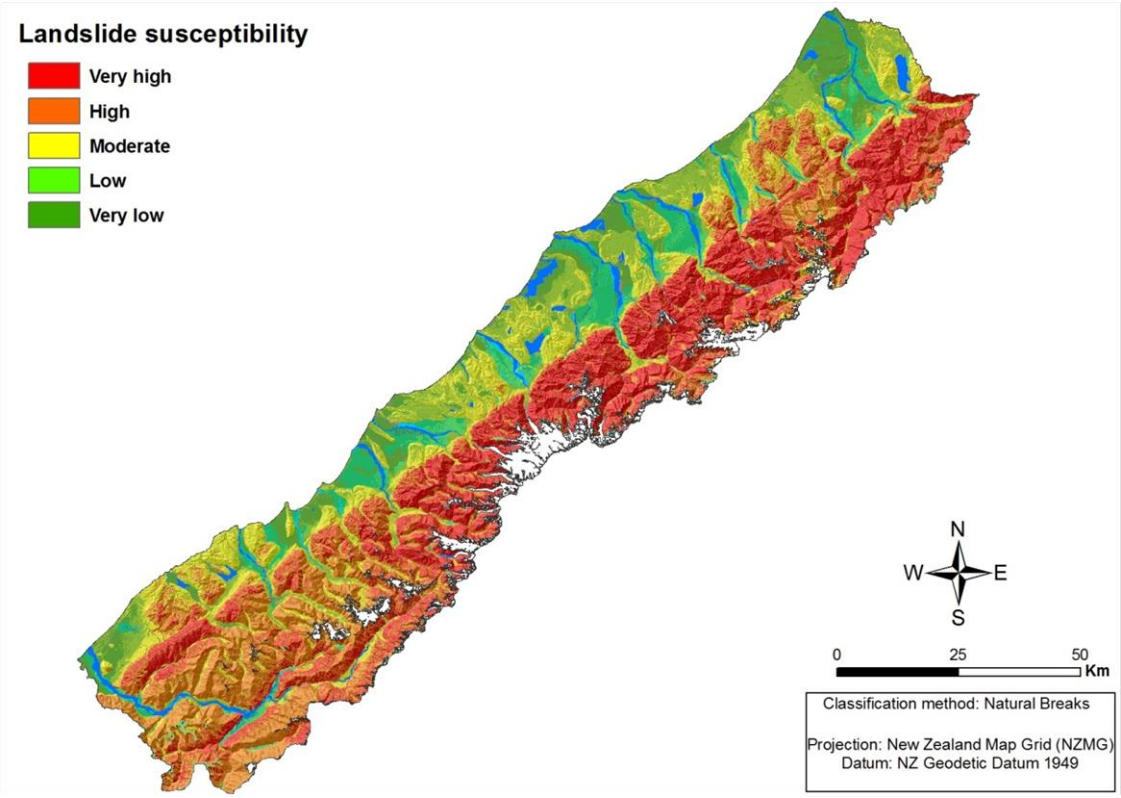

Figure 5.4 Rainfall-triggered shallow landslide / debris-flow susceptibility map.

The flood hazard assessment was carried out in two stages. Initially a GIS-based spatially distributed unit hydrograph model was developed in order to investigate the hydrologic response (i.e. the intrinsic tendency of different catchments to produce runoff) of major ungauged river catchments in the study area based on their morphometry, land cover and soil characteristics. Findings revealed that steep, relatively short mountainous catchments generally produce more runoff per unit area compared to larger catchments, thus having greater potential to induce flooding downstream. The spatial variation of rainfall characteristics within the catchment and antecedent runoff conditions emerged as key factors in the modelling approach. A model based on fuzzy logic in GIS environment was also developed using terrain, land cover and soil parameters, aiming to evaluate the flood susceptibility in the study area (Fig. 5.5). The height above nearest drainage, slope gradient, land cover, soil permeability and proximity to stream channels were identified as the as the most important flood susceptibility parameters in the area. The specific factors were selected as they are related to critical flood characteristics such as flow velocity, inundation extent, flood duration and depth. Their relationship with flood occurrence was established based on historical flood events and user-defined fuzzy membership functions. The implementation of fuzzy logic allows a more realistic representation of the predisposing factors as it takes into account uncertainties related to insufficient knowledge, data limitations and non-linear relationships between conditioning factors and flood susceptibility. The procedures, input parameters and evaluation for the spatially

distributed unit hydrograph and the fuzzy flood susceptibility models are described in detail in chapter 4.

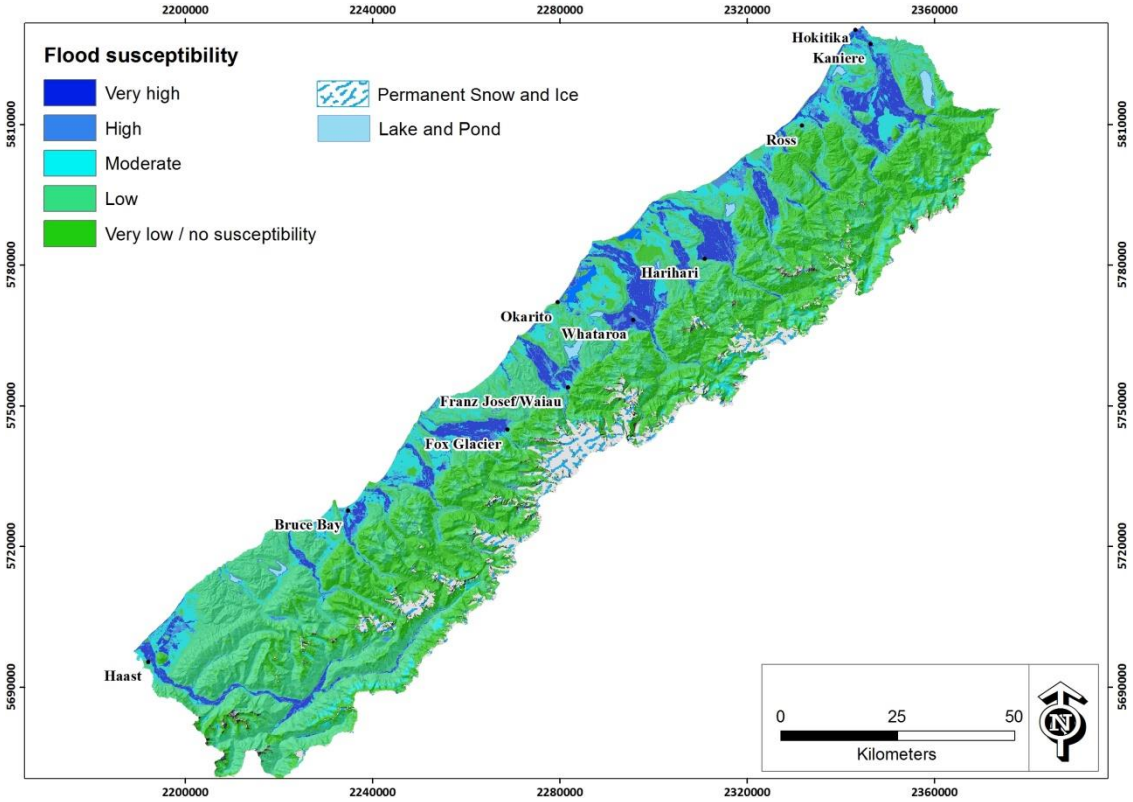

Figure 5.5 River flood susceptibility map.

Since rainfall-induced shallow landslides and river floods overlap in time and space, the output of their joint analysis can be represented by a map overlay (Fig. 5.3A). In order to combine the susceptibility indices from the two maps into a single output, the continuous susceptibility scale of each map is classified into the same classes, ranging from very high to very low. Different methods are available in GIS to perform this task (e.g. equal intervals, geometric intervals, natural breaks and quantile). Although there is no optimum procedure to classify the susceptibility into specific categories, the criterion for the most appropriate classification method is that the higher susceptibility classes should explain a large proportion of hazard occurrences (floods or landslides) in a relatively small proportion of the total area. Details on the classification methods selected for the shallow landslide and river flood susceptibility maps are provided in chapters 3 and 4 respectively. Following the classification of both maps into a common susceptibility scale, the matrix shown in Table 5.2 was used to derive a combined output. The final map shows the spatial variation of combined susceptibility (Fig. 5.6). It reveals areas highly susceptible to both hazards as well as locations that are not affected by any of these processes, which are not easily identified when examining the output from each process separately.

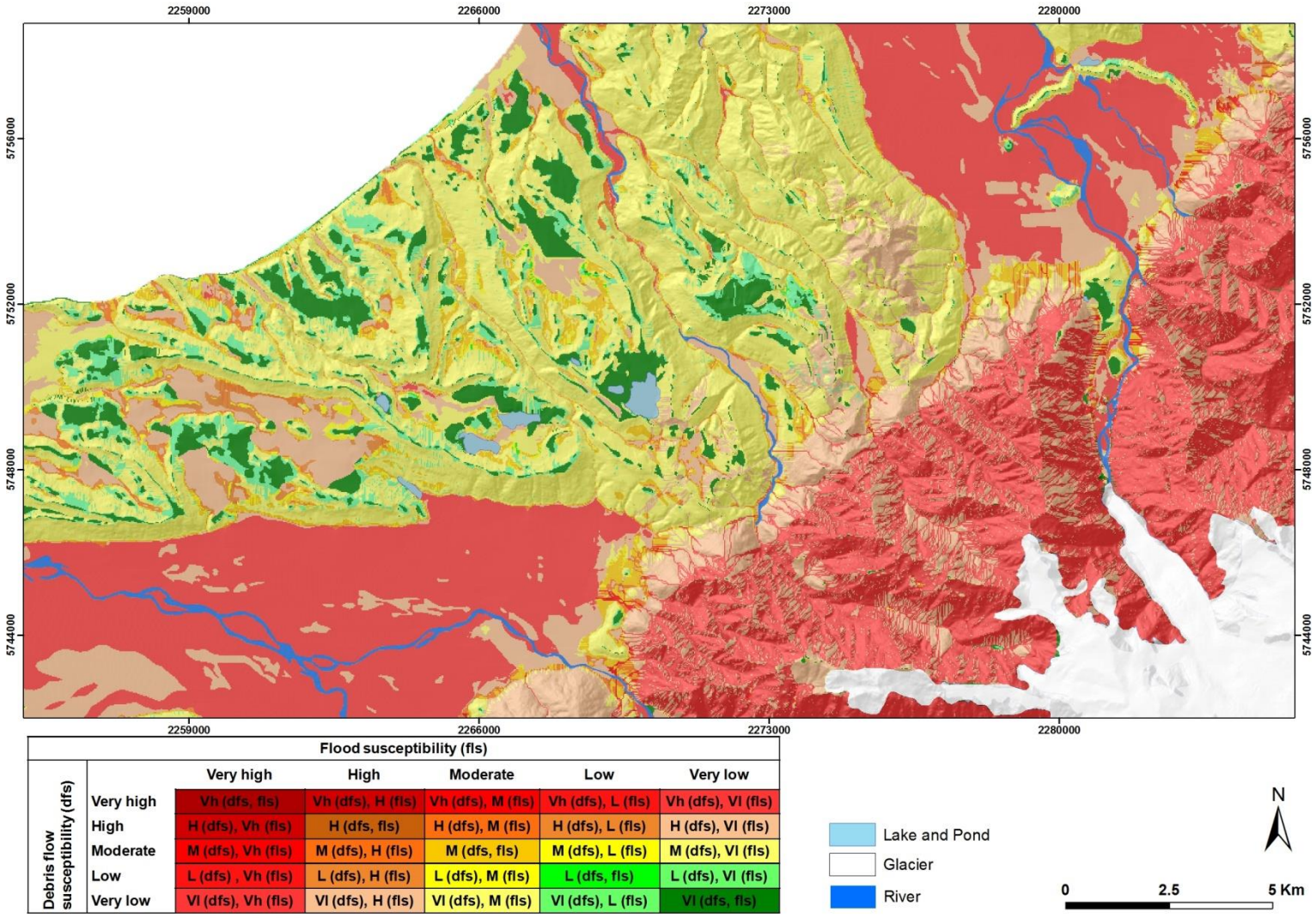

Figure 5.6 Integrated shallow landslide and river flood susceptibility. The map shows the variation of relative combined susceptibility in the area. Classes with the same total combined susceptibility are represented by the same colour, for example Vh (dfs), Vl (fls) and Vl (dfs), Vh (fls). (Note: the very low susceptibility class implies that the geomorphic hazard does not occur in the specific location)

Riverbed aggradation is another common geomorphic process in WSA related to debris flows and river flooding. Aggradation occurs when the volume of sediment input to a stream channel reach exceeds its transport capacity. Sediment is therefore deposited in the channel. It is generally observed at the head of an active fan, where a river emerges from the steep confined mountain valley, and accumulates on broader, flatter basin, valley or coastal plain (Davies et al. 2003; Davies et al. 2005; Davies & McSaveney 2006). Adverse consequences associated with aggradation include increased flood hazard, as less discharge is needed to overflow the banks and channel avulsion (complete abandonment and initiation of a new channel).

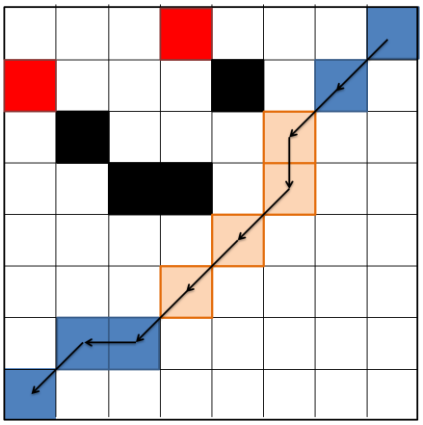

Figure 5.7 GIS-based calculation of channel length susceptible to sediment input. Black arrows indicate flow directions. Blue squares represent cells belonging to the drainage network. Red squares represent modelled debris flow sources and black squares show their runout paths. Light orange squares delineate the intersection of debris-flows runout paths with drainage network cells. These cells are considered susceptible to sediment input. The total susceptible length is calculated by the cumulative flow length of the light orange squares. Given a cell size of 25m the total susceptible to sediment input length in the above example is 120.7m.

Combining the runout susceptibility model with the drainage network, locations where the runout paths of shallow landslides intersect with stream channels were delineated (Fig. 5.7). Although the volume of the landslides cannot be estimated, the length of susceptible channel reach in each catchment was extracted as an indirect measure of their relative susceptibility to sediment input (Table 5.3). Combining the affected channel length with a simplified stream power model applied to examine the spatial distribution of fluvial erosion and deposition in the study area (see chapter 2), channel reaches prone to aggradation were indentified (Fig. 5.8). The result is based on the assumption that drainage systems with significant channel length susceptible to sediment input from debris-flows and limited transport capacity are the most susceptible to river aggradation. These channel reaches are also prone to flooding as less water is required to reach overbank flow. It should be noted that the above method only provides a first order identification of channel reaches susceptible to aggradation and more detailed analysis is required to estimate their relative susceptibility and consequent flood proneness.

Table 5.3 Channel length affected by debris-flows.

Catchment	Affected channel length (km)				Total affected length (km)	Total stream length (km)	Normalized affected length				
	Very high	High	Moderate	Low			Very high	High	Moderate	Low	Total
Hokitika	872.3	997.6	743.7	191.2	1282.5	1965.6	0.444	0.508	0.378	0.097	0.652
Totara	12.9	108.2	108.2	28.8	132.9	268.8	0.048	0.403	0.403	0.107	0.494
Mikonui	54.1	219.2	190.5	41.1	244.9	301.2	0.180	0.728	0.632	0.136	0.813
Waitaha	275.6	341.3	267.9	45.3	415.8	574.5	0.480	0.594	0.466	0.079	0.724
Wanganui	441.0	442.8	324.3	54.0	569.6	875.3	0.504	0.506	0.370	0.062	0.651
Poerua	134.1	138.3	130.9	49.9	209.7	471.9	0.284	0.293	0.277	0.106	0.444
Whataroa	596.5	599.8	396.7	43.7	713.2	960.4	0.621	0.625	0.413	0.046	0.743
Waitangitaona (lower)	11.7	14.7	20.2	10.1	26.1	193.3	0.061	0.076	0.105	0.052	0.135
Waitangitaona (upper)	93.4	84.8	55.7	7.4	110.6	135.4	0.690	0.626	0.411	0.055	0.817
Waiho	194.4	189.0	122.4	17.6	238.3	398.8	0.488	0.474	0.307	0.044	0.598
Waikukupa	38.0	41.5	56.8	29.6	80.1	106.7	0.356	0.389	0.533	0.278	0.750
Fox-Cook	224.5	236.5	157.1	23.9	296.1	469.4	0.478	0.504	0.335	0.051	0.631
Ohinematea	33.5	46.7	46.2	19.4	70.6	168.2	0.199	0.278	0.275	0.116	0.420
Karangarua	444.8	511.9	301.2	24.7	579.4	718.5	0.619	0.712	0.419	0.034	0.806
Makawhio	91.8	191.4	145.1	24.1	226.4	314.6	0.292	0.608	0.461	0.077	0.720
Mahitahi	55.7	245.6	222.3	48.4	287.1	367.1	0.152	0.669	0.606	0.132	0.782
Ohinemaka	5.4	39.1	49.9	23.3	58.5	131.1	0.041	0.299	0.381	0.178	0.446
Paringa	65.4	378.5	365.1	97.5	464.1	644.6	0.101	0.587	0.566	0.151	0.720
Moeraki	37.1	106.3	103.8	22.9	131.4	192.4	0.193	0.553	0.540	0.119	0.683
Whakapohai	41.1	79.9	72.2	14.3	88.2	100.8	0.408	0.792	0.717	0.142	0.876
Waita	45.2	95.4	94.4	33.0	118.9	241.6	0.187	0.395	0.391	0.136	0.492
Haast	601.9	1801.9	1296.4	176.6	1912.9	2354.3	0.256	0.765	0.551	0.075	0.813

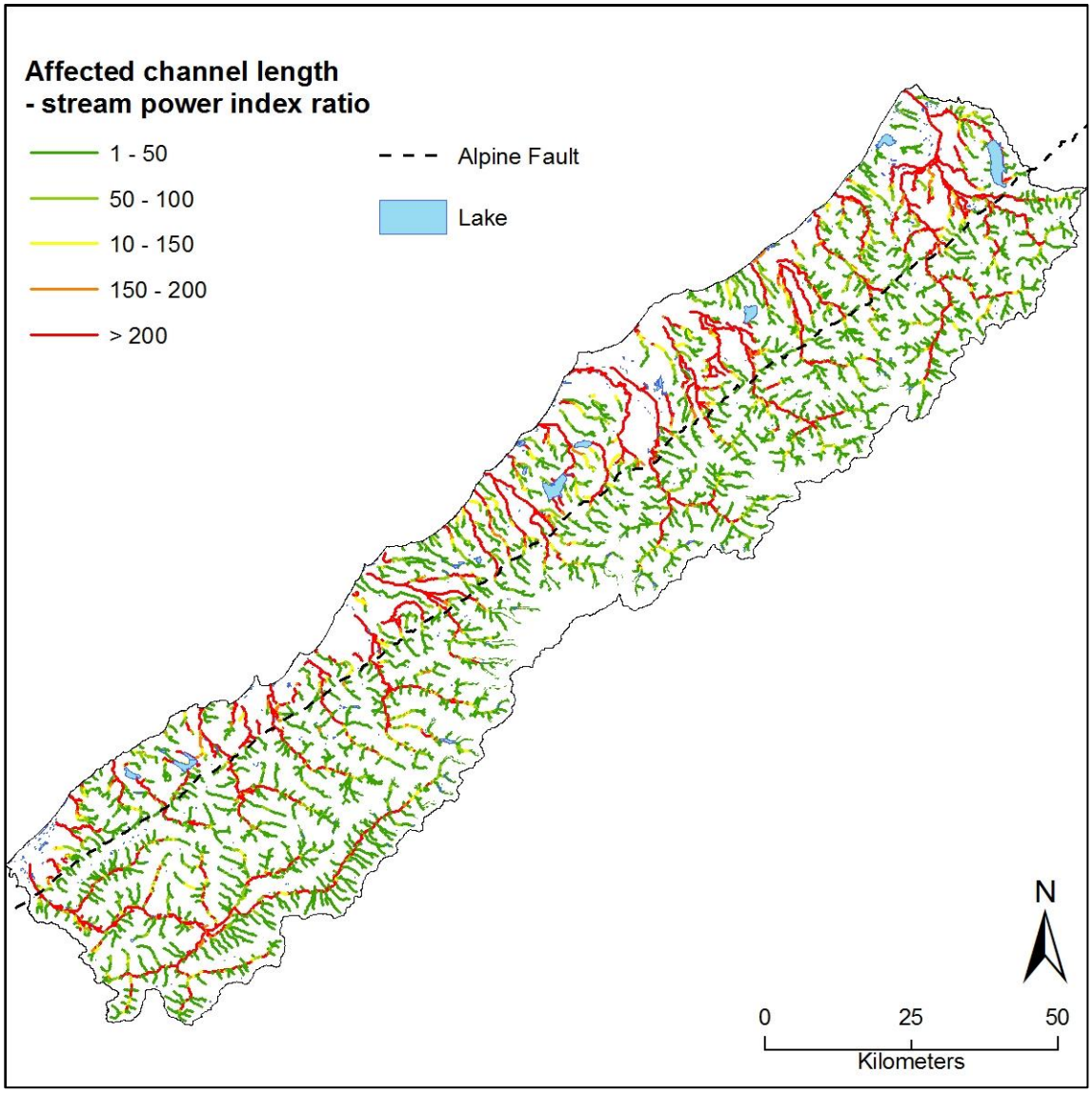

Figure 5.8 Sediment input can be generated from debris flows, rock avalanches, river bank collapses, and glacial outburst floods. Herein only the input from rainfall induced shallow landslides / debris flows is considered based on the shallow landslide and runout susceptibility models. The map delineates aggradation-prone channel reaches based on the length affected by debris flows and the spatial variation of a simplified stream power index.

5.3.2 Earthquake hazard and co-seismic landslides

5.3.2.1 The Alpine Fault Earthquake Scenario

Of all the natural hazards in the region, an Alpine Fault earthquake poses the single largest known risk, as its impact will be devastating for the entire region. In addition to the ground shaking a range of other geomorphic hazards will affect the area on time scales varying from immediately after the earthquake up to decades (Hewitt et al. 2008; Robinson & Davies 2013). Due to the severe expected impacts from an Alpine fault earthquake on the region, several studies have investigated the Alpine Fault's characteristics, its paleo-seismicity and its consequent geomorphic hazards (Benn 1992; Bull

1996; Sutherland et al. 2007; Yetton et al. 1998; Berryman et al. 1998; Wells et al. 1999; Yetton 2000; Wells & Goff 2007; Robinson & Davies 2013).

Paleoseismic studies based on post-earthquake aggradational terraces (Adams 1980), lichenometric dating of coseismic rock falls (Bull 1996), trenching along the fault (Berryman et al. 1998), tree-ring dating (Wells et al. 1999), deformed river terraces and fallen trees (Yetton 2000), and coastal dune progradation sequences (Wells & Goff 2007), age constraints for surface-rupturing earthquakes on or near the Alpine fault in the last c. 1000 years have been dated c. AD 1717, c. AD 1615, c. AD 1460 and c. AD 1230. These studies suggest a recurrence interval between 200-300 years and earthquake magnitudes of up to Mw ≈ 8. Recent studies by Berryman et al. (2012) and De Pascale & Langridge (2012) suggest a mean recurrence interval of 329±68 years and magnitude up to M_w 8.2 respectively.

Since no major earthquake has occurred on the Alpine Fault during the short historical period in New Zealand (180 years) the fault is considered to be due for another significant earthquake ($M_w \approx 8$) (Sutherland et al. 2007) posing a substantial seismic hazard for the West Coast and most of the South Island.

The predominant effect of earthquakes is ground shaking as seismic waves generated by the release of crustally-stored elastic strain energy at the fault propagate through the crust. These waves are amplified or reduced by the underlying geology, soils and topography, and generally reduce in severity with distance from the earthquake source. The shaking hazard is commonly defined directly in terms of the maximum accelerations caused by the seismic waves (peak ground acceleration), or indirectly in terms of effects using an intensity scale (e.g. Modified Mercalli intensity scale). The spatial variation in Modified Mercalli shaking intensity from a hypothetical M_w 8 Alpine Fault earthquake is shown for the South Island in Figure 5.9. The whole of the West Coast will experience strong shaking, expected to be most intense in the WSA as they are enclosed by the MMI 9 isoseismal.

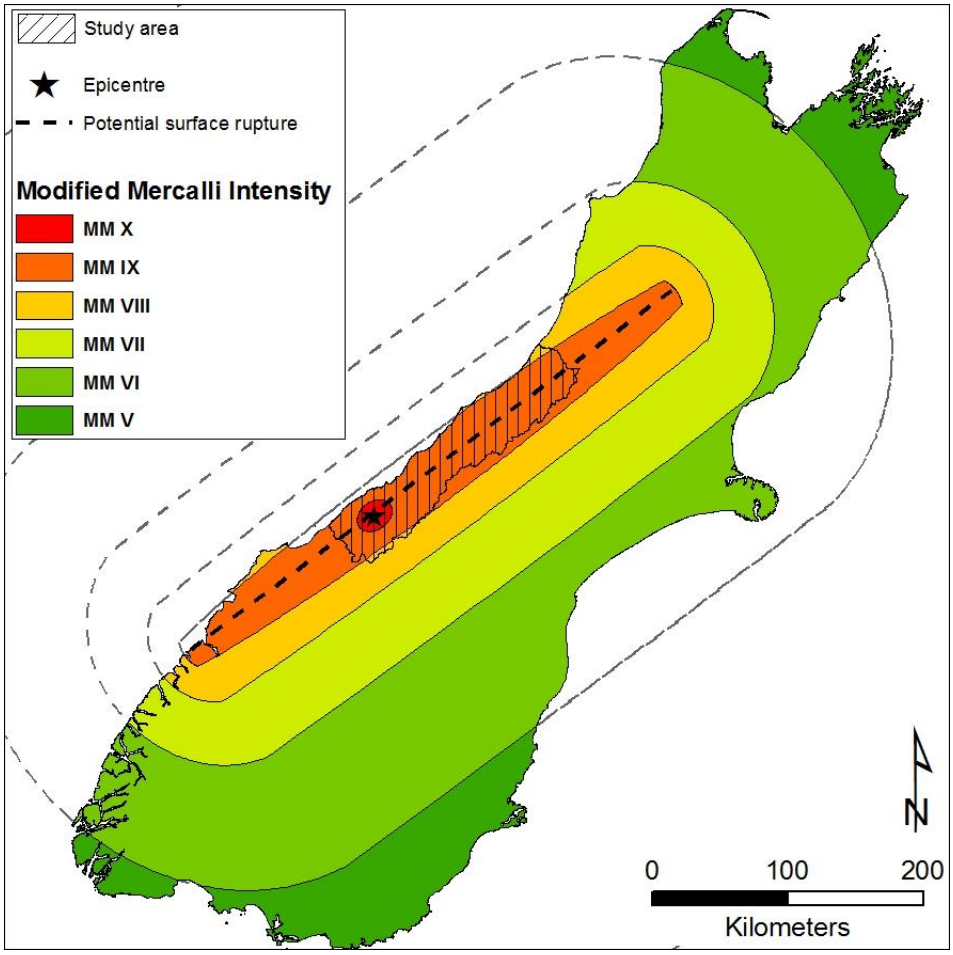

Figure 5.9 Isoseimal map that corresponds to Mw 8 Alpine Fault earthquake scenario (isoseimals from Robinson & Davies 2013).

Several studies investigating the amplification of seismic ground motion by topography (Davis & West 1973; Spudich et al. 1996; Athanasopoulos et al. 1999; LeBrun et al. 1999; Havenith et al. 2003; Wald & Allen 2007; Buech et al. 2010) have illustrated that different parts of mountains or hills (e.g. ridge, mid-slope, base) respond differently to seismic shaking. Additionally, areas underlain with deep, recent soils can be expected to have increased shaking intensities, particularly at longer periods, relative to areas underlain with strong rock at shallow depths (McCahon et al. 2006). This is mainly because soft soils amplify ground shaking due to lower shear wave velocities (Wald & Allen 2007). Therefore spatial variation of shaking intensity is expected due to local site conditions such as the physical characteristics of the soils and underlying rock (relative thickness, grain-size, depth, density) as well as topography, geometry and distance to the seismic source (McCahon et al. 2006; Buech et al. 2010). This phenomenon has major implications for the triggering of co-seismic processes such as mass movements, liquefaction and lateral spreading.

Given sufficient knowledge about the underlying geology, soils and topographic amplification of seismic shaking is available, it would be possible to classify the study area into different zones. This

would allow estimating a specific shaking intensity or peak ground acceleration value for each cell and infer its susceptibility to seismic shaking. The spatial variation of susceptibility to seismic shaking would then be possible to combine with the debris-flow and flood susceptibilities using a three dimensional version of the combination matrix described above (Fig 5.10).

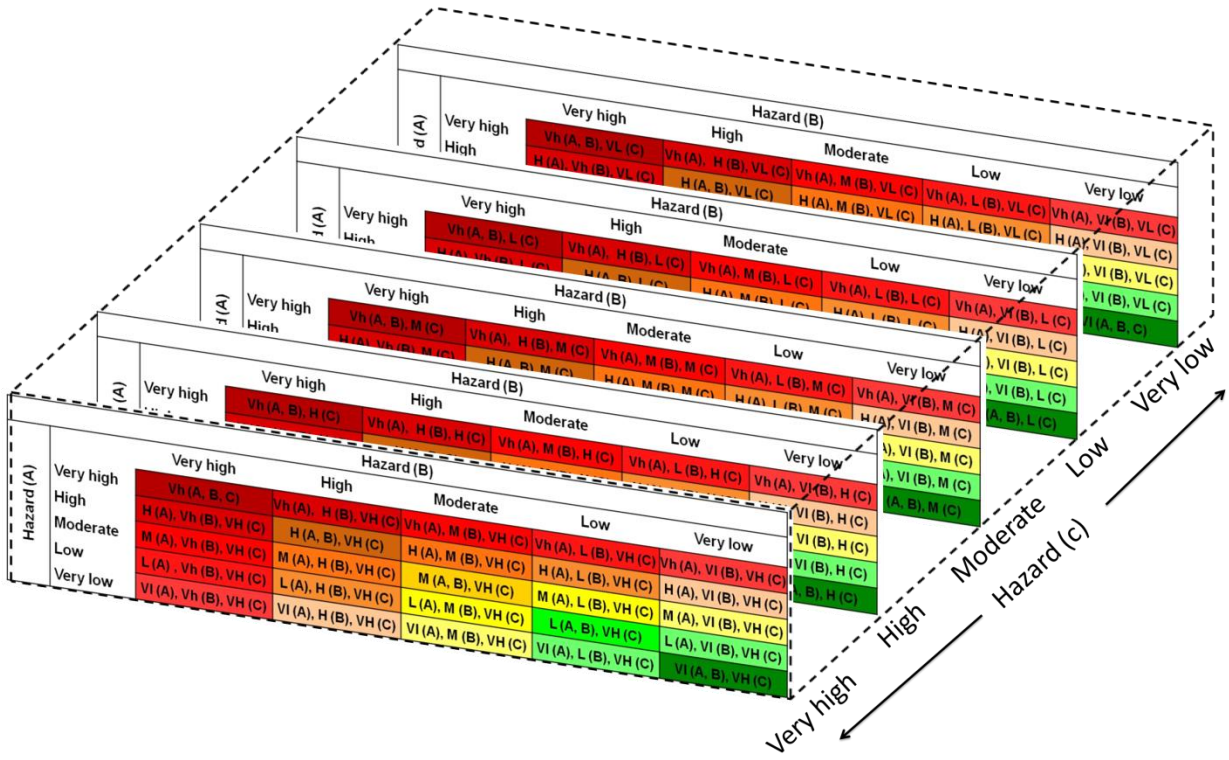

Figure 5.10 Three dimensional matrix for estimating the combined relative hazard or susceptibility from three processes.

However, the topographic amplification requires analysis of detailed ground-motion records and therefore it has not been considered in this case study. The recent New Zealand loadings standard (Standards New Zealand 2004: NZS 1170.5:2004) recognizes the local variation of shaking intensity using five general subsoil categories (A: strong rock, B: rock, C: shallow soil, D: deep or soft soil, E: very soft soil) based on their geological and geotechnical properties. Some indication about underlying geology and soils can be acquired from existing geological maps. Nevertheless these broad geological divisions are indicative only and a region wide zoning has not been attempted for the study area. Areas that fall into the C – E subsoil categories (mainly recent alluvial soils) are particularly interesting as most of the populated areas and infrastructure are located on them. In addition to their greater ground shaking potential due to generally lower shear-wave velocities

compared to A and B categories, recent alluvial soils are often related to high and very high flood susceptibility zones. These areas were directly extracted from published geological maps (QMAPs 1:250000) for the region (Fig. 5.11). Given a Mw 8 Alpine fault earthquake these locations are expected to experience strong ground shaking and therefore it is assumed that they have high seismic shaking susceptibility. Figure 5.12 shows the integrated ground shaking, debris-flow and flood susceptibility at the Fox River catchment.

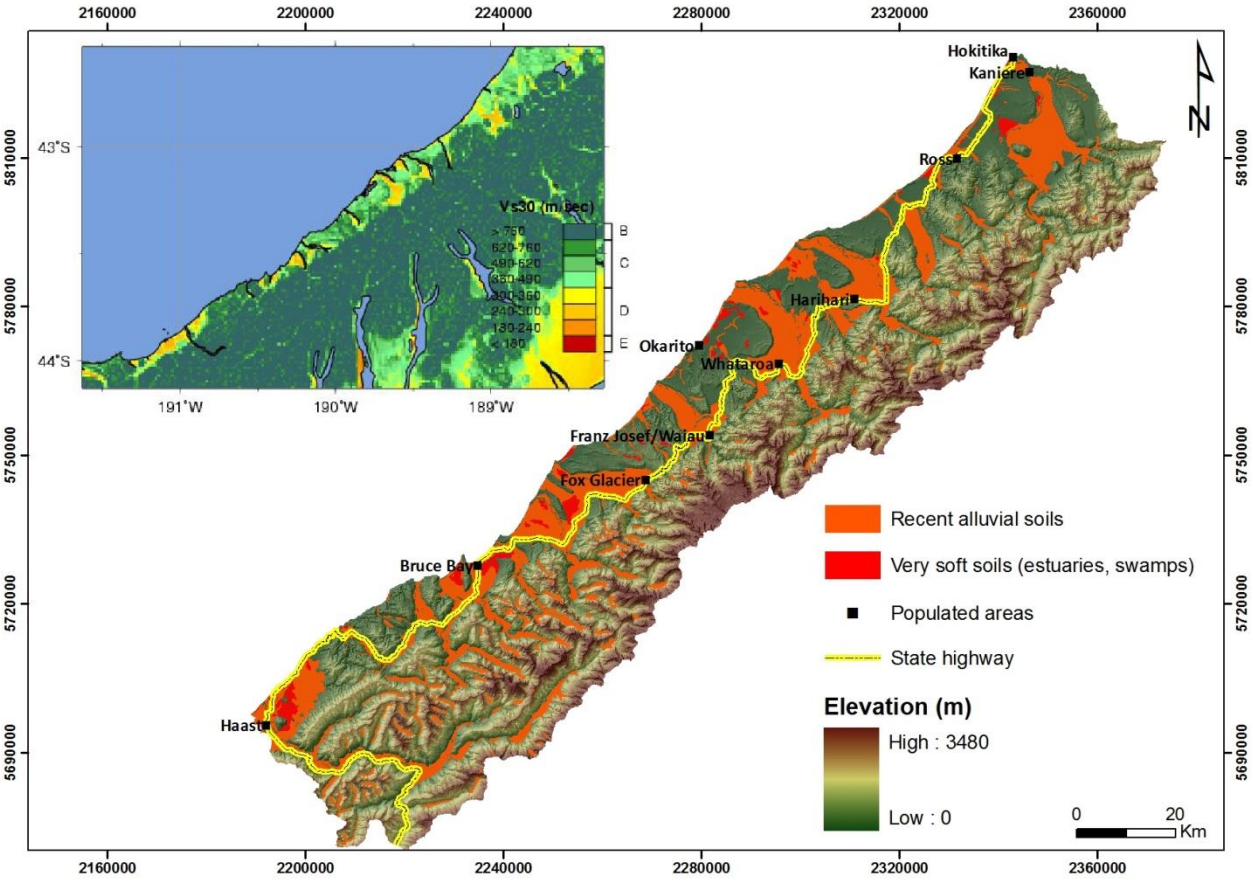

Figure 5.11 Recent alluvial deposits in the study area associated with subsoil classes D and E. Populated areas and significant length of the principal road network are located on these areas. Inset figure shows the variation of average shear-velocity in the upper 30 m (Wald & Allen 2007). The recent alluvial deposits generally exhibit Vs_s^{30} < 360 m s^{-1}.

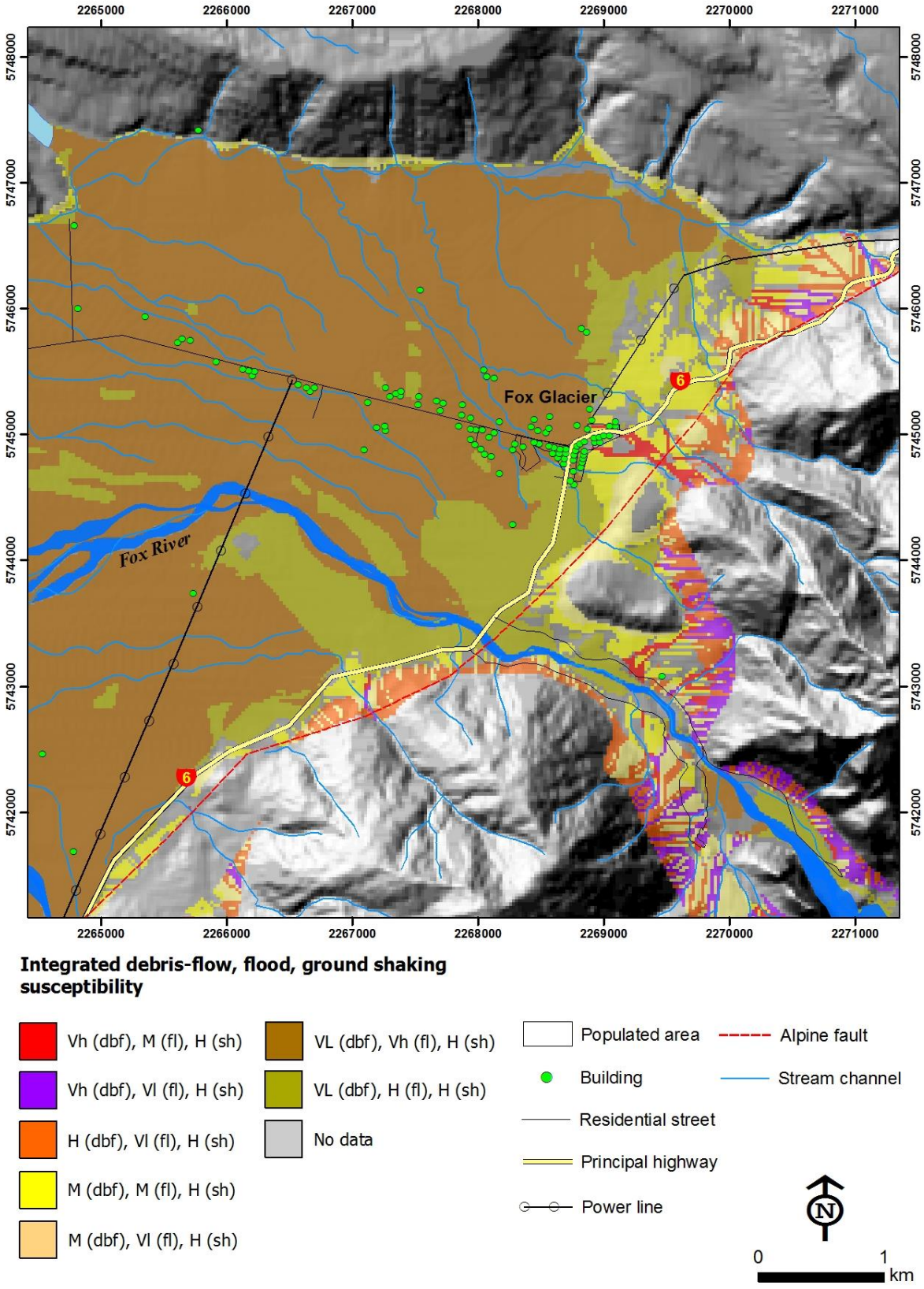

Figure 5.12 Integrated ground shaking, debris-flow and flood susceptibility. The analysis carried out only on areas assumed to have high ground shaking susceptibility based on the subsoil classes by NZS 1170.5:2004 and average shear-velocities. Fox Glacier is mostly located on a very high flood, high shaking susceptibility zone. The north-east part of the township has the highest total susceptibility as it is located on the very high debris-flow, moderate flood and high shaking susceptibility zone.

5.3.2.2 Co-seismic landslides

Landslides are a common effect of earthquakes especially when shaking occurs in steep terrain. The process of co-seismic landsliding has received considerable attention in recent years as the seismically induced slope failures often result in a great number of casualties and have long term geomorphic and socio-economic impacts (e.g landslides triggered by the 1989 Loma Prieta, U.S, the 1999 Chi-Chi, Taiwan and the 2008 Wenchuan, China earthquakes).

Although small-magnitude, high-frequency, rainfall-induced events have caused the most damage to property and infrastructure and at least 36 fatalities in WSA (Benn 2005), prehistoric earthquakes are inferred to have triggered deep-seated slides with deposits of the order of 10^6 - 10^8 m^3 (Whitehouse & Griffiths 1983).

A large number of landslides can be expected in WSA given a M_w 8 Alpine Fault earthquake due to the combination of steep topography coinciding with the region of the strongest shaking intensity. Liquefaction is also expected to occur in susceptible soils and extensive lateral spreading along river banks. Based on the empirical formulas proposed by Keefer (1984) and Malamud et al. (2004), Robinson & Davies (2013) indicate order-of-magnitude estimates of the expected total affected area, total landslide volume, largest landslide area, and largest landslide volume. According to their estimates an area of up to 10^5 km^2 will be potentially affected by co-seismic landslides.

Large magnitude earthquakes on mountain range bounding faults such as the M_w 7.6 Chi Chi 1999 and M_w 8 Wenchuan 2008 have triggered tens of thousands landslides, both shallow- and deep-seated. In both events the highest landslide density is observed in the highest shaking intensity region which is also the area closest to the fault-rupture (Gorum et al. 2011; Lee 2013).

Therefore according to the estimated maximum affected area of the order of 10^5 km^2 and the spatial distribution of landslides induced by great earthquakes such as the 1999 Chi-Chi, Taiwan and the 2008 Wenchuan, China, co-seismic landslides from a M 8 Alpine Fault earthquake can occur anywhere over the narrow strip of rugged terrain (c. 4800 km^2) between the potential fault rupture and the main divide. Although the exact locations of the slope failures cannot be determined, it is realistic to assume that the entire mountainous area between the AF and the main divide is expected to be highly susceptible to both shallow and deep-seated landslides, while gentle slopes west of the AF, especially close to major rivers, will be susceptible to lateral spreading. In addition, large volume (> 10^6) seismically-induced rock avalanches can have very long runout distances of the order of few kilometres. The largest landslide triggered by the 2008 Wenchuan earthquake, the Daguangbao landslide, with estimated volume of 750-840 x 10^6 m^3 travelled a distance of about 4.5

km (Zhang et al. 2013). In Westland, a large volume (45 x 10^6 m^3) rock avalanche from Round Top, potentially triggered by an AF earthquake, has an estimated runout distance of > 4km (Dufresne et al. 2009; Wright 1998). These findings indicate that populated areas, infrastructure and lifelines located within a few kilometres away from the mountain front are exposed to both strong seismic shaking and the runout path of large rock avalanches.

5.3.3 Exposure analysis and risk

Exposure analysis was performed by combining the output maps from the multi-hazard assessment with elements-at-risk. The task was carried out in GIS by means of overlay analysis of the integrated shallow landslide / river flood susceptibility map with populated areas, buildings, road network and powerlines. Table 5.4 shows the potentially affected lengths of road network classified in two major categories. The results indicate that the road network is primarily exposed to flooding. Significant length is also exposed to both debris flows and flooding. Tables 5.5 - 5.7 illustrate the exposure of populated areas, buildings and powerlines to debris flows and river floods. The results indicate that all populated areas, most buildings and the longest length of powerlines are mainly affected by river floods. However, Fox Glacier, Franz Josef and Harihari as well as a significant number of buildings and few km of powerlines are exposed to at least moderate, if not higher, debris-flow and flood susceptibilities demonstrating the highest total risk.

Table 5.4 Exposed length of road network to debris-flows and floods.

Susceptibility	Affected length (km)	
	Principal highways	Residential or district
Vh (DBF, FL)	-	-
H (DBF), Vh (FL)	-	-
M (DBF), Vh (FL)	-	0.05
L (DBF) , Vh (FL)	-	0.03
Vl (DBF), Vh (FL)	126.60	368.73
Vh (DBF), H (FL)	1.10	1.25
H (DBF, FL)	3.83	2.55
M (DBF), H (FL)	10.33	16.15
L (DBF), H (FL)	5.88	9.63
Vl (DBF), H (FL)	120.88	170.20
Vh (DBF), M (FL)	2.70	0.40
H (DBF), M (FL)	9.08	2.85
M (DBF, FL)	17.93	17.20

L (DBF), M (FL)	7.83	7.45
Vl (DBF), M (FL)	18.03	29.18
Vh (DBF), L (FL)	-	-
H (DBF), L (FL)	0.13	0.05
M (DBF), L (FL)	0.85	1.55
L (DBF, FL)	0.68	1.28
Vl (DBF), L (FL)	1.15	2.73
Vh (DBF), Vl (FL)	2.85	1.68
H (DBF), Vl (FL)	27.25	13.65
M (DBF), Vl (FL)	52.00	56.85
L (DBF), Vl (FL)	5.90	15.35
Vl (DBF, FL)	8.78	37.20

Table 5.5 Number of buildings exposed to debris-flows and floods.

Susceptibility	No. of buildings
Vh (DBF, FL)	-
H (DBF), Vh (FL)	-
M (DBF), Vh (FL)	-
L (DBF) , Vh (FL)	2
Vl (DBF), Vh (FL)	2061
Vh (DBF), H (FL)	1
H (DBF, FL)	4
M (DBF), H (FL)	50
L (DBF), H (FL)	50
Vl (DBF), H (FL)	661
Vh (DBF), M (FL)	3
H (DBF), M (FL)	1
M (DBF, FL)	26
L (DBF), M (FL)	9
Vl (DBF), M (FL)	18
Vh (DBF), L (FL)	-
H (DBF), L (FL)	1
M (DBF), L (FL)	1
L (DBF, FL)	-
Vl (DBF), L (FL)	8
Vh (DBF), Vl (FL)	17
H (DBF), Vl (FL)	18
M (DBF), Vl (FL)	24
L (DBF), Vl (FL)	11
Vl (DBF, FL)	62

Table 5.6 Length of powerlines (distribution and transmission lines) exposed to debris-flows and floods (power line data from the LINZ digital topographic database: http://www.linz.govt.nz/).

Susceptibility	Power lines (affected length km)
Vh (DBF, FL)	-
H (DBF), Vh (FL)	-
M (DBF), Vh (FL)	-
L (DBF) , Vh (FL)	-
Vl (DBF), Vh (FL)	63.7
Vh (DBF), H (FL)	0.1
H (DBF, FL)	0.4
M (DBF), H (FL)	1.5
L (DBF), H (FL)	1.8
Vl (DBF), H (FL)	37.1
Vh (DBF), M (FL)	0.0
H (DBF), M (FL)	0.2
M (DBF, FL)	3.4
L (DBF), M (FL)	1.3
Vl (DBF), M (FL)	1.7
Vh (DBF), L (FL)	-
H (DBF), L (FL)	-
M (DBF), L (FL)	0.1
L (DBF, FL)	0.0
Vl (DBF), L (FL)	0.0
Vh (DBF), Vl (FL)	0.2
H (DBF), Vl (FL)	3.1
M (DBF), Vl (FL)	15.3
L (DBF), Vl (FL)	2.5
Vl (DBF, FL)	2.4

Furthermore all the above elements-at-risk are expected to experience shaking intensity of MM 9 from a M8 AF earthquake. Most of the populated areas and road network are located on recent alluvial soils classified in subsoil category D (NZS 1170.5:2004) and may experience very strong ground shaking and liquefaction due to low shear-wave velocities associated with these soft, deep sediment deposits.

Table 5.7 Populated areas exposed to debris-flows and floods (populated areas dataset was obtained from: http://koordinates.com/layer/3658-nz-populated-places-polygons/).

Susceptibility	Populated areas (m^2, % area affected)									
	Franz Josef	Fox Glacier	Hokitika	Whataroa	Kaniere	Haast	Harihari	Ross	Bruce Bay	Okarito
Vl (DBF), Vh (FL)	31250 (20)	86875 (59.7)	1295625 (78)	128750 (100)	135625 (68.9)	116875 (67.3)	199375 (89.9)	-	25000 (100)	165625 (99.6)
Vh (DBF), H (FL)	-	2500 (1.7)	-	-	-	-	-	-	-	-
M (DBF), H (FL)	6875 (4.4)	2250 (15.5)	-	-	-	-	13125 (5.9)	-	-	-
L (DBF), H (FL)	-	1875 (1.3)	20000 (1.2)	-	-	-	5000 (2.3)	1250 (0.4)	-	-
Vl (DBF), H (FL)	106875 (68.4)	20000 (13.7)	341250 (20.6)	-	61250 (31.1)	56875 (32.7)	1875 (0.8)	319375 (98.5)	-	625 (0.4)
Vh (DBF), M (FL)	-	5625 (3.9)	-	-	-	-	-	-	-	-
M (DBF, FL)	-	5625 (3.9)	-	-	-	-	-	-	-	-
L (DBF), M (FL)	-	625 (0.4)	-	-	-	-	-	625 (0.2)	-	-
Vl (DBF), M (FL)	-	-	-	-	-	-	-	3125 (1)	-	-
M (DBF), Vl (FL)	10625(6.8)	-	-	-	-	-	2500 (1.1)	-	-	-
Vl (DBF, FL)	625 (0.4)	-	3125 (0.2)	-	-	-	-	-	-	-
Total area (m^2)	156250	145625	1660000	128750	196875	173750	221875	324375	25000	166250

With regard to co-seismic landsliding exposure, Franz Josef, Fox Glacier and Harihari are located close to the mountain-front and are highly susceptible to potential rock avalanches. Additionally, approximately 130 km of the principal highways are also less than 4km (Round Top rock avalanche estimated runout) distance from the mountain-front and are thus at risk from long runout seismically-induced rock avalanches.

5.4 Discussion – conclusions

Acknowledging the challenges of effective hazard assessment in highly dynamic environments such as tectonically active mountains, an approach for multi-hazard analysis is developed and applied in western Southern Alps. The approach aims to provide a conceptual framework of the key tasks underlying effective hazard and risk analysis in environments where geomorphic processes and consequent hazards are strongly interrelated. The proposed framework is based on two fundamental characteristics of complex systems, these are: (1) a system consists of multiple interactive components and (2) the interactions give rise to emergent properties which do not correspond to the sum of the individual components of observed system (Bründl et al. 2010; Keiler 2011). Therefore, multi-hazard analysis involves the concepts of both interaction and emergent properties (cascade effects) which are not identified by single hazard assessments or by just summing the various single processes.

The procedure developed in this study comprises seven consecutive stages that bring together geomorphology, hazards and GIS in order to evaluate hazard and risk from multiple geomorphic processes and provide a simple way to communicate the complexity of multi-hazard and risk assessment to decision makers, emergency managers and stakeholders. The key strengths of the approach are summarized below. The implementation of geomorphology at the initial stage provides the means to investigate the interplay between tectonics, climate and surface processes controlling the evolution of dynamic environments and acquire an in-depth understanding of the geomorphic system, its components and the interactions between them. This is especially useful when available data concerning the dominant geomorphic hazards are not available. For example, if no sufficient information exists on active faults and seismic hazard to inform planning, studying the distinct landforms generated by differential uplift rates in tectonically active settings can be used as a reconnaissance tool in assessing regional earthquake hazards. Findings from this fundamental step serve as the basis for the hazard or susceptibility assessments at the next stages.

Particular focus is given to the various types of interactions between processes that indicate the complexity of the environment and the most appropriate multi-hazard assessment approach that

should be followed. An attempt has been made to classify the various interaction types in specific categories: spatial coincidence, common trigger, amplification of magnitude, change in susceptibility during consecutive hazards and cascade effects. However, geomorphic processes often interact in more than one way, thus two hazards triggered by the same event (temporal coincidence) are is very likely to also overlap in space (spatial coincidence) and perhaps have greater magnitude (magnitude amplification). Likewise, by altering the susceptibility to a process after an event (e.g. susceptibility to flooding after a fire) the probability of occurrence of this process also changes.

The proposed approach can be applied focusing on a single hillslope, a catchment or a large region. This provides the user with the flexibility to perform the multi-hazard analysis in different scales depending on the aims and scale of planning as well as the availability of resources.

As previously discussed single hazard assessments are the core of multi-hazard analysis. In this study the outputs from two regional scale susceptibility models were combined focusing on the spatial distribution of rainfall induced debris-flows and river floods rather than on their temporal probabilities. Alternatively if adequate data exist to estimate probabilities the proposed framework can be applied using hazard instead of susceptibility models. This also provides the user with the option to implement the appropriate types of multi-hazard analyses according to the purpose of planning. However, the consistency of the input hazard models throughout the multi-hazard analysis is essential in order to produce comparable outputs.

Additionally, viewing the hazardscape as a system and incorporating hazard mitigation measures in the multi-hazard analysis as system components raises awareness regarding the crucial role of human activity in disaster occurrence and enhances effective risk mitigation in the context of sustainability. Finally, the relatively low data requirements and the capability to produce useful results make the proposed approach suitable for areas with limited available information on hazards.

To demonstrate the practical application of the proposed approach, a regional multi-hazard analysis was carried out in the central WSA. The processes considered in the case study were mainly rainfall induced shallow landslides/debris flows and river flooding. The impacts of a potential Alpine fault earthquake and consequent co-seismic landsliding were also considered and the findings were discussed in relation to the spatial distribution of the rainfall triggered debris-flow and river flood susceptibilities. The output from the joint analysis of shallow landslides and river floods provides information not available from single hazard assessments. For instance, the final map reveals areas characterized by high river flood and debris-flow susceptibilities, which are likely to be affected by at

least one geomorphic hazard during a heavy rainfall. These areas demonstrate the highest total susceptibility and they have to be prioritized in terms of hazard mitigation. Furthermore, this information can be useful to identify locations with the *lowest* combined susceptibility suitable for development or relocation of existing infrastructures in the context of hazard risk reduction through land-use planning. These are generally gentle-slope elevated areas away from the mountain-front and steep hillslopes, often located on the glacial moraines between major floodplains (Fig. 5.13).

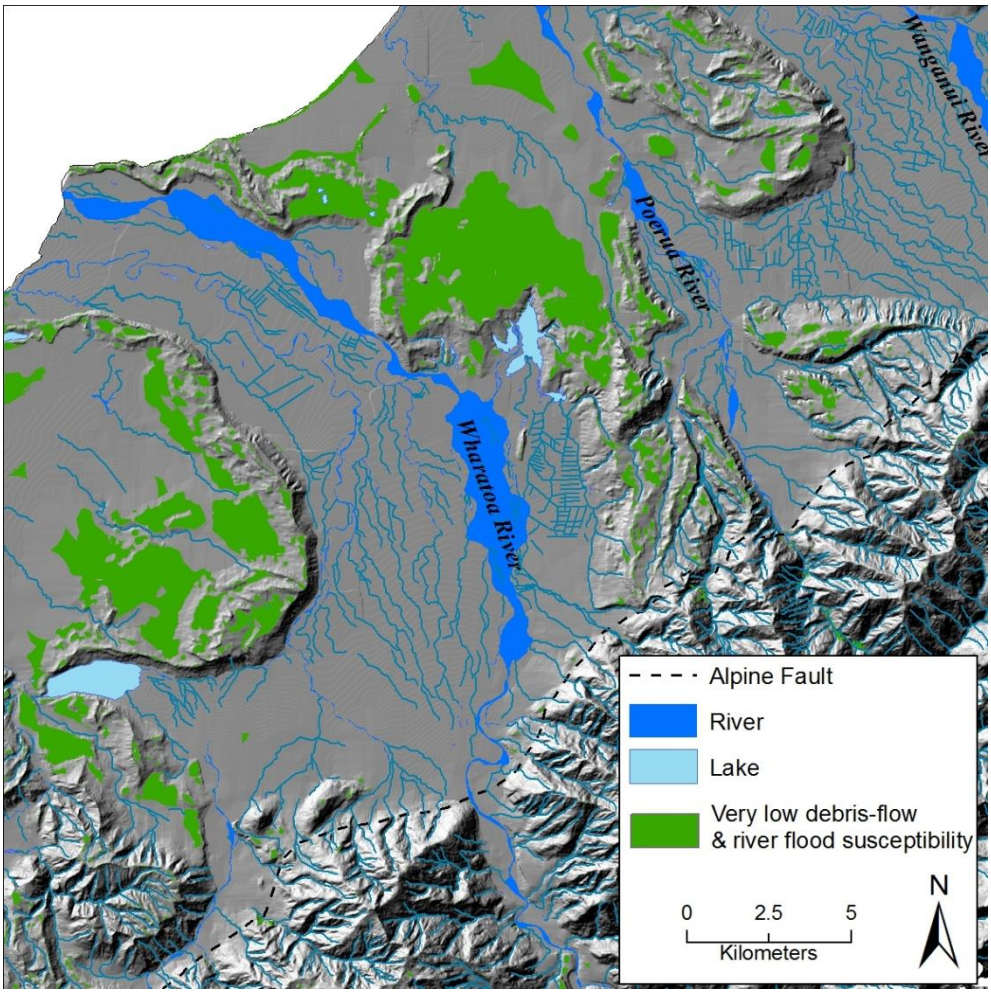

Figure 5.13 Areas with the lowest total susceptibility are mainly located on glacial moraines that offer gentle-slope elevated terrain away from steep hillslopes.

Conversely areas associated with fan deposits, especially those in close proximity to the mountain-front, demonstrate the *highest* susceptibility to multiple geomorphic hazards. These areas are the least suitable for directing future development. The low-gradient, semi-cone-shaped deposits that form where sediment transported by streams exits from the steep, narrow mountain valleys and accumulates on floodplains immediately east of the Alpine Fault, are particularly prone to debris-flows, aggradation and flooding. In terms of ground shaking fan formations are mainly composed by soft, deep, recent alluvial soils and may experience stronger shaking compared to sites underlain by

rock. Also their proximity to the mountain-front significantly increases their susceptibility to co-seismic rock avalanches.

The exposure analysis results indicate that significant lengths of main lifelines (road network, powerlines) and almost all populated areas are exposed to flooding. Flooding, either rainfall-induced or as a consequent effect of earthquakes, landslides and sediment input, is the most frequently occurring hazard in the region. A considerable length of the road network is also exposed to debris flows. An interesting outcome however, concerns locations susceptible to both debris flows and flooding. These locations have the highest total risk to rainfall-induced geomorphic processes. Further, all infrastructure and populated areas are exposed to seismic hazard and strong ground shaking in the event of a M8 AF earthquake. Additionally, two of the most popular tourist attractions in South Island, Franz Josef and Fox Glacier townships, due to their close proximity to the mountain-front, are also potentially exposed to earthquake-triggered rock avalanches (Davies 2007).

However a number of major challenges still remain. The first concerns the comparability and combination of different hazards. Herein, standardizing the processes to a common hazard or susceptibility scale and their combination using a matrix was trialled. The matrix can be extended to integrate up to three processes and derive a unique value of combined relative susceptibility for each location. However, this is a simplification that involves many uncertainties when transforming, for example, flood depth, PGA or landslide occurrence into hazard or susceptibility classes. So, the outputs from different hazard models are still very difficult to combine unless a similar methodology for their assessment is applied.

Linking various hazard assessments is also subject to propagation of uncertainty. As the different assessments are connected through their outputs, the uncertainty from the first model propagates and increases as the chain of events grows. Thus, flood depth and extent from a dam-break flood will include the uncertainties of the seismic hazard, rock avalanche and dam-break flood models. To overcome this major limitation the uncertainties must be estimated at each stage and linked. This task requires separate analyses in order to model the uncertainties which at the current stage are extremely difficult due to the complexity of the geomorphic processes and limitations of their modelling procedures.

Another challenge stems from the system's boundaries. Despite the assumption that the system functions within its hypothetical boundaries, it is still linked and interacts with other systems. As a result hazard, susceptibility and risk are dynamic, as changes occur in the hazard processes, human activities and the environment in response to external perturbations such as global changes.

Finally, incorporating non-quantifiable components such as social and cultural vulnerabilities that potentially affect the system's resilience is still a major challenge. Within the system's boundaries these components might significantly change the exposure to geomorphic hazards as they interact with the other sub-systems.

The proposed approach does not provide a complete solution to the extremely challenging task of hazard and risk analysis in highly dynamic environments, as further research needs to be done to address the above limitations and incorporate more processes and interactions at different scales. However, as an initial attempt at a multi-hazard analysis, it has yielded useful indications of the way forward.

5.5 References

Adams J 1980. Paleoseismicity of the Alpine fault seismic gap, New Zealand: Geology, v. 8, p. 72–76.

Alexander D 2001. Encyclopedia of environmental science, Chapter Natural hazards. Kluwer Academic Publishers.

Ambrose JE, Vergun D 1995. Simplified building design for wind and earthquake forces, Wiley, New York. 368p.

Arnaud-Fassetta G, Cossart E, Fort M 2005. Hydro-geomorphic hazards and impact of man-made structures during the catastrophic flood of June 2000 in the Upper Guil catchment (Queyras, Southern French Alps). Geomorphology, 66, 41–67.

Ashby WR 1956. An Introduction to Cybernetics, Chapman & Hall, London, 1956, 295p. Internet (1999): http://pcp.vub.ac.be/books/IntroCyb.pdf

Athanasopoulos GA, Pelekis PC, Leonidou EA 1999. Effects of surface topography on seismic ground response in the Egion (Greece) 15 June 1995 earthquake. Soil Dynamics and Earthquake Engineering, 18(2): 135-149.

Axelrod C, Killam, PP, Gaston, MH (1994). Primary health care and the Midwest flood disaster. Public Health Report, 109 (Sept./Oct.), 601–605.

Becker J, Saunders W, Hopkins L, Wright K, Kerr J 2008. Pre-event recovery planning for land-use in New Zealand: An updated methodology. GNS Science Report 2008/11. 39 p.

Bell R, Glade T 2004. Multi-hazard analysis in natural risk assessments.- In: Brebbia C.A. (ed): International Conference on Computer Simulation in Risk Analysis and Hazard Mitigation. WIT Press, 26.-29. September, Rhodes (GR), 197-206.

Benn JL 1990. A Chronology of Flooding on the West Coast, South Island, New Zealand: 1846 – 1990. The West Coast Regional Council, Greymouth. 159p

Benn JL 1992. Review of Earthquake Hazards on the West Coast. The West Coast Regional Council, Greymouth. 62p.

Benn JL 2005. Landslide events on the West Coast, South Island, 1867-2002. New Zealand Geographer 61: 3-13.

Berryman K, Cooper AF, Norris RJ, Sutherland R, Villamor P 1998. Paleoseismic investigation of the Alpine Fault at Haast and Okuru. Geological Society of New Zealand Miscellaneous Publication, 101A, 44.

Berryman KR, Cochran UA, Clark KJ, Biasi GP, Langridge RM, Villamor P 2012. Major Earthquakes Occur Regularly on an Isolated Plate Boundary Fault. Science 336, 1690. DOI: 10.1126/science.1218959.

Brabb EE 1984. Innovative approaches to landslide hazard and risk mapping, Proceedings of the 4th International Symposium on Landslides, 16–21 September, Toronto, Ontario, Canada (Canadian Geotechnical Society, Toronto, Ontario, Canada), 1:307–324.

Bründl M, Bartelt P, Schweizer J, Keiler M, Glade T 2010. Geomorphological hazards and disaster prevention. Camebridge University Press. Chap. Snow avalanche risk analysis - review and future challenges, 49–61.

Buchanan M 1996. ‘‘Is earthquake prediction just literature?’’ New Statesman, 130, 16–17.

Buech F, Davies TR, Pattinga JR 2010. The Little Red Hill Seismic Experimental Study: Topographic Effects on Ground Motion at a Bedrock-Dominated Mountain Edifice. Bulletin of the Seismological Society of America, 100(5A): 2219–2229, doi: 10.1785/0120090345.

Bull WB 1996. Prehistorical earthquakes on the Alpine fault, New Zealand: Journal of Geophysical Research, v. 101, no. B3, p. 6037–6050, doi:10.1029/95JB03062.

Burby RJ 1998. Natural hazards and land use: an introduction. In: Burby RJ (ed) Cooperating with nature: confronting natural hazards with land-use planning for sustainable communities. Joseph Henry Press, Washington, DC, pp 1–26.

Burby RJ, Deyle RE, Godschalk DR, Olshansky RB, 2000. Creating hazard resilient communities through land-use planning. Natural Hazards Rev. Vol.1, Issue 2, 99 – 106.

Central American Probabilistic Risk Assessment (CAPRA) 2013. http://www.ecapra.org/ (accessed 23 April 2013).

Carpignano A Golia E Di Mauro C Bouchon S and Nordvik J-P (2009) A methodological approach for the definition of multi-risk maps at regional level: first application. J Risk Res 12:513–534.

Chorley RJ 1962. Geomorphology and General Systems Theory. Theoretical papers in the hydrologic and geomorphic sciences. US Geological Survey Professional Paper 500-B.

Clinton JJ, Hagebak BR, Sirmons JG 1995. Lessons from the Georgia floods. *Public Health Reports 110* (Nov./Dec.), 684-688.

Comfort LK 1994. Self-organization in complex systems. J. Public Admin. Res. Theory, 4, 393–410.

Davies TRH 2002. Landslide dambreak flood hazards at Franz Josef Glacier township, NewZealand: a risk assessment. Journal of Hydrology (New Zealand) 41: 1-17.

Davies TR, McSaveney MJ, Clarkson PJ 2003. Anthropic Aggradation of the Waiho River, Westland, New Zealand: Microscale Modelling. Earth Surf. Process. Landforms 28, 209–218.

Davies TR, McSaveney MJ, Doscher C 2005. Final Report on Research Project No. 03/499 Monitoring and effects of landslide-induced aggradation in the Poerua Valley, Westland. Earthquake Commission, Wellington, N.Z.

Davies TR, McSaveney MJ 2006. Geomorphic constraints on the management of bedload dominated rivers. Journal of Hydrology (New Zealand) 45 (2): 69-88.

Davies TR 2007. Potential for rock avalanche hazard at Franz Josef Glacier village, Westland. Confidential report to West Coast regional council. Natural Hazard Research Center, Department of Geological Sciences, University of Canterbury, New Zealand. 14 p.

Davies TR, Manville V, Kunz M, Donadini L 2007. Modeling Landslide Dambreak Flood Magnitudes: Case Study. Journal of hydraulic engineering. doi: 10.1061/(ASCE)0733-9429(2007)133:7(713).

Davis LL, West LR 1973. Observed effects of topography on ground motion. Bull. Seismol. Soc. Am. 63, 283–298.

De Graff JV, Cannon SH, Gallegos AJ 2007. Reducing post-wildfire debris flow risk through the burned area emergency response (BAER) process. In: Proceedings of the 1st North American Landslide Conference, AEG Special Publication no. 23.

Delmonaco G, Margottini C, Serafini S 1999. Multi-hazard risk assessment and zoning: an integrated approach for incorporating natural disaster reduction into sustainable development. TIGRA (The Integrated Geological Risk Assessment) Project (Env4-CT96-0262) Summary Report.

Delmonaco G, Margottini C, Spizzichino D 2006. ARMONIA methodology for multi-risk assessment and the harmonisation of different natural risk maps. Deliverable 3.1.1, ARMONIA.

De Pascale GP, Langridge RM 2012. New on-fault evidence for a great earthquake in A.D. 1717, central Alpine fault, New Zealand. Geology, doi: 10.1130/G33363.1.

De Pippo T, Donadio C, Pennetta M, Petrosino C, Terlizzi F, Valente A 2008. Costal hazard assessment and mapping in Northern Campania, Italy. Geomorphology, 97, 451–466.

Drabek TE 1986. Human system responses to disaster: An inventory of sociological findings, Springer, New York, 479 p.

DTec Consulting Ltd 2002. West Coast Regional Council: Natural Hazards Review. Report prepared for West Coast Regional Council by Dtec Consulting Ltd. Client Reference: 1065.136WCRC, Greymouth. 140 p.

Dufresne A, Davies TR, McSaveney MJ 2009. Influence of runout-path material on emplacement of the Round Top rock avalanche, New Zealand. Earth Surface Processes and Landforms. DOI: 10.1002/esp.1900.

Dunbar P, McCullough H, Mungov G, Varner J, Stroker K 2011. 2011 Tohoku earthquake and tsunami data available from the National Oceanic and Atmospheric Administration/National Geophysical Data Center, Geomatics, Natural Hazards and Risk, 2:4, 305-323.

Ericksen NJ, Berke PR, Crawford JL, Dixon JE 2004. Plan-making for sustainability: The New Zealand experience. Ashgate, Aldershot, 350 pp

European Commission DG XII, Environment and Climate Program, 2000. TEMRAP: The European Multi-Hazard Risk Assessment Project, contract ENV4-CT97-0589.

European Commission 2010. Commission staff working paper: "Risk assessment and mapping guidelines for disaster management", European Commission, Brussels, December 2010.

FEMA 1997. Multi hazard identification and risk assessment: a cornerstone of the national mitigation strategy, 1th Edition, United States.http://www.fema.gov/library/viewRecord.do?id=2214

FEMA 2004. HAZUS-MH. FEMA's Methodology for Estimating Potential Losses from Disasters. US Federal Emergency Management Agency. http://www.fema.gov/hazus (accessed 19 April 2013)

Forrester JW 1961. Industrial Dynamics, Cambridge, MA: Productivity Press. 464 pp

Forrester J W 1969. Urban Dynamics, Cambridge, MA: Productivity Press. 285 pp.

Garcia-Aristizabal A, Marzocchi W (primary authors), 2011. Review of existing procedures for multi-hazard assessment. Deliverable D3.1 of MATRIX project (New methodologies for multihazard and multi-risk assessment methods for Europe), Grant agreement No. 265138.

Gillespie DF, Banerjee MM 1993. Prevention planning and disaster preparedness. J. Appl. Social Sci., 17(2), 237–253.

Glavovic BC, Saunders WS, Becker JS 2010. Land-use planning for natural hazards in New Zealand: the setting, barriers, 'burning issues' and priority actions. Nat Hazards, doi: 10.1007/s11069-009-9494-9.

Gorum T, Fan X, van Westen CJ, Huang RQ, Xu Q, Tang C, Wang G 2011. Distribution pattern of earthquake-induced landslides triggered by the 12 May 2008 Wenchuan earthquake. Geomorphology, 133, 152–167.

Griffiths GA, McSaveney MJ 1983. Distribution of mean annual precipitation across some steepland regions of New Zealand: New Zealand Journal of Science, v. 26, p. 197–209.

Gude M, Barsch D 2005. Assessment of geomorphic hazards in connection with permafrost occurrence in the Zugspitze area (Bavarian Alps, Germany). Geomorphology, 66, 85–93.

Hancox GT, McSaveney MJ, Manville VR, Davies TRH 2005. The October 1999 Mt Adams rock avalanche and subsequent landslide dam-break flood and effects in Poerua River, Westland, New Zealand. New Zealand Journal of Geology & Geophysics 48: 683-705.

Havenith H-B., Vanini M, Jongmans D, Faccioli E 2003. Initiation of earthquake-induced slope failure: influence of topographical and other site specific amplification effects, J. Seismol. 7, 397–412.

Herman F, Braun J 2006. Fluvial response to horizontal shortening and glaciations: A study in the Southern Alps of New Zealand. J. Geophys. Res., 111, F01008, doi:10.1029/2004JF000248.

Hewitt K, Clague JJ, Orwin JF 2008. Legacies of catastrophic rock slope failures in mountain landscapes. *Earth-Science Reviews* 87, 1-38.

Hovius N, Stark CP, Allen PA 1997. Sediment flux from a mountain belt derived from landslide mapping. Geology 25, 231– 234.

Huang R, Fan X 2013. The landslide story Nature Geoscience, 6 (5), 325-326.

Jacobson AD, Blum JD, Chamberlain CP, Craw D, Koons PO 2003. Climatic and tectonic controls on chemical weathering in the New Zealand Southern Alps. Geochimica et Cosmochimica Acta, Vol. 67, No 1, pp. 29-46.

Kanaori Y 1997. Earthquake proof design and active faults, Elsevier, Amsterdam. 268p.

Kappes M, Keiler M, Glade T 2010. From single- to multi-hazard risk analyses: a concept addressing emerging challenges.- In: Malet J.-P., Glade T. & Casagli N. (Editors): Proceedings of the International Conference 'Mountain Risks: Bringing Science to Society', Firenze, 24-26 November 2010, 351-356.

Kappes MS, Gruber K, Frigerio S, Bell R, Keiler M, Glade T 2012. The MultiRISK platform: The technical concept and application of a regional-scale multihazard exposure analysis tool. Geomorphology, 151–152, 139–155.

Keefer DK 1984. Landslides caused by earthquakes, Bull. Geol. Soc. Am., 95(4), 406.

Keiler M 2011. Geomorphology and complexity – inseparably connected? Zeitschrift für Geomorphologie Vol. 55, Suppl. 3, 233-257.

Kim DH 1994. Systems thinking tools: A user's reference guide, Pegasus Communications, Cambridge, 55p.

Korup O 2005. Geomorphic hazard assessment of landslide dams in South Westland, New Zealand – fundamental problems and approaches. Geomorphology 66, 167-188. doi:10.1016/j.geomorph.2004.09.013.

Korup O, Tweed F 2007. Ice, moraine, and landslide dams in mountainous terrain. Quaternary Science Reviews 26, 3406–3422.

Larsen SH, Davies TRH 2005. A possible coseismic landslide origin of late Holocene moraines of the Southern Alps, New Zealand. New Zealand Journal of Geology and Geophysics, Vol. 48: 311-314.

Laszlo A, Krippner S 1998. Systems theories: Their origins, foundations and development, in J. Scott Jordon (ed.), Systems Theories and a Priori Aspects of Perception, Amsterdam: Elsevier: 47–74.

LeBrun B, Hatzfeld D, Bard PY, Bouchon M 1999. Experimental study of the ground motion on a large scale topographic hill in Kitherion (Greece), J. Seismol. 3, 1–15.

Lee C-T 2013. Re-Evaluation of Factors Controlling Landslides Triggered by the 1999 Chi–Chi Earthquake. In: Earthquake-Induced Landslides. Proceedings of the International Symposium

on Earthquake-Induced Landslides, Kiryu, Japan, 2012 (eds) Keizo Ugai , Hiroshi Yagi , Akihiko Wakai: Springer Berlin Heidelberg, pp 213-224.

Li L, Simonovic SP 2002. System dynamics model for predicting floods from snowmelt in North American prairie watersheds. Hydrol. Process. 16, 2645–2666.

Luino F 2005. Sequence of instability processes triggered by heavy rainfall in the northern Italy. Geomorphology, 66, 13–39.

Malamud BD, Turcotte DL, Guzzetti F, Reichenbach P 2004. Landslides, earthquakes, and erosion, Earth Planet. Sc. Lett., 229(1-2), 45-59.

Marzocchi W, Mastellone M, Ruocco A Di, Novelli P, Romeo E, Gasparini P 2009. Principles of multi-risk assessment: interactions amongst natural and man-induced risks. European Commission.

Marzocchi W, Garcia-Aristizabal A, Gasparini P, Mastellone ML, Di Ruocco A 2012. Basic principles of multi-risk assessment: a case study in Italy. Natural Hazards, Vol. 62, Issue 2, pp 551-573.

McCahon I, Elms D, Dewhirst R 2006. West Coast Engineering Lifelines Group Study: Alpine fault earthquake scenario. A report prepared for the West Coast Engineering Lifelines Group and the West Coast Regional Council. Greymouth, 204 p.

McSaveney MJ, Davies TR 1998. Natural hazard assessment for the township of Franz Josef Glacier and its environs. Client Report 43714B.10, Institute of Geological and Nuclear Sciences, Lower Hutt, 58 p.

MfE 2008. Meeting the challenges of future flooding in New Zealand. MfE, Wellington, 48 pp

Miles SB, Keefer DK 2009. Evaluation of camel – comprehensive areal model of earthquake-induced landslides. Engineering Geology, 104, 1–15.

Mileti DS 1999. Disasters by Design: A reassessment of natural Hazards in the United States. Washington, D.C. Joseph Henry Press. 351p.

Norris RJ, Cooper AF 2000. Late Quaternary slip rates and slip partitioning on the Alpine Fault, New Zealand. *Journal of Structural Geology 23*: 507–520.

Patterson K, Boehm S 1992. How can human service agencies be ready? Public Welfare, 50 (4), 6–9.

Phillips JD 2003. Sources of nonlinearity and complexity in geomorphic systems. Progress in Physical Geography 27, 1, pp. 1–23.

Platt RH 1999. Disasters and democracy: The politics of extreme natural events, Island Press, Washington, D.C. 344p.

Reese S, Bell R, King A (2007) RiskScape: a new tool for comparing risk from natural hazards. Water and Atmosphere 15:24–25.

Reiner JM, Spiegelman S 1945. The energetics of transient and steady states, with special reference to biological systems: Phys. Chem. Jour., v. 49, p. 81-92.

Remondo J, Soto J, Gonzalez-Dıez A, de Teran JRD, Cendrero A 2005. Human impact on geomorphic processes and hazards in mountain areas in northern Spain. Geomorphology, 66, 69–84.

Remondo J, Bonachea J, Cendrero A 2008. Quantitative landslide risk assessment and mapping on the basis of recent occurrences. Geomorphology 94: 496-507.

Robinson TR, Davies TRH 2013. Review Article: Potential geomorphic consequences of a future great (Mw = 8.0+) Alpine Fault earthquake, South Island, New Zealand. Nat. Hazards Earth Syst. Sci., 13, 2279–2299.

Saunders W, Forsyth J, Johnston D, Becker J 2007. Strengthening linkages between land-use planning and emergency management in New Zealand. Aust J Emerg Manag 22(1):36–43.

Schiff AJ 1995. Northridge earthquake: Lifeline performance and post-earthquake response, ASCE, New York. 339p.

Schmeidl S, Jenkins JC 1998. The early warning of humanitarian disasters: Problems in building an early warning system. Int. Migr. Rev., 32(2), 471–486.

Schmidt-Tomé P, Kallio H, Jarva J, Tarvainen T, Greiving S, Fleischhauer M, Peltonen L, Kumpulainen S, Olfert A, Schanze J, Bärring L, Persson G, Relvão AM, Batista MJ, 2006. The Spatial Effects and Management of Natural and Technological Hazards in Europe (ESPON) project 1.3.1. Geological Survey of Finland (http://www.espon.lu – last visited: July 2011).

Schmidt J, Matcham I, Reese S, King A, Bell R, Henderson R, Smart G, Cousins J, Smith W, Heron D 2011. Quantitative multi-risk analysis for natural hazards: a framework for multi-risk modeling. Nat Hazards 58(3):1169-1192.

Selva J 2013. Long-term multi-risk assessment: statistical treatment of interaction among risks. Natural Hazards, 67(2), 701-722, DOI: 10.1007/s11069-013-0599-9.

Shulmeister J, Davies TR, Evans DJA, Hyatt OM, Tovar DS 2009. Catastrophic landslides, glacier behaviour and moraine formation – A view from an active plate margin. Quaternary Science Reviews 28: 1085–1096.

Shroder JF, Bishop MP 2004. Mountain geomorphic systems. In Bishop MP, Shroder JF ed. Geographic Information Science and Mountain Geomorphology. Chichester UK, Springer, Praxis Publishing. Pp. 33-66.

Spudich PA, Hellweg M, Lee WHK 1996. Directional topographic site response at Tarzana observed in aftershocks of the 1994 Northridge, California, earthquake: Implications for mainshock motions, Bull. Seismol. Soc. Am. 86, (1 Part B, suppl.), 193–208.

Sutherland R, Eberhart-Phillips D, Harris RA, Stern T, Beavan J, Ellis S et al. 2007. Do great earthquakes occur on the Alpine Fault in central South _Island, New Zealand? Geophysical Monograph, SIGHT, 175, 235-251.

Tang C, Zhu J, Qi Z, Ding J 2011 Landslides induced by the Wenchuan earthquake and the subsequent strong rainfall event: A case study in the Beichuan area of China, Eng. Geol. doi:10.1016/j.enggeo.2011.03.013

Tate E, Burton CG, Berry M, Emrich CT, Cutter SL 2011. Integrated Hazards Mapping Tool. Transactions in GIS, 15(5): 689–706.

Tovar DS, Shulmeister J, Davies TR, 2008. A landslide origin of the New Zealand's Waiho Loop Moraine. Nature Geosciences 10.1038/ngeo249.

Van Westen CJ, Montoya L, Boerhoom L, Coto EB 2002. Multi-hazard Risk Assessment using GIS in Urban areas: A case study for the city of Turrialba, Costa Rica. Proceedings of Regional Workshop on Best Practices in Disaster Mitigation, Lessons learned from the Asian Urban Disaster Mitigation Program and other initiatives, 24-26 September, Bali, Indonesia, 53-72.

Van Westen CJ 2010. GIS for the assessment of risk from geomorphological hazards. In: Alcantara-Ayala I, Goudie A ed. Geomorphological hazards and disaster prevention. Cambridge, Cambridge University Press, pp. 205-218.

Van Westen C, Kappes MS, Luna BQ, Frigerio S, Glade T, Malet JP 2014. Medium-scale multi-hazard risk assessment of gravitational processes. In Van Asch T, Corominas J, Greiving S, Malet JP, Sterlacchini S ed. Mountain Risks: From Prediction to Management and Governance. Advances in Natural and Technological Hazards Research. Springer Netherlands, pp. 201-231.

Varnes DJ 1984. Landslide Hazard Zonation: a review of principles and practice. Commission on landslides of the IAEG, UNESCO, Nat Hazards 3:61

von Bertalanffy L 1951. An outline of general system theory: Jour. British Phil. Sci., v. 1, p. 134-165.

von Bertalanffy L 1952. Problems of life: Watts and Co., London, 216 p.

von Bertalanffy L 1968. General system theory: Essays on its foundation and development, rev. ed. New York: George Braziller.

Waddington CH 1977. Tools for thought. Jonathan Cape, London 250p.

Wald DJ, Allen TI 2007. Topographic Slope as a Proxy for Seismic Site Conditions and Amplification, B. Seismol. Soc. Am., 97(5), 1379–1395, doi:10.1785/0120060267.

Wallace WA, De Balogh F 1985. Decision support systems for disaster management. Public Admin. Rev., 45 (special issue), 134– 46.

Wells A, Goff J 2007. Coastal dunes in Westland, New Zealand, provide a record of paleoseismic activity on the Alpine fault: Geology, v. 35, p. 731–734, doi:10.1130/G23554A.1.

Wells A, Yetton MD, Duncan RP, Stewart GH 1999, Prehistoric dates of the most recent Alpine fault earthquakes, New Zealand: Geology, v. 27, p. 995–998, doi:10.1130/0091-7613(1999)027<0995:PDOTMR>2.3.CO;2.

Welsh A, Davies T 2011. Identification of alluvial fans susceptible to debris-flow hazards. Landslides 8:183–194.

West Coast Regional Council (WCRC) 2010. Report on West Coast Weather Event 27 & 28 December 2010. 43p.

Whitehouse IE, Griffiths GA 1983. Frequency and Hazard of Large Rock Avalanches in the Central Southern Alps, New Zealand. Geology, Vol. 11, pp 331-334.

Whitehouse IE 1988. Geomorphology of the central Southern Alps, New Zealand: the interaction of plate collision and atmospheric circulation. Zeitschrift fur Geomorphologie Supplement Band N.F 69, 105– 116.

Wiener N 1954. The Human Use of Human Beings: Cybernetics and Society. Houghton Mifflin, 1950. Second Edition Revised, Doubleday Anchor, 1954, 199p.

Wilford DJ, Sakal ME, Innes JL, Sidle RC, Bergerud WA (2004) Recognition of debrisflow, debris-flood and flood hazard through watershed morphometrics. Landslides 1:61–66.

Wobus CW, Whipple KX, Kirby E, Snyder NP, Johnson J, Spyropolou K, Crosby B, Sheehan D 2006. Tectonics from topography: Procedures, promise, and pitfalls, in Willett, S.D., Hovius, N., Brandon, M.T., and Fisher, D.M., editors, Tectonics, Climate, and Landscape Evolution, Geological Society of America Special Paper 398, p. 55-74, doi: 10.1130/2006.2398(04).

Wright CA 1999. The AD 930 long-runout Round Top debris avalanche, Westland, New Zealand. New Zealand Journal of Geology and Geophysics 41: 493–497.

Yetton MD 1998. Progress in understanding the paleoseismicity of the central and northern Alpine Fault, Westland, New Zealand. New Zealand Journal of Geology & Geophysics, Volume 41: 475-483.

Yetton MD, Wells A, Traylen NJ 1998. The Probability and Consequences of the Next Alpine Fault Earthquake. EQC Research Report 95/19 Prepared by Geotech Consulting Ltd, Christchurch. 161p.

Yetton MD 2000. The probability and consequences of the next Alpine Fault earthquake, South Island, New Zealand. Unpublished Ph.D. thesis, Christchurch, New Zealand, University of Canterbury, 312 p.

Zarn B, Davies TR 1994. The significance of processes on alluvial fans to hazard assessment. Zeitschrift fór Geomorphologie 38: 487-500.

Zhang Y, Chen G, Zheng L, Li Y 2013. Numerical analysis of the largest landslide induced by the Wenchuan earthquake, may 12, 2008 using DDA. In: Earthquake-Induced Landslides. Proceedings of the International Symposium on Earthquake-Induced Landslides, Kiryu, Japan, 2012 (eds) Keizo Ugai , Hiroshi Yagi , Akihiko Wakai: Springer Berlin Heidelberg, pp 617-626.

Chapter 6: Discussion and conclusions

The primary aim of this research project was to develop an approach for the analysis of geomorphic hazards in highly dynamic environments, with particular focus on tectonically active mountains. This aim was approached through four main objectives integrating quantitative geomorphology, hazard assessments and GIS. The first objective was to identify the dominant geomorphic processes, their spatial distribution and interrelationships and explore their implications in hazard assessment and modelling. This was achieved through regional geomorphic analysis based on a GIS analysis using the available DEM. The focus of the analysis was mainly on catchment morphometry and structure of the drainage network, as they are linked to tectonic forcing and contain useful information on differential rock uplift rates across the landscape; in addition as they reflect critical relationships between tectonic, climatic and surface processes. The second and third objectives were to assess the spatial variation of rainfall-generated shallow landslides and river flood susceptibilities respectively. To achieve these objectives a series of GIS-based models were developed, applied and evaluated in western Southern Alps. The final objective was to develop an approach for multi-hazard and risk analysis suitable for highly dynamic environments. The approach aimed to provide a conceptual framework of the key stages underlying effective hazard and risk analysis in environments where geomorphic processes and their hazards are strongly interrelated. The objective was achieved by combining the findings from the previous objectives and developing a seven-stage framework based on the concepts of *interaction* and *emergent properties* (cascade effects) inherent to complex systems. A summary of the key findings from the four main objectives is outlined, followed by a discussion on the implications of this research for land-use planning in the context of sustainable hazard mitigation.

6.1 Regional geomorphic analysis

Results from drainage network, catchment morphometry and channel long profile analyses indicated two distinct geomorphic environments on either side of the Alpine Fault. On the NW side, between the mountain front and the coast, a narrow strip of low-slope terrain occupied by large braided rivers, lakes and glacial moraines is predominantly shaped by fluvial processes, the intensity and character (erosional-depositional) of which is largely controlled by the processes taking place in the upstream catchments SE of the Alpine fault. Between the Alpine Fault and the main divide a narrow

zone of rugged terrain is shaped by fluvial processes, orogrpahically-enhanced precipitation, various types of mass movements (debris-flows, rockfalls and rock avalanches), glaciers and tectonic activity manifested through high uplift rates and earthquakes. These processes interact and affect both the structure of the drainage network and catchment topography creating short, steep, elongated catchments sub-perpendicular to the Main Divide, often occupied in their headwaters by permanent snow and ice. The spatial variations of the mean normalized channel steepness index and valley-floor width valley-height ratio indicate highest relative tectonic activity, expressed through uplift rates, at the central WSA with a decreasing trend to the south.

These findings have significant implications for hazard assessment and modelling. The strongly interrelated geomorphic processes controlling the landscape evolution of the region are the source of geomorphic hazards which are also interrelated. Therefore, effective hazard assessment in such a dynamic landscape requires approaches which incorporate the interactions between geomorphic processes and potential cascade effects.

In rapidly-changing environments the spatial variation and temporal changes of landforms and topographic parameters complicate meaningful hazard modelling. As a result, hazard models based on highly dynamic topographic parameters (e.g. hydraulic models using detailed channel cross-section data to estimate flow velocity, depth and flood extent) are meaningful only for a short period of time and limited spatial extent.

Although earthquakes and intense or prolonged rainfall are considered as the main triggering factors of slope failures in the region, significant landslide events have also occurred without an obvious trigger mechanism (Benn 2005). Several studies (Korup 2006; Hewitt 2006; Hewitt et al. 2008; Korup et al. 2009; Crozier 2009) as well as the present research recognize landslides as fundamental processes of landscape evolution. This significantly affects the predictive capability of landslide models that assume rainfall or earthquakes as the only triggering factors and do not take into account the response of hillslopes to uplift rates and threshold slope angles as a fundamental geomorphic process in landform evolution.

The observation that the central WSA are characterized by the highest uplift rates, which implies a rapidly changing environment affected by various geomorphic processes, and the fact that it is a very popular area with growing annual visitor numbers with the prospect of further development, substantially increase the total risk. This stresses the need for innovative geomorphic hazard assessment methods which can provide reliable quantitative estimation of individual and coupled events to guide land-use planning and hazard mitigation strategies.

Another critical implication concerns the role of human interventions in the form of protection works for hazard mitigation, in the geomorphic system of WSA. In a dynamic open geomorphic system which constantly recovers from various geomorphic disturbances (Hewitt 2006) any interference with the system will trigger a series of other processes in order for the landscape to adjust to the new regime. This implies that engineering controls of geomorphic processes as hazard mitigation options may interfere with the geomorphic system and trigger other processes with potentially adverse effects for human developments. A prominent example of this type of chain reaction in the area is illustrated by Davies et al. (2003, 2013) who observed that the presence of stopbanks at Waiho River, installed as flood mitigation measure, has induced significant riverbed aggradation which has repeatedly damaged the river-control works and reduced their effectiveness. This emphasises that any hazard mitigation approach in order to be effective and sustainable must be seamlessly integrated in the geomorphic system.

6.2 Rainfall-generated shallow landslide susceptibility

The assessment of shallow landslide/debris-flow susceptibility in the western Southern Alps of New Zealand was based on the development of a fuzzy logic model in GIS environment. A GIS-based model was also developed to estimate the runout path and distance of the potential future shallow slope failures. Evaluation of the final output in a test area using an independent population of landslides demonstrated satisfactory predictive capability (AUC ≈ 0.72 ± 0.01). The evaluation results illustrate that the assessment of regional landslide susceptibility using the GIS-based fuzzy logic approach is feasible. Although ten parameters were initially identified as significant factors in generating shallow slope failures in the study area, sensitivity analyses indicated that a six-parameter model including slope angle, lithology, slope aspect, proximity to faults, soil induration and proximity to drainage network demonstrates the highest predictive performance (AUC=0.734). The slightly improved performance compared to the ten-parameter model may be attributed to redundancy of the four excluded factors and/or spatial inaccuracy issues between these information layers and the other input thematic maps that potentially aggravate the prediction of susceptibility. It is also possible that the effect of controlling factors on landslide susceptibility is spatially variable particularly in a regional-scale assessment. Thus, the same factor category (e.g. schist formations or west facing slopes) may affect the susceptibility to different extents across the study area. Interestingly, the spatial variation of rainfall intensity does not appear to be a significant parameter for mapping the spatial variation of rainfall-generated landslide susceptibility in the region. This may be because rainfall intensity varies little across the area studied (the entire area is subject to intense

and prolonged rainfall above critical thresholds), or perhaps because some other rainfall parameter such as mean annual or monthly rainfall has greater significance.

Although the highest susceptibility to debris-flows is generally observed at the steep slopes between the Alpine fault and the main divide, the susceptibility values demonstrate a spatial variation in the NE-SW direction (Fig. 6.1). Relatively higher values are observed at the NE and central sections of the mountain range and lower at the SW. This spatial pattern is captured by the model and it seems to agree with the inferred spatial variation of uplift rates from the regional geomorphic analysis. This observation implies that uplift rates are an important factor in shallow landslide susceptibility and corroborate the role of landslides as landscape evolution processes. The outputs from the runout susceptibility model overlaid by populated areas and road network reveal several locations potentially affected by debris-flows which need to be prioritized in terms of hazard mitigation.

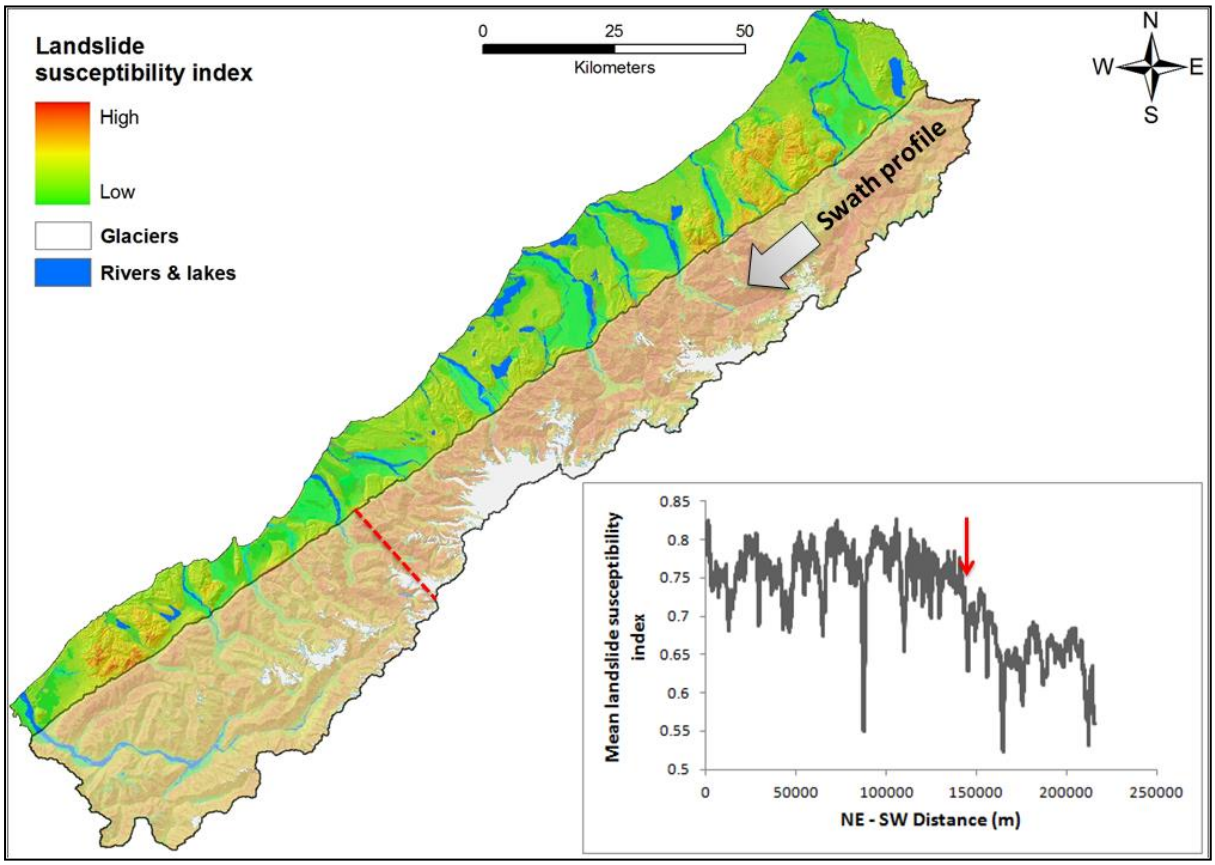

Figure 6.1 NE-SW swath profile between the Alpine fault and the main divide of the Southern Alps. Inset graph shows the variation of mean landslide susceptibility index in NE-SW direction. The distinct sharp decrease of values between high mean susceptibility is due to the effect of large valley-floors. The dotted line on the map indicates where the reduction to systematically lower values occurs.

During the modelling procedure the availability and quality of the landslide inventory were of the utmost importance. The effectiveness and reliability of the final output, derived from statistical relationships between predisposing factors and landslide occurrence, is directly related to the

quality of information of the landslide inventory. Therefore, it is necessary that landslide inventories be developed and updated on a regular basis to ensure continuity of observational information. Furthermore, developing time series of such inventories including measurements of deposit volumes is important for establishing frequency-magnitude relationships and estimating landslide erosion rates.

6.3 River flood susceptibility

A GIS-based spatially distributed unit hydrograph (SDUH) model was developed in order to investigate the hydrologic response of major ungauged catchments in the study area based on their morphometry, land cover and soil characteristics, as well as provide a tool to predict runoff hydrographs using real rainfall intensity data.

The spatial variation of unit peak flow rate normalized by contributing catchment area (Q_p A^{-1}) indicates that steep, relatively short mountainous catchments generate more runoff per unit area compared to larger catchments. Therefore, due to their increased runoff efficiency (greater amounts of precipitation become surface runoff) these catchments have greater potential to generate overbank flows and consequent flooding downstream.

Evaluation results using measured hydrograph data from two catchments illustrate that the GIS-based SDUH is able to predict the peak discharge and time to peak with reasonable accuracy (coefficient of efficiency =0.82, error in peak =-0.43%). However, the predictive performance of the simulated hydrographs varies significantly primarily depending on the method applied to estimate flow velocity and input rainfall data (spatial variation of rainfall characteristics within the catchment).

An approach based on fuzzy logic in GIS environment was also developed, aiming to identify flood-prone areas. The height above nearest drainage, slope gradient, land cover, soil permeability and distance from river channels were used as input parameters as they are related to critical flood characteristics such as flood water velocity, inundation extent, flood duration and flood depth. Evaluation of the final map using a flood event database compiled from various sources showed that the model has very good predictive capability and it can be effectively used to identify flood-prone locations at regional scale. Interpretation of the above findings:

- The extremely high orographically-enhanced precipitation, and the fact that most settlements are located on active floodplains close to rivers that source from steep, short mountain catchments, significantly increasing the flood hazard in the region.

- The high denudation rates due frequent landsliding (Hovius et al 1997; Korup et al. 2005; Korup 2005) in western Southern Alps generate very high sediment input and flux through the drainage network, constantly altering the channels' geometry (width, depth, radius) and their position on the flood plains (braided rivers and fans). Additionally, glacier cover significantly affects catchment hydrological response altering the annual and seasonal flow discharge patterns through the storage and release of precipitation water. These processes make flood hazard assessment in WSA extremely difficult using available modelling approaches. Despite these complexities the proposed approach offers a simple way to predict the peak flow rate and time to peak of ungauged river catchments using real rainfall scenarios, and to identify areas susceptible to flooding at regional scale with reasonable accuracy. Future research should focus on incorporating into flood hazard assessment modelling other critical geomorphic processes such as landslide dam break floods, glacier bursts and river aggradation as well as the impact of large magnitude earthquakes that can induce both landslide dams and river aggradation.

- The development of a comprehensive flood catalogue or inventory that includes the specific geospatial information (i.e., latitude and longitude) of flood events accompanied by parameters such as peak flow discharge and velocity, flood depth, extent and damage, is critical for quantifying the spatial and temporal distribution of flood occurrence as well as in the development of effective flood hazard assessment models.

- Finally, as the flood hazard in the region is controlled by tectonic, climatic and surface processes as well as their interrelationships, flood hazard mitigation activities either through engineering works, flood proofing of buildings and infrastructure or relocation of existing developments, should consider the catchment as a geomorphic system (not only the drainage system) in order to effectively mitigate the impact of flooding in the context of sustainability without inducing other potentially damaging processes (e.g. river aggradation due to flood protection works).

6.4 Regional multi-hazard analysis

The multi-hazard analysis approach developed in this study comprises seven consecutive stages which integrate geomorphology, hazard assessments and GIS in order to evaluate susceptibility and exposure to multiple geomorphic processes. The strengths, limitations and most important findings emerged from the implementation of the multi-hazard analysis approach in western Southern Alps are summarized below.

The proposed approach is based on two fundamental concepts of complex systems, those of *interaction* (cascade effects) and *emergent properties* and recognizes the western Southern Alps as an open geomorphic system with various interrelated components. Therefore, the implementation of geomorphology at the initial stage of the approach is essential in order to investigate the interplay between tectonics, climate and surface processes controlling the landscape evolution of the mountain range and acquire an in-depth understanding of the geomorphic system and its components. This step is especially useful when information concerning the mechanisms, controlling and triggering factors of the dominant geomorphic hazards is not available. Particular attention is given to the various types of interactions between processes that indicate the complexity of the environment and the most appropriate multi-hazard assessment approach that should be followed. An attempt has been made to classify the various interaction types in specific categories: spatial coincidence, common trigger, amplification of magnitude, change in susceptibility during consecutive hazards, and cascade effects. However, geomorphic processes often interact in more than one way requiring various types of interactions to be considered in the assessment.

The proposed approach can be applied focusing on a single hillslope, a catchment or a large region. This provides the user with the flexibility to perform the multi-hazard analysis at different scales depending on the aims and scale of planning as well as the availability of resources.

Single hazard assessments are the core of multi-hazard analysis. Traditionally, hazard assessment is performed by identifying areas potentially affected by a hazard, quantifying the probability of its occurrence and estimating its magnitude. In order to establish the temporal frequency of hazards and quantify the probability of occurrence, accurate and reasonably complete catalogues of historical records are required. However, adequate historical records are not often available to estimate probabilities with useful accuracy for decision making. Furthermore, even if this information exists, a number of implicit assumptions in probabilistic hazard assessments (Davies 1993) may result in misleading conclusions especially in rapidly changing environments. In this study the outputs from two regional-scale *susceptibility* models were combined focusing on the spatial variation of areas potentially affected by rainfall induced debris-flows and river floods rather than on the temporal probabilities of these events. Susceptibility is related to the spatial probability, concerned with identifying areas which will potentially be affected by a geomorphic event given a set of predisposing factors, and does not consider the temporal probability or the magnitude of the event. By not estimating the temporal probability, which always involves a degree of uncertainty, the assessment is not less meaningful. On the contrary, susceptibility provides a more realistic result as it implies that a specific location can be affected by a process anytime, unless the predisposing

factors change. However if adequate data are available to estimate probabilities, the proposed framework can be applied using hazard instead of susceptibility models. This also provides the user with the option to implement the appropriate types of multi-hazard analyses according to the purpose of planning. Nevertheless, consistency of the input hazard models throughout the multi-hazard analysis is essential in order to produce comparable outputs.

The integrated analysis of shallow landslides and river floods provides information not available from single hazard assessments. The final map reveals areas characterized by high river flood and debris-flow susceptibilities, which are likely to be affected by at least one geomorphic hazard during a heavy rainfall. These areas demonstrate the highest total susceptibility and they need to be prioritized in terms of hazard mitigation. In particular, areas associated with fan deposits, especially those in close proximity to the mountain-front, demonstrate the *highest* susceptibility to multiple geomorphic hazards. These areas are the least suitable for future development. The low-gradient, semi-cone-shaped deposits that form where sediment transported by streams exits from the steep, narrow mountain valleys and accumulates on floodplains immediately east of the Alpine Fault, are particularly prone to debris-flows, aggradation and flooding. In terms of ground shaking, fan formations are mainly composed by unconsolidated, deep, recent alluvial materials and may experience stronger shaking compared to sites underlain by rock. Also their proximity to the mountain-front significantly increases their susceptibility to co-seismic rock avalanches. Conversely, areas with the *lowest* combined susceptibility are generally gentle-slope elevated areas away from the mountain-front and steep hillslopes, often located on the glacial moraines between major floodplains.

The exposure analysis results indicate that significant lengths of main lifelines (road network, powerlines) and almost all populated areas are exposed to flooding. Flooding, either rainfall-induced or as a consequent effect of earthquakes, landslides and sediment input, is the most frequently occurring hazard in the region. A considerable length of the road network is also exposed to debris flows. An interesting outcome however, concerns locations susceptible to both debris flows and flooding demonstrating the highest total risk. Further, all infrastructure and populated areas are exposed to seismic hazard and strong ground shaking in the event of a M8 AF earthquake. Additionally, two of the most popular tourist attractions in South Island, Franz Josef and Fox Glacier townships, due to their close proximity to the mountain-front, are also potentially exposed to earthquake-triggered rock avalanches (Davies 2007).

Viewing the hazardscape as a system and incorporating hazard mitigation measures in the multi-hazard analysis as system components raises awareness regarding the crucial role of human activity

in disaster occurrence and promotes sustainable risk mitigation. Finally, the relatively low data requirements and the ability to produce useful results make the proposed approach suitable for areas with limited information on hazards.

However a number of limitations also emerged. The first concerns the comparability and combination of different hazards. Herein, standardizing the processes to a common hazard or susceptibility scale and their combination using a matrix was trialled. The matrix can be extended to integrate up to three processes and derive a unique value of combined relative susceptibility for each location. However, this is a simplification that involves many uncertainties when transforming, for example, flood depth, PGA or landslide occurrence into common hazard or susceptibility classes. So, the outputs from different hazard models are still very difficult to combine unless a similar methodology for their assessment is applied.

Linking various hazard / susceptibility assessment models is inevitably subject to propagation of errors. As the individual assessments are connected through their outputs, the uncertainties of the various input parameters and modelling assumptions propagate in the multi-hazard analysis and often increase as the chain of events grows. Thus, the predicted flood depth and extent from a potential earthquake-generated landslide dam-break event will incorporate the uncertainties of the seismic hazard, rock avalanche and runout as well as dam-break flood assessment models.

Modelling complex physical systems inherently involves various types of uncertainties that affect the predicted system response. Two main sources of uncertainties are common in complex system modelling, the stochastic (aleatory) uncertainty, which results because the system can behave in many different ways and is thus a property of the system itself and the subjective (epistemic) uncertainty which results from a lack of knowledge about the system (Helton 1997). An example of aleatory uncertainty in landslide susceptibility assessment is the spatially variable contribution of a landslide susceptibility controlling factor in the slope instability. Thus the same factor (e.g. schist formations or > 45^{o} slopes) may affect the landslide susceptibility to a different extent within the study area. An example of epistemic uncertainty lies in the selection of the most appropriate modelling approach for landslide or flood susceptibility assessment.

The benefit of making the distinction between stochastic and subjective uncertainties is that, in general, subjective uncertainties can be reduced with improved knowledge, whereas stochastic uncertainties cannot. However, a clear distinction between stochastic and subjective uncertainty is not always possible in that some of the observed stochastic uncertainties could be due to lack of knowledge, resulting from for example, the simplified nature of the landslide susceptibility model.

Error propagation analysis aims to assess how the various types of uncertainties in the modelling process propagate in model calculations to yield an uncertainty range in the output. The multi-hazard approach proposed in this research integrates different susceptibility assessment models and their associated parameters and is subject to a range of stochastic and subjective uncertainty sources such as formulation of conceptual and computational models, selection and processing of input parameters, calculation, interpretation, and representation of the results. Of these, only uncertainties associated with input parameters can be quantified. The input parameters include topographic features, land cover types, geological formations, soil characteristics as well as previous landslide and flood occurrences which have been obtained from different sources with variable accuracies. Input parameters such as the DEM and its derivatives (slope, curvature, slope aspect) have clearly defined errors whereas the accuracy of soil characteristics is highly variable mainly due to the wide variation in map scale and quality of the underlying soil surveys and the limited measurements of soil chemical and physical attributes. Therefore only for a limited number of the input parameters the associated errors are available with meaningful accuracy and can be used in error propagation analysis.

Furthermore, error refers to the disagreement between measured (or predicted) and true or accepted values. This implies a “true” or “acceptable” value is known in order to estimate the error. In a highly dynamic physical system such as the WSA a “true” value is often very difficult to obtain. Thus, although the input 25 m DEM has a known RMS error of 8.15 m, due to the high uplift and denudation rates in the study area this value is more likely to have changed since the development and evaluation of the DEM in 2002.

Despite these limitations, a number of steps have been followed to reduce the effect of several uncertainties to the final output. Fuzzy logic was implemented to minimize spatial uncertainties between conditioning factors and landslide as well as flood occurrence. Sensitivity analyses were performed to assess the impact of changes in input parameters on the models outputs (e.g. landslide susceptibility, simulated runoff hydrographs) and help identify the most important variables which influence the models’ performance. Evaluation procedures using actual observations were also performed to provide a quantitative estimation of models’ predictive capabilities (e.g. success rate curves, coefficient of efficiency, relative volume error, % error in peak). However due to the issues and limitations discussed above a robust assessment of the error propagation from the individual models to the final output was not attempted.

Another limitation is associated with the system’s boundaries. Despite the assumption that the system functions within its hypothetical boundaries, it is still linked to and interacts with other

systems. As a result hazard, susceptibility and risk are dynamic, as changes occur in the hazard processes, human activities and the environment in response to external perturbations such as global changes.

Finally, another challenge involved taking into account non-quantifiable system components such as social and cultural vulnerabilities that affect the system's resilience. Within the system's boundaries these components might significantly change the exposure and risk to geomorphic hazards as they interact with the other sub-systems.

6.5 Land-use planning and sustainable hazard mitigation

The critical role of land-use planning in sustainable hazard mitigation and risk reduction has received increased attention in recent years from both academics and practitioners (Mileti 1999; Burby et al. 2000; Saunders et al. 2007; Becker et al. 2008; CAE 2009, Glavovic et al. 2010). Mileti (1999) states that "No single approach to bringing sustainable hazards mitigation into existence shows more promise at this time than the increased use of sound and equitable land-use management" (pp.155-156). Furthermore, Burby et al. (2000) conclude that "Land-use planning for hazard mitigation is an essential ingredient in any recipe for building disaster-resilient communities" (p.105). They argue that communities with a coherent land-use plan and hazard-mitigation strategy are able to build settlements resistant to natural disasters, able to recover quickly from a natural event, and able to last for many years with little cost to their inhabitants in money or lives. In the New Zealand context, Becker et al. (2008) indicate that pre-event land-use planning is directly related to the first of the 4Rs (risk reduction) and it is also very important to recovery activities (short- and long-term).

Although the role of land-use planning in building sustainable and hazard resilient communities is fundamental, its full potential has yet to be realised (Glavovic et al. 2010). The locations of populated areas and infrastructure in New Zealand are based on historical land-use decisions, and are often prone to a variety of hazards such as floods, landslides and earthquakes. Risk reduction in these areas was achieved traditionally through centralised government action and a tendency to rely on protective works such as flood stopbanks (Ericksen et al. 2000; MfE 2008; Glavovic et al. 2010). These issues are reflected in communities located on the floodplains close to the western Southern Alps mountain-front. Multi-hazard analysis revealed that all populated areas, significant lengths of road network and powerlines are exposed to river floods and high seismic hazard. Additionally, some populated areas and infrastructure are also exposed to debris-flows and co-seismic landslides. Prolonged or high-intensity rainfall repeatedly induces river floods and debris flows with widespread impacts such as road closures, bridge collapses, destroyed buildings and farmland as well as loss of

lives (Benn 2005; DTec 2002). Furthermore, a great Alpine Fault earthquake is expected to induce severe impacts on the region and trigger a range of other geomorphic hazards which will affect the area on various time scales (Hewitt et al. 2008; Robinson & Davies 2013). Dealing with these geomorphic hazards by implementing protective works or by focusing on relief after the disaster clearly does not enhance community resilience and does not lead to effective risk reduction. Therefore there is a pressing need to address risk reduction in a proactive way by implementing sustainable mitigation strategies in order to effectively improve the safety of these communities. However, given the prospect of economic growth and future development along WSA the challenge lies in these communities choosing land use on the basis of susceptibility to multiple geomorphic processes, and not driven only by economic benefits and short-term interests based on the assumption that low-probability risks will not occur in individuals' lifetimes.

In this context an approach delineating low susceptibility / hazard areas suitable for future development is an essential prerequisite. The value of delineating low hazard areas is highlighted by Burby et al. (2000) who argue that "Cities need safety valves for growth pressures, and every jurisdiction with extremely hazardous areas should also have areas of lower hazard designated for development." (p.104). Identifying low hazard / susceptibility areas in a highly dynamic environment that is subject to a variety of interrelated geomorphic hazards can be useful in all phases (pre- and post-event) of emergency management (Kirschenbaum 1996; Mileti & Passerini 1996; Perry & Lindell 1997; Lindell & Prater 2003). In particular, knowing the location of relatively safer sites facilitates activities such as partial or complete relocation of critical infrastructures and communities, establishing temporary emergency operation centres immediately after an event or directing future development in the context of pre-event land use planning.

Since the late nineteenth century in the form of hand-drawn maps, to the present day using artificial intelligence and GIS technologies, the process of identifying the most suitable areas for locating future land uses, known as land-use suitability analysis, enables environmental managers and planners to analyze the interactions between location, development actions, and environmental elements in order to set policies and make decisions regarding the use of land (Collins et al. 2001). In this context, 'Planning for the development of land on or close to active faults' (also known as the Active Fault Guidelines) is a set of guidelines published by the NZ Ministry for the Environment that aim to assist planners, emergency managers, earth scientists and people in the building industry in planning for the avoidance and / or mitigation of fault rupture hazard (Kerr et al. 2003). The guidelines are based on four main principles which recognise that different planning approaches are

required for areas which have not been developed and areas that have already been developed or subdivided. These principles are:

1. Gather accurate active fault hazard information
2. Plan to avoid fault rupture hazard before development and subdivision
3. Consider, and as appropriate, account for the fault rupture hazard in areas already developed or subdivided
4. Communicate risk in built-up areas subject to fault rupture.

The first principle involves data acquisition in order to evaluate the seismic hazard while the second principle aims to determine areas suitable for development by combining information on the seismic hazard with building codes. These assume that adequate information about earthquake characteristics (recurrence interval, magnitude, shaking intensity) can be obtained with meaningful accuracy and the impacts of earthquake-induced geomorphic hazards and other potential cascade effects in short-and long-term time scales are also considered.

The recurrence interval for an earthquake is often determined in terms of the average length of time between events of a certain size. The main drawback with this approach is that limited historical records usually reflect only a fraction of landscape evolution time scales, and are not sufficient for estimating the occurrence of these events with meaningful accuracy for planning purposes. Furthermore, high impact geomorphic events occurring in highly dynamic environments generally trigger other potentially damaging processes that may result in greater impacts than the main event (e.g. co-seismic landslides, landslide dams and dam-break floods, river aggradation).

Note that even with adequate statistical data, the probabilities derived do not accurately represent the future occurrence of events over the short timescales (< a century) of interest to society (Davies, 1993), and thus cannot realistically be used for risk management planning. This is because the number of hazard events that will occur during a century is by definition small, and applying probabilities (no matter how robust) to a small sample cannot result in reliable predictions.

Therefore, land-suitability analyses must not rely only on identifying areas with low probability of hazard occurrence but consider the inherent susceptibility of the landscape to multiple interrelated geomorphic hazards. Herein, in an attempt to address some of these issues, a set of steps is proposed as a framework for land-use suitability analysis in highly dynamic environments by modifying the multi-hazard analysis approach introduced in chapter 5 to focus on low susceptibility areas (Fig. 6.2).

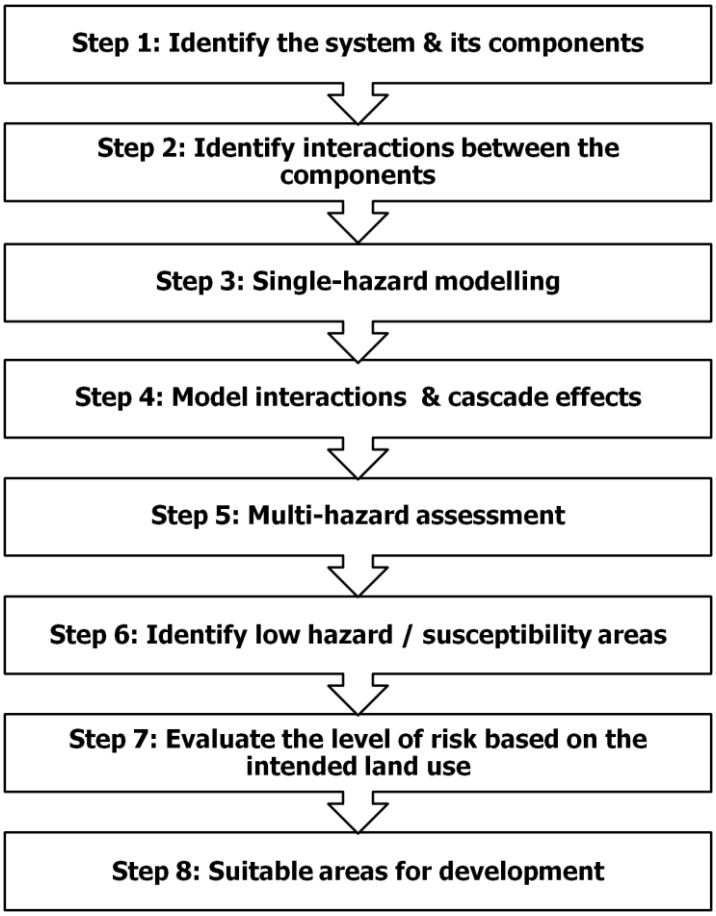

Figure 6.2 Land-suitability analysis approach (based on the multi-hazard analysis framework; Chapter 5)

The steps 1 - 5 aim to evaluate the spatial variation of susceptibility or hazard from multiple processes. Identifying the geomorphic system and its various interconnected components provides understanding of the potential hazards in the context of landscape evolution. In particular, geomorphic analysis provides the means to reconstruct the history of occurrence of past hazardous events, identify potential cascade effects, estimate their frequencies and magnitudes and identify the location of future events. This step is especially useful when available data concerning the dominant geomorphic hazards are not available. Results from geomorphic analysis can then be used to develop susceptibility models that essentially delineate the spatial probability of future events without requiring long time series of records. Next, depending on the identified hazard interaction types and model complexity the individual susceptibility models are combined to yield the spatial variation of total susceptibility in the area. The steps 6 - 8 aim to identify low susceptibility / hazard areas more suitable for development. Key outputs of the multi-hazard analysis performed in WSA are the areas with the *highest* and *lowest* total susceptibilities to multiple geomorphic hazards. In order to identify areas suitable for development, however, the *lowest* total susceptibility areas require further assessment based on their intended land-use to ensure that the consequences from a potential event is acceptable (Fig. 6.3). For example locations with very low debris-flow, very low

flood and high ground shaking susceptibilities may be suitable to be used as farmlands but not for building critical facilities. Finally, the intended land-use needs to be examined as part of the broader geomorphic system to ensure that it will not induce other processes with adverse consequent effects on the community or the environment. For instance, the construction of transport infrastructure, especially roads, at mountainous terrain may increase the landslide susceptibility as a result of undercutting (Petley 2007). The strength of this approach when combined with susceptibility analyses primarily is that it does not depend on multi-temporal data; it accounts for multiple processes; and it can be implemented at a range of scales.

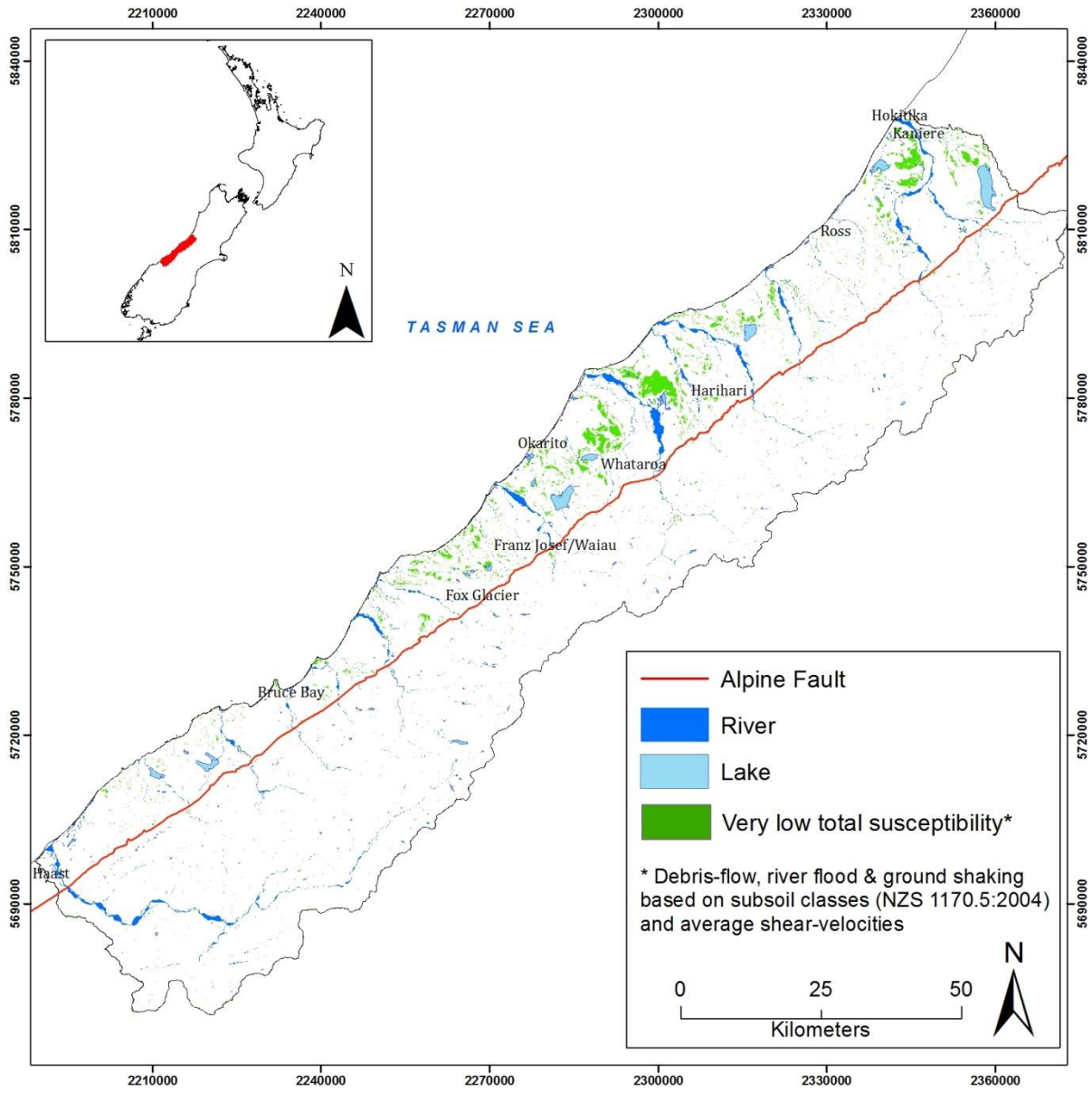

Figure 6.3 Areas with very low relative total susceptibility. These areas cover approximately 2.2% of the study area.

In the WSA case study, the gentle-slope elevated areas located on the glacial moraines between major floodplains demonstrate very low debris-flow and river-flood susceptibilities. Additionally, the sediments which comprise these landforms (mainly glacial-age outwash gravel and till) have generally higher shear-wave velocities compared to recent alluvial deposits, thus may experience relatively lower ground shaking. However, these areas are still exposed to strong shaking from a great Alpine fault earthquake and the intended land-uses have to be further analysed according to steps 7 and 8 of the proposed approach. Moreover, other processes such as climatic and coastal hazards need to be considered before any decision is made. The purpose of the WSA case study was to demonstrate the key stages of multi-hazard analysis in a tectonically-active mountainous environment and its contribution to land-use planning in sustainable hazard mitigation and risk reduction.

6.6 Future research

Several limitations and unresolved issues have been identified in this thesis, which require further research. Below is an outline of future research recommendations within the field of hazard and disaster management. The focus is mainly on landslide and flood hazard assessments as well as multi-hazard analyses.

Assessment of rainfall-generated landslides

Future research should continue to explore new methods concerning regional assessment of rainfall-generated landslide hazard and susceptibility. Efforts should focus on: 1) the development, application and comparison of different landslide hazard and susceptibility methods such as physically-based models, statistical analyses and GIS techniques, 2) investigating different landslide types, 3) exploring the complex relationships between predisposing, triggering factors (e.g. critical rainfall thresholds) and landslide occurrence, 4) improvement of runout and deposition models and 5) developing comprehensive landslide inventories. Progress in these areas will help to reduce some critical uncertainties in the predictive capability of landslide models and increase their reliability in land-use planning and decision making.

Improvement of co-seismic landslide hazard / susceptibility assessments

The improvement of regional-scale assessments of co-seismic landslide susceptibility and hazard is a research priority, especially in areas with high relief and high seismic hazard such as tectonically active mountains. Particular focus is required on the initiation of deep-seated slope failures and

catastrophic rock avalanches in response to ground motion. This task involves identifying critical conditioning factors (e.g. mechanical properties of geological formations, hydrologic conditions, and earthquake characteristics) and in-depth understanding of topographic amplification and directivity phenomena. It also requires the development and analysis of comprehensive co-seismic landslide inventories to establish statistical relationships between conditioning factors and landslide occurrence. Modelling the runout of these failures is also essential for effective landslide hazard and risk assessment. This can be achieved through a combination of high resolution digital topography coupled with multiple flow direction algorithms and distance-volume empirical relationships based on observed data.

Investigate landsliding in response to tectonic forcing and bedrock incision

Recognizing the fundamental role of landslides in landscape evolution, the response of hillslope processes to tectonic and fluvial forcing requires further investigation to understand the occurrence of landslides without obvious triggers (rainfall or earthquakes). This requires information on uplift and landslide erosion rates as well as the implementation of a spatially distributed stream power model. Quantitative analysis of high resolution digital terrain models can be used to infer uplift rates, extract slope angles and develop the stream power model. Landslide mapping through remote sensing and the implementation of landslide volume-frequency distributions can be used to estimate regional landslide erosion rates. Static and dynamic fatigue (i.e. the reduction of slope stability caused by long-term, relatively low stresses) associated with the presence of water or glacial cycles, also needs to be considered. The joint analysis of the above information will provide insights into threshold hillslope angles and landslide occurrence in response to uplift and bedrock incision.

Linking catchment hydrologic response to flood susceptibility

In this research a GIS-based spatially distributed unit hydrograph model was developed in order to investigate the hydrologic response of major ungauged catchments in the study area based on their morphometry, land cover and soil characteristics, followed by a GIS-based flood susceptibility model using fuzzy logic. According to the evaluation results the SDUH model is able to predict the peak flow rate and time to peak of ungauged river catchments for different rainfall scenarios with reasonable accuracy while the GIS-based fuzzy logic model performed well in delineating flood-prone areas in regional scale. However, an attempt to link the two models was not made. This can be achieved by converting the peak-flow rate into flow stage and using the height above nearest drainage information layer to identify the hydrologically connected areas that will be flooded. This requires the use of high resolution topographic data and adequate information on the spatial distribution of

rainfall within catchments. The combination of the two models will provide a regional scale assessment of flood hazard or susceptibility based on various rainfall scenarios and inform decision making.

Regional downstream variation of channel geometry

A critical limitation emerged during the development of the spatially distributed unit hydrograph and the GIS-based flood susceptibility models concerns the estimation of channel geometry. Many hydrological and hydraulic models require channel geometric parameters as input in order to calculate flow velocity and depth. Although several empirical relationships have been proposed to estimate the downstream changes in channel geometry, more research is required to improve these relationships and be suitable for rapidly changing drainage systems in highly dynamic environments (e.g. braided rivers). As the most important factor affecting channel geometry is the sediment input and flux through the drainage system, the models need to incorporate spatio-temporal variation of erosion rates. Multi-temporal LiDAR digital terrain models can be used to extract channel geometry in various time-steps. The extracted geometries could then be compared with erosion rates and discharge, to establish relationships between downstream channel geometry, discharge and sediment input.

Catchment hydrology and glacier cover

Another research priority is linked to the impact of glaciers in catchment hydrology and flood hazard. The presence of glaciers in the mountainous catchments significantly affects the rainfall-runoff transformation primarily through storage and release of water from the glacier. This modifies the variability of annual and seasonal discharge and complicates the assessment of flood susceptibility and hazard. This requires the modelling of the three interlinked drainage systems, supraglacial, englacial and subglacial. For this task, more research is needed for the development of spatially distributed glacio-hydrological models based on high resolution digital elevation models of glacier surface, climatic data (temperature, precipitation, solar radiation) and discharge measurements at the glacier terminus. Glaciers can also store and release substantial quantities of sediment, affecting downstream river processes.

Investigate the effects on river flooding of geomorphic events such as sediment input from landslide erosion and landslide dams.

Flood hazard in the WSA is a function of extreme precipitation totals, steep topography as well as several geomorphic processes. In this research only the rainfall-induced flood susceptibility was

considered. More research is required to investigate flood hazard in response to geomorphic processes such as river aggradation and landslide dams. River aggradation involves estimating erosion rates and consequent sediment input, the movement of the sediment through the drainage system (flux) and its relation to overbank flows. The assessment of landslide dam-break flood hazards assumes that the potential locations and volumes of landslide deposits can be predicted with reasonable accuracy. This may eventually be achieved using sophisticated landslide modelling (co-seismic, rainfall-triggered or in response to tectonic forcing) that estimates the area or directly the volume of the slope failure and identifies the runout path and distance of the material. Additionally the development of robust empirical models for estimating the breaching parameters of landslide dams based on information of real landslide dam failure cases is also essential.

Improvement of multi-hazard analysis

Chapter 5 develops an approach for multi-hazard and risk analysis in environments where geomorphic processes and consequent hazards are strongly interrelated. To demonstrate the practical application of the proposed approach, a regional multi-hazard analysis was performed in the WSA. The processes considered in the case study were mainly rainfall-induced shallow landslides and river flooding. The impacts of a potential Alpine fault earthquake and consequent co-seismic landsliding were also considered. The geomorphic system of the WSA, however, includes several other important components (processes) and interactions which they have not been included in the analysis. More research is necessary to incorporate these important processes into the multi-hazard analysis. One way to achieve this is by modelling each process individually and linking the various models. For example, separately develop a co-seismic landslide hazard and a flood hazard model. Then establish the link between them the by calculating the runout, estimating the volume (e.g. using area-volume empirical relationships) of future slope failures in order to identify potential landslide dam locations, identifying the breaching parameters and ultimately assess the flood hazard. Another option to model the geomorphic system with its various interrelated processes, and assess the potential consequent hazards, is to link landscape evolution models with multi-hazard analyses. Landscape evolution models can be described in general as models (qualitative, physical or numerical) based on physical laws and principles that simulate the evolution of landscape over time. They have been applied in research fields such as hydrology, soil erosion, hillslope stability, volcanology and general landscape evolution studies aiming to provide insight into processes and laws governing landscape evolution. Integrating elements-at-risk in a changing landscape as a result of various interrelated tectonic, climatic and surface processes may provide useful information for planning and decision making.

6.7 References

Becker J, Saunders W, Hopkins L, Wright K, Kerr J 2008. Pre-event recovery planning for land-use in New Zealand: An updated methodology. GNS Science Report 2008/11. 39 p.

Benn JL 2005. Landslide events on the West Coast, South Island, 1867-2002. New Zealand Geographer 61: 3-13.

Burby RJ, Deyle RE, Godschalk DR, Olshansky RB, 2000. Creating hazard resilient communities through land-use planning. Natural Hazards Rev. Vol.1, Issue 2, 99 – 106.

CAE (2009). Land use planning for natural hazards—Stewardship for the future. CAENZ Comments, 5. Centre for Advanced Engineering, Christchurch, 24 pp

Collins MG, Steiner FR, Rushman MJ 2001. Land-Use Suitability Analysis in the United States: Historical Development and Promising Technological Achievements. Environmental Management Vol. 28, No. 5, pp. 611–621.

Crozier MJ 2009. Landslide geomorphology: An argument for recognition, with examples from New Zealand, Geomorphology, doi:10.1016/j.geomorph.2009.09.010.

Davies 1993. Fallacies in flood hydrologic design.New Zealand Journal of Hydrology, Vol. 31 (2), p. 73-77.

Davies TR, McSaveney MJ, Clarkson PJ 2003. Anthropic Aggradation of the Waiho River, Westland, New Zealand: Microscale Modelling. Earth Surf. Process. Landforms 28, 209–218.

Davies T 2007. Potential for rock avalanche hazard at Franz Josef glacier village, Westland. Confidential report to west coast regional council. Natural Hazards Research Centre Dept of Geological Sciences University of Canterbury, New Zealand, 14p.

Davies TRH, Campbell B, Hall RJ, Gomez C (2013 in press). Recent behaviour and sustainable future management of the Waiho River, Westland, New Zealand. Journal of hydrology (New Zealand).

DTec Consulting Ltd 2002. West Coast Regional Council: Natural Hazards Review. Report prepared for West Coast Regional Council by Dtec Consulting Ltd. Client Reference: 1065.136WCRC, Greymouth. 140 p.

Ericksen NJ, Berke PR, Crawford JL, Dixon JE 2004. Plan-making for sustainability: The New Zealand experience. Ashgate, Aldershot, 350 pp.

Glavovic BC, Saunders WS, Becker JS 2010. Land-use planning for natural hazards in New Zealand: the setting, barriers, 'burning issues' and priority actions. Nat Hazards, doi: 10.1007/s11069-009-9494-9.

Helton JC 1997. Uncertainty and sensitivity analysis in the presence of stochastic and subjective uncertainty, Journal of Statistical Computation and Simulation, 57: 1-4, 3-76.

Hewitt K 2006. Disturbance regime landscapes: mountain drainage systems interrupted by large rockslides. Progress in Physical Geography, Vol. 30, No. 3, 365-393.

Hewitt K, Clague JJ, Orwin JF 2008. Legacies of catastrophic rock slope failures in mountain landscapes. Earth-Science Reviews 87, 1-38.

Hovius N, Stark CP, Allen PA 1997. Sediment flux from a mountain belt derived from landslide mapping. Geology 25, 231– 234.

Kerr J, Nathan S, Van Dissen R, Webb P, Brunsdon D, King A 2003. Planning for Development of Land on or Close to Active Faults. A guideline to assist resource management planners in New Zealand. Ministry for the Environment, 67 p.

Kirschenbaum A 1996. Residential Ambiguity and Relocation Decisions: Population and Areas at Risk. International Journal of Mass Emergencies and Disasters. Vol.14(1): p. 79-96.

Korup O 2005. Large landslides and their effect on alpine sediment flux: South Westland, New Zealand. Earth Surface Processes and Landforms 30, 305-323.

Korup O, Schmidt J, McSaveney MJ 2005. Regional relief characteristics and denudation pattern of the western Southern Alps, New Zealand. Geomorphology 71, 402-423.

Korup O 2006. Effects of deep-seated bedrock landslides on hillslope morphology, Southern Alps, New Zealand. Journal of Geophysical Research 111, F01018, doi:10.1029/2004JF000242.

Korup O, Densmore AL, Schlunegger F 2009. The role of landslides in mountain range evolution. Geomorphology, doi:10.1016/j.geomorph.2009.09.017.

Lindell MK, Prater C 2003. Assessing community impacts of natural disasters. Natural Hazards Review 4(4): 176-185.

MfE 2008. Meeting the challenges of future flooding in New Zealand. MfE, Wellington, 48 pp.

Mileti DS 1999. Disasters by Design: A reassessment of natural Hazards in the United States. Washington, D.C. Joseph Henry Press. 351p.

Mileti DS, Passerini E 1996. Social Explanation of Urban Relocation after Earthquakes. International Journal of Mass Emergencies and Disasters, Vol. 14, No. 1, pp. 97-110.

Perry R, Lindell M 1997. Principles for managing community relocation as a hazard mitigation measure. Journal of Contingencies and Crisis Management Vol. 5(1): pp 49-59.

Petley DN, Hearn G J, Hart A, Rosser NJ, Dunning SA, Oven K, Mitchell WA 2007. Trends in landslide occurrence in Nepal. Natural hazards, 43 (1): pp. 23-44.

Robinson TR, Davies TRH 2013. Review Article: Potential geomorphic consequences of a future great (Mw = 8.0+) Alpine Fault earthquake, South Island, New Zealand. Nat. Hazards Earth Syst. Sci., 13, 2279–2299.

Saunders W, Forsyth J, Johnston DM, Becker J 2007. Strengthening linkages betweenland-use planning and emergency management in New Zealand. Australian Journal of Emergency Management, 22(1): 36-43.

Appendix 1

Table A1.1 Drainage network analysis results. Comparison of observed stream numbers, lengths and contributing catchment areas with values estimated from Horton's laws.

Catchment	Stream Order	Law of stream numbers (% deviation)	Law of stream lengths (% deviation)	Law of stream areas (% deviation)
Hokitika	1	-3.0	0.0	0.0
	2	-15.4	2.6	16.1
	3	-21.6	25.8	38.3
	4	-21.5	17.2	34.5
	5	-5.3	38.6	73.8
	6	0.0	126.4	140.4
Totara	1	-17.4	0.0	0.0
	2	-31.8	79.5	41.5
	3	-30.8	48.6	78.9
	4	-44.6	235.7	207.3
	5	0.0	-60.3	85.3
Mikonui	1	-21.1	0.0	0.0
	2	-30.7	-5.0	11.0
	3	-44.3	19.7	87.1
	4	-50.2	-11.6	81.1
	5	0.0	81.3	123.9
Waitaha	1	-10.0	0.0	0.0
	2	-17.9	9.1	19.7
	3	-17.6	4.5	28.7
	4	-34.0	108.9	105.0
	5	0.0	98.8	132.7
Wanagui	1	-5.0	0.0	0.0
	2	2.2	-1.4	-6.8
	3	31.1	-39.1	-25.0
	4	17.8	-5.3	1.3
	5	0.0	74.5	93.8
Poerua	1	-28.5	0.0	0.0
	2	-35.1	32.2	10.3
	3	-32.6	74.0	39.0
	4	-54.5	310.3	201.8
	5	0.0	-98.4	40.6
Whataroa	1	-22.5	0.0	0.0
	2	-38.0	16.0	26.2
	3	-52.0	32.9	50.7
	4	-54.6	16.0	95.8
	5	-49.0	53.5	175.2

	6	0.0	129.9	130.9
Waitangitaona (upper)	1	-1.8	0.0	0.0
	2	-10.1	-6.5	3.6
	3	6.0	36.8	32.5
	4	0.0	119.1	123.3
Waiho	1	-41.1	0.0	0.0
	2	-62.5	11.5	43.5
	3	-72.4	20.3	82.8
	4	-40.0	-3.2	106.1
	5	-41.5	58.8	103.4
	6	0.0	116.1	139.3
Waikukupa	1	-31.2	0.0	0.0
	2	-36.4	-66.2	-44.4
	3	-57.4	21.1	69.4
	4	0.0	-90.6	-33.0
Fox-Cook	1	-4.3	0.0	0.0
	2	-14.1	-16.8	-5.2
	3	7.4	-44.8	-15.0
	4	-7.3	43.2	71.3
	5	0.0	30.1	95.3
Ohinematea	1	-2.5	0.0	0.0
	2	-0.9	-20.1	-8.6
	3	-15.1	82.0	52.0
	4	0.0	68.2	116.3
Karangarua	1	-41.3	0.0	0.0
	2	-49.2	-19.6	6.1
	3	-59.0	8.8	39.5
	4	-74.2	136.7	182.3
	5	-49.2	43.3	154.7
	6	0.0	52.2	77.8
Makawhio	1	-5.0	0.0	0.0
	2	-20.6	-5.0	15.1
	3	-26.5	0.7	49.0
	4	-22.5	-7.8	62.8
	5	0.0	91.3	138.0
Mahitahi	1	-24.6	0.0	0.0
	2	-27.5	-9.8	1.5
	3	-40.1	62.6	46.2
	4	-53.3	107.7	148.7
	5	0.0	111.4	109.8
Ohinemaka	1	-17.1	0.0	0.0
	2	-33.6	50.1	58.5
	3	-50.0	165.3	136.3

	4	-36.8	321.7	138.9
	5	0.0	-40.1	118.2
Paringa	1	-11.9	0.0	0.0
	2	-12.4	4.5	1.6
	3	-20.9	19.2	2.7
	4	-37.1	152.4	118.2
	5	0.0	75.8	85.0
Moeraki	1	-4.0	0.0	0.0
	2	-5.6	-74.5	-29.1
	3	19.0	-97.4	-72.1
	4	0.0	-90.6	-19.1
Whakapohai	1	-31.0	0.0	0.0
	2	-33.7	-10.9	17.6
	3	-56.5	114.6	126.5
	4	0.0	50.1	103.5
Waita	1	-16.5	0.0	0.0
	2	-31.0	63.0	49.5
	3	-39.3	171.0	111.3
	4	-44.9	312.7	213.5
	5	0.0	-23.9	90.6
Haast	1	-28.5	0.0	0.0
	2	-31.7	-7.9	5.4
	3	-40.6	-1.0	19.6
	4	-54.9	68.0	150.7
	5	-57.5	-42.8	165.2
	6	0.0	12.5	74.3

Appendix 2

Figure A2.1 Hokitika River

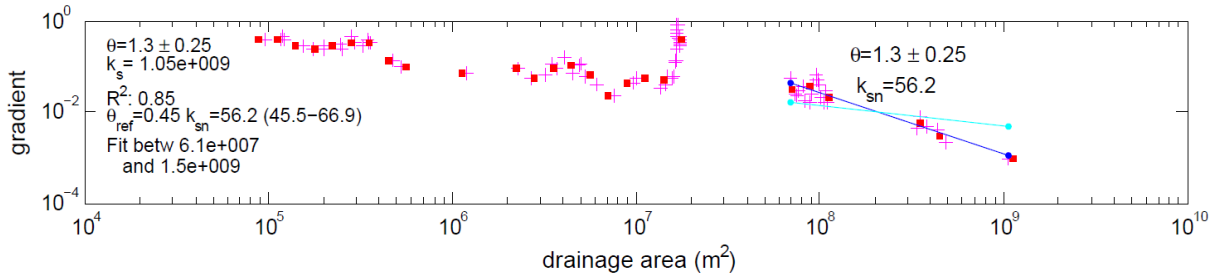

Figure A2.2 Mikonui River

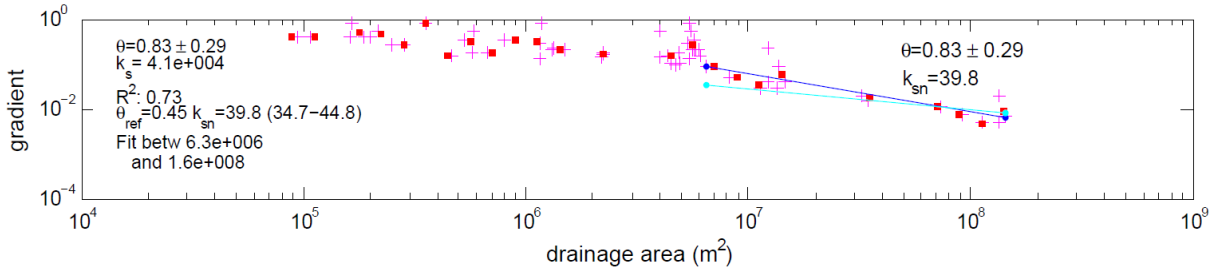

Figure A2.3 Waitaha River

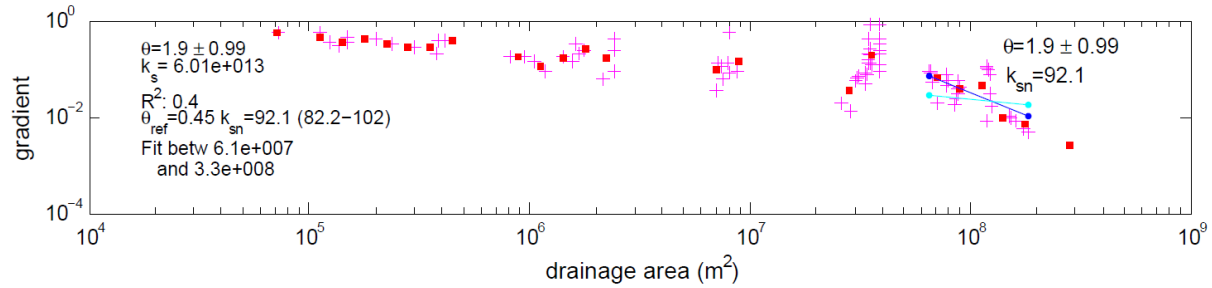

Figure A3.4 Wanganui River

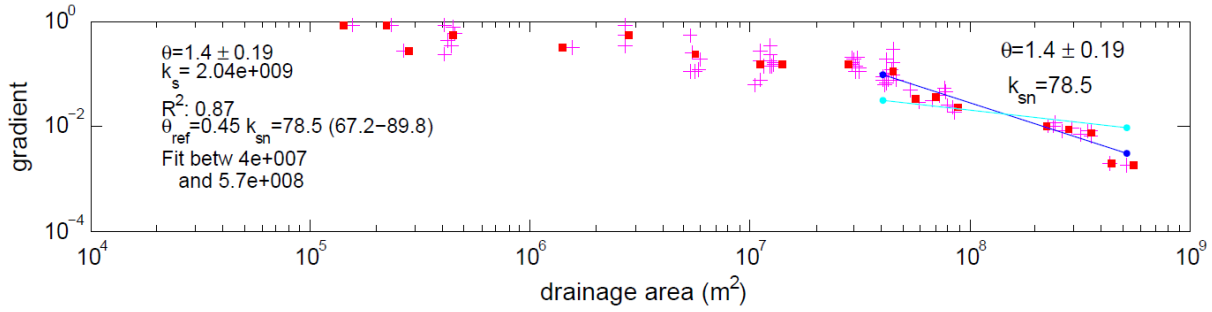

Figure A2.5 Poerua River

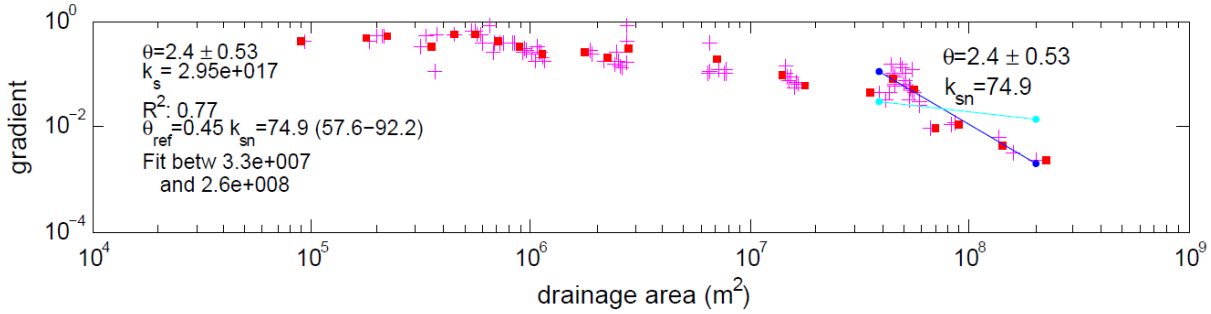

Figure A2.6 Whataroa River

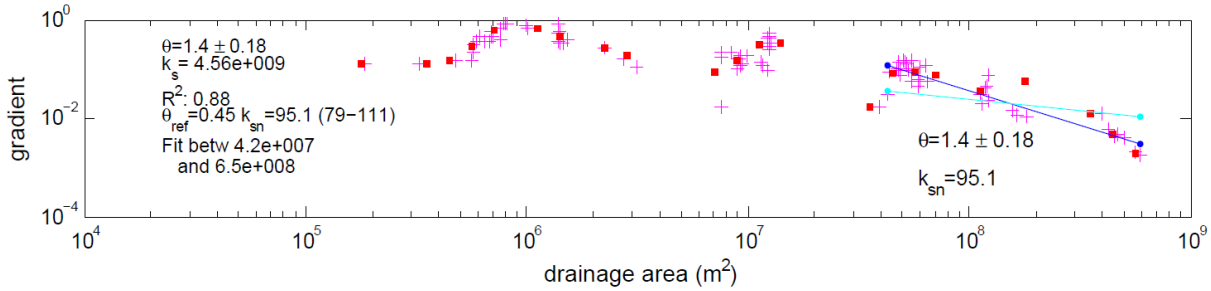

Figure A2.7 Waitangitaona River (upper)

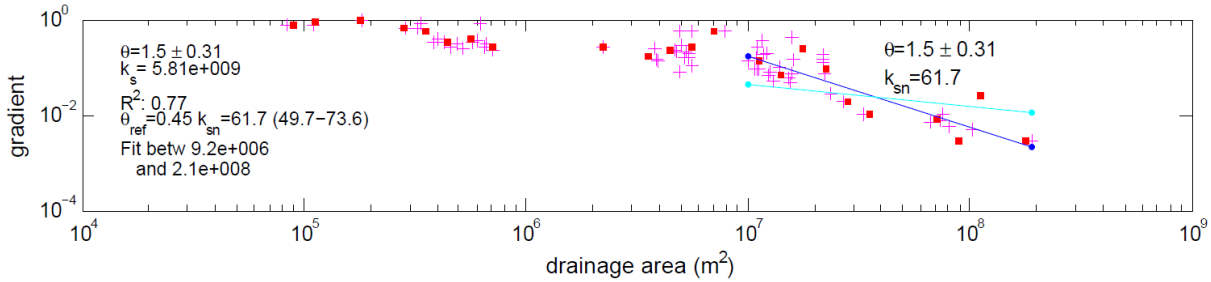

Figure A2.8 Callery River

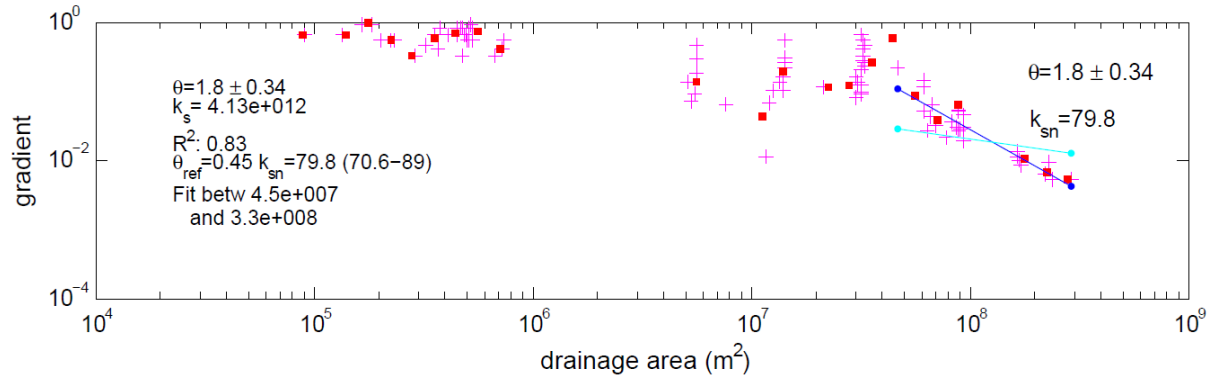

Figure A2.9 Waikukupa River

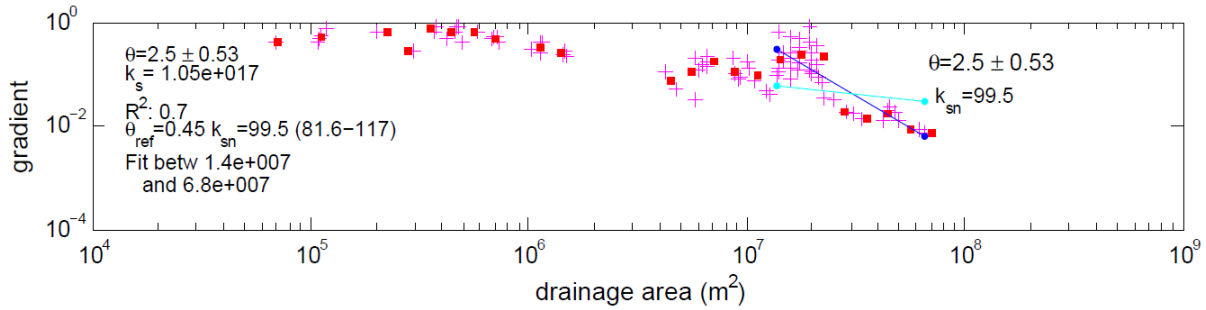

Figure A2.10 Cook River

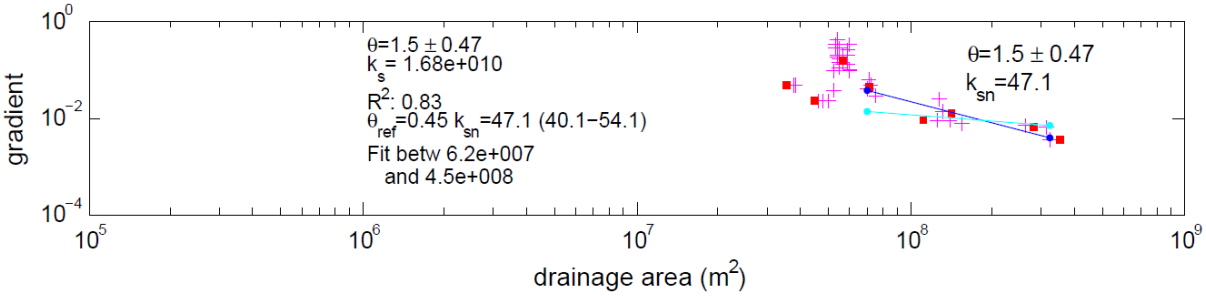

Figure A2.2 Karangarua river

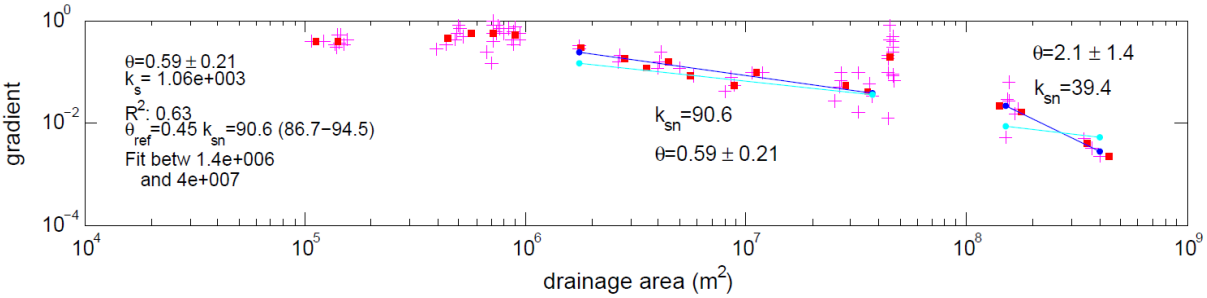

Figure A2.3 Makawhio River

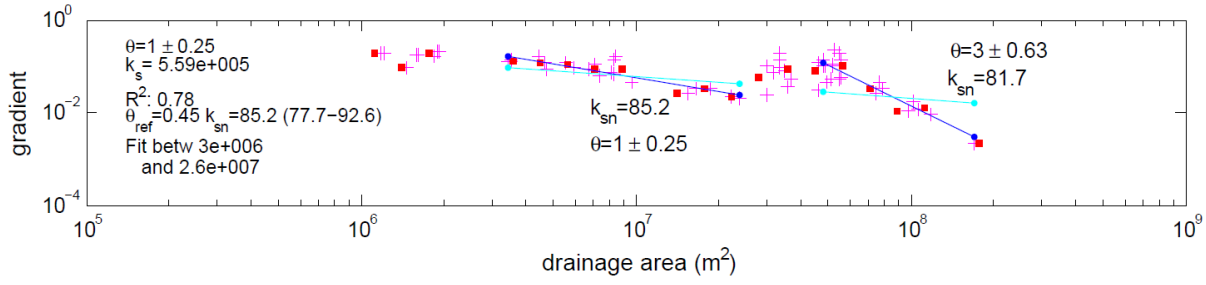

Figure A2.4 Mahitahi River

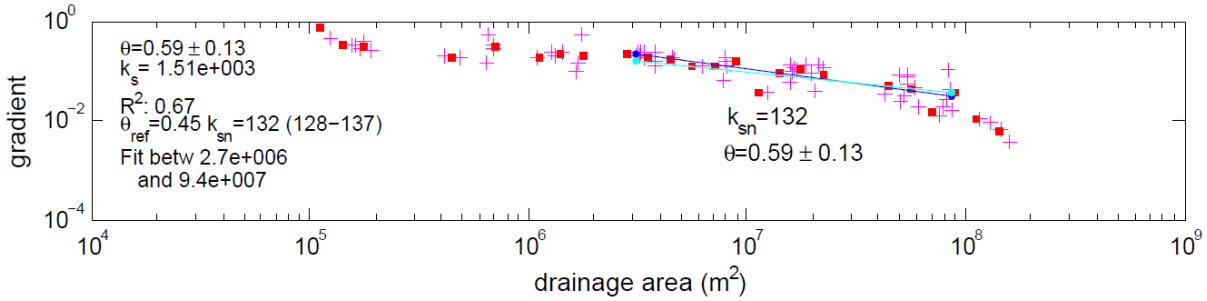

Figure A2.5 Paringa River

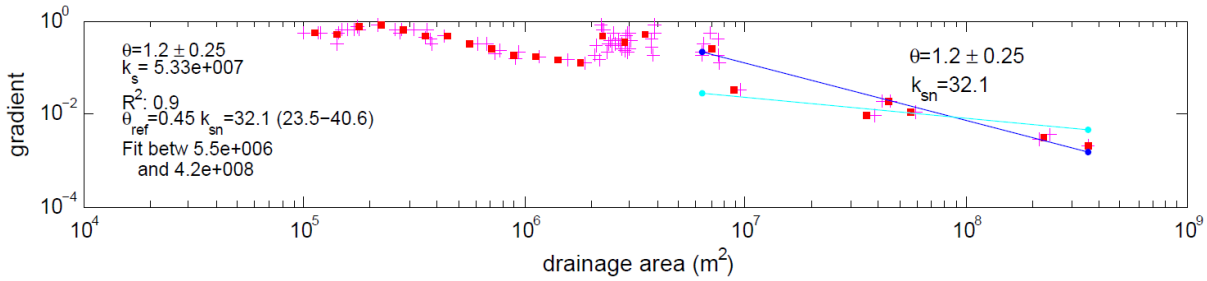

Figure A2.6 Moeraki River

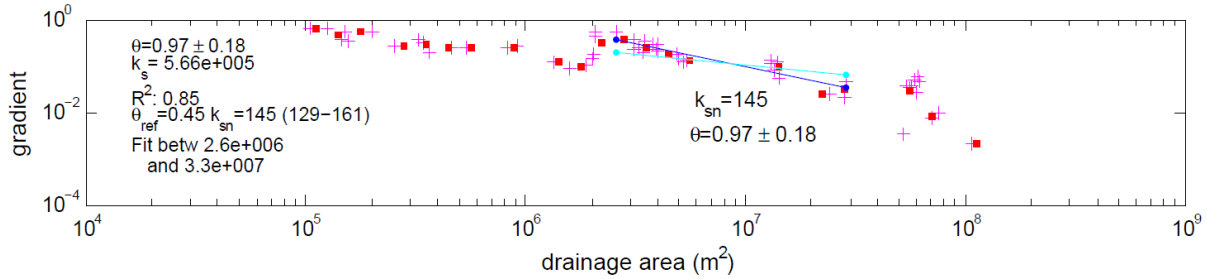

Figure A2.16 Haast River

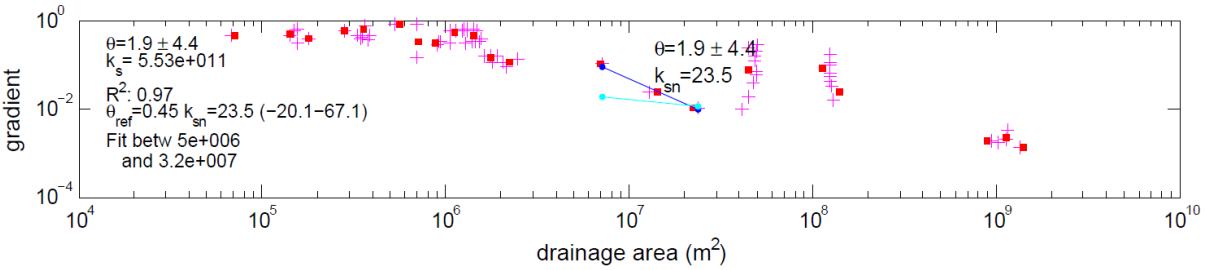

Appendix 3

Table A3.1 Valleys' topographic paramaters and V_f ratios. The coordinates indicate the centre of the valley cross-section.

Name	Easting	Northing	A_{rd} (m)	A_{ld} (m)	V_{fw} (m)	A_{sc} (m)	V_f
Hokitika River	2346810	5799020	960	1242	124	118	0.126
Hokitika River	2350260	5798080	980	987	50	172	0.062
Hokitika River	2351980	5797830	1349	1310	75	200	0.066
Hokitika River	2353750	5797100	1180	1340	75	311	0.079
Hokitika River	2354350	5795140	1169	1180	25	360	0.031
Whitcombe River	2349300	5796440	822	830	99	140	0.144
Whitcombe River	2350410	5794900	1228	1059	100	198	0.106
Whitcombe River	2349250	5792050	1814	1586	124	239	0.085
Whitcombe River	2349050	5789440	1693	949	50	278	0.048
Whitcombe River	2348350	5787980	1888	1470	50	340	0.037
Whitcombe River	2347300	5784000	2070	1252	75	494	0.064
Whitcombe River	2346820	5781960	2198	1743	50	595	0.036
Whitcombe River	2345950	5780370	2091	1680	100	639	0.080
Whitcombe River	2345910	5778590	1900	1460	50	777	0.055
Whitcombe River	2345830	5776720	1960	1912	75	1011	0.081
Mungo River	2355830	5794600	1009	1457	49	417	0.060
Mungo River	2358010	5794780	1751	1626	25	505	0.021
Mungo River	2361630	5795400	1791	1759	50	638	0.044
Toaroha River	2356970	5805890	1487	840	100	279	0.113
Toaroha River	2357480	5804660	760	1298	50	346	0.073
Toaroha River	2358910	5802970	1721	1536	349	440	0.294
Toaroha River	2357970	5800930	1000	1541	75	513	0.099
Toaroha River	2358730	5799300	1080	1199	25	634	0.049
Kokatahi River	2360240	5809580	761	1060	894	113	1.121
Kokatahi River	2361800	5808630	814	1036	25	146	0.032
Kokatahi River	2363360	5808220	1157	850	25	201	0.031
Kokatahi River	2363640	5806540	1499	1202	75	280	0.070
Kokatahi River	2364540	5804920	1288	1259	50	360	0.055
Kokatahi River	2365870	5802300	1978	1193	50	547	0.048
Kokatahi River	2364760	5801260	1978	1400	49	699	0.049
Kokatahi River	2362700	5801270	1860	1690	50	986	0.063
Crawford creek	2366810	5805150	1234	1752	50	540	0.052
Crawford creek	2368140	5806250	1801	1836	25	720	0.023
Styx River	2361500	5811630	907	736	150	120	0.214
Styx River	2363270	5811450	1156	914	199	175	0.231
Styx River	2365190	5811470	1137	958	25	300	0.033
Styx River	2367050	5811300	1320	1838	100	356	0.082
Styx River	2368800	5811460	1159	1715	25	460	0.026

Mikonui River	2342670	5794180	1581	1220	74	1182	0.339
Dickson River	2341170	5794700	1203	970	25	544	0.046
Dickson River	2341990	5793270	1313	1524	25	783	0.039
Healey Creek	2340000	5793760	944	1250	25	760	0.074
Healey Creek	2340820	5792360	1488	1620	123	1217	0.365
Tuke River	2337720	5791890	1602	1313	50	451	0.050
Tuke River	2336890	5790900	1135	1250	25	678	0.049
Tuke River	2337490	5789290	1340	1658	74	899	0.123
Tuke River	2338600	5788060	1600	1984	100	1028	0.131
Waitaha	2324940	5784210	1201	1264	124	173	0.117
Waitaha	2329120	5783720	1119	726	125	320	0.207
Waitaha	2330840	5783190	1460	1219	99	379	0.103
Waitaha	2332740	5782910	900	1276	50	459	0.079
Waitaha	2334800	5784270	1658	1358	74	896	0.121
Waitaha	2336780	5784180	1852	1840	25	1050	0.031
Whirling	2327560	5782440	813	1101	323	405	0.585
Whirling	2328350	5780750	934	1863	149	741	0.227
Whirling	2329210	5779890	1442	1839	50	1022	0.081
County stream	2334370	5782540	1545	1283	124	776	0.194
County stream	2334920	5780840	2041	1882	149	932	0.145
County stream	2336290	5779290	1878	1560	50	1038	0.073
County stream	2338550	5779130	2040	2229	50	1290	0.059
Macgregor creek	2328340	5786430	842	1128	25	555	0.058
Macgregor creek	2330090	5786110	1306	1100	25	839	0.069
Kakapotahi river	2333100	5788780	1293	1539	50	480	0.053
Kakapotahi river	2335060	5788490	1276	1261	25	900	0.068
Wanganui	2316810	5778590	803	1192	275	100	0.306
Wanganui	2318130	5777390	832	1529	200	120	0.189
Wanganui	2319890	5776660	904	1386	1123	138	1.115
Wanganui	2321200	5775590	1114	1225	324	159	0.321
Wanganui	2322990	5775100	880	1182	200	176	0.234
Wanganui	2324710	5774150	1347	792	199	198	0.228
Wanganui	2326360	5773280	1469	1411	99	260	0.084
Wanganui	2328530	5773940	1516	1721	125	256	0.092
Wanganui	2330350	5774410	1839	1934	374	319	0.239
Wanganui	2332090	5775050	1794	2134	50	392	0.032
Wanganui	2333870	5775450	1852	1977	25	557	0.018
Evans R	2338050	5776140	1958	2278	175	1077	0.168
Lambert R	2328510	5770120	747	717	25	260	0.053
Lambert R	2327890	5771810	1638	1349	199	523	0.205
Lord R	2330420	5769380	1665	1430	74	793	0.098
Lord R	2332660	5769340	1933	2174	50	933	0.045
Lord R	2334870	5770520	2313	2047	74	1220	0.077

Adams R	2325540	5771990	1132	635	75	278	0.124
Adams R	2324000	5770990	1560	1335	74	320	0.066
Adams R	2323540	5769100	1794	1436	25	480	0.022
Adams R	2322200	5767770	1241	1660	724	742	1.022
Adams R	2321940	5765550	1900	1599	99	967	0.127
Hot Spring Creek	2319620	5774720	497	775	74	220	0.178
Hot Spring Creek	2320950	5773620	1294	879	174	620	0.373
Hot Spring Creek	2320650	5772000	1076	1217	75	876	0.277
Hot Spring Creek	2319060	5770950	1281	1618	50	1041	0.122
Tribute Creek	2315940	5774740	886	1089	75	512	0.158
Tribute Creek	2316470	5772770	1552	1596	50	1268	0.163
Hendes Creek	2322560	5777090	1086	827	50	345	0.082
Hendes Creek	2324110	5777920	1211	1415	50	581	0.068
Amethyst Ravine	2319340	5779100	800	880	50	561	0.179
Amethyst Ravine	2321130	5779920	1050	1185	100	616	0.199
Amethyst Ravine	2322630	5780730	1389	1208	50	700	0.084
Poerua	2309340	5772320	985	1195	750	275	0.920
Poerua	2310330	5771040	1509	1654	25	322	0.020
Poerua	2311960	5769950	1208	2004	49	486	0.044
Poerua	2313910	5768200	1305	1225	74	658	0.122
Poerua	2315410	5766780	1381	1532	25	992	0.054
Wilberg	2314340	5770950	1640	1402	75	725	0.094
Wilberg	2316140	5770230	1645	1627	75	1032	0.124
Wilberg	2314870	5772830	1515	1563	50	1146	0.127
Whataroa river	2300420	5764500	1349	1259	574	99	0.476
Whataroa river	2300960	5762680	1256	1628	200	100	0.149
Whataroa river	2301640	5761470	1583	1353	275	118	0.204
Whataroa river	2302100	5757050	1446	1480	50	180	0.039
Whataroa river	2301070	5755500	1637	1551	50	349	0.040
Whataroa river	2301010	5753710	1505	1283	50	277	0.045
Whataroa river	2300090	5751910	1382	1477	25	340	0.023
Whataroa river	2298640	5750660	1904	1911	25	498	0.018
Whataroa river	2297510	5749150	2064	1950	25	978	0.024
Perth river	2306180	5759160	930	1329	225	180	0.237
Perth river	2308170	5759390	1339	1511	25	217	0.021
Perth river	2310600	5758070	1667	1147	25	279	0.022
Perth river	2312090	5757040	1925	1679	50	378	0.035
Perth river	2315210	5757300	1590	1367	25	525	0.026
Perth river	2316370	5758740	1676	2219	50	691	0.040
Perth river	2317640	5760150	1990	1247	49	818	0.061
Perth river	2319340	5760250	1943	1822	99	997	0.112
Perth river	2321350	5760730	1745	2239	25	1089	0.028
Gunn river	2299230	5755890	1182	1262	25	627	0.042

Gunn river	2297370	5755620	1367	1520	25	760	0.037
Gunn river	2295630	5755110	1817	1530	100	1121	0.181
Gunn river	2294290	5753770	1693	1841	49	1223	0.090
Butler river	2302210	5751240	1246	1420	75	539	0.094
Butler river_n	2303920	5751770	1477	1949	25	700	0.025
Butler river_n	2305740	5752560	1796	2230	274	917	0.250
Butler river_s	2302560	5749210	2238	1893	124	896	0.106
Butler river_s	2302240	5747580	2113	2014	347	1150	0.380
Barlow creek	2310210	5760870	1081	1875	25	300	0.021
Barlow creek	2310650	5762680	1631	1923	25	400	0.018
Gaunt Creek	2294540	5761280	829	1362	25	568	0.047
Gaunt Creek	2296310	5760900	1498	1570	25	1050	0.052
Darnley Creek	2292160	5759730	1035	1150	75	444	0.116
Darnley Creek	2293770	5758660	1386	1740	25	732	0.030
Darnley Creek	2295560	5758910	1536	1287	25	1096	0.079
Waitangitaona River	2288910	5758120	841	656	25	339	0.061
Waitangitaona River	2289070	5756610	1076	1203	50	506	0.079
Waitangitaona River	2290800	5756040	1490	1133	25	860	0.055
Waitangitaona River	2290350	5755340	1101	1579	50	821	0.096
Waitangitaona River	2292000	5754500	1614	2004	50	1450	0.139
Potters Creek	2286470	5756000	919	1129	25	340	0.037
Potters Creek	2288240	5755180	1318	1600	25	844	0.041
Callery	2283250	5751160	1103	760	74	220	0.104
Callery	2283990	5749850	1386	1188	25	280	0.025
Callery	2285690	5748920	1232	2005	25	344	0.020
Callery	2287480	5749160	1494	1582	25	417	0.022
Callery	2289610	5748980	1671	1027	49	633	0.068
Callery	2291600	5749700	1780	2013	25	1041	0.029
Callery	2292890	5750960	1975	2125	49	1080	0.051
Callery_str	2289740	5747150	1660	1787	25	681	0.024
Tatare	2284410	5752610	980	1084	25	868	0.152
Tatare	2286370	5752780	1218	1309	25	601	0.038
Tatare	2288210	5752360	1684	1608	25	698	0.026
Tatare	2290580	5752400	1699	1759	25	1172	0.045
Waiho	2281170	5750400	727	1017	997	212	1.511
Waiho	2281080	5748290	1255	1446	25	241	0.023
Waikukupa River	2273520	5745350	1318	1278	25	406	0.028
Waikukupa River	2275180	5744750	1377	1693	25	871	0.038
Waikukupa River	2277080	5744200	1720	1840	50	940	0.060

Waikukupa River	2278660	5743670	1578	1799	100	1137	0.181
Fox	2270270	5741950	999	1436	100	236	0.102
Fox	2271870	5741130	1559	1680	125	255	0.092
Victoria glacier/Fox	2276420	5741490	1657	1586	75	1035	0.128
Boyd creek	2273830	5739260	1499	1561	50	1195	0.149
Cook	2265840	5739190	933	900	25	140	0.032
Cook	2266260	5737530	639	811	25	178	0.046
Cook	2265240	5735840	798	1295	25	320	0.034
Cook	2264940	5734090	1183	1860	25	676	0.030
Cook	2266430	5733130	1444	1734	25	739	0.029
Cook	2268300	5732640	1563	2062	25	806	0.025
Craig creek	2268480	5737770	1244	689	25	473	0.051
Craig creek	2270370	5738000	1674	1580	25	1140	0.051
Mc Bain Creek	2267340	5735520	949	1452	25	573	0.040
Balfour	2268020	5736770	695	929	25	306	0.049
Balfour	2269670	5736050	1330	1710	25	600	0.027
Balfour	2271560	5736370	1816	1676	174	739	0.173
Karangarua	2252770	5730550	882	861	150	40	0.180
Karangarua	2253530	5728840	833	817	75	57	0.098
Karangarua	2254280	5726880	1446	683	175	78	0.177
Karangarua	2253620	5725370	1356	1542	75	100	0.056
Karangarua	2254020	5723700	921	1742	200	159	0.171
Karangarua	2254550	5722250	859	1429	99	177	0.102
Karangarua	2254090	5720380	1182	1468	25	180	0.022
Karangarua	2255180	5719050	1460	1708	25	500	0.023
Karangarua	2256870	5718240	1620	1600	99	519	0.091
Karangarua	2258470	5717380	1864	1733	25	597	0.021
Karangarua	2260320	5716710	1658	1139	25	717	0.037
Troyte river	2259180	5715900	1637	1549	25	818	0.032
Troyte river	2259380	5714270	1413	2253	25	999	0.030
Copland river	2257130	5728160	1193	1576	175	80	0.134
Copland river	2258880	5728040	1670	1513	150	113	0.101
Copland river	2260840	5727480	1260	1604	25	197	0.020
Copland river	2262620	5726870	1812	1990	25	339	0.016
Copland river	2264220	5725870	1953	2204	225	437	0.137
Copland river	2266800	5725480	941	2399	100	459	0.083
Copland river	2268450	5725140	1893	1763	25	519	0.019
Copland river	2271400	5723670	1815	3062	25	926	0.017
Copland river	2273170	5724290	1861	2288	25	1052	0.024
Douglas river	2256700	5721160	1207	1543	25	532	0.030
Douglas river	2258640	5721290	1484	1771	25	680	0.026
Douglas river	2260240	5720370	1807	1805	25	849	0.026

Douglas river	2261890	5719610	2118	1681	25	408	0.017
Regina creek	2256280	5722890	1078	1206	49	400	0.066
Regina creek	2257930	5723750	1468	1420	149	539	0.165
Regina creek	2259870	5723890	1540	1803	25	780	0.028
Architect creek	2259090	5729840	1220	909	25	481	0.043
Architect creek	2260760	5730560	1605	1219	124	580	0.149
Architect creek	2262600	5731430	1784	1662	200	715	0.198
Ruera river	2266240	5727870	1611	1477	25	802	0.034
Ruera river	2268000	5728650	2049	1734	75	1057	0.090
Ohinetamatea River	2260150	5737160	662	652	74	274	0.193
Ohinetamatea River	2260690	5735360	1439	1265	75	797	0.135
Ohinetamatea River	2261040	5733810	1339	1445	221	1063	0.672
Ohinetamatea River	2261750	5736450	1231	1261	75	856	0.192
Havelock Creek	2258050	5734750	797	1041	50	484	0.115
Havelock Creek	2259440	5733410	1394	1499	75	895	0.136
Makawhio (Jacobs) River	2243650	5724560	1144	1176	125	60	0.114
Makawhio (Jacobs) River	2244930	5722990	1295	1350	250	99	0.204
Makawhio (Jacobs) River	2246280	5721890	846	1649	149	152	0.136
Makawhio (Jacobs) River	2247350	5720200	1423	1476	100	315	0.088
Makawhio (Jacobs) River	2249820	5717910	1936	1682	99	570	0.080
Makawhio (Jacobs) River	2251550	5717170	1849	1824	75	640	0.063
Makawhio (Jacobs) River	2253150	5716260	1649	1799	75	699	0.073
Makawhio (Jacobs) River	2254950	5715450	1543	2125	124	827	0.123
Mahitahi River	2236210	5719930	820	1038	598	174	0.792
Mahitahi River	2237340	5718120	1381	1519	599	58	0.430
Mahitahi River	2238700	5716710	724	1640	399	60	0.356
Mahitahi River	2240120	5715670	1161	1607	274	84	0.211
Mahitahi River	2241400	5713840	899	1067	299	137	0.353
Mahitahi River	2245520	5713660	1742	2178	175	252	0.102
Mahitahi River	2247240	5712990	1989	1988	250	351	0.153
Mahitahi River	2249970	5712540	1806	1767	50	592	0.042
Mahitahi River	2251820	5712180	1948	2022	100	794	0.084
Morse River	2239540	5713390	785	1620	25	360	0.030
Morse River	2240290	5711620	1199	1547	50	665	0.071

Morse River	2241740	5710700	1489	1780	100	820	0.123
Morse River	2243360	5709580	2002	1890	100	1129	0.122
Doughboy Creek	2233390	5717920	1208	972	75	820	0.278
Blackwater Creek	2232140	5716890	902	644	100	453	0.313
Blackwater Creek	2231920	5716480	720	887	50	556	0.202
Blackwater Creek	2231190	5715680	868	931	50	838	0.813
Paringa River	2227900	5713560	923	880	598	40	0.694
Paringa River	2228820	5711860	754	1215	548	58	0.591
Paringa River	2228950	5707260	1409	1152	399	76	0.331
Paringa River	2229320	5705970	647	1493	224	94	0.230
Paringa River	2230780	5704640	1088	820	174	134	0.212
Paringa River	2232390	5703710	1429	1640	124	152	0.090
Otoko River	2231560	5710400	1000	988	200	60	0.214
Otoko River	2234070	5710770	1152	957	175	797	0.680
Otoko River	2235940	5709870	1685	1598	250	118	0.164
Otoko River	2237880	5708980	1599	1873	125	197	0.081
Otoko River	2239450	5708060	1556	1439	399	261	0.323
Otoko River	2241100	5707110	1823	2206	299	456	0.192
Otoko River	2242710	5706130	1989	2281	75	600	0.049
Otoko River	2244200	5705410	2159	2598	225	797	0.142
Moeraki River	2216950	5705450	730	1341	1100	174	1.277
Moeraki River	2218610	5705020	985	1157	846	215	0.988
Moeraki River	2219980	5704320	1031	1169	797	218	0.904
Moeraki River	2221900	5704560	1337	1500	625	219	0.521
Moeraki River	2223560	5704240	736	1697	149	258	0.155
Moeraki River	2225000	5703180	1442	1688	150	391	0.128
Moeraki River	2226750	5703350	1238	1545	324	616	0.418
Moeraki River	2225920	5701530	1491	1899	75	831	0.087
Haast River	2196870	5690950	789	1357	1572	19	1.491
Haast River	2198430	5690060	1035	1381	648	20	0.545
Haast River	2203770	5687350	1376	1398	1470	39	1.091
Haast River	2208150	5687750	1247	1421	1525	57	1.194
Haast River	2209370	5689570	1459	1480	925	59	0.656
Haast River	2213650	5689010	1427	1482	375	78	0.272
Haast River	2218410	5688330	2060	1483	525	79	0.310
Haast River	2220500	5687400	1144	1182	1425	79	1.315
Haast River	2222520	5686980	795	457	873	88	1.623
Haast River	2222430	5684630	1502	664	949	97	0.962
Haast River	2221450	5682930	1296	1606	500	99	0.370
Haast River	2219830	5681650	1314	1517	500	100	0.380
Haast River	2219880	5678980	1255	1549	99	175	0.081
Haast River	2220240	5676900	1365	1541	75	400	0.071
Haast River	2220730	5674850	2109	1470	100	459	0.075

Haast River	2219390	5673520	1904	1500	75	479	0.061
Thomas River	2202280	5691270	1046	1006	124	58	0.128
Thomas River	2203650	5692940	1141	1401	424	79	0.356
Thomas River	2204340	5694550	1123	1462	124	160	0.109
Thomas River	2206120	5695610	1110	1260	375	178	0.372
Thomas River	2207890	5696600	1172	1379	349	179	0.318
Thomas River	2209970	5697290	1005	1408	125	200	0.124
Thomas River	2211400	5698510	848	1492	75	220	0.079
Thomas River	2212320	5700390	1241	1340	100	276	0.099
Thomas River	2214070	5701450	1220	1385	75	336	0.078
Thomas River	2216080	5701910	1266	1340	50	434	0.058
Thomas River	2218040	5701950	1090	1541	25	520	0.031
Landsborough River	2225160	5686940	672	1713	1574	97	1.437
Landsborough River	2226920	5688270	1182	1773	998	115	0.732
Landsborough River	2227840	5690000	1584	2034	1422	120	0.842
Landsborough River	2230830	5689710	474	1897	1274	140	1.219
Landsborough River	2232170	5691310	472	1903	499	158	0.485
Landsborough River	2234110	5692140	1036	1941	175	178	0.134
Landsborough River	2235910	5692870	1042	1977	125	197	0.095
Landsborough River	2238090	5692820	1130	2121	75	214	0.053
Landsborough River	2240150	5693160	1491	2104	100	239	0.064
Landsborough River	2242090	5693040	1264	2020	374	250	0.269
Landsborough River	2243730	5693010	1458	2223	724	260	0.458
Landsborough River	2245150	5695200	1431	2170	674	294	0.447
Landsborough River	2246290	5696920	1420	2055	375	316	0.264
Landsborough River	2247200	5698590	1519	2103	375	336	0.254
Landsborough River	2248880	5700300	1744	2261	275	358	0.167
Landsborough River	2249810	5701820	1703	2116	500	379	0.327
Landsborough River	2250840	5703400	2144	2402	150	400	0.080
Landsborough River	2252330	5704770	2510	2264	225	438	0.115

Landsborough River	2254030	5706030	2282	2257	274	477	0.153
Landsborough River	2256160	5706810	1481	1620	149	519	0.144
Landsborough River	2257610	5708050	1840	2299	124	613	0.085
Landsborough River	2259220	5709610	2111	1780	50	757	0.042
Landsborough River	2260790	5710840	2008	2259	50	918	0.041
Landsborough River	2263000	5712810	1788	2287	149	1095	0.158
Landsborough River	2263680	5715060	1534	2642	25	1218	0.029
Clarke River	2228910	5691640	1809	481	1097	136	1.087
Clarke River	2229770	5693320	1713	574	699	138	0.695
Clarke River	2230810	5694940	1380	864	475	139	0.483
Clarke River	2232390	5695730	1775	979	100	140	0.081
Clarke River	2236320	5696780	1338	1140	250	318	0.271
Clarke River	2237770	5697680	1615	1450	175	360	0.149
Clarke River	2239570	5698900	2084	1701	199	390	0.132
The Roaring Billy	2213600	5692210	844	1340	250	320	0.324
The Roaring Billy	2214290	5693900	1182	1433	174	372	0.186
The Roaring Billy	2214840	5695580	1422	1469	299	475	0.308
The Roaring Billy	2215460	5697420	1399	1657	299	590	0.319
The Roaring Billy	2216380	5699090	1381	1712	99	715	0.119
Wills River	2222230	5679160	1284	2017	25	404	0.020
Wills River	2224130	5679250	1319	2155	249	518	0.204
Wills River	2226230	5679600	1557	1749	298	538	0.267
Wills River	2228060	5679910	1640	1774	224	559	0.195
Wills River	2229960	5680730	1667	1747	125	599	0.113
Wills River	2231600	5681580	1759	1591	75	714	0.078
Wills River	2233410	5682080	1761	1885	200	839	0.203
Wills River	2234700	5683760	1986	2120	100	974	0.093

Appendix 4

Table A4.1 Frequency ratios and data-driven fuzzy memberships of input factor categories.

Factors	Factor class	Area (km^2)	Number of pixels	Number of pixels %	Number of pixels classified as landslides	Number of pixels classified as landslides %	Frequency Ratio	r_{ij}	Fuzzy membership (normalized freq. ratio)
Landslide inventory map	Landslides	202.2	323470	2.58	-	-	-	-	-
	No landslides	7637.7	12220305	97.42	-	-	-	-	-
Geological formations / lithological groups	Quaternary sediments - unconsolidated clastic sediments	2976.6	4762628	40.13	31510	9.81	0.245	0.313	0.139
	Coarse grained sediments	12.0	19196	0.16	78	0.02	0.150	0.016	0.085
	Medium grained sediments	450.4	720583	6.07	10585	3.30	0.543	0.182	0.308
	Fine grained sediments	24.7	39457	0.33	73	0.02	0.068	0.015	0.039
	Low - medium grade metamorphics	3554.6	5687320	47.92	270966	84.39	1.761	0.919	1.000
	High grade metamorphics	231.3	370080	3.12	7475	2.33	0.747	0.153	0.424
	Granitoids	70.2	112267	0.95	336	0.10	0.111	0.032	0.063
	Mafic extrusive	1.6	2522	0.02	30	0.01	0.440	0.010	0.250
	Limestones	1.6	2500	0.02	21	0.01	0.311	0.008	0.176

	Peat	95.0	152057	1.28	0	0.00	0.000	0.000	0.000
Slope (degrees)	**0-5**	1998.6	3197713	25.51	3973	1.23	0.048	0.111	0.028
	5-10	456.3	730008	5.82	7823	2.42	0.415	0.156	0.238
	10-15	464.5	743188	5.93	15695	4.85	0.818	0.220	0.469
	15-20	474.0	758446	6.05	23474	7.26	1.200	0.269	0.687
	20-25	679.6	1087439	8.67	46161	14.27	1.645	0.378	0.942
	25-30	728.0	1164726	9.29	52485	16.23	1.746	0.403	1.000
	30-35	722.8	1156524	9.23	51275	15.85	1.718	0.398	0.984
	35-40	939.5	1503256	11.99	60417	18.68	1.558	0.432	0.892
	40-45	603.9	966209	7.71	31979	9.89	1.283	0.314	0.734
	>45	768.2	1229136	9.80	30184	9.33	0.952	0.305	0.545
Landcover	**Bare or lightly vegetated surfaces**	810.2	1296348	11.33	59508	18.73	1.652	0.433	1.000
	Forest	3966.6	6346580	55.49	162649	51.18	0.922	0.715	0.558
	Grassland	1424.4	2279005	19.92	54141	17.04	0.855	0.413	0.518
	Scrub and shrubland	849.7	1359445	11.89	41493	13.06	1.099	0.361	0.665
	Wetland	91.6	146503	1.28	2	0.00	0.000	0.003	0.000
	Cropland	0.1	82	0.00	0	0.00	0.000	0.000	0.000
	Artificial areas	6.4	10276	0.09	0	0.00	0.000	0.000	0.000
Proximity to faults (m)	**0-100**	474.6	759309	6.05	21852	6.76	1.116	0.260	0.803
	100-500	1590.2	2544282	20.28	82342	25.46	1.255	0.505	0.903
	500-1000	1278.3	2045308	16.31	73325	22.67	1.390	0.476	1.000
	1000-2000	1484.0	2374418	18.93	79212	24.49	1.294	0.495	0.931
	2000-3000	899.1	1438544	11.47	31642	9.78	0.853	0.313	0.614

	>3000	2113.7	3381914	26.96	35097	10.85	0.402	0.329	0.289
Soil drainage	**Very poor**	795.3	1272401	10.36	10594	3.28	0.316	0.181	0.214
	Poor	109.9	175859	1.43	2	0.00	0.000	0.002	0.000
	Imperfect	540.3	864476	7.04	680	0.21	0.030	0.046	0.020
	Moderate	535.4	856577	6.98	33283	10.30	1.477	0.321	1.000
	Good (well drained)	5691.9	9107008	74.18	278468	86.21	1.162	0.928	0.787
Soil induration	**Non-indurated**	1329.0	2126333	17.32	11259	3.49	0.201	0.187	0.119
	Very weakly indurated	324.2	518777	4.23	762	0.24	0.056	0.049	0.033
	Weakly indurated	1844.7	2951507	24.04	18664	5.78	0.240	0.240	0.142
	Strongly indurated	4080.0	6528020	53.18	291166	90.14	1.695	0.949	1.000
	Very strongly indurated	94.8	151684	1.24	1176	0.36	0.295	0.060	0.174
Proximity to streams (m)	**0-100**	2193.7	3509995	27.98	95131	29.41	1.051	0.542	0.995
	100-200	1803.8	2886136	23.01	78607	24.30	1.056	0.493	1.000
	200-300	1410.6	2256941	17.99	58970	18.23	1.013	0.427	0.959
	300-400	1041.3	1666012	13.28	41824	12.93	0.974	0.360	0.922
	400-500	704.1	1126497	8.98	25252	7.81	0.869	0.279	0.823
	>500	686.4	1098194	8.75	23686	7.32	0.836	0.271	0.792
Slope aspect	**Flat**	103.6	1035921	8.26	456	0.14	0.017	0.038	0.012
	North	104.7	1046764	8.35	25446	7.87	0.942	0.280	0.670
	Northeast	149.6	1495865	11.93	23189	7.17	0.601	0.268	0.428
	East	90.7	906887	7.23	17388	5.38	0.743	0.232	0.529
	Southeast	97.7	977285	7.80	32858	10.16	1.303	0.319	0.927
	South	110.8	1108024	8.84	32626	10.09	1.141	0.318	0.812

	Southwest	153.5	1534732	12.24	32342	10.00	0.817	0.316	0.581
	West	155.2	1551905	12.38	55800	17.25	1.394	0.415	0.992
	Northwest	220.8	2207783	17.61	80057	24.75	1.405	0.497	1.000
	North	67.1	671479	5.36	23304	7.20	1.345	0.268	0.957
Curvature	**Concave**	1346.7	2154794	17.12	74239	22.95	1.340	0.089	1.000
	Less concave	2387.1	3819409	30.35	92242	28.52	0.940	0.083	0.701
	Flat	712.7	1140315	9.06	11690	3.61	0.399	0.019	0.298
	Less convex	1812.1	2899382	23.04	72203	22.32	0.969	0.075	0.723
	Convex	1607.3	2571680	20.43	73096	22.60	1.106	0.080	0.825
Rainfall intensity (mm day^{-1})	**< 200**	116.9	187087	1.49	5	0.00	0.001	0.000	0.000
	200-250	976.8	1562842	12.46	23138	7.15	0.574	0.033	0.267
	250-300	1606.5	2570321	20.49	34455	10.65	0.520	0.038	0.242
	300-350	1761.8	2818872	22.47	37682	11.65	0.518	0.039	0.241
	350-400	971.7	1554764	12.39	57961	17.92	1.446	0.082	0.672
	400-450	1113.0	1780851	14.20	71811	22.20	1.564	0.095	0.727
	450-500	1008.0	1612853	12.86	89510	27.67	2.152	0.124	1.000
	500-550	209.1	334621	2.67	8249	2.55	0.956	0.025	0.444
	>550	76.0	121564	0.97	659	0.20	0.210	0.003	0.098

Table A4.2 Selected fuzzy membership functions and associated input parameters.

Factors	Fuzzy membership function	Parameters			
		Minimum	Maximum	Midpoint	Spread
Lithology	Near	-	-	Low- medium grade metamorphics	1
Slope	Gaussian	-	-	$\sim 30^0$	0.075
Land cover	Near	-	-	Bare or lightly vegetated areas	0.7
Proximity to faults	Linear	> 3000 m	< 100 m	-	-
Soil drainage	Large	-	-	3.75	6
Soil induration	Small	-	-	1.7	5
Proximity to streams	Linear	> 500 m	< 100 m	-	-
Slope aspect	Linear	Flat slopes	Northwest	-	-
Curvature	Large	-	-	2	-
Rainfall intensity	Gaussian	-	-	400 - 500 mm day^{-1}	0.3

Table A4.3 Predictive performance of different factor combinations (* ten parameter model).

Factor combinations	AUC
Slope/ lithology/ prox. to faults/ prox. to streams/ aspect/ soil induration	0.734
Slope/ lithology/prox. to faults/prox. to streams/ soil induration	0.730
Slope/ lithology/ prox. to faults/prox. to streams/ aspect	0.725
Slope/ rainfall/ lithology/prox. to faults/prox. to streams/ aspect/ curvature/soil drainage/soil induration	0.723
Slope/ rainfall/ lithology/prox. to faults/prox. to streams/ aspect/ curvature/ land cover/soil induration	0.722
Slope/ lithology/ prox. to faults/ prox. to streams/ aspect/ land cover/ curvature/ soil drainage/ soil induration	0.722
Slope/ rainfall/ lithology/ prox. to faults/ prox. to streams/ aspect/ land cover/ soil drainage/ soil induration	0.719
Slope/ rainfall/ soil induration	0.718
Slope/ rainfall/ lithology/prox. to faults/prox. to streams/ aspect/ curvature/soil drainage/soil induration/ land cover *	0.717
Slope/ rainfall/ lithology/ prox. to faults/ aspect/ land cover/ curvature/ soil drainage/ soil induration	0.716
Slope/ rainfall/ lithology/ soil drainage/ soil induration/ prox. to streams	0.714
Slope/ rainfall/ lithology/ prox. to faults/ prox. to streams/ land cover/ curvature/ soil drainage/ soil induration	0.714
Rainfall/ lithology/ prox. to faults/ prox. to streams/ aspect/ land cover/ curvature/ soil drainage/ soil induration	0.711
Slope/ rainfall/ lithology/ prox. to streams/ aspect/ land cover/ curvature/ soil drainage/ soil induration	0.711
Slope/ rainfall/ lithology/ soil induration	0.711
Slope/ lithology/prox. to faults/ prox. to streams/ aspect/ curvature/ land cover	0.709
Slope/ rainfall/ lithology/ prox. to faults/ prox. to streams/ aspect/ curvature/ land cover	0.709
Slope/ rainfall/ lithology/prox. to faults/ prox. to streams/ aspect/ curvature/ land cover/ soil drainage	0.704

Slope/ rainfall/ lithology	0.703
Slope/ rainfall/ prox. to faults/ prox. to streams/ aspect/ land cover/ curvature/ soil drainage/ soil induration	0.701
Slope/ rainfall/ prox. to streams	0.678
Slope/ rainfall/ soil drainage	0.678
Slope/ rainfall	0.675
Slope/ rainfall/ aspect	0.671
Slope/ rainfall/ prox. to faults	0.670
Slope/ rainfall/ aspect/ curvature	0.669
Slope/ rainfall/ land cover	0.669
Slope/ rainfall/ curvature	0.668